Magnetic Fusion Energy (UC-20)
MFE--Reactor Materials (UC-20c)
MFE--Fusion Systems (UC-20d)
MFE--Environment and Safety
Analyses (UC-20e)

ANL-84-55

ANL--84-55

DE85 008345

ARGONNE NATIONAL LABORATORY
9700 South Cass Avenue
Argonne, Illinois 60439

THE TRIO EXPERIMENT

by

R. G. Clemmer, P. A. Finn, R. F. Malecha, B. Misra, M. C. Billone, D. L. Bowers, A. K. Fischer, L. R. Greenwood, R. F. Mattas, S. W. Tam, R. B. Poeppel, and G. T. Reedy

Argonne National Laboratory

I. T. Dudley, F. F. Dyer, E. D. Clemmer, J. S. Watson, P. W. Fisher, J. R. Conlin, R. L. Childs, and J. L. Scott

Oak Ridge National Laboratory

R. M. Arons

Celanese Research Company
Summit, N. J.

A. E. Scandora

Science Applications, Inc.
Schaumberg, Ill.

September 1984

TABLE OF CONTENTS

TABLE OF CONTENTS (Contd.)

TABLE OF CONTENTS (Contd.)

LIST OF FIGURES

LIST OF FIGURES (Contd.)

LIST OF FIGURES (Contd.)

LIST OF FIGURES (Contd.)

LIST OF FIGURES (Contd.)

LIST OF TABLES

LIST OF TABLES (Contd.)

ABSTRACT

The TRIO experiment is a test of in-situ tritium recovery and heat transfer performance of a miniaturized solid breeder blanket assembly. The assembly (capsule) was monitored for temperature and neutron flux profiles during irradiation and a sweep gas flowed through the capsule to an analytical train wherein the amounts of tritium in its various chemical forms were determined. The capsule was designed to operate at different temperatures and sweep gas conditions. At the end of the experiment the amount of tritium retained in the solid was at a concentration of less than 0.1 wppm. More than 99.9% of tritium generated during the experiment was successfully recovered. The results of the experiment showed that the tritium inventories at the beginning and at the end of the experiment follow a relationship which appears to be characteristic of intragranular diffusion. The derived diffusivity for tritium in lithium aluminate is expressed by $D = 1.1 \times 10^{-6} e^{(-35.8\ Kcal/RT)}$, where D in cm^2/s is the absolute temperature in K, and R is the gas constant, 0.001987 Kcal/mol-K. It was found that the addition of hydrogen to the sweep gas appeared to enhance the release of tritium - this enhancement is attributed to a surface effect. The predominant form of tritium observed was the noncondensible, or HT, form. Thermodynamic calculations are consistent with this observation. The conditions of irradiation, equivalent to about two months in a fusion reactor, did not appreciably change the morphology of the breeder material and there was no significant change in thermal conductivity of the lithium aluminate.

SECTION I

INTRODUCTION

I. INTRODUCTION

Lithium aluminate, $LiAlO_2$, is representative of a group of ceramics, called the "Solid Breeders," that are candidate materials for use as the tritium breeding medium in fusion reactors. In the past several years, a number of conceptual blanket designs for fusion reactors have used solid breeders,[1-16] and the data base has been reviewed.[17-24] Although the data base is limited, experimental programs are in progress and more results are becoming available.[25-39] The solid breeders include Li_2O, $LiAlO_2$, Li_2ZrO_3, Li_4SiO_4, and Li_2SiO_3. The ternary oxides, in general, have much better chemical and thermophysical stability than Li_2O, but owing to its high lithium atom density, Li_2O has better tritium breeding potential.

The TRIO experiment involved the irradiation of $LiAlO_2$ in the Oak Ridge Research Reactor (ORR) under well-defined conditions of temperature, neutron flux, sweep gas flow, and sample configuration. Lithium aluminate was selected for the experiment because of its attractive properties (discussed later). Tritium, in its various chemical forms (and other gases evolved from the $LiAlO_2$ during irradiation), was moved by a sweep gas to an analytical train in which measurements on the composition of the effluent were performed.

SECTION II

PURPOSE

II. PURPOSE

The primary purpose of the TRIO experiment was to test in-situ tritium recovery from a candidate solid breeder material under conditions representing those expected in a fusion reactor blanket. The tritium recovery results tested the feasibility of in-situ tritium recovery from solid breeders. The results also provided tritium transport data from which models can be developed to predict tritium inventories in fusion reactor blankets. Heat transfer performance of the $LiAlO_2$ was a key part of the experiment. The heat transfer data (heat transfer coefficients, thermal conductivity, etc.) derived from the experimental results will be of considerable value for the design of fusion reactor blankets.

Seven objectives were proposed for this experiment:

(1) Demonstrate tritium release and recovery for a miniaturized solid breeder blanket assembly. This objective is the most important one of the experiment. The capsule is a small-scale but operational solid breeder blanket which will be tested under limited conditions. The experiment will demonstrate for these limited conditions whether in-situ tritium recovery is feasible.

(2) Determine the effects of key operational factors upon tritium release. These factors include temperature, time, tritium partial pressure, sweep gas flow rate, H_2 partial pressure, neutron fluence (to a limited extent), and impurities. It is necessary to know how tritium release is affected by operational factors so that an understanding of tritium transport can be acquired. This should enable predictions to be made of blanket performance under conditions that have not been or cannot be determined experimentally.

(3) Demonstrate heat transfer performance in a miniaturized solid breeder blanket assembly. The control of temperatures and temperature profiles to maintain solid breeder blankets within operating limits is regarded as a significant design issue. Thus, experimental demonstration of the ability to control temperature profiles is important. In addition, data from the experiment will be used to

determine values of heat transfer coefficients and thermal conductivity of the $LiAlO_2$ and to access the effects of radiation damage upon these values.

(4) Measure tritium permeation through primary cladding. A measurable quantity of tritium may permeate through the primary cladding into the gas gap of the breeder capsule. This tritium which permeates will be collected and assayed.

(5) Investigate the form of the tritium species (e.g., $T_2O:T_2$ ratio) in the sweep gas stream. The amount of tritium released in each chemical form is to be quantitatively determined.

(6) Establish the methodology for in-pile testing. This experiment is the first truly comprehensive test of in-situ tritium recovery from solid breeders. Thus, a methodology for this kind of test will be developed.

(7) Measure radioactive species in the sweep gas stream. Certain impurities in the $LiAlO_2$ (e.g., uranium, potassium, sodium, chlorine, etc.) produce volatile radionuclides during irradiation. These will be quantified to ensure that tritium monitoring is not affected. In addition, transport data on other species (mostly nobel gases), which may provide some insight into transport of helium, will be obtained. Helium transport is potentially important for solid breeders because it can cause bubbles, which may act as traps for tritium and may also cause swelling.

SECTION III

APPROACH

III. APPROACH

The experimental approach included provision for safe operation of the experiment and acceptable uncertainty in tritium release behavior. Conditions were chosen to be favorable for tritium release, and the monitoring and control systems were provided with appropriate redundancy and flexibility. The experimental plan included a test matrix in which certain parameters were systematically varied; these parameters were time, temperature, and sweep gas conditions. Other factors, notably sample configuration and microstructure, were fixed. The grain size and the microstructure were kept essentially unchanged so that they would be well defined throughout the course of the experiment. Quality assurance was judiciously applied in the planning, design, installation, and operation of the experiment. The quality control thus ensured the validity of results from the experiment.

A. Breeder Material Selection

The first consideration was selection of the appropriate breeder material for the experiment. The selection criteria were:

(1) It must be a candidate solid breeder. The choice was limited to Li_2O and certain ternary oxides, viz., $LiAlO_2$, Li_4SiO_4, and Li_2ZrO_3. Other materials for testing can be considered as data on them is developed; an example of such a material is Li_8ZrO_6.[37]

(2) It must maintain structural and microstructural integrity during the experiment, so that temperature profiles and microstructural properties are well defined throughout.

(3) It must be readily fabricated in appropriate form, and there must be a sufficient data base such that extensive property measurements are not required to be able to design the experiment.

(4) Chemical inertness is desirable.

Based upon these criteria, $LiAlO_2$ was selected as the breeder material for TRIO.

B. Experimental Design

A test capsule was designed to function as a small-scale blanket assembly with temperature control and with continuous, in-situ tritium recovery. Parameters such as tritium production rates, temperatures, temperature profiles, damage rates, and sample configuration were, in general, selected to correspond to STARFIRE.[1] Selected features for the STARFIRE and TRIO blankets are compared in Table III-1.

TABLE III-1

Design and Operating Conditions of STARFIRE and TRIO Breeder Blankets

	TRIO	STARFIRE
Breeder Material		
$LiAlO_2$ allotrope	γ	α
Pore size distribution	Bimodal	Bimodal
Grain radius, μm	0.1-0.2	0.1-0.2
Agglomerate diameter, μm	50-100	100
Temperatures/Heat Transfer		
Minimum temperature, °C	400	500
Maximum temperature, °C	900	900
Temperature range, °C	150	400
Tritium Generation		
Production rate, $T/cm^3 \cdot s$	8×10^{12}	8×10^{12}
Lithium burnup, %/mo	0.08	0.08
Atomic displacements in $LiAlO_2$, dpa/mo	0.2	0.2
Dose, rads/mo	3×10^{12}	3×10^{12}
^6Li isotopy, %	0.5	30
Configuration		
Sweep gas composition	He/H_2 or O_2	He
Tritium partial pressure, Pa	0.1-10	1
Purge channel spacing, cm	1	1
Purge channel location	High-temp. zone	High-temp. zone

The TRIO and STARFIRE features are similar with respect to configuration, microstructure, tritium production, damage rates, and temperature range. However, some features of TRIO are different. The gamma phase of $LiAlO_2$ was chosen for TRIO because it is the stable form at high temperature and does not revert to the alpha form. The ^6Li content was reduced to compensate for differences in the neutron spectrum; ORR has a mixed spectrum, with roughly equal fluxes of thermal, epithermal, and fast neutrons -- each about 1.4 10^{14} $n/cm^2.s$. Because the ^6Li cross section is very much larger at low neutron energies, the isotope is diluted to have the same tritium production rate as that in a fusion reactor, which has a much "harder" neutron spectrum (more high-energy neutrons). The "softer" spectrum of the TRIO experiment (more low-energy neutrons) has another effect; namely, the ^6Li burns up in a rather short time, and the tritium production rate decreases by about 12% every month. The temperature and sweep gas conditions are fixed in STARFIRE but the TRIO-01 experimental design allows for variation of both temperature and sweep-gas flow rate. In addition, the temperature range at a given point in time is minimized so that the effects of temperature upon tritium transport can be determined. As later discussed, the experiment includes a matrix of 33 tests involving different combinations of temperature and flow conditions.

SECTION IV

EXPERIMENTAL APPARATUS

IV. EXPERIMENTAL APPARATUS

The TRIO experimental configuration is schematically illustrated in Fig. IV-1. The sweep gas flows through the capsule and then passes to the gas analysis system. The essential components of the experimental apparatus are the capsule containing the breeder material, the gas analysis system, the core mockup test, and the instrumentation system. Each of these components is discussed below, as is the core mockup test.

A. Capsule

The design for the capsule is illustrated schematically in Fig. IV-2. The $LiAlO_2$ breeder pellets are in the form of hollow cylinders, designed to limit the radial temperature gradients to about 100°C. The pellets are enclosed in the inner capsule, which is separated from the outer capsule by a gas gap. The heat generated in the inner capsule flows radially outward to the reactor coolant, which is water at 60°C. The gap acts as a resistance to heat flow, and temperature control is achieved by varying the helium/argon ratio in the flowing gap gas. The sweep gas flows down through the center of the capsule, back up through the annulus between the inner tube and the inside surface of the breeder pellets, and out to the gas analysis system. Temperature is monitored by ten thermocouples located on the inside and outside surfaces of the breeder pellets. Neutron flux is monitored by three self-powered neutron detectors wrapped around the outside of the capsule. In addition, dosimetry wires are placed in the center of the capsule and on the outside of the capsule assembly.

Table IV-1 presents various characteristics of the $\gamma LiAlO_2$ pellets used in the TRIO capsule, and Table IV-2 gives various characteristics of the capsule itself and capsule instrumentation. A detailed capsule design is illustrated in Fig. IV-3. In general, the TRIO design conforms with the criteria selected for the design concept (see Table III-1). The major exception is the maximum temperature, which was limited by stress considerations. The essential elements of the experimental design are discussed below.

The pellet dimensions were selected so that the radial temperature gradients were limited to 100°C, i.e., the inside surface of the pellets was 100°C hotter than the outside surface. The sweep gas flows past the inside surface

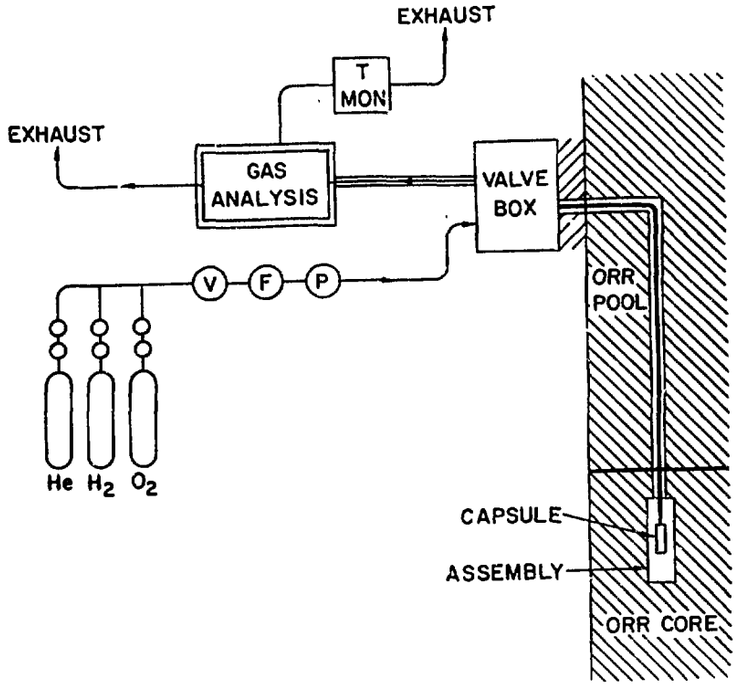

Fig. IV-1. TRIO sweep gas flow path.

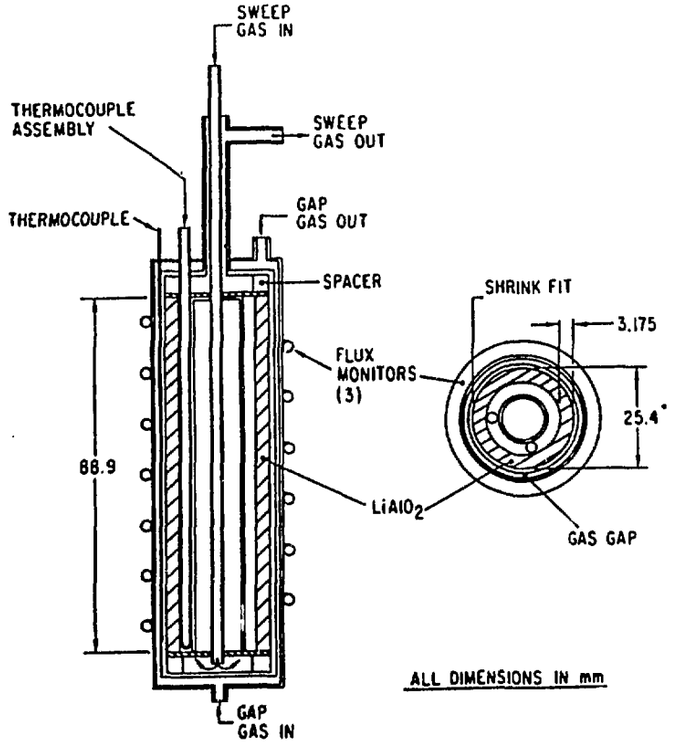

Fig. IV-2. TRIO design concept.

TABLE IV-1

Characteristics of γ-$LiAlO_2$ Breeder Material for TRIO Capsule

Characteristics	Values
Number of pellets	7
Mass,[a] g	42.9
Pellet dimensions, mm (in.)	
Inside diameter	15.87 (5/8)
Outside diameter	25.4 (0.999)
Height	~13 (1/2)
Smear density, % of theoretical	65
Elemental impurities, wppm	<100
Carbonate impurity, %	<0.5
Moisture content, %	<0.5
^6Li isotopy, %	0.55
Grain radius, μ	0.1
Nominal diameter agglomerates, μm	~50
Maximum temperature,[b] °C	800
Minimum temperature, °C	400
Radial temperature gradient, °C	100
Total temperature range, °C	150

[a]Total of the seven pellets.

[b]Limited by capsule stresses.

TABLE IV-2

Characteristics of TRIO Capsule
and Capsule Instrumentation

Capsule Characteristics	Values
Breeder material	γ-$LiAlO_2$
Structural material	304 SS
Maximum temperature,[a] °C (°F)	815 (1500)
Inner capsule dimensons, mm (in.)	
Minimum wall thickness	2.59 (0.0625)
Inside diameter	25.40 (1.000)
Outside diameter	31.75 (1.250)
Outer capsule dimensions, mm (in.)	
Minimum wall thickness	1.59 (0.0625)
Inside diameter	32.77 (1.290)
Outside diameter	39.12 (1.540)
Pressure, kPa (psig)	
Sweep gas	340 (35)
Gap gas	450 (50)
Coolant water	340 (35)
Coolant water temperature, °C	60
Average (nominal) breeder temperature, °C	400-700
Sweep gas flow, cm^3/min	30-300
Sweep gas composition	He + 0-1% H_2 or 0-0.2% O_2
Capsule instrumentation	
Temperature	10 thermocouples
Thermal flux	3 self-powered neutron detectors
Dose	Dosimetry wire (inside and outside capsule)
Sweep gas pressure and flow	Gas instrumentation
Tritium release, sweep gas	SGAS[b]
Sweep gas chemistry	SGAS
Radionuclides in sweep gas	SGAS
Tritium permeation	Gap gas monitor

[a]Limited by stress, ASME code.

[b]SGAS = sweep gas analysis system.

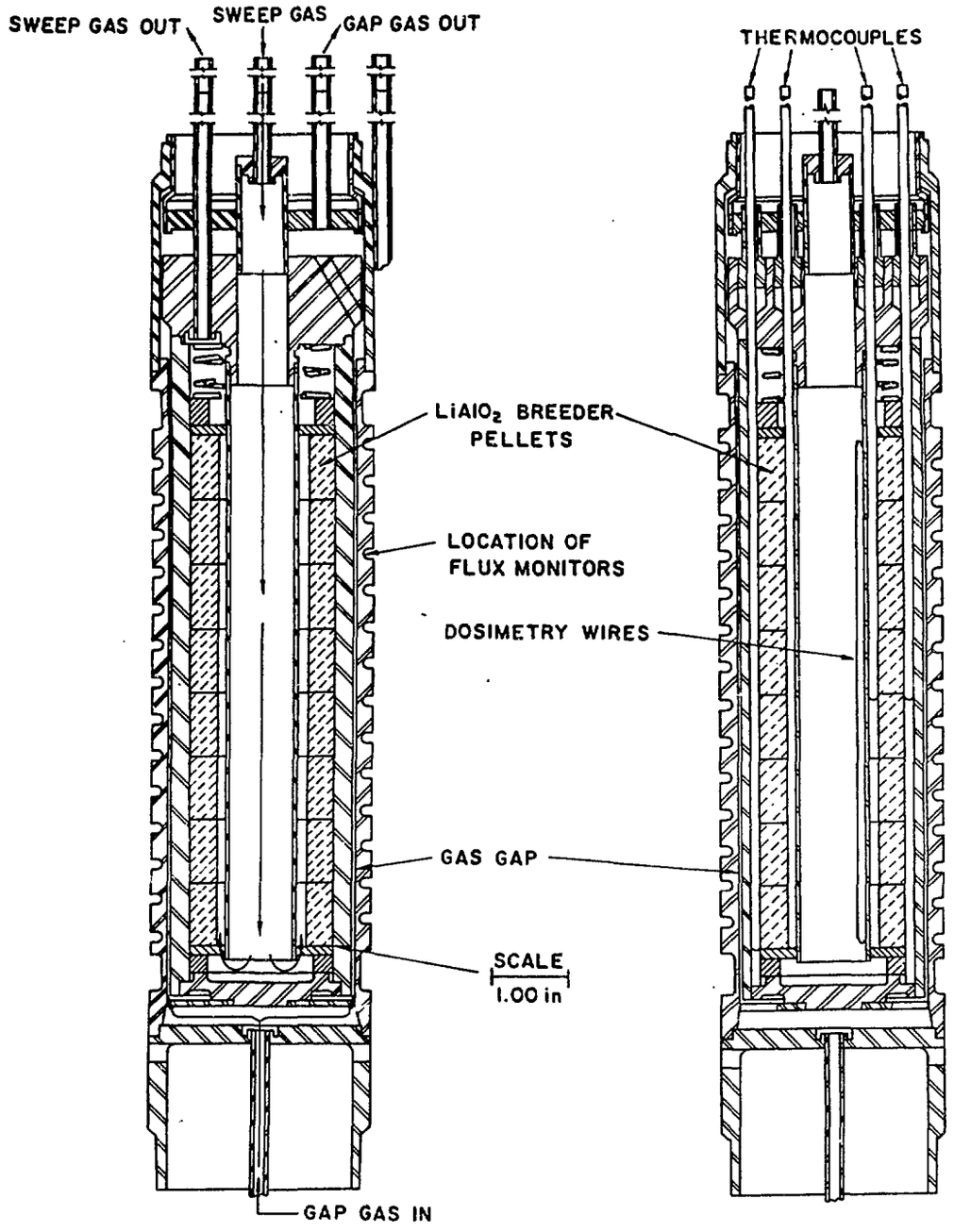

Fig. IV-3. Detailed design of TRIO capsule.

of the breeder pellets, which is the hot zone. In STARFIRE, the purge channels are also located in the hot zone. The breeder thickness for TRIO is about 5 mm, compared to a nominal purge channel spacing of 1 cm in STARFIRE.

The capsule assembly (Fig. IV-3) includes an inner capsule, which is separated from an outer capsule by the gas gap. The gas gap has a nominal

thickness of 0.50 mm (0.020 in.) at room temperature. This gap decreases by up to 50% during operation of the experiment owing to the greater thermal expansion of the inner capsule, which is at significantly higher temperatures than the outer capsule. Attached to the bottom end of the inner capsule is a guide plate that contacts the bevelled inside surface of the outer cladding. The purpose of this cladding is to center the inner capsule and maintain the gap. The inner cladding has two grooves machined into the inside surface to hold the thermocouples in position. The outer cladding has spiral grooves on the outside surface for holding the three self-powered neutron detectors in place.

There are a number of monitors for the capsule. Thermocouples (Type K Chromel-Alumel) measure temperature at 10 locations. Two of them are single-element thermocouples located on the east side of the capsule. Two are four-element thermocouple assemblies, located on the west side of the capsule. The thermocouple locations are given in Table IV-3. The thermocouples were subjected to extensive inspection by X-radiography to ensure that failures would

TABLE IV-3

Location of Capsule Thermocouples

Thermocouple Type	Element No.	Geographic Direction	Distance from Bottom (cm)	Location with Respect to Breeder
Single element	TE-1	East	4.32	Inside
Single element	TE-2	East	4.32	Outside
Multi-element	TE-3	West	6.22	Inside
Multi-element	TE-4	West	4.32	Inside
Multi-element	TE-5	West	2.54	Inside
Multi-element	TE-6	West	0.73	Inside
Multi-element	TE-7	West	6.22	Outside
Multi-element	TE-8	West	4.32	Outside
Multi-element	TE-9	West	2.54	Outside
Multi-element	TE-10	West	0.73	Outside

not occur. The accuracy (tolerance) of the thermocouples as per specifications is ±3/8% for the single-element ones and ±3/4% for the four-element ones. Further, these thermocouples normally read, at 400°C, high by about half of the tolerance.[36] Radiation effects, which are primarily important with respect to transmutation, are negligible for the experimental conditions. At 500°C, the absolute error is thus estimated to be 2°C for the single-element units and 4°C for the multi-element units.

Neutron flux is measured by active and passive methods. The active measurement consists of three self-powered neutron detectors wound around the outside of the capsule. The passive dosimetry consists of sets of dosimetry wires encapsulated in Type 316 stainless steel tubing with an o.d. of 1.6 mm (1/16 in.), having a length of 8.9 cm (3 1/2 in). There are three such dosimetry packets, one located near the center of the capsule, and two located outside the capsule on the east and west sides. As discussed later in this section, a core mockup test was performed to characterize the neutronic environment of the A2 core position, wherein the TRIO experiment was subsequently performed. The precision of the self-powered neutron detectors appears to be better than 5%, on the basis of the observed agreement of the three detectors. The accuracy of the self-powered neutron detectors is approximately 10%. The accuracy in total fluence as measured by the dosimetry wires is 10-15%.

B. $LiAlO_2$

The $LiAlO_2$ powder (alpha form) was prepared by mixing stoichiometric quantities of Al_2O_3 and Li_2CO_3, which were then ball-milled in a water slurry, spray dried, and calcined in air at 800°C for 8 h. Chemical analyses (Table IV-4) showed that the powder was reasonably pure (impurities <100 wppm) except for chloride, which was 2000 wppm.

The chloride level was a matter of considerable concern because of the corrosiveness of that ion. After exploration of several methods, it was found that vacuum heat treatment of the lithium aluminate powder for 20 h at 830°C reduced the chloride levels to less than 500 wppm. This heat treatment apparently reduced the sinterability of the final product, because the final pellet firing required more stringent conditions in comparison to procedures developed earlier to fabricate "bimodal" lithium aluminate from powder that had not

TABLE IV-4

Chemical Analysis of $LiAlO_2$ Powder

Impurity	Amount of Impurity[a] (wppm)		
	Emission Spectroscopy	Neutron Activation	Other
Ag	<10, <10, <1		
As	<500, <500, <300	0.05, 0.04	
Au	b	0.00051	
B	<10, <10, (5)		
Ba	<100, <100, <20		
Be	<10, <10, <5		
Bi	<10, <10, <10		
Br	b	0.10, 0.065	
Ca	30, 50?, <50		
Cd	<1000, <1000, <100		
Cl[c]	b	1960	2300 ± 100
Co	<30, <30, <5	0.22	
Cr	<30, <30, 50	25.5, 27.	
Cu	FT, FT, 2		
Fe	30, 70, 100	99.0	
Ga	b, 20, 15	17.1, 15.0	
In	b	0.03	
K	<500, (<1000), <100	<18, 7.8	18.0 ± 6.
La	b	0.14, 0.086	
Mg	(10), 20, 40		
Mn	<10, FT, 2	1.55	
Mo	<30, <30, <30		
Na	50, 100, 200	83.5	
Ni	20?, 30, 40	(400.0)	
P	<500, <500, <500		
Pb	<10, <10, <2		
Rb	b, <1000, <50		
Sb	<100, <1000, <10	1.2	
Sc	b	0.08, 0.015	
Si	(50), (70), (150)		
Sn	<30, <30, <5		
Sr	<1000, <1000, <100	4.90	
Ti	<30, <100, <30		
U	b	0.19	
Zn	<500, <300, <100	48.6, 52.0	
Zr	<100, <300, <300		

[a]Entries with question marks indicate presence of impurity uncertain; those values in parentheses have uncertain accuracies; FT = faint trace, 1-10 wppm.

[b]Not reported.

[c]The Cl level of the final product was 15 ± 5 wppm.

been heat treated. In particular, somewhat higher temperatures (1050°C instead of 1000°C) and longer firing times (17 h instead of 1 h) were necessary to achieve the target density of 65%. The final firing procedures reduced the chloride level to 15 wppm.

The pellets were fabricated by preparing agglomerates of appropriate size and then cold pressing and firing them. The agglomerates were prepared by first mixing 12 g of polyvinyl alcohol (PVA) in 300 cm^3 of water at 60°C, mixing in 120 g of $LiAlO_2$ powder, and then heating the mixture until a thick paste was obtained. The paste was then vacuum dried at 80°C for 8 h with periodic stirring. The resultant agglomerates were weakly bound; ball-milling produced an excessively high fraction of fine particles. The lithium aluminate was then mixed with water (200 cm^3), dried into a cake, and manually ground with a mortar and pestle; and once again there were too many fines. The material was then added to 300 cm^3 of warm water with an additional 3.6 g PVA, dried as before, manually ground with a mortar and pestle, and sieved to retain the fraction passing a 200-mesh screen but not a 325-mesh one. The fines were again added to water and reworked to produce 200- to 325- mesh agglomerates. These agglomerates from the second batch were added to those of the first batch to use for pellet fabrication.

The prepared material was then cold-pressed at 62 x 10^3 N (14,000 lb), producing a green pellet having dimensions of 3.00-cm o.d. x 1.76-cm i.d. x 1.30-cm high (1.18-in. o.d. x 0.695-in. i.d. x 0.512-in. high). The pellet firing data for the first test pellet are shown in Table IV-5. After the firing conditions were verified, the subsequent pellets, i.e., those used in the TRIO experiment, were fired for 17 h at 1050°C. Scanning electron microscopy showed that the microstructure had the desired bimodal pore-size distribution, with a grain diameter of about 0.2 μm (see Fig. IV-4).

The preparation procedures involved exposure of the pellets to humid ambient air. Chemical analysis of a pellet showed that the water content was 0.4 wt%. Nearly all (>99%) of this moisture was removed by heating the pellet to 300°C for 20 min. Before final assembly of the capsule, the finished pellets (which had been ground to the desired dimension) were dried by heating to 400°C for 1 h and kept in a desiccator until they were loaded into the capsule in an inert atmosphere box. These procedures involved a very brief exposure

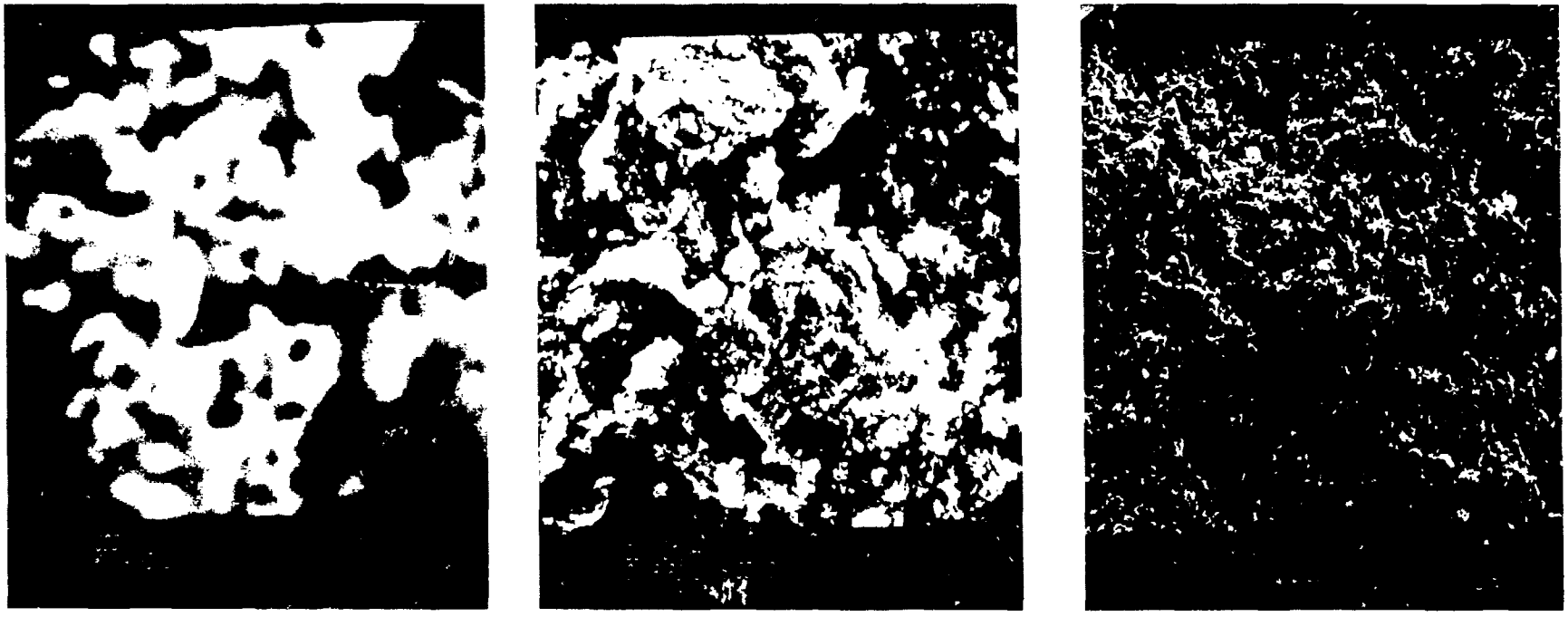

Fig. IV-4. Scanning electron micrographs of γ-$LiAlO_2$ pellet. Note the bimodal pore distribution.

TABLE IV-5

Density Data for the Firing of the First Test Pellet

	Weight (g)	o.d. (in.)	i.d. (in.)	Height (in.)	Density (g/cm^3)	% TD
Green	9.1413	1.180	0.695	0.512	1.524	59.5
First firing[a]	7.2318	1.137	0.670	0.495	1.345	52.5
Second firing[b]	7.2050	1.095	0.645	0.476	1.502	58.7
Third firing[c]	7.2074	1.078	0.635	0.467	1.580	61.7
TRIO	42.9	1.000	0.625	3.20	1.709	65.4

[a]Firing schedule: 15 h to 500°C, 8 h at 1000°C, 1 h to 1000°C, 4 h of cooling.

[b]Firing schedule: 10 h to 1050°C, 6.5 h at 1050°C, 4 h of cooling.

[c]Firing schedule: 10 h to 1050°C, 10 h at 1050°C, 4 h of cooling.

to the ambient air. The moisture content of the pellets in the experiment was estimated to be less than 0.1 wt.%.

A sample of a pellet exposed to air for one week had a CO_2 content of 0.4 wt.%. Another sample, exposed to air for four weeks, had a carbonate (CO_2) content of 1 wt.%. The heat-treatment procedure was estimated to reduce the carbonate content of the TRIO pellets to about 0.1 wt.%.

C. Gas Analysis System

The gas analysis system was designed to quantitatively measure both the amounts of tritium released in its various chemical forms and the real-time tritium release rates. The components of the system were designed as modular units that could be easily replaced and could be grouped as needed to meet the needs of the experiment. The performance of each component was verified in a mockup rig prior to assembly of the gas analysis system.

1. Design Basis

The TRIO experiment required a gas analysis system with capabilities for quantitatively determining amounts of tritium released in its various chemical

forms and for continuously measuring tritium release rates. Also, measurement of chemical impurities, radionuclides, and tritium permeation through the inner cladding into the gas gap were required. In view of considerable uncertainties regarding tritium release, the experimental system had to handle many contingencies. Proper and safe operation was necessary for the duration of the experiment, including provision for unattended operation over weekends.

The flow paths for the sweep gas and the control gas (gap gas) are shown schematically in Fig. IV-5. The sweep gas is routed sequentially to (1) a cleanup system which purifies the gas; (2) the capsule, where tritium released from the lithium aluminate is removed by the flowing sweep gas; (3) the sweep gas analysis train, where the tritium is collected and analyzed; and (4) the exhaust. The sweep gas analysis train is enclosed in a glove box, which has an atmosphere of dry ("instrument") air. The atmosphere of the glove box is routed to the ORR cell vent and exhaust. The sweep gas line leading from the capsule to the glove box is enclosed within a purged jacket to provide secondary containment of tritium. The control gas flows sequentially from its supply station through (1) a cleanup system, (2) the gas gap between the inner

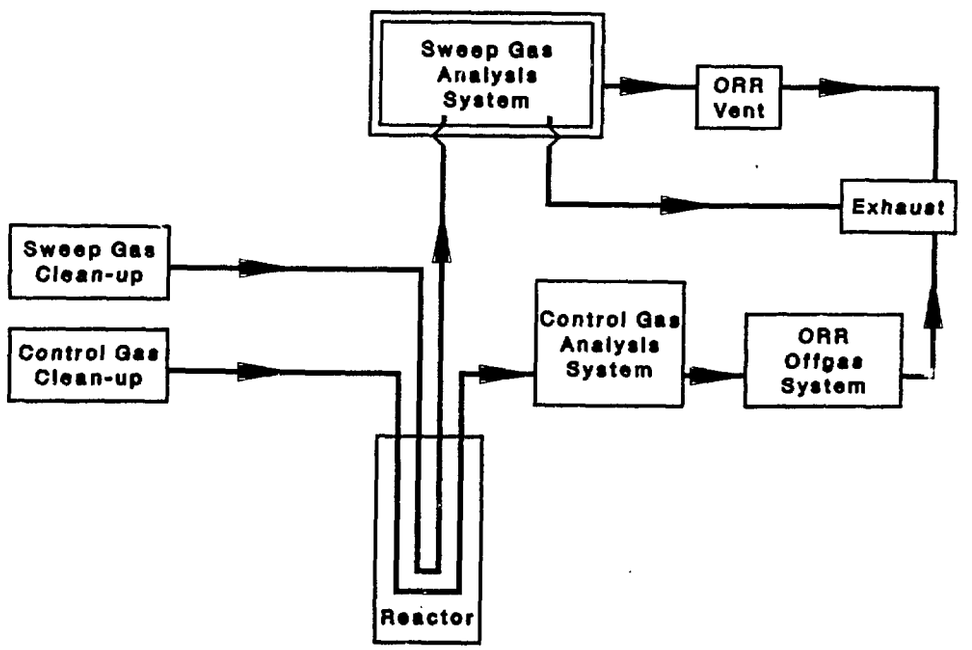

Fig. IV-5. Flow diagram for the gas analysis system.

and outer cladding of the capsule, (3) the control gas analysis system, a small scrubber which collects permeated tritium, (4) the ORR off-gas system, which consists of a charcoal bed, and (5) the exhaust. The cleanup systems consist of 4A molecular sieve beds operating at room temperature and, for all gases except oxygen and hydrogen, titanium getter beds operated at 400°C.

2. Components

The components for the gas analysis system were designed to be replaceable units that could be grouped as needed for the experiment. The performance of selected units was tested in a mockup of the gas analysis train prior to final design of the gas analysis system. The purpose of each component is described below.

Unit	Purpose
Oxidation bed	Converting HT to HTO
Ethylene glycol trap	Collecting HTO
Mole seive bed	Collecting HTO
Reduction bed	Converting HTO to HT
Getter bed	Collecting HT
Kanne chamber	Measuring HT concentration in gas stream
Gas sampler	Analyzing of composition and radionuclides
Stainless steel tubing	Proving gas lines
Furnace/controller	Controlling bed temperature
Glove box	Providing secondary containment of tritium
Data logger	Collecting data collection

a. Oxidation Bed

The oxidation beds, as well as the mole sieve beds, reduction beds, getter beds and the gas sampler, were constructed from Whitey sample cylinders, Part No. 304-HDF4-300. These cylinders have an internal volume of 300 cm^3 and are constructed of Type 304 stainless steel. The cylinders were loaded with appropriate material, and pipe thread adapter fittings were attached to each end. For the beds which operated at high temperature (oxidation beds, reduction beds, and getter beds), the pipe thread seals were welded to ensure that leakage did not occur. The ends of the cylinder were then connected to stain-

less steel tubing (1/4 in. o.d.) with Swagelock fittings. The stainless steel tubing was then fitted with quick-connects to the rest of the system so that components could be readily replaced.

The oxidation beds were used in the experiment for converting tritium in the noncondensable form (HT) to the condensable form (HTO). Reagent-grade copper oxide wire was used as the oxidant. In the sweep gas system, 0.1% oxygen in helium was added upstream of the oxidation bed to ensure that the oxidant was not consumed. In the control gas system, oxygen was not added; however, the bed was designed to have a lifetime of one year for that system. Tests of a prototype bed showed that the conversion efficiency (HT to HTO) was 99.5% at a temperature of 500°C, for a sweep gas with nominal conditions (helium-0.1% H_2 flowing at 100 cm^3/min). The mean residence time of tritium in the bed was approximately 30 min.

b. Ethylene Glycol Trap

Ethylene glycol is used as a liquid sorbent for HTO at room temperature. The use of ethylene glycol for this purpose has been demonstrated.[40] For the TRIO experiment, the traps are so arranged that the sweep gas flows through a coarse glass frit and bubbles up through 20 mL of ethylene glycol in the traps. The traps are operated as two in series so that the HTO which is not collected by the first trap is collected in the second one. Each set of such traps is backed by a bed of 4A molecular sieves to ensure removal of HTO. The traps are constructed of Pyrex glass and attached to the metal system with glass-to-metal seals having flexible metal tubing to reduce strain and shock. The outer portion of each trap is removable, having an O-ring seal joint. This outer portion serves as a container for the ethylene glycol. Samples were changed by bypassing flow, opening the seal, and removing and replacing the container. The removed container was then sealed, placed in a special carrying container, bagged and taken to the analytical laboratory for performing dilutions and preparing solutions for scintillation counting. Extreme care was taken not to drop or spill the solutions of ethlylene glycol, which, in some instances, contained upwards of one curie of HTO.

Estimates based on existing data[41] indicated that the traps removed more than 98% of the HTO when operated at nominal sweep gas conditions for three

days. It is estimated that increasing the flow rate to 1 liter/min would reduce the efficiency to about 92%. The vapor pressure of ethylene glycol at 25°C is 0.9 MPa (0.12 torr). With nominal sweep gas flow, about 60 mg is transported from the bubblers each day. The ethylene glycol vapor is expected to be removed by the molecular sieve bed. The carryover of ethylene glycol from one sample to the next was measured to be 0.30% for the first bubbler (which was minimized by blowing out the grit with a momentary pulse of sweep gas) and 0.6% for the second bubbler. The effect of ethylene glycol upon quenching the scintillation signal was a decrease of about 4% for an addition of 1% ethylene glycol to the liquid scintillator solution.[42] Since the lowest dilution used has a factor of 100 less ethylene glycol and the quenching curve is almost linear, the error introduced from this factor is less than 0.05%.

The following analytical procedure was used to determine the tritium content of a trap sample. Using an Eppindorf pippete, a 0.5-mL sample of the ethylene glycol solution was diluted to 25 mL. If necessary, a second dilution was made by diluting 0.5 mL of the first solution to 25 mL. In some cases, a third dilution was prepared from 0.5 mL of the second dilution. After appropriate dilution, a 0.10-mL sample of the diluted solution was added to 15.0 mL of Beckman GP scintillator solution, and the mixture was counted for tritium. After background corrections, the counts were ratioed to NBS standards so that the tritium activity in the sample could be determined. The accuracy of all pipettes was ensured by weighing the amounts of liquid delivered in not less than ten tests. It was found that the test pipettes delivered to within 1% of the nominal value. The absolute accuracy of a single determination is estimated to be 5%, including random errors from the NBS standard (<2%), the dilution (3%), and the counting statistics (<1%).

A technique was developed to remove some samples from a trap without removing the trap. For this procedure, the trap had a side arm with a rubber septum, and 2.0-μL samples were taken with a syringe. The 2.0-μL sample was then added directly to the scintillator solution and counted. This procedure is not as accurate as the above one, owing to sampling errors of approximately 5%. (overall absolute error, <10%), but it did permit frequent samples to be taken. Such a procedure was used for many HTO determinations.

c. Molecular Sieve Bed

Beds containing Type 4A molecular sieves were used to back up the scintillation traps and to collect permeated tritium from the gap gas. The molecular sieve beds were operated at ambient temperature. Tritium was removed from the molecular sieves by refluxing in water for a period of not less than four hours. The water was then analyzed for tritium by liquid scintillation counting.

d. Reduction Bed

Although not used in the experiment, the gas analysis system was provided with reduction beds designed to convert HTO to HT. The beds contained reagent grade magnesium turnings and were to be operated at 400°C. Mockup tests of a prototype bed showed that the conversion efficiency was 99.5%, with negligible holdup of tritium. The residence time was approximately one hour.

e. Getter Bed

A getter bed, consisting of titanium sponge, was provided for the purpose of removing HT from the sweep gas stream. The bed was to be operated at 230°C and regenerated at 600°C. The bed was not used for the experiment.

f. Kanne Chamber

Kanne chambers were used to monitor tritium concentration of the sweep gas and to measure tritium levels in the glove box and in the room. These instruments are particularly useful because a continuous measure of tritium level is provided. When calibrated, the instruments have an absolute accuracy of about 10%. The instruments operate properly over a range of about two decades. However, exposure of a meter to very high levels of tritium causes a significant increase in background levels for an extended period of time -- this is called a "memory" effect. Tritium monitors used for the room and for the glove box were calibrated with a commercially available unit that supplies known amounts of tritiated methane. The sweep-gas line monitors were tested and calibrated at levels of up to 1000 $\mu C/m^3$ with this unit. However, the tritium levels in the sweep gas during the experiment were three orders of magnitude higher, and the calibration unit could not operate at this level.

Therefore, the Kanne chambers used as sweep gas monitors were calibrated using the integral data obtained from scintillation counting during operation of the experiment.

g. Gas Sampler

The purpose of the gas sampler was to provide samples of the sweep gas for chemical analysis. The unit consisted of a 300-cm^3 cylinder in a flow-through configuration fitted with quick-disconnects. As later discussed, the unit was modified for measuring radionuclides.

h. Stainless Steel Tubing

The sweep gas, upon leaving the capsule, must traverse a 15-m (50-ft) length of stainless steel tubing (1/8 in. o.d.) leading to the analytical train. To determine the tritium holdup of such a line, a 15-m long coil of stainless steel tubing was tested in the mockup rig. It was found that the holdup time was less than 30 min for the reference gas flow conditions.

i. Furnace/Controller

Replaceable furnace units, constructed of semi-cylindrical heating elements, were provided for the purpose of operating beds at elevated temperature. The heating elements were coated with Sauerisen paste, dried, provided with insulation, and installed. Temperature was controlled with a Variac rheostat and a Leeds on-off type controller.

j. Glove Box

The above units were located in a glove box. The purpose of the glove box was to provide secondary containment of the tritium for protection of personnel. The atmosphere of the glove box was dry instrument air which is available at the ORR site as a utility. The glove box is maintained at a negative pressure of one inch of water, and the air is flushed through the box at a rate of 100-200 liters/min. Pressure control is provided to ensure against pressurization of the box.

k. Data Logger

Data from tritium monitors, flow rates, pressures, bed temperatures, etc., from the above units were collected at timed intervals on a Fluke data logger and recorded both on paper and magnetic tape. Alarm levels were specified where appropriate. Alarms that could affect safety were wired directly to the control room. Alarms that could affect only the operation of the experiment were combined into a single alarm for the reactor control room. In the event the latter alarm was tripped, the cause was investigated and proper actions were taken to clear the alarm or the experimenter was contacted for advice.

3. Modes of Operation

The sweep gas analysis system was designed to operate in four different modes, as illustrated in Fig. IV-6. The different modes were selected by appropriate manipulation of valves in the glovebox. Mode 1 was found to be most appropriate for the experiment, and it was the only mode used. In this mode, the sweep gas flows in the following sequence: (1) the tritium-containing gas is sent through the gas sampler, (2) HTO is removed by the

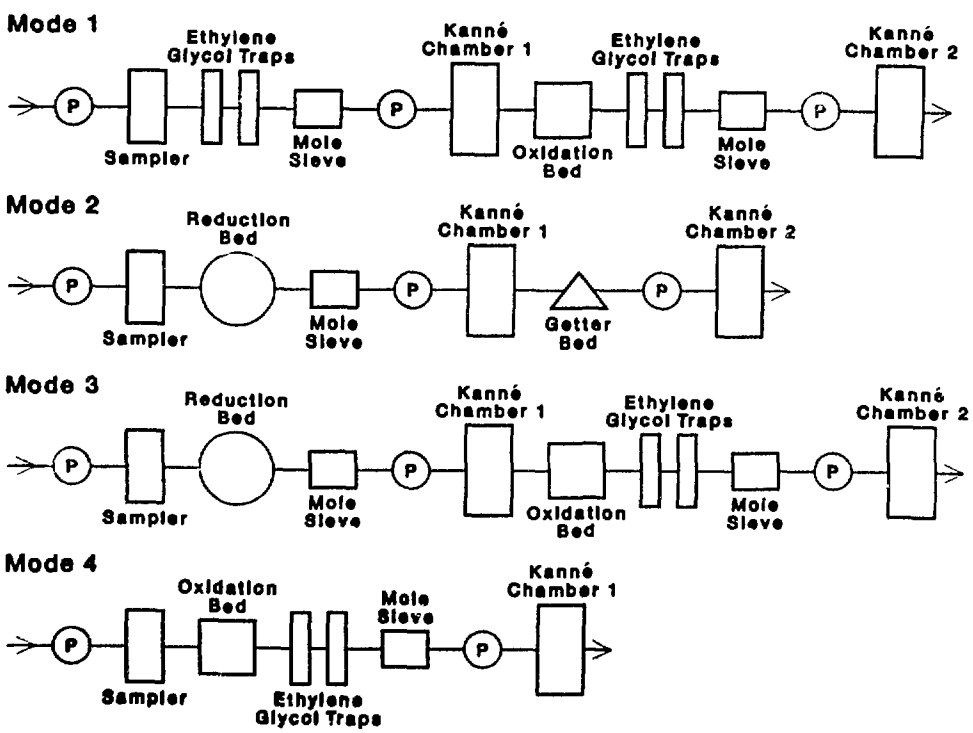

Fig. IV-6. Modes of operation for the sweep gas analysis system.

ethylene glycol traps and the mole sieve bed, (3) the HT level is monitored with Kanne Chamber 1, (4) the HT is oxidized to HTO, (5) the converted HTO is trapped, and (6) the exhaust stream is monitored by Kanne chamber 2. Owing to instrumental problems, the exhaust monitor did not function for most of the experiment.

4. Control Gas

The analysis system was provided with an arrangement designed to collect the tritium that permeated into the control gas. Such tritium was oxidized, then collected on molecular sieves. Owing to radioactivity, the system was accessible only when the reactor was down (every two weeks). The molecular sieve bed was then removed and replaced every two weeks. The tritium content was determined as previously discussed.

D. Instrumentation

The experimental system includes a number of on-line monitors which record data from the components described above. The data from the gas analysis system include tritium production, temperatures, and flow conditions in the train. These data were recorded on a Fluke data logger and magnetic tape. Monitors record the ORR power parameters, which were manually recorded in ORR logbooks. Capsule monitors and some gas supply system data were recorded on the ORRDACS (ORR data acquisition system) and on ORRDACS magnetic tapes. From these monitors, data were transferred to computer disc storage at ANL. The parameters so recorded are defined in Table IV-6.

E. Core Mockup Test and Nuclear Measurements

Before irradiation of the capsule, the core mockup test was performed to characterize the nuclear environment and to calibrate the flux monitors. A mockup of the TRIO capsule assembly (Fig. IV-7) was fabricated and installed in the A2 core position of ORR. The configuration of the ORR core, with the grams of fuel in each position during the mockup test, is schematically shown in Fig. IV-8. The mockup included three of the self-powered neutron detectors and provision for inserting tubes in eight different locations, as illustrated in Fig. IV-9. The test included a comprehensive dosimetry experiment used to measure the neutron spectrum in a number of appropriate geometric locations.

TABLE IV-6

Parameter List for TRIO

Parameter Name	Description	Units
	Gas Analysis System	
KC1	Line monitor Kanne chamber KC1	μCi/min
KC1C	Corrected line monitor KC1	μCi/min
KC1R	Line monitor Kanne chamber KC1	Ci/m^3
PI-3	PI-3 line monitor pressure for KC1	psi
PI-3R	PI-3 pressure for KC1 (raw)	psi
FI-3	FI-3 line monitor flow for KC1	cm^3/min
KC2	Exhaust monitor Kanne chamber KC2	μCi/min
KC2R	Exhaust monitor Kanne chamber KC2	Ci/m^3
PI-2	PI-2 exhaust monitor pressure for KC2	psi
PI-2R	PI-2 pressure for KC2 (raw)	psi
FI-2	FI-2 exhaust monitor flow for KC2	cm^3/min
KC3	Box monitor Kanne chamber KC3	μCi/min
KC3R	Box monitor Kanne chamber KC3	$\mu Ci/m^3$
PI-4	PI-4 box monitor pressure for KC3	psi
PI-4R	PI-4 box pressure for KC3 (raw)	psi
FI-4	FI-4 box monitor flow for KC3	cm^3/min
TC2	TC2 temperature from Box OB-1	°C
TC4	TC4 temperature from Box RB-1	°C
TC6	TC6 temperature from Box RB-2	°C
TC8	TC8 temperature from Box OB-2	°C
TC10	TC10 temperature from Box GB-1	°C
TC12	TC12 temperature from Box GB-2	°C
PI-1	PI-1 inlet sweep gas pressure	psi
PI-1R	PI-1 inlet sweep gas pressure (raw)	psi
TE-1	TE-1 capsule temperature	°C
TE-2	TE-2 capsule temperature	°C
TE-3	TE-3 capsule temperature	°C
TE-4	TE-4 capsule temperature	°C
TE-5	TE-5 capsule temperature	°C

TABLE IV-6 (Contd.)

Parameter Name	Description	Units
	Gas Analysis System (Contd.)	
TE-6	TE-6 capsule temperature	°C
TE-7	TE-7 capsule temperature	°C
TE-8	TE-8 capsule temperature	°C
	Power History	
POWER	Daily power (energy)	MWh
CPOWER	Cumulative power (energy)	MWh
FPD	Daily FPD (full-power days)	
CFPD	Cumulative FPD	
T	Daily tritium	Ci
CT	Cumulative tritium	Ci
DFLUX	Daily average flux	10^{14} nv
SHIELD	Self-shielding	
6LIBU	^{6}Li burnup	%
6LIBUT	^{6}Li total burnup	%
BUDAY	% burnup/day	
BUTOT	Total burnup	
LILEFT	% lithium left	
TDAY	Tritium production	Ci/day
TNET	Total tritium production	Ci
	ORRDACS	
T901	TE-1 capsule temperature	°C
T902	TE-2 capsule temperature	°C
T903	TE-3 capsule temperature	°C
T904	TE-4 capsule temperature	°C
T905	TE-5 capsule temperature	°C
T906	TE-6 capsule temperature	°C

TABLE IV-6 (Contd.)

Parameter Name	Description	Units
	ORRDACS (Contd.)	
T907	TE-7 capsule temperature	°C
T908	TE-8 capsule temperature	°C
TR801	TE-9 capsule temperature	°C
TR901	TE-10 capsule temperature	°C
F12	Helium inlet flow-gap gas	cm^3/min
F18	Argon inlet flow-gap gas	cm^3/min
F25	Flow-gap gas exhaust	cm^3/min
F26	Flow-gap gas exhaust	cm^3/min
F52	Helium flow-sweep gas	cm^3/min
F53	Helium/4% H_2 flow-sweep gas	cm^3/min
F64	Sweep gas exhaust	cm^3/min
REAPWR	ORR reactor power	W
TREF6	Reference thermocouple	
R100	R100 neutron flux	10^{14} nv
R100R	R100 neutron flux (raw)	10^{14} nv
R200	R200 neutron flux	10^{14} nv
R200R	R200 neutron flux (raw)	10^{14} nv
R300	R300 neutron flux	10^{14} nv
R300R	R300 neutron flux (raw)	10^{14} nv
R400	Average neutron flux	10^{14} nv

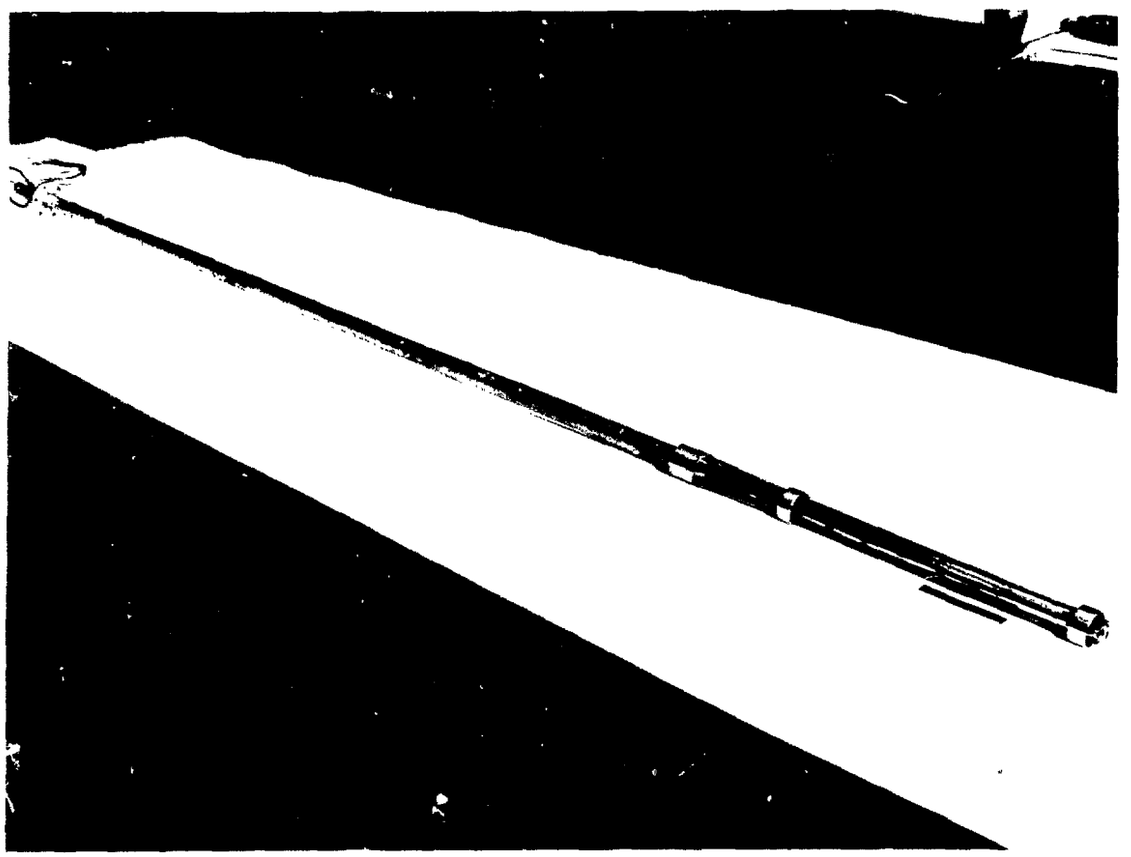

Fig. IV-7. Core mockup test assembly.

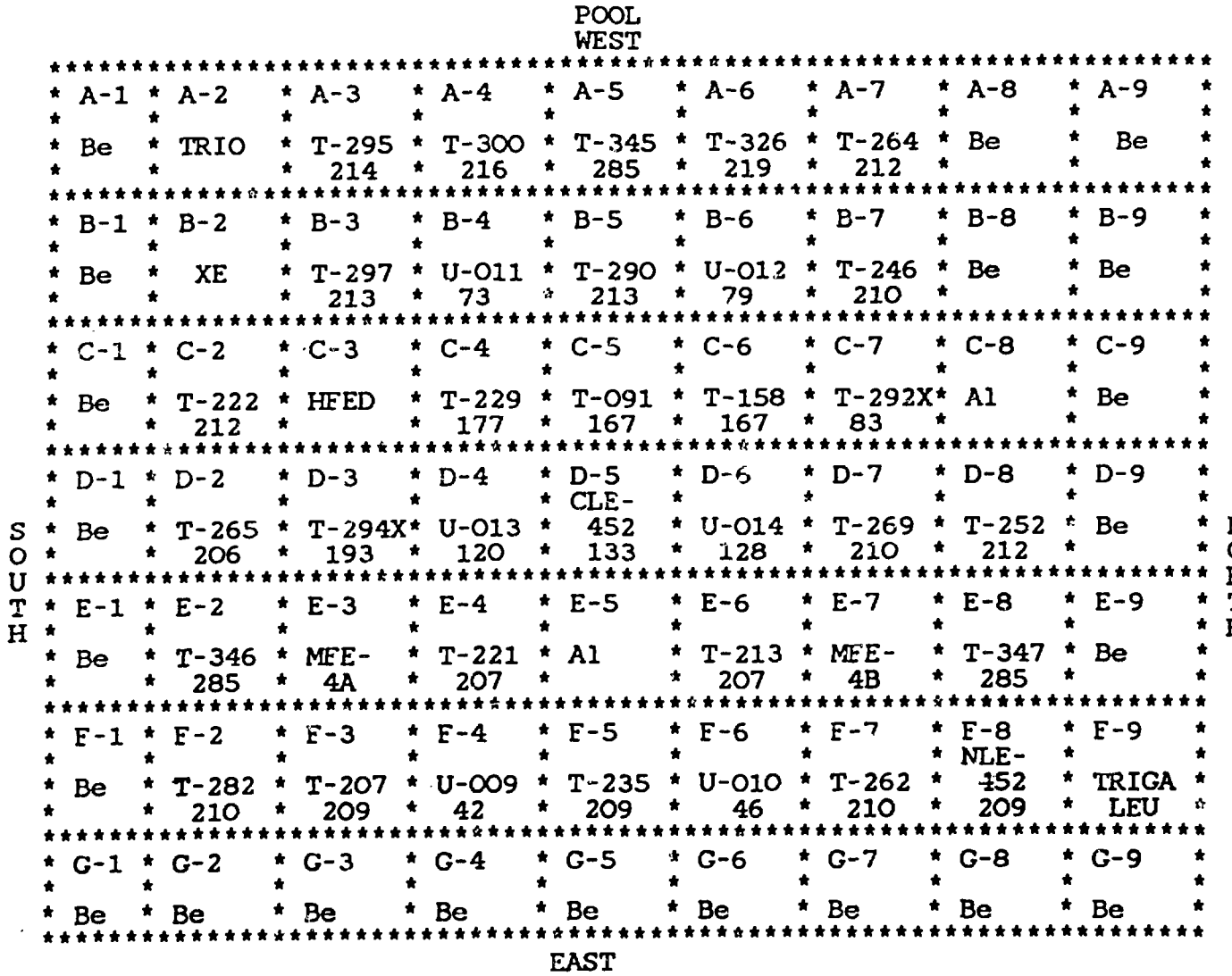

Note: T - is fuel element.
V - is control element.
Grams of fuel shown, other designations are other experiments.

Fig. IV-8. ORR fuel loading diagram (Cycle 160-E, core mockup test, from April 5, 1983, to April 16, 1983).

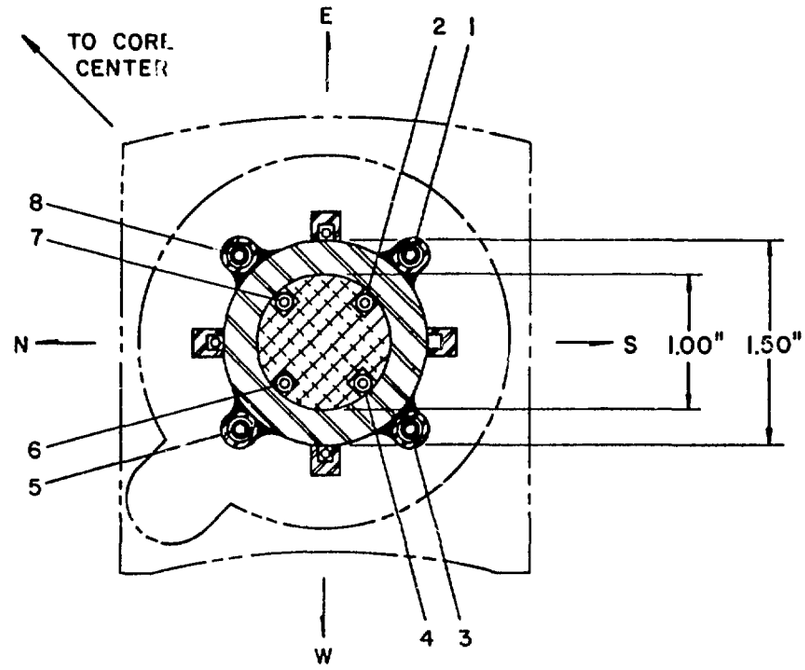

Fig. IV-9. Cross section of TRIO core mockup.

Tritium production in samples of the isotopically tailored breeder material used for the TRIO experiment was also measured. In related but separate tests, neutron flux profiles and gamma heating rates were measured in the A2 core position of ORR. Described herein are the calibration of the self-powered neutron detectors, and measurements of essential nuclear parameters, including gamma heating rates, neutron spectrum, and tritium production.

1. Self-Powered Neutron Detectors

The three self-powered neutron detectors were found to consistently give thermal flux readings that agreed within one percent. Typical values for the three detectors were 1.33, 1.32, and 1.34 10^{14} x $n \cdot cm^{-2} \cdot s^{-1}$ ($n \cdot cm^{-2} \cdot s^{-1}$ = nv), or an average of 1.33×10^{-14} nv. The precision of these detectors is thus very good. Since the three detectors used in the TRIO experiment are from the same batch, their precision is expected to also be very good.

2. Tritium Production Tests

Before the tritium production was measured in the core mockup test, experiments were conducted to verify the tritium assay techniques. Specimens

of lithium carbonate (natural abundance, ^6Li = 7.5%) and the $LiAlO_2$ powder used to fabricate the TRIO pellets (isotopically tailored, ^6Li = 0.55%) were sealed in quartz capillaries and irradiated in the pneumatic tube of the Oak Ridge High Flux Isotope Reactor (HFIR) at a nominal thermal neutron flux of 4.6×10^{-14} nv. The neutron fluence was monitored using wires of aluminum alloys containing known amounts of manganese and gold. After irradiation, each quartz capillary containing a sample of lithium aluminate or lithium carbonate was dissolved in concentrated HF in a sealed polyethylene vial. The solutions were diluted with water, made basic with NaOH, diluted to a known volume, and distilled to recover the HTO. The tritium was then measured by beta counting in a Packard liquid scintillation counter. The counter was calibrated using known aliquots of an NBS standard.

Comparisons of predicted and measured amounts of tritium ai presented in Table IV-7. Predicted activities of tritium (A) were based on the relation:

$$A = N \times P_{th}[S_o + (P_r/P_{th})I](1 - \exp\{-lt\}) ,$$

where

N = number of ^6Li atoms irradiated

P_{th} = thermal neutron flux

S_o = 2200 m/s* neutron cross section of ^6Li (940 b)

P_r = resonance neutron flux

I = resonance integral for the reaction of ^6Li (425 b)

l = decay constant for tritium (half life = 12.33 y)

t = the irradiation time

As can be seen from Table IV-7, the agreement between predicted and measured tritium activities is quite good. Uncertainties in predicted activities are thought to be mainly due to uncertainties in the measured neutron flux, estimated to be 5%. The error in the NBS standard is about 2%. The results

*This value is the nominal velocity of a thermal neutron.

TABLE IV-7

Comparison of Predicted and Measured Activities of Tritium in Irradiated Samples of Lithium Carbonate and Lithium Aluminate

Sample No.	Tritium Activity, Bq/mg		
	Predicted	Measured	% Diff.
	Lithium Carbonate[a]		
1	5.98×10^4	5.84×10^4	-2.3
2	5.98×10^4	6.10×10^4	+2.0
3	5.98×10^4	6.05×10^4	+1.2
			+0.3
	Lithium Aluminate (TRIO)[b]		
1	7.07×10^4	6.87×10^4	-2.8
2	7.07×10^4	6.93×10^4	-2.0
3	7.07×10^4	7.24×10^4	+2.4
4	7.07×10^4	6.97×10^4	-1.4
5	7.07×10^4	7.44×10^4	+5.2
6	7.07×10^4	6.94×10^4	-1.8
			-0.1

[a] Thermal flux* = 4.68×10^{14} nv; irradiation time = 61.6 s.

[b] Thermal flux* = 4.61×10^{14} nv; irradiation time = 1800 s.

*The thermal-to-resonance flux ratio was measured to be 36.

demonstrate that the analytical techniques developed for the core mockup test yield quantitative recovery of tritium.

Tritium production in the core mockup test was determined by inserting quartz ampoules containing the isotopically tailored $LiAlO_2$ into various locations in the mockup assembly (Fig. IV-9) and assaying for tritium. The measured tritium activities for the core mockup test are given in Table IV-8.

Table IV-8

Tritium Production in the Core Mockup Test
(April 27, 1982)

Sample No.	Irradiation Location	Sample Weight[a] (mg $LiAlO_2$)	Measured Tritium Activity (μCi/mg)
1	2 top	2.415	6.58
2	2 bottom	1.173	7.04
3	4 top	1.396	6.72
4	4 bottom	1.509	6.23
5	6 top	1.358	6.24
6	6 bottom	1.569	6.41
7	8 top	1.858	6.55
8	8 bottom	1.920	6.53

[a]The lithium aluminate used is isotopically tailored, having a ^6Li content of 0.55%.

3. Dosimetry Measurements

A comprehensive dosimetry experiment was conducted as a part of the core mockup test to characterize the nuclear environment.[43] Flux monitor wires were irradiated in the A2 core position of ORR (see Fig. IV-8) for 8.93 h, which amounted to a total exposure of 253.35 MWh. Eight aluminum tubes were positioned in the core mockup assembly (Fig. VI-9) to measure flux and spectral gradients. Seven tubes contained titanium, iron, nickel, and cobalt-aluminum gradient wires, 15 cm (6 in.) in length. These wires were positioned to span the flux peak, which is located about 15 cm (6 in.) below the reactor midplane. The eighth tube measured 89 cm (35 in.) in length and contained 17 different materials, including gadolinium covers and fission monitors for a

spectral analysis. Gradient wires were also included to span the entire length of the core mockup assembly.

The activities of the samples were counted with Ge(Li) spectrometers, and the resultant saturated activities are listed in Table IV-9. These results were then used to adjust a calculated neutron spectrum using the STAYSL computer code.[54] The resultant neutron flux values are listed in Table IV-10.

TABLE IV-9

Activation Rates for TRIO[a]

Reaction	Activation Rate (atom/atom•s)	Gd Cover
$^{58}Fe(n,\gamma)^{59}Fe$	1.08×10^{-10}	No
$^{59}Co(n,\gamma)^{60}Co$	2.70×10^{-9}	No
$^{176}Lu(n,\gamma)^{177m}Lu$	3.92×10^{-9}	No
$^{45}Sc(n,\gamma)^{46}Sc$	2.53×10^{-10}	Yes
$^{197}Au(n,\gamma)^{198}Au$	2.15×10^{-8}	Yes
$^{237}Np(n,\gamma)^{238}Np$	7.22×10^{-9}	Yes
$^{238}U(n,\gamma)^{239}Np$	1.02×10^{-10}	Yes
$^{238}U(n,fission)$	2.26×10^{-11}	Yes
$^{54}Fe(n,p)^{54}Mn$	5.38×10^{-12}	No
$^{58}Ni(n,p)^{58}Co$	6.86×10^{-12}	No
$^{46}Ti(n,p)^{46}Sc$	7.30×10^{-13}	No
$^{47}Ti(n,p)^{47}Sc$	1.26×10^{-12}	No
$^{48}Ti(n,p)^{48}Sc$	1.99×10^{-14}	No
$^{27}Al(n,\alpha)^{24}Na$	4.59×10^{-14}	No
$^{55}Mn(n,2n)^{54}Mn$	1.69×10^{-14}	No
$^{93}Nb(n,2n)^{92m}Nb$	3.05×10^{-14}	No

[a]Determined on April 26, 1982, at ORR, A2 position. Values renormalized to 30-MW reactor power. Maximum flux height is in position 8.

Table IV-10

Neutron Flux Values for TRIO
(April 26, 1982)

Energy Range	Flux (10^{14} n/cm²-sec)	Uncertainty (%)
Total	3.79	5.0
Thermal (<0.5 eV)	1.31	6.0
Thermal (2200 m/s)[a]	1.16	6.0
Epithermal (0.5 eV-0.11 MeV)	1.20	9.0
Fast (>0.11 MeV)	1.27	7.0
Fast (>1 Mev)	0.58	6.0

[a]Nominal velocity of a thermal neutron.

The flux spectrum is shown in Fig. IV-10 for the A2 position. The dotted and dashed lines represent errors for each flux group; however, the groups are highly correlated. A covariance error matrix must then be used to calculate errors in integral quantities. Integral flux errors are typically 5-10%, as listed in Table IV-10.

The measured spectrum was also used to calculate the tritium production rate from ^{6}Li. The result agrees quite well with the measured tritium production rate (Table IV-7) and related helium dosimetry results,[44] as shown in Table IV-11. The measured thermal neutron flux also agrees well with the self-powered neutron detector readings (1.31 vs. 1.33 × 10^{14}).

TABLE IV-11

Tritium Production Rates in the
TRIO Core Mockup Test

Method Used	Production Rate (10^{-8} T/^{6}Li•s)
Dosimetry (calculated)	9.22
Measured (Table IV-8)	8.91
Helium dosimetry (Ref. 44)	8.45

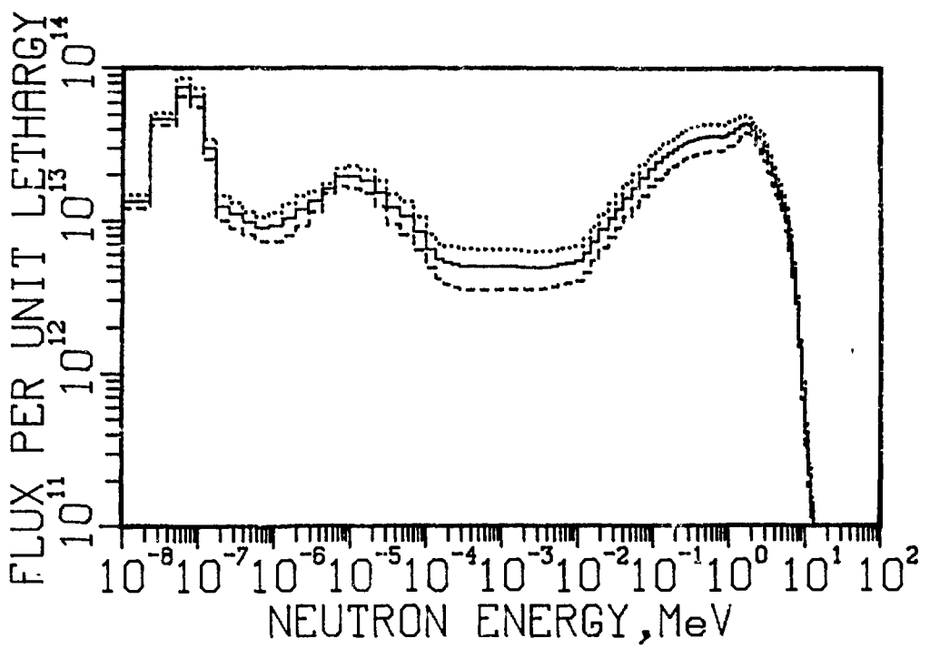

Fig. IV-10. Flux spectrum measured in the A2 core position of ORR for the TRIO experiment. (Dotted and dashed lines represent one standard deviation; however, the flux groups are highly correlated.)

Vertical flux gradients are shown in Figure IV-11. The maximum flux occurs about 13 cm (5 in.) below the reactor midplane, as expected at the start of a fuel cycle in ORR. Over the course of a fuel cycle, the flux peak moves upward about 10 cm (4 in.). Thus, the TRIO capsule, centered at 8 cm (3 in.) below reactor midplane, is near or on the flux peak throughout the fuel cycle.

Horizontal flux gradients are summarized as follows: (1) the thermal flux decreases about 21% across the assembly (4.5 cm) from east to west [away from the center of the core (Fig. IV-7)]; (2) the thermal flux is about 23% lower inside the mockup assembly, owing to absorption by the stainless steel cladding; (3) the fast flux decreases sharply (about 60%) from northeast to southwest on a line roughly pointing away from the center of the core; (4) the thermal flux varies less than 10% inside the mockup assembly, representing the region where the lithium aluminate breeder material will be located during operation of the TRIO experiment.

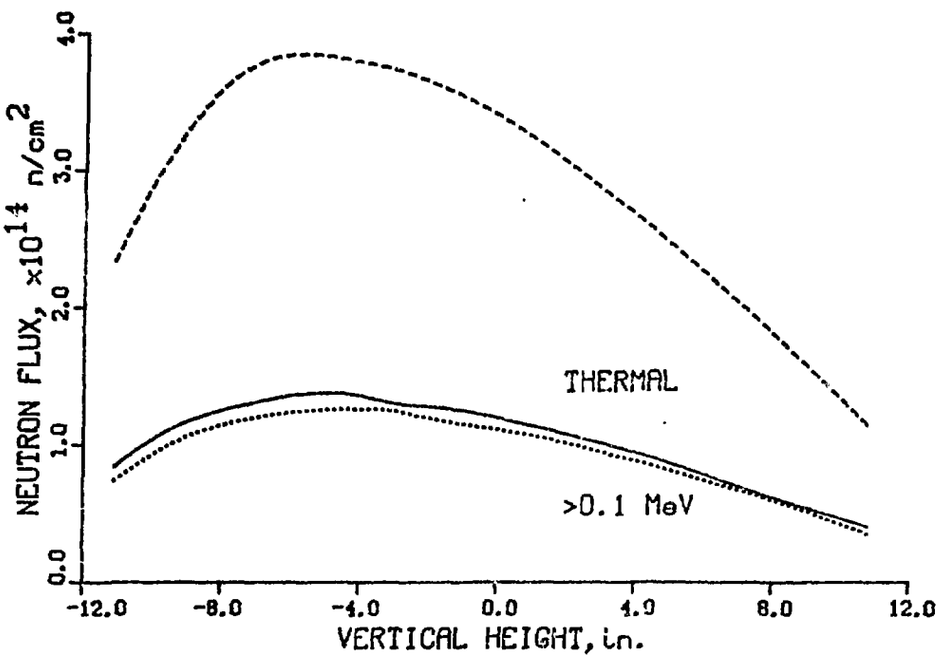

Fig. IV-11. Vertical flux gradients measured in position A2 of ORR. The maximum flux is 5 in. below midplane at the start of the fuel cycle, but will rise to 3 in. below midplane where TRIO is centered.

4. Gamma Heating Rates

Gamma flux profiles in the A2 core position were measured with an ionization chamber. The fuel loading diagram for the measurement is given in Figure IV-12. The values of ionization current were correlated to a prior experiment with known gamma heating rates, and the heating rates derived as a function of axial position. It was found that the gamma heating rate in stainless steel in the region of the TRIO capsule is 4.8 W/g. The estimated accuracy of this value is 5-10% (42) for a given core loading in ORR. However, changes in core loading in ORR cause significant variations in the local nuclear environment. The uncertainty in gamma flux owing to fuel changes is estimated to be 20%. The overall accuracy of the values is thus estimated to be about 25%. The value of 4.8 W/g was used for the capsule. Because gamma heating in units of watts per gram is roughly the same for most materials, the measured value was used for both the stainless steel and the $LiAlO_2$ in the capsule.

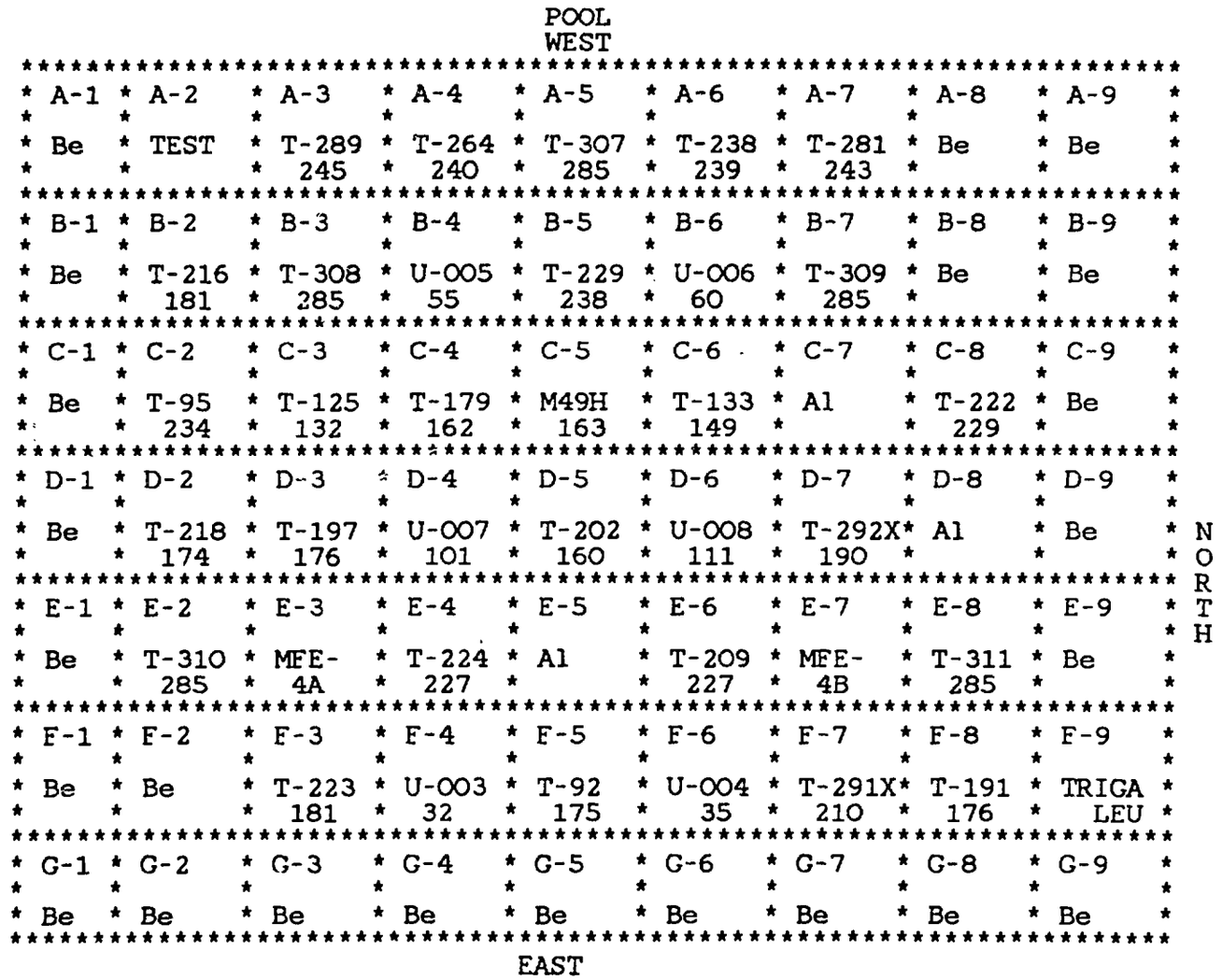

Fig. IV-12. Fuel loading diagram for the gamma heating measurements (July 12, 1981).

SECTION V

EXPERIMENTAL PLAN

V. EXPERIMENTAL PLAN

Tritium release is a function of operational parameters such as temperature, purge gas conditions, radiation damage, etc. In the TRIO experiment, three parameters were independently controlled: temperature, sweep gas flow rate, and sweep gas composition. Average (nominal) temperature was varied from 400 to 700°C by changing the composition of the gap gas; the flow rate was operated at 30 to 300 cc/min; and up to 1% H_2 or O_2 was added to the helium sweep gas. The TRIO test matrix (Table V-1) is composed of combinations of the three parameters. The matrix was designed to systematically investigate the parameter space. Temperature is the most important variable, and for most runs the sweep gas was maintained at standard conditions, namely, a flow rate of 100 cm^3/min and 0.1% H_2 added to the helium sweep gas.

The basic strategy was to operate under preset conditions and to monitor the tritium release rate until steady state was achieved. Steady state was observable when the release rate was invariant in time, and also when the release rate was equal to the generation rate. Upon completion of such a test run, the conditions were changed and another run was performed. It was expected that, when the second run was at steady state, the release rate would be the same as that of the first run.

The conditions selected for the first run were predicted to achieve steady state within about one day. Thus, the temperature was chosen to be moderately high so that there would be a good chance of achieving steady state. The second run was set at maximum temperature so that it could be checked that the first test had actually reached steady-state conditions.

The next several runs (up to Run 8) tested the effects of the temperature range, with the exception of Run 3, which tested the effect of increased hydrogen in the sweep gas. Runs 9 through 14 tested the effect of temperature when no hydrogen was added to the sweep gas. Runs 10 and 11 were used to measure low-temperature release rates of radionuclides. The next series, Runs 16-20, tested the effects of sweep gas composition and flow rate. The later series of runs tested low temperatures in an effort to obtain steady state at as low a temperature as possible. Finally, the temperature was increased to standard conditions so that the amount of tritium retained in the solid breeder could be minimized.

TABLE VI-1

TRIO Test Matrix

Run No.	Time (d)	Nominal Temp. (°C)	Sweep Gas		Test Purpose
			Composition	Flow Rate (cm^3/min)	
1	2	600	He/0.1% H_2	100	
2	2	700	He/0.1% H_2	100	Temperature
3	1	700	He/1% H_2	100	H_2 level
4	5	550	He/0.1% H_2	100	Temperature
5	2	500	He/0.1% H_2	100	Temperature
6	1	550	He/0.1% H_2	100	Repeat Run 4
7	3	600	He/0.1% H_2	100	Repeat Run 1
8	2	650	He/0.1% H_2	100	Standard run
9	6	650	100% He	100	H_2 level
10	1	400	100% He	100	Radionuclides
11	1	500	100% He	100	Radionuclides
12	4	550	100% He	100	H_2 level
13	5	600	100% He	100	H_2 level
14	2	700	100% He	100	H_2 level
15	1	700	He/0.1% H_2	100	H_2 level, temperature
16	1	700	He/0.1% H_2	100	H_2 level, temperature
17	3	700	He/0.1% H_2	30	Flow rate
18	1	700	He/0.1% H_2	100	Flow rate
19	1	650	He/0.1% H_2	100	Standard run
20	4	650	He/0.2% O_2	100	O_2
21	2	650	He/0.1% H_2	100	Standard run
22	1	600	He/0.1% H_2	100	Repeat Runs 1,7
23	3	550	He/0.1% H_2	100	Repeat Runs 4,6
24	1	600	He/0.1% H_2	100	Repeat Runs 1,7,22
25	2	560	He/0.1% H_2	100	New temperature
26	3	550	He/0.1% H_2	100	Repeat Runs 4,6,23
27	7	525	He/0.1% H_2	100	Low temperature
28	7	500	He/0.1% H_2	100	Low temperature
29	3	480	He/0.1% H_2	300	Flow rate
30	4	480	He/0.1% H_2	100	Low temperature
31	2	500	He/0.1% H_2	100	Repeat Run 28
32	2	550	He/0.1% H_2	100	Repeat Run 26
33	3	650	He/0.1% H_2	100	Standard run

SECTION VI

EXPERIMENTAL RESULTS - ON LINE DATA

VI. EXPERIMENTAL RESULTS - ON-LINE DATA

The measurement of in-situ tritium release and the correlation of relationships between tritium release and operational parameters constitute the essential part of the TRIO experiment. The most important operational parameters in the experiment are time, neutron flux, temperature and temperature profiles, and sweep gas chemistry. Presented herein are the data on operational parameters and the observed release behavior of tritium in its various chemical forms.

A. Time and Recorded Experimental History

The TRIO experiment was installed in ORR on January 14, 1983. Installation of the experiment occurred during a time when the reactor was down for a three-month period for coolant system repairs. The full-power irradiation began on March 12, 1983, and the 33 tests performed in subsequent months. The operating history is given in Table VI-1. In addition to the 33 runs, there are a large number of (about 50) transient runs. The transients provide useful dynamic data.

B. Neutron Flux and Dosimetry

Thermal neutron flux incident on the capsule was continuously monitored with the three self-powered neutron detectors wound around the outside of the capsule. Calibration of the self-powered neutron detectors was done in the core mockup test, as previously discussed. The recorded fluxes for the entire experiment are shown in Fig. VI-1. The variation in local neutron flux was considerably more than that of the reactor power (Fig. VI-2). The reason for the rather large variations in local flux was that the entire fuel for the reactor is changed every two weeks. The core loading diagrams, showing the grams of fuel in each core position for the six different fuel loadings used in the experiment, are given in Figs. VI-3a through -3g. In addition to these effects, the flux levels are approximately 30% lower than those in the core mockup test so that tritium production is correspondingly reduced. The flux data, in conjunction with dosimetry results, are used to calculate instantaneous tritium production rates.

TABLE VI-1

TRIO Operating History

Run No.	1983 Date	Time[a]	Nominal Temp. (°C)	Sweep Gas		Comments[b]
				Composition	Flow Rate (cm^3/min)	
0	1/14	1500	30	--	0	TRIO experiment installed in A2 core position
	1/27	1200	30	100% He	20	
	2/28	0900	30	100% He	0	Pressure check
	3/2	0930	30	100% He	100	
	3/9	1400	30	100% He	100	ORR rod calibrations, R = 3-30 kW
	3/10	1000	30	He/0.1% H_2	100	
	3/10	1900	35	He/0.1% H_2	100	nL run, 2 h @ 0.30 MW
	3/11	0357	200	He/0.1% H_2	100	ORR @ 12 MW for 1 h
		1013	35	He/0.1% H_2	100	nL run (0.30 MW ORR power)
		1051	35	He/0.1% H_2	100	nL run (0.30 MW ORR power)
		1625	35	He/0.1% H_2	100	nL run (0.30 MW ORR power)
		1701	35	He/0.1% H_2	100	nL run (0.30 MW ORR power)
		1720	100	He/0.1% H_2	100	ORR @ 3 MW
		1746	35	He/0.1% H_2	100	ORR @ nL
		1826	35	He/0.1% H_2	100	ORR @ nl
		1846	100	He/0.1% H_2	100	ORR @ 3 MW
		2025	200	He/0.1% H_2	100	ORR @ 12 MW
		2125	35	He/0.1% H_2	100	ORR @ nL for 25 min
1	3/12	0754	35	He/0.1% H_2	100	ORR @ nL
		0838	50	He/0.1% H_2	100	ORR @ 3 MW
		0841	87	He/0.1% H_2	100	ORR @ 6 MW
		0848	150	He/0.1% H_2	100	ORR @ 9 MW
		0849	180	He/0.1% H_2	100	ORR @ 12 MW
		0850	214	He/0.1% H_2	100	ORR @ 15 MW
		0851	242	He/0.1% H_2	100	ORR @ 18 MW
		0852	269	He/0.1% H_2	100	ORR @ 21 MW
		0853	300	He/0.1% H_2	100	ORR @ 24 MW for 30 min
		0900	350	He/0.1% H_2	100	ORR @ 24 MW for 30 min
		0924	380	He/0.1% H_2	100	ORR increased 1.5 MW
		0937	450	He/0.1% H_2	100	ORR @ 30 MW
		1050	450	He/0.1% H_2	100	ORR adjusted +0.5 MW to 30 MW
		1100	450	He/0.1% H_2	100	Begin changing gap gas to go to 600°C
		1200	600	He/0.1% H_2	100	Run 1 conditions established
	3/14	1016	600	He/0.1% H_2	100	ORR power setback
		1226	600	He/0.1% H_2	100	ORR setback
2	3/14	1300	700	He/0.1% H_2	100	Begin Run 2
	3/15	0930	700	He/0.1% H_2	100	ORR setback
3	3/16	1124	700	He/0.1% H_2	100	Begin Run 3
		1525	700	He/0.1% H_2	100	Power reduced 0.12 MW to 30 MW
4	3/17	1405	550	He/0.1% H_2	100	Begin Run 4
	3/19	1206	550	He/0.1% H_2	100	Temperature of breeder reduced 8 deg
	3/21	0856	30	He/0.1% H_2	100	ORR shut down for 1 h
		0956	550	He/0.1% H_2,	100	Resume Run 4
5	3/22	1127	500	He/0.1% H_2	100	Begin Run 5
6	3/24	1052	550	He/0.1% H_2	100	Begin Run 6
7	3/25	1050	600	He/0.1% H_2	100	Begin Run 7
8	3/28	1300	650	He/0.1% H_2	100	Begin Run 8; flux up 3%
9	3/30	1015	650	100% He	100	Begin Run 9
	4/4	1424	650	100% He	100	Temperature of breeder increased 8 deg
	4/5	0400	30	0.1% H_2	100	ORR shutdown
	4/6	0800	30	0.1% H_2	100	Duration 45 min during shutdown
		0915	150	100% He	100	Orr up to 9 MW and down
10	4/6	1230	400	100% He	100	Begin Run 10
11	4/7	0922	500	100% He	100	Begin Run 11
12	4/8	0915	550	100% He	100	Begin Run 12
	4/11	0900	30	100% He	100	ORR shutdown
		1011	550	100% He	100	Resume Run 12
13	4/12	0920	600	100% He	100	Regin Run 13
	4/13	1345	35	100% He	100	Set back to nL
		1350	600	100% He	100	Resume Run 13
		1408	30	100% He	100	ORR shutdown

TABLE VI-1 (Contd.)

Run No.	1983 Date	Time[a]	Nominal Temp. (°C)	Sweep Gas		Comments[b]
				Composition	Flow Rate (cm^3/min)	
	4/14	1420	35	100% He	100	ORR @ nL
		1440	30	100% He	100	ORR shutdown
		1614	600	100% He	100	Resume Run 13, ORR @ 29 MW
	4/15	0840	600	100% He	100	ORR to 30 MW, readjust temp.
14	4/18	0951	700	100% He	100	Begin Run 14
15	4/20	1400	700	0.1% H_2	100	Begin Run 15
16	4/21	0946	700	0.1% H_2	300	Begin Run 16
17	4/22	1230	700	0.1% H_2	30	Begin Run 17
18	4/25	1300	700	0.1% H_2	100	Begin Run 18
19	4/26	1000	650	0.1% H_2	100	Begin Run 19
	4/27	0400	30	0.1% H_2	100	ORR shutdown
20	4/28	1130	400	100% He	100	
	4/29	0810	400	He/0.2% O_2	100	
		1110	650	He/0.2% O_2	100	Begin Run 20
	5/2	0915	650	100% He	100-200	
21	5/2	1425	650	He/0.1% H_2	100	Begin Run 21
	5/3	0837	650	He/0.1% H_2	100	Temperature adjusted - increased 9 deg
22	5/4	0900	600	He/0.1% H_2	100	Begin Run 22
23	5/5	0900	550	He/0.1% H_2	100	Begin Run 23
	5/6	0001	30	He/0.1% H_2	100	ORR shutdown
	5/6	1400	550	He/0.1% H_2	100	Resume Run 23 @ 28.5 MW
	5/7	1710	300	He/0.1% H_2	100	ORR set back to 15 MW
		1720	550	He/0.1% H_2	100	Resume Run 23 @ 28.5 MW
		1730	300	He/0.1% H_2	100	ORR set back to 15 MW
		1743	550	He/0.1% H_2	100	Resume Run 23 @ 28.5 MW
		2051	550	He/0.1% H_2	100	ORR @ 29 MW
		2106	550	He/0.1% H_2	100	ORR @ 29.5 MW
	5/8	0305	30	He/0.1% H_2	100	ORR shutdown
		0351	550	He/0.1% H_2	100	Resume Run 23 @ 29.5 MW
24	5/9	1100	600	He/0.1% H_2	100	Begin Run 24 @ 29.5 MW
25	5/10	1351	560	He/0.1% H_2	100	Begin Run 25 @ 29.5 MW
	5/11	10:45	35	He/0.1% H_2	100	ORR set back to nL (0.30 MW)
		1129	560	He/0.1% H_2	100	ORR @ 30 MW; resume Run 25
26	5/12	0815	550	He/0.1% H_2	100	Begin Run 26 @ 30 MW
	5/16	0400	30	He/0.1% H_2	100	ORR shutdown
27	5/16	1600	525	He/0.1% H_2	100	Begin Run 27 @ 28 MW
	5/17	1400	525	He/0.1% H_2	100	ORR @ 28.5 MW
28	5/23	1050	500	He/0.1% H_2	100	Begin Run 28 @ 28.5 MW
	5/31	0400	30	He/0.1% H_2	100	ORR shutdown
	6/1	0125	500	He/0.1% H_2	100	ORR up 2 h, then down
29	6/1	1357	480	He/0.1% H_2	300	Begin Run 29 @ 29 MW
30	6/3	1500	480	He/0.1% H_2	100	Begin Run 30 @ 29 MW
31	6/6	0900	500	He/0.1% H_2	100	Begin Run 31 @ 30 MW
32	6/10	0830	650	He/0.1% H_2	100	Begin Run 32
33	6/10	0830	650	He/0.1% H_2	100	Begin Run 33
	6/13	0400	30	He/0.1% H_2	100	ORR shut down; end of experiment

[a]Local time at Oak Ridge, EST or EDT.

[b]Note: nL is the lowest power at which the automatic reactor control system will function - it corresponds to a reactor power of ~0.30 MW. R refers to reactor power.

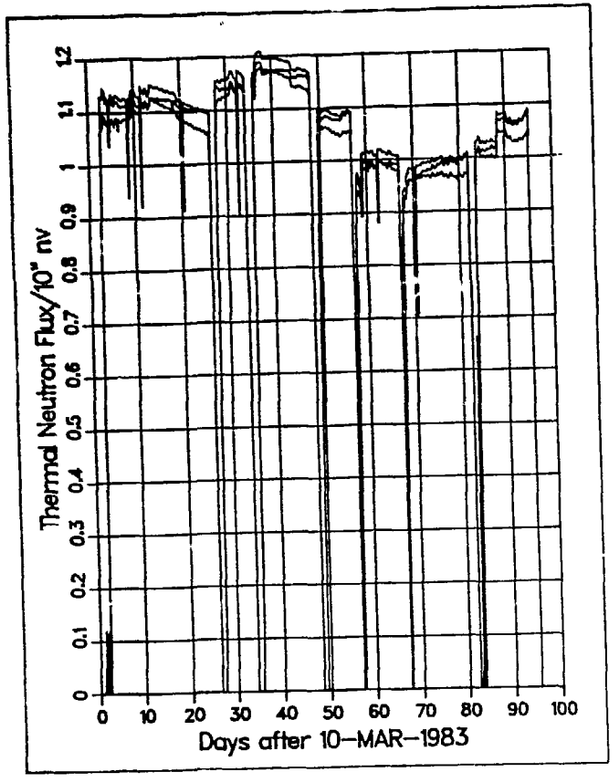

Fig. VI-1. TRIO flux history.

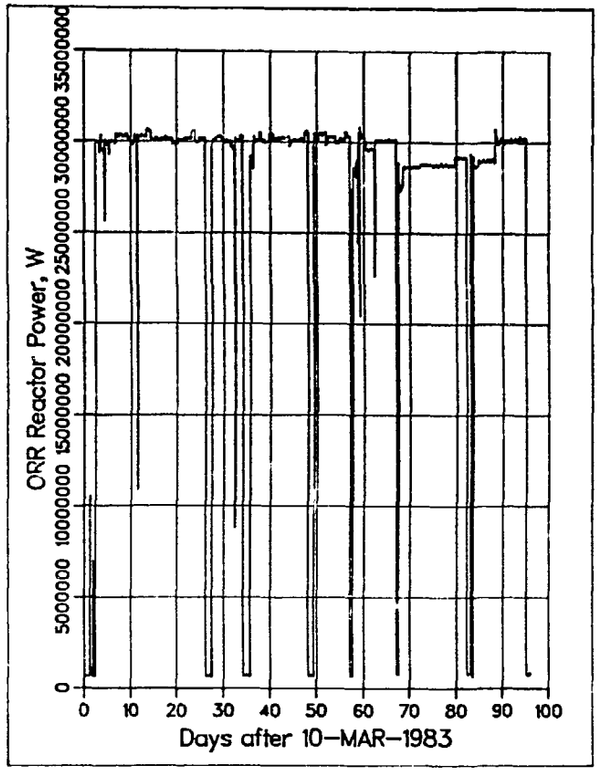

Fig. VI-2. ORR reactor power history.

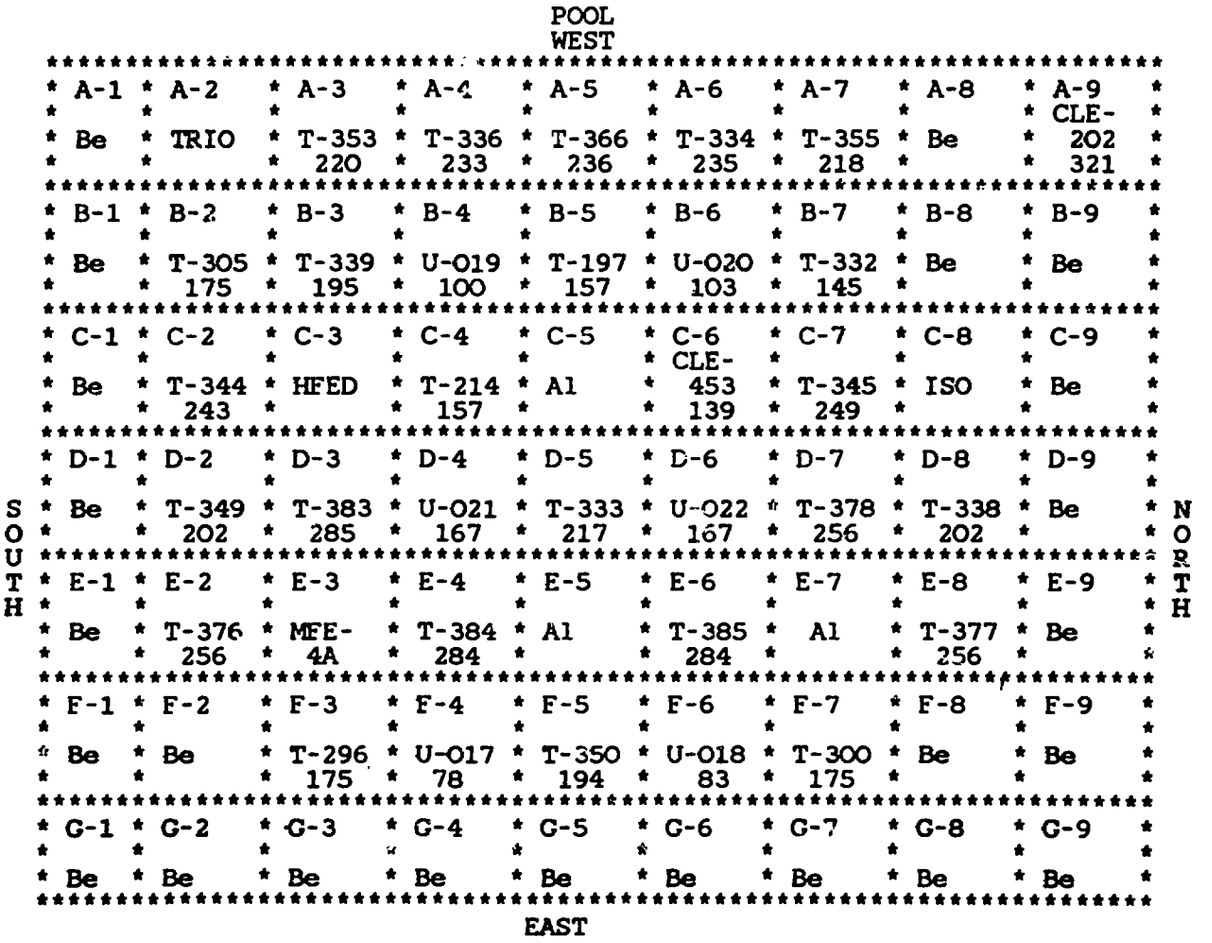

Note: - T-xxx refers to a fuel element

- U-xxx is a control rod.

- Other alphanumeric designations refer to experiments.

Fig. VI-3a. ORR fuel loading diagram: Cycle 164-A. (March 10, 1983 to April 6, 1983).

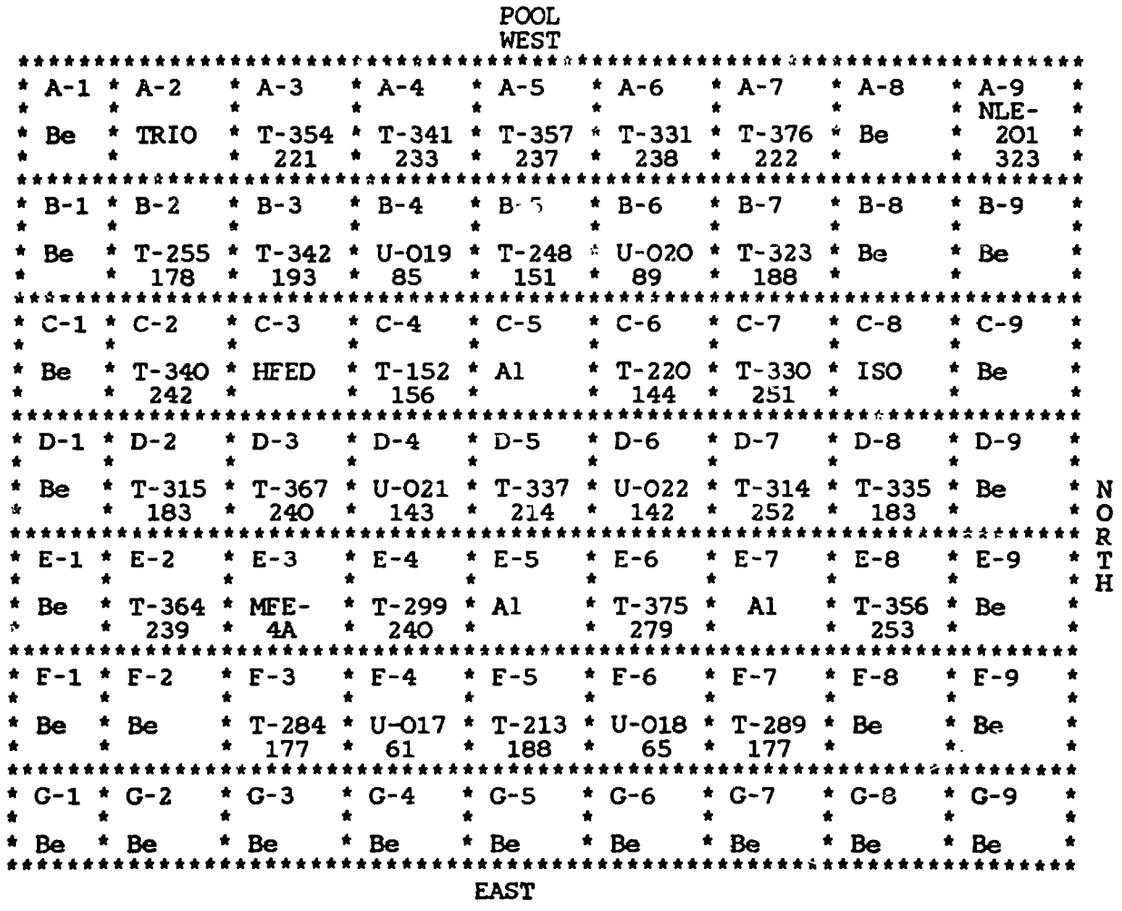

Fig. VI-3b. ORR fuel loading diagram: Cycle 164-B.
(April 6, 1983 to April 13, 1983).

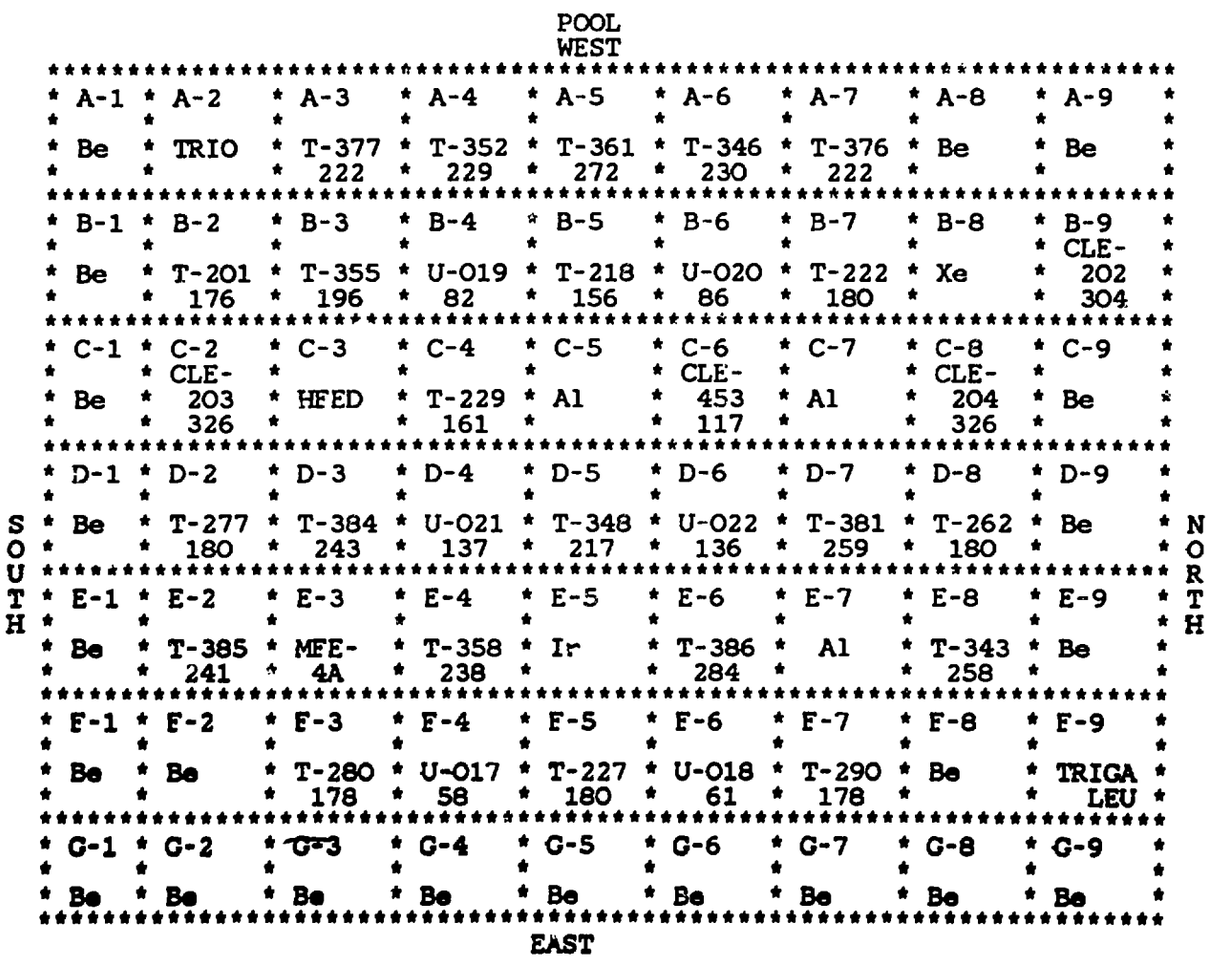

Fig. VI-3c. ORR fuel loading diagram: Cycle 164-C (April 14, 1983 to April 27, 1983).

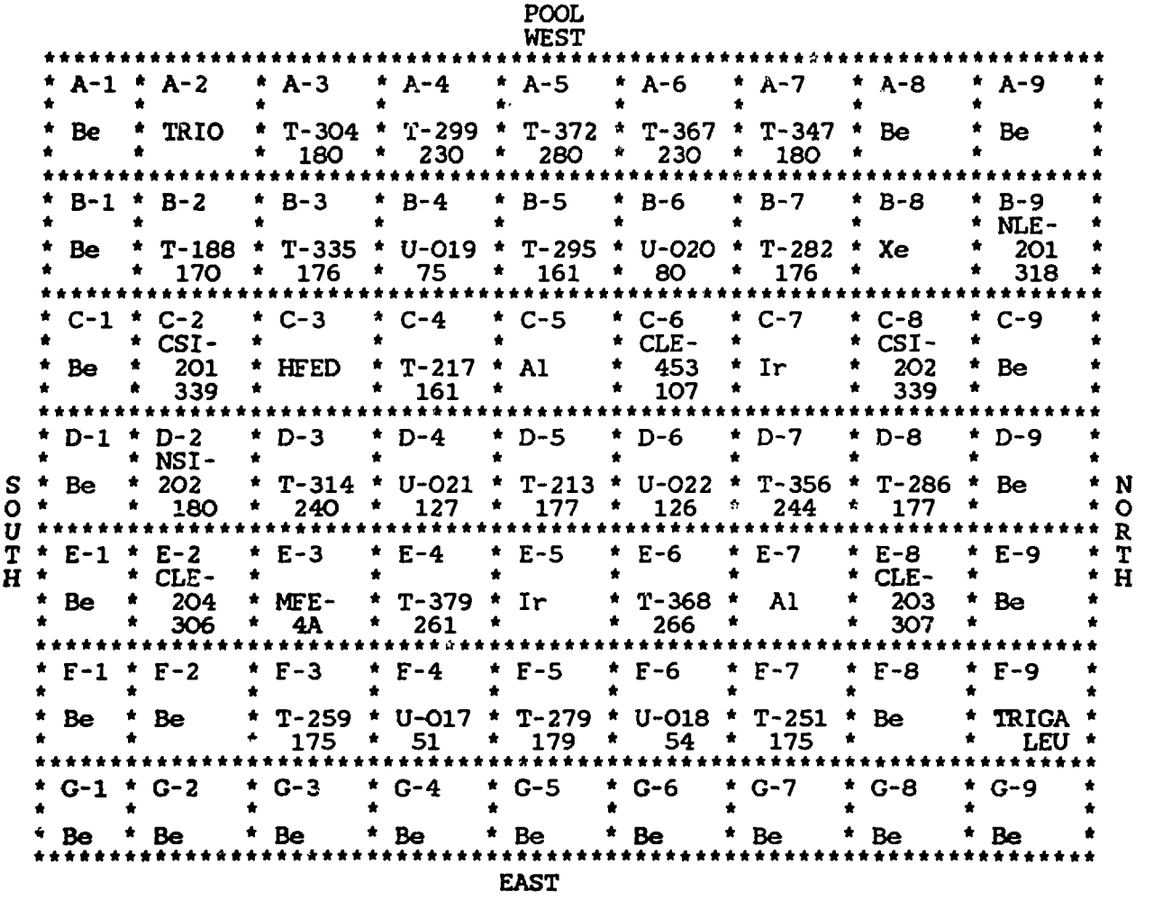

Fig. VI-3d. ORR fuel loading diagram: Cycle 164-D.
(April 28, 1983 to May 6, 1983).

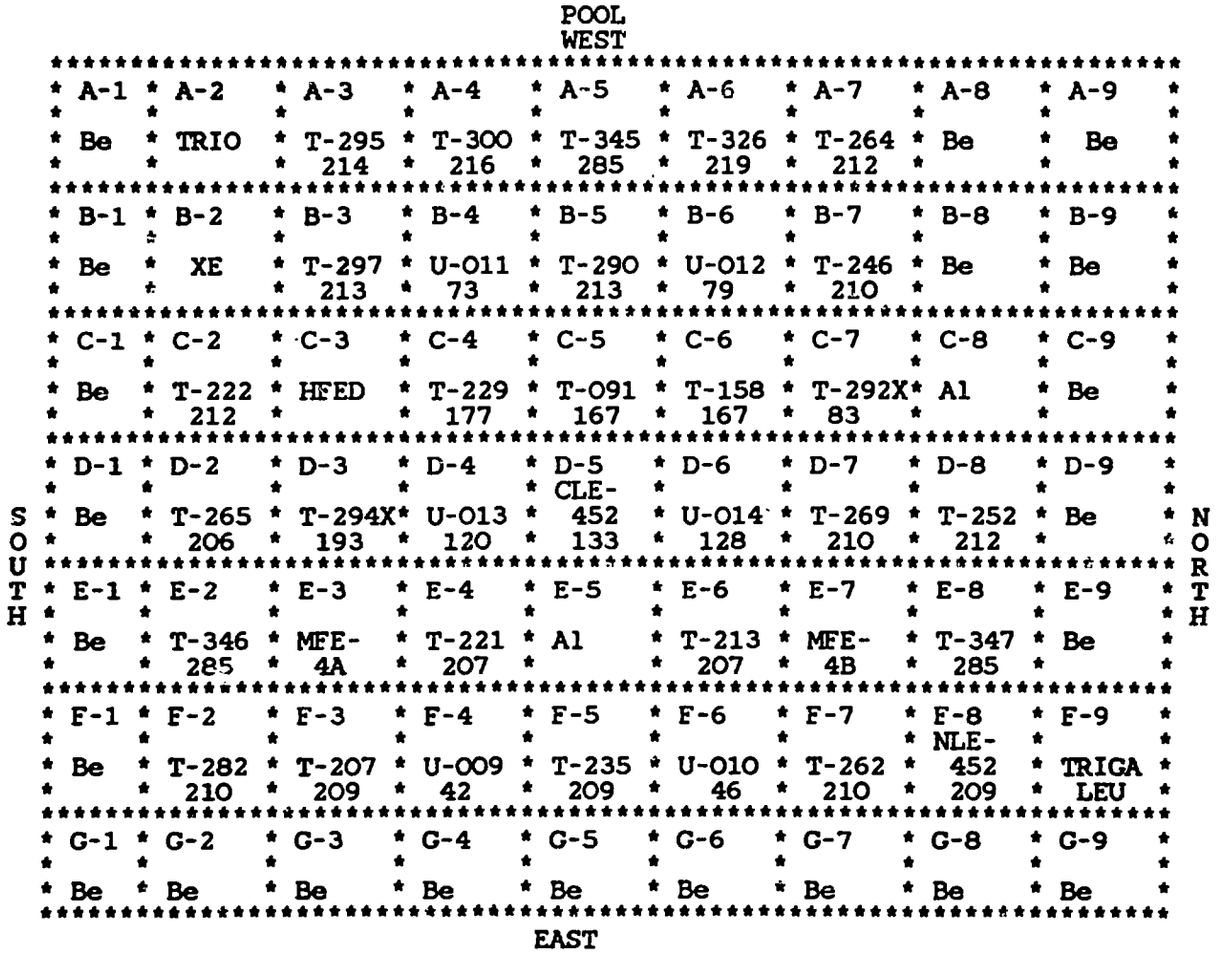

Fig. VI-3e. ORR fuel loading diagram: Cycle 164-E.
(May 6, 1983 to May 16, 1983).

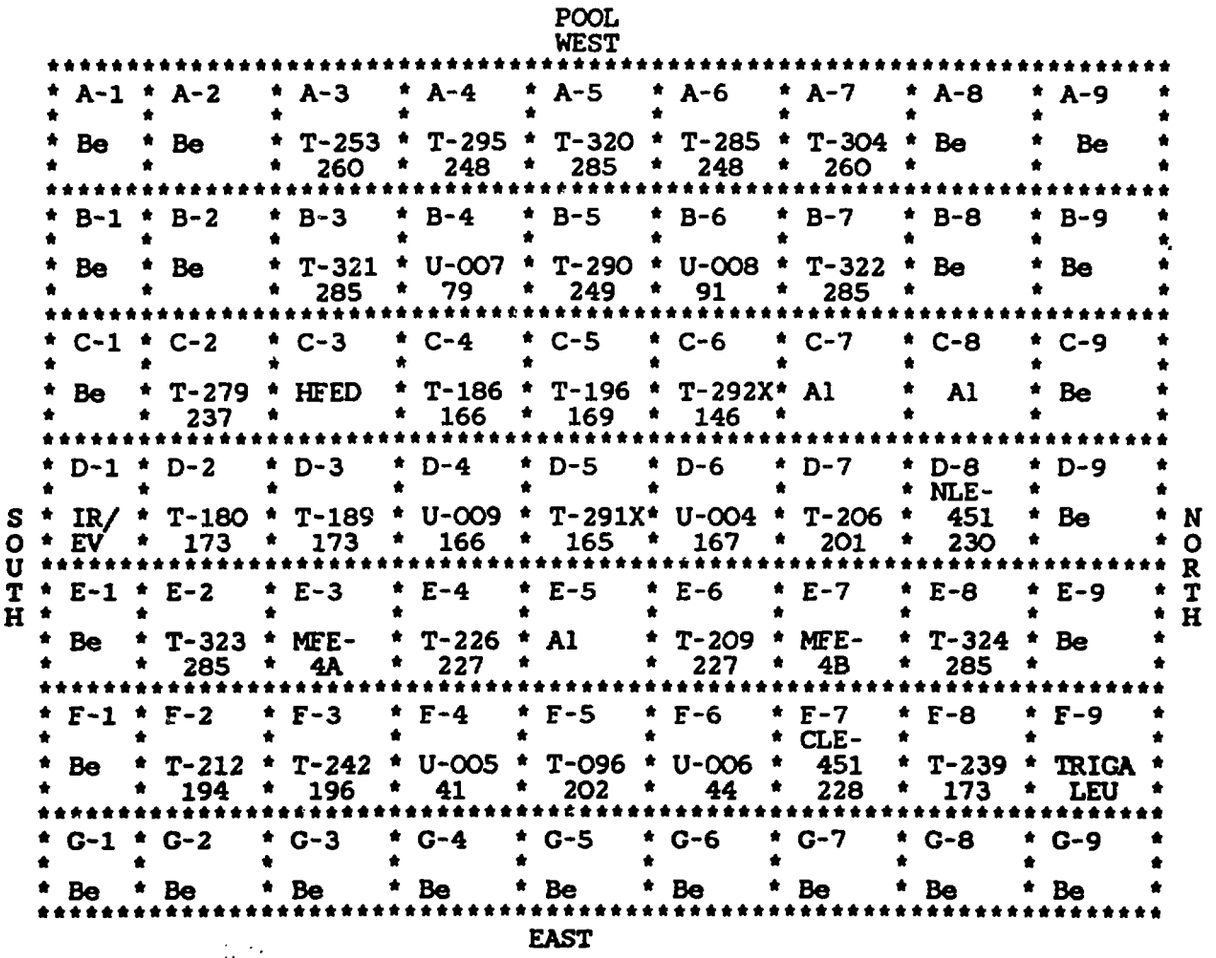

Fig. VI-3f. ORR fuel loading diagram: Cycle 164-F.
(May 16, 1983 to May 31, 1983).

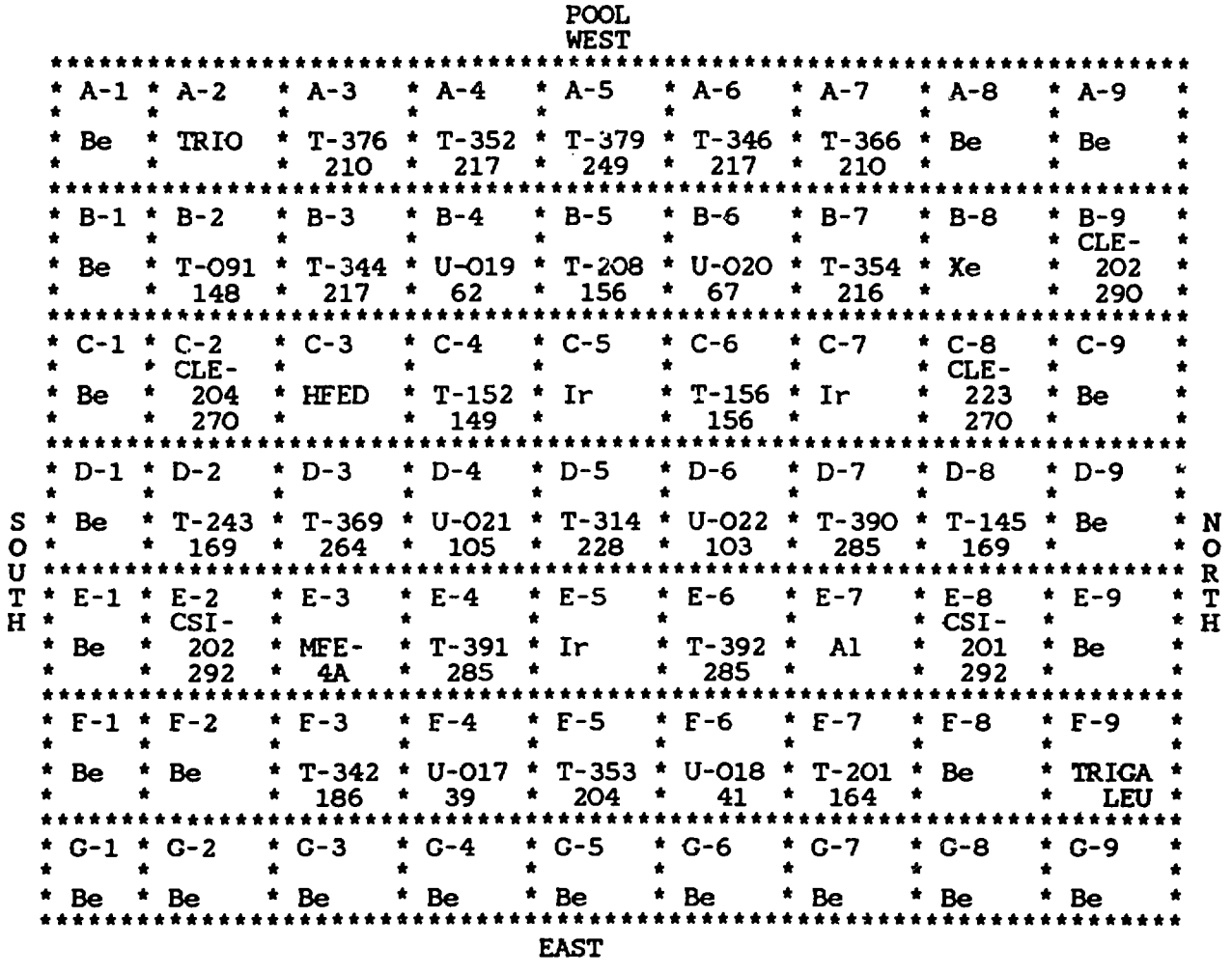

Fig. VI-3g. ORR fuel loading diagram: Cycle 164-G.
(May 31, 1983 to June 13, 1983).

C. Temperature Profiles

The recorded temperatures for the entire experiment are given in Fig. VI-4. The location of the thermocouples is shown in a cross-sectional diagram of the capsule (Fig. VI-5). Besides defining the temperature profiles for the tritium release, a number of observations were made regarding temperature. First, the readings from the thermocouples have a distinct pattern; the highest temperatures are always on the west side and the inside surface. These are from thermocouples T903, T904, T905, and T906. Of these four, T906, the one on the capsule bottom, consistently shows the lowest temperature by about 10°C. The next highest temperature is from T902, located on the east side and the inside surface of the breeder. The four thermocouples on the west outside (T907, T908, TR801, and TR901) read within 20°C of one another. The lowest temperature is always from T902, located on the east outside surface of the breeder. The fact that this pattern remained the same throughout the course of the experiment provides evidence that the heat transfer pathways did not change as a result of effects of temperature and radiation. Therefore, the integrity of the capsule was maintained throughout the experiment. The lower temperature on the east side of the capsule is attributed to asymmetry in the gap, i.e., the gap is smaller on the east side. The temperature profiles for each run are presented later.

D. Sweep Gas Analyses

The total level of contaminants in the supply cylinders was less than 30 vppm. Significant impurities were neon (<20 vppm) and N_2 + CO (<6 ppm). Oxygen was less than 2 vppm, and the gas purifier ensured that levels <1 ppm were maintained. Samples of the effluent sweep gas were taken during the time when no hydrogen was added to the system. The results (shown in Table VI-2) show that no measurable amounts of impurities were added to the sweep gas stream by the capsule. The concentrations of the tritium species noted in the effluent were not high enough to provide truly quantitative data.

E. Tritium Collected

The tritium released to the sweep gas was collected and quantitatively analyzed by liquid scintillation counting. The tritium collected is in three

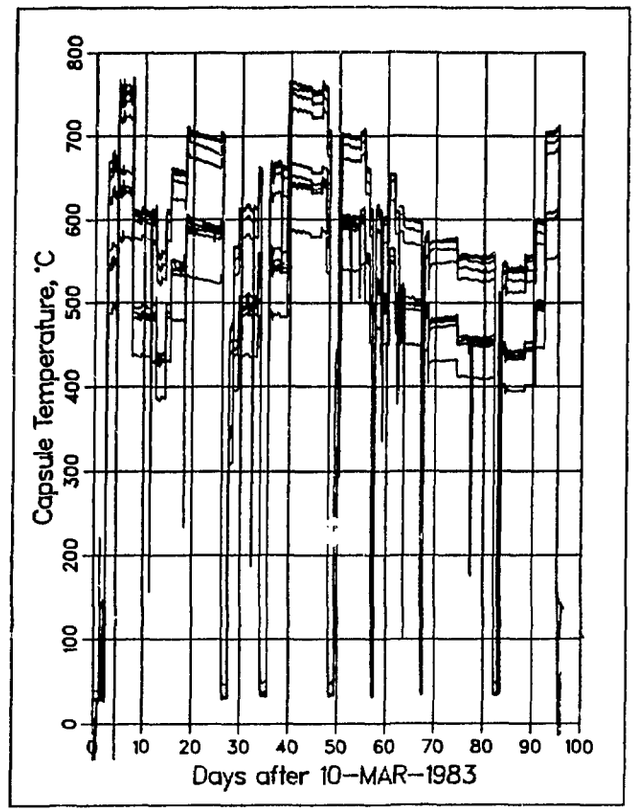

Fig. VI-4. TRIO capsule temperature.

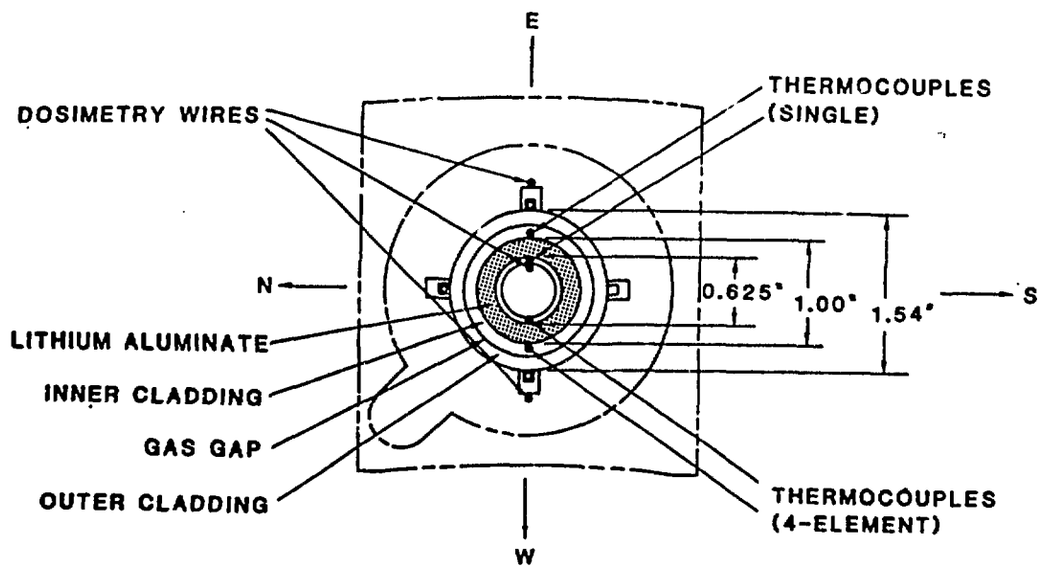

Fig. VI-5. TRIO capsule assembly.

TABLE VI-2

Sweep Gas Analysis

Species	Concentration (%)		
	Supply	Exhaust (1)	Exhaust (2)
H_2	0.0003	0.0003	0.0003
He	99.997	99.998	99.997
CH_4	<0.0002	<0.0002	<0.0002
H_2O	<0.0002	<0.0002	<0.0002
N_2 + CO	0.0005	<0.0005	<0.0005
O_2	<0.0002	<0.0001	0.0001
Ar	0.0001	<0.0001	<0.0001
CO_2	<0.0001	<0.0001	<0.0001
Ne	0.0020	0.0018	0.0020
T_2	-	<0.0001	<0.0001
HT	-	-	<0.0002

forms: (1) tritium as HT or noncondensable form, (2) tritium as HTO or condensable form, and (3) tritium that permeated from the sweep gas through the inner capsule to the gap gas stream. Data for tritium collected in these three forms for the 33 experimental runs are presented below.

1. HT Collected

Tritium in the sweep gas which passed the first set of traps was monitored by the line monitor (KCl), oxidized, and then trapped and analyzed as described in Sec. IV-C. The samples represent noncondensable tritium collected a specified time interval. The data for HT thus collected are given in Table VI-3.

The predominant form of tritium collected was HT, representing more than 95% of all the tritium. The data in Table VI-3 show the amount of HT collected during the amount of 33 experimental runs. In those instances when a sample overlapped two runs, the amount collected was apportioned between the two runs.

TABLE VI-3

Tritium Collected, Noncondensable or HT Form
(November 25, 1983)

Sample I.D.	Time On		Time Off		HT μCi
	Date	Hour	Date	Hour	
5-1	3/10	1530	3/11	0328	0.02×10^6
6-1	3/10	1530	3/11	0328	9.0×10^9
5-2	3/11	0338	3/11	1440	9.29×10^4
6-2	3/11	0338	3/11	1440	9.4×10^7
5-3	3/11	1443	3/11	2243	9.25×10^4
6-3	3/11	1443	3/11	2243	2.1×10^8
Run 0	3/10	1530	3/11	2400	0.0019 Ci HT Start full power test
5-4	3/12	0814	3/12	1201	4.95×10^3
6-4	3/12	0814	3/12	1201	2.0×10^7
	3/12	1201	3/12	1209	2.24×10^3
5-5	3/12	1209	3/12	1420	0.0366
6-5	3/12	1209	3/12	1420	1.8×10^6
	3/12	1420	3/12	1423	7.8×10^4
5-6	3/12	1423	3/12	1601	0.0285
6-6	3/12	1423	3/12	1601	0.6×10^6
	3/12	1601	3/12	1608	2.1×10^3
5-7	3/12	1608	3/12	2219	0.12
6-7	3/12	1608	3/12	2219	1.08×10^6
	3/12	2219	3/12	2227	2.4×10^3
5-8	3/12	2227	3/13	1415	0.307
6-8	3/12	2227	3/12	1415	3.5×10^6
	3/13	1415	3/13	1422	2.1×10^3
5-9	3/13	1422	3/14	1240	0.455
6-9	3/13	1422	3/14	1240	0.0134
	3/14	1240	3/14	1245	3.6×10^3
5-10(1)*	3/14	1245	3/14	1300	0.006
Run 1	3/12	0814	3/14	1300	0.985 Ci HT
5-10	3/14	1300	3/14	1448	0.041
6-10	3/14	1245	3/14	1448	4.5×10^5
	3/14	1448	3/14	1453	3.8×10^3
5-11	3/14	1453	3/15	1731	0.593
6-11	3/14	1453	3/15	1731	7.4×10^3
	3/15	1731	3/15	1736	0.0
5-12	3/15	1736	3/16	1047	0.336
6-12	3/15	1736	3/16	1047	7.4×10^4
	3/16	1047	3/16	1050	1.0×10^3
5-13(2)	3/16	1050	3/16	1124	0.009

TABLE VI-3 (Contd.)

Sample I.D.	Time On		Time Off		HT μCi
	Date	Hour	Date	Hour	
Run 2	3/14	1300	3/16	1124	0.985 Ci HT
5-13	3/16	1124	3/16	1437	0.0504
6-13	3/16	1050	3/16	1437	1.74×10^3
	3/16	1437	3/16	1441	1.2×10^3
5-14	3/16	1441	3/17	1125	0.07245
6-14	3/16	1441	3/17	1125	8.5×10^3
	3/17	1125	3/17	1129	1.2×10^3
5-14	3/16	1441	3/17	1125	0.336[a]
5-15	3/17	1129	3/17	1344	0.0444
6-15	3/17	1129	3/20	1747	6.0×10^4
	3/17	1344	3/17	1347	9.0×10^3
5-16(3)	3/17	1347	3/17	1405	0.005
Run 3	3/16	1124	3/17	1405	0.513 Ci HT
5-16	3/18	1405	3/18	1600	0.0428
	3/18	1600	3/18	1603	0.0009
5-17	3/18	1603	3/19	2132	0.541
	3/19	2132	3/19	2135	0.0009
5-18	3/19	2135	3/20	1747	0.36
	3/20	1747	3/20	1753	0.0018
5-19	3/20	1753	3/21	0815	0.291
6-16	3/20	1753	3/21	0815	0.00381
	3/21	0815	3/21	0820	0.0015
5-20	3/21	0820	3/22	1127	0.47
Run 4	3/18	1405	3/22	1127	2.099 Ci HT
5-20(5)	3/22	1127	3/22	1606	0.081
	3/22	1606	3/22	1611	0.001
5-21	3/22	1611	3/23	0834	0.179
	3/23	0834	3/23	0841	0.0014
5-22	3/23	0841	3/24	1053	0.355
Run 5	3/22	1127	3/24	1052	0.617 Ci HT
	3/24	1053	3/24	1058	0.001
5-23	3/24	1058	3/24	1538	0.18
6-17	3/21	0820	3/28	0855	0.0098
	3/24	1538	3/24	1543	0.0015
5-24	3/24	1543	3/25	1018	0.505
	3/25	1018	3/25	1022	0.0024
5-25(6)	3/25	1022	3/25	1050	0.025

TABLE VI-3 (Contd.)

Sample I.D.	Time On		Time Off		HT μCi
	Date	Hour	Date	Hour	
Run 6	3/24	1053	3/25	1050	0.72 5 Ci HT
5-25	3/25	1050	3/25	1423	0.194
	3/25	1423	3/25	1428	0.004
5-26	3/25	1428	3/27	1751	1.21
	3/27	1751	3/27	1756	0.002
5-27	3/27	1756	3/28	0855	0.321
	3/28	0855	3/28	0858	0.0012
5-28(7)	3/28	0858	3/28	1300	0.079
Run 7	3/25	1050	3/28	1300	1.811 Ci HT
5-28	3/28	1300	3/29	0906	0.539
	3/29	0906	3/29	0907	0.0004
5-29	3/29	0907	3/30	0920	0.452
	3/30	0920	3/30	0925	0.0015
5-30(8)	3/30	0925	3/30	1015	0.015
Run 8	3/28	1300	3/30	1015	1.008
5-30	3/30	1015	4/04	1355	1.525
	4/04	1355	4/04	1402	0.0014
5-31	4/04	1402	4/05	0754	0.285
6-18	3/28	0858	4/04	1355	0.012
Run 9	3/30	1015	4/0	0400	1.823 Ci HT
5-32	4/06	0855	4/07	0811	0.033
	4/07	0811	4/07	0825	0.0014
5-33(10)	4/07	0825	4/07	0922	0.006
Run 10	4/06	0855	4/07	0922	0.0404 Ci HT
5-33	4/07	0922	4/08	0915	0.3
Run 11	4/07	0922	4/08	0915	0.3 Ci HT
5-33(12)	4/08	0915	4/11	1430	0.828 Ci HT
	4/11	1430	4/11	1432	0.0004
5-34	4/11	1432	4/12	0847	0.246
6-19	4/04	1402	4/11	1430	0.0805
6-20	4/11	1432	4/13	0913	0.0807
	4/12	0847	4/12	0903	0.0048
5-35(12)	4/12	0903	4/12	0920	0.005

TABLE VI-3 (Contd.)

Sample I.D.	Time On		Time Off		
	Date	Hour	Date	Hour	HT μCi
Run 12	4/08	0915	4/12	0920	1.245 Ci HT
5-35	4/12	0920	4/13	1109	0.77
	4/13	1109	4/13	1113	0.0012
5-36	4/13	1113	4/15	0908	0.0858
	4/15	0908	4/15	0910	0.0
5-37	4/15	0910	4/18	0913	1.324
5-38(13)	4/18	0913	4/18	0951	0.016
Run 13	4/12	0920	4/18	0951	2.197 Ci HT
6-21	4/18	0913	4/21	0917	0.00687
5-38	4/18	0951	4/19	0853	0.976
	4/19	0853	4/19	0857	0.002
5-39	4/19	0857	4/19	1604	0.177
	4/19	1604	4/19	1607	0.0009
5-40	4/19	1607	4/20	1245	0.366
	4/20	1245	4/20	1248	0.0012
5-41(13)	4/20	1248	4/20	1400	0.03
Run 14	4/18	0951	4/20	1400	1.560 Ci HT
5-41	4/20	1400	4/21	0917	0.705
	4/21	0917	4/21	0921	0.002
5-42(14)	4/21	0921	4/21	0946	0.008
Run 15	4/20	1400	4/21	0946	0.715 Ci HT
5-42	4/21	0946	4/22	0852	0.434
6-22	4/21	0921	5/02	0856	0.0203
	4/22	0852	4/22	0856	0.001
5-43(16)	4/22	0856	4/22	1230	0.048
Run 16	4/21	0946	4/22	1230	0.503 Ci HT
5-43	4/22	1230	4/22	1543	0.0434
	4/22	1543	4/22	1546	0.0006
5-44	4/22	1546	4/25	1300	1.065
Run 17	4/22	1230	4/25	1300	1.109 Ci HT
5-44(18)	4/25[b]	1300	4/25	1319	0.005
	4/25	1319	4/25	1322	0.0005
5-45	4/25	1322	4/26	1000	0.374
Run 18	4/25	1300	4/26	1000	0.380 Ci HT
5-45(19)	4/26	1000	4/26	1047	0.015
	4/26	1047	4/26	1052	0.0012
5-46	4/26	1052	4/27	0920	0.277
	4/27	0920	4/27	0923	0.0006

TABLE VI-3 (Contd.)

Sample I.D.	Time On		Time Off		HT μCi
	Date	Hour	Date	Hour	
Run 19	4/26	1000	4/27	0923	0.294 Ci HT
5-47	4/27	0923	5/02	0856	0.0278
	5/02	0856	5/02	0902	0.0
Run 20	4/29	1110	5/02	0915	0.0278 Ci HT
5-48	5/02	0902	5/03	0915	0.671
6-23	5/02	0902	5/06	0810	0.00311
	5/03	0915	5/03	0920	0.002
5-49	5/03	0920	5/04	0835	0.385
	5/04	0835	5/04	0840	0.0063
5-50(21)	5/04	0840	5/04	0900	0.025
Run 21	5/02	1425	5/04	0900	1.092 Ci HT
5-50	5/04	0900	5/05	0830	0.347
	5/05	0830	5/05	0837	0.0014
-51(22)	5/05	0837	5/05	0900	0.003
Run 22	5/04	0900	5/05	0900	0.351 Ci HT
5-51	5/05	0900	5/06	0840	0.191
	5/06	0840	5/06	0850	0.0
5-52	5/06	1440	5/09	0858	0.855
6-24	5/06	0850	5/09	0858	0.00712
	5/09	0858	5/09	0903	0.001
5-53(23)	5/09	0903	5/09	1100	0.023
Run 23	5/05	0900	5/09	1100	1.077 Ci HT
5-53	5/09	1100	5/10	0920	0.476
6-25	5/09	0903	5/19	0816	0.0308
	5/10	0920	5/10	0926	0.0018
5-54(24)	5/10	0926	5/10	1351	0.067
Run 24	5/09	1100	5/10	1351	0.576 Ci HT
5-54	5/10	1351	5/11	0835	0.218
	5/11	0835	5/11	0840	0.001
5-55	5/11	0840	5/12	0815	0.319
Run 25	5/10	1351	5/12	0815	0.537 Ci HT
5-55(26)	5/12	0815	5/12	0829	0.003
	5/12	0829	5/12	0833	0.0008
5-56	5/12	0833	5/13	0815	0.294
	5/13	0815	5/13	0819	0.0008
5-57	5/13	0819	5/16	0944	0.914
	5/16	0944	5/16	0948	0.0008

TABLE VI-3 (Contd.)

Sample I.D.	Time On		Time Off		HT μCi
	Date	Hour	Date	Hour	
Run 26	5/12	0815	5/16	0948	1.213 Ci HT
5-58	5/16	0948	5/17	1102	0.416
	5/17	1102	5/17	1109	0.0014
5-59	5/17	1109	5/18	0903	0.243
	5/18	0903	5/18	0909	0.0012
5-60	5/18	0909	5/19	0816	0.263
	5/19	0816	5/19	0822	0.0012
5-61	5/19	0822	5/20	0911	0.338
	5/20	0911	5/20	0915	0.0017
5-62	5/20	0915	5/23	1008	0.687
5-62	5/20	0915	5/23	1008	0.16[c]
5-63(27)	5/23	1008	5/23	1050	0.01
Run 27	5/16	0948	5/23	1050	2.128 Ci HT
5-63	5/23	1050	5/24	0844	0.206
	5/24	0844	5/24	0848	0.0007
5-64	5/24	0848	5/25	1259	0.298
	5/25	1259	5/25	1303	0.0005
6-26	5/19	0822	5/31	0846	0.0257
5-65	5/25	1303	5/26	0954	0.245
	5/26	0954	5/26	0958	0.0008
5-66	5/26	0958	5/27	0812	0.247
	5/27	0812	5/27	0816	0.0008
5-67	5/27	0816	5/31	0846	1.08
Run 28	5/23	1050	5/31	0400	2.1045 Ci HT
5-68	5/31	0859	6/02	1004	0.242
	6/02	1004	6/02	1008	0.0008
5-69	6/02	1008	6/03	0802	0.209
	6/03	0802	6/03	0806	0.0008
6-27	5/31	0859	6/03	0802	0.0191
5-70	6/03	0806	6/03	1508	0.0714
Run 29	6/01	1357	6/03	1500	0.543 Ci HT
	6/03	1508	6/03	1512	0.0008
5-71	6/03	1512	6/04	1229	0.213
	6/04	1229	6/04	1232	0.0005
5-72	6/04	1232	6/05	1621	0.305
	6/05	1621	6/05	1624	0.0005
6-28	6/03	0806	6/13	0845	0.0157
5-73	6/05	1624	6/06	0831	0.179
3	6/06	0832	6/06	0835	0.0006
-74(30)	6/06	0835	6/06	0900	0.006

TABLE VI-3 (Contd.)

Sample I.D.	Time On		Time Off		HT μCi
	Date	Hour	Date	Hour	
Run 30	6/03	1500	6/06	0900	0.721 Ci HT
5-74	6/06	0900	6/07	0836	0.345
4	6/07	0836	6/07	0840	0.0008
5-75	6/07	0840	6/08	0846	0.342
4	6/08	0846	6/08	0850	0.0008
5-76	6/08	0850	6/08	1228	0.049
4	6/08	1228	6/08	1232	0.0008
-77(31)	6/08	1232	6/08	1240	0.002
Run 31	6/06	0900	6/08	1240	0.74 Ci HT
5-77	6/08	1240	6/09	0831	0.767
4	6/09	0831	6/09	0835	0.0008
5-78	6/09	0835	6/10	0808	0.498
	6/10	0808	6/10	0812	0.0008
5-79	6/10	0812	6/10	0830	0.004
Run 32	6/08	1240	6/10	0830	1.271 Ci HT
5-79	6/10	0830	6/11	0725	0.987
	6/11	0725	6/11	0728	0.0006
5-80	6/11	0728	6/13	0819	0.675
5-81	6/13	0819	6/13	0845	3.85×10^3
Run 33	6/10	0830	6/13	0845	1.666 Ci HT

*Note: Parentheses refer to run proapportioned samples which overlapped two runs.

[a]Calculated loss, copper oxide bed of fluorine.

[b]Time changed to Eastern Daylight Time.

[c]Leak into glovebox, calculated to g.

The data show tritium collected in the first and the second HT trap (Nos. 5 and 6). The sample identification numbers indicate which trap was used. The blanks represent HT which was calculated to pass during the short time intervals when the traps were not on-line. The absolute accuracy of a single determination is 5%. The tritium collected in the second trap (No. 6) is consistently less than 1% of the tritium collected in the first trap. The exhaust monitor recorded tritium levels less than one per cent of the levels of the line monitor. Thus, a single trap removes about 99% of the tritium.

2. Tritium Collected as HTO

The HTO was scrubbed from the sweep gas stream as previously described (Sec. IV.C). The HTO data are presented in Table VI-4. The first trap is either No. 1 or 3 and the second trap is either No. 2 or 4. Designations A, B, C, etc., as the last character of the sample identification number refer to 2 μL, samples taken from the ethylene glycol during operation by means of inserting a calibrated syringe through a septum. These samples were then added directly to the scintillator solution without dilution. The designations D as the first character of the sample identification number refers to HTO collected over intervals between different syringe samples. The absolute accuracy for the syringe samples is estimated to be 10%. The absolute accuracy of the regular samples is again 5%. The amounts of HTO were much less (generally by a factor of 100 to 1000) than those of HT.

3. Tritium Permeation

The tritium which permeated through the wall of the inner capsule into the gap gas was collected by passing the gap gas through an oxidizer and then trapping the tritium on Type 4A molecular sieves. The molecular sieves were removed at times when the ORR was down and analyzed for tritium by refluxing in water for not less than four hours and then analyzing an aliquot by liquid scintillation. Seven such samples were collected and analyzed. Each sample thus represents several runs. For each sample, the amounts were apportioned to each run using the temperature, the amount of HT released (Table VI-2) and the duration of each run by a method described below. Temperatures used were the average of the recorded thermocouple readings on the two sides (east and west) of the capsule for the thermocouple elements in contact with the inner cladding. The permeation data are given in Table VI-5.

TABLE VI-4

Tritium Collected, Condensable, or HTO FORM
(January 26, 1983)

Sample I.D.	Time On		Time Off		HTO, μCi
	Date	Hour	Date	Hour	
1-1	3/11	0340	3/11	0540	56.9
2-1	3/11	0340	3/11	0540	0.28
1-2	3/11	1443	3	2230	2.4
2-2	3/11	1443	3	2230	0.0
Run 0	3/11	0340	3/11	2230	59.6
1-3	3/12	0812	3/12	1033	153.0
2-3	3/12	0812	3/12	1033	0.77
	3/12	1033	3/12	1043	500.0
1-4	3/12	1043	3/12	1243	6218.0
2-4	3/12	1043	3/12	1243	4.7
	3/12	1243	3/12	1255	121.0
1-5	3/12	1255	3/12	1411	849.0
2-5	3/12	1255	3/12	1411	1.7
	3/12	1411	3/12	1413	60.0
1-6	3/12	1413	3/12	1531	3718.0
2-6	3/12	1413	3/12	1531	0.91
	3/12	1531	3/12	1544	260.0
1-7	3/12	1544	3/12	1714	1218.0
2-7	3/12	1544	3/12	1714	0.73
	3/12	1714	3/12	1725	110.0
3-1	3/12	1725	3/12	2211	2910.0[a]
1-8	3/12	2216	3/13	0458	4045.0
2-8	3/12	2216	3/13	0458	0.0
3-2	3/13	0458	3/13	1407	5490.0[a]
Run 1	3/12	0812	3/13	1407	2.566×10^4
1-9	3/13	1407	3/14	1313	3490.0
2-9	3/13	1407	3/14	1313	0.4
3-3	3/14	1313	3/14	1439	172.0[a]
1-10	3/14	1439	3/14	1548	133.0
2-10	3/14	1439	3/14	1548	0.043
3-4	3/14	1548	3/14	1745	234.0[a]
1-11A	3/14	1745	3/14	2304	565.0
2-11A	3/14	1745	3/14	2304	0.0
3-5/6	3/14	2304	3/16	1410	4000.0
Run 2	3/13	1407	3/16	1410	8.594×10^3
3-7	3/16	1410	3/17	0850	11200.0
1-11B	3/17	0857	3/17	1344	259.0
	3/17	1344	3/17	1359	10.0

TABLE VI-4 (Contd.)

Sample I.D.	Time On		Time Off		HTO, μCi
	Date	Hour	Date	Hour	
Run 3	3/16	1410	3/17	1359	1.147×10^4
1-12A	3/17	1359	3/18	0827	747.0
3-8/11	3/18	0827	3/21	0943	4243.0
1-13A	3/21	0943	3/22	1008	768.0
	3/22	1008	3/22	1012	2.0
Run 4	3/17	1359	3/22	1012	5.76×10^3
2-11B	3/17	0950	3/24	1104	9.4
1-12BA	3/22	1012	3/22	1445	(109.0)[b]
1-12BB	3/22	1012	3/23	0851	(683.0)
1-12B	3/22	1012	3/24	1104	1383.0[c]
D1-12BB	3/22	1445	3/23	0851	(574.0)
D-112B	3/23	0851	3/24	1104	(500.0)
	3/24	1104	3/24	1110	3.0
Run 5	3/17	0950	3/24	1110	1.395×10^3
1-13BA	3/24	1110	3/24	1355	(62.0)
1-13BB	3/24	1110	3/24	1546	(172.0)
1-13BC	3/24	1110	3/25	1025	(718.0)
Run 6	3/24	1110	3/25	1025	7.18×10^2
1-13BD	3/24	1110	3/25	1428	(906.0)
1-13BE	3/24	1110	3/27	1748	(1910.0)
1-13BF	3/24	1110	3/28	0906	(2320.0)
1-13BG	3/24	1110	3/25	1200	(2110.0)
1-13B	3/24	1110	3/25	1200	2420.0
D1-13BB	3/24	1355	3/24	1546	(110.0)
D1-13BC	3/24	1546	3/25	1025	(546.0)
D1-13BD	3/25	1025	3/25	1428	(188.0)
D1-13BE	3/25	1428	3/27	1748	(1004.0)
D1-13BF	3/27	1748	3/28	0906	(410.0)
D1-13BC	3/28	0906	3/28	1200	(-210.0)
D1-13B	3/28	0906	3/28	1200	(100.0)
2-12	3/24	1110	4/05	0759	5.2
	3/28	1200	3/28	1205	2.0
Run 7	3/25	1025	3/28	1205	1.71×10^3
1-14A	3/28	1205	3/28	1537	(169.0)
1-14B	3/28	1205	3/29	0901	(604.0)
1-14C	3/28	1205	3/30	0915	(1350.0)
1-14D	3/28	1205	3/30	1100	(1400.0)

TABLE VI-4 (Contd.)

Sample I.D.	Time On		Time Off		HTO, μCi
	Date	Hour	Date	Hour	
Run 8	3/28	1205	3/30	1100	1.40×10^3
1-14E	3/28	1205	3/30	1300	(1460.0)
1-14F	3/28	1205	3/30	1500	(1500.0)
1-14G	3/28	1205	3/30	1624	(1430.0)
1-14H	3/28	1205	3/31	0918	(1600.0)
1-14F	3/28	1205	4/04	1353	(2466.0)
1-14	3/28	1205	4/05	0754	2950.0
D1-14B	3/28	1537	3/29	0901	(435.0)
D1-14C	3/29	0901	3/30	0915	(746.0)
D1-14D	3/30	0915	3/30	1100	(50.0)
D1-14E	3/30	1100	3/30	1300	(60.0)
D1-14F	3/30	1300	3/30	1500	(40.0)
D1-14G	3/30	1500	3/30	1624	(-70.0)
D1-14H	3/30	1624	3/31	0918	(170.0)
D1-14I	3/31	0918	4/04	1353	(866.0)
D1-14	4/04	1353	4/05	0754	(481.0)
Run 9	3/30	1100	4/05	0754	1.55×10^3
	4/05	0754	4/06	0842	0.0
1-15A	4/06	0842	4/07	0825	(90.8)
Run 10	4/05	0754	4/07	0825	91.0
1-15B	4/06	0842	4/07	1558	(1360.0)
1-15C	4/06	0842	4/08	0824	(2445.0)[c]
1-15D	4/06	0842	4/08	1530	(2511.0)
Run 11	4/07	0825	4/08	1530	2.51×10^3
1-15	4/06	0842	4/11	1415	2988.0
2-13	4/06	0842	4/11	1415	15.0
D1-15B	4/07	0829	4/07	1558	(1269.1)
D1-15C	4/07	1558	4/08	0824	(1085.0)
D1-15D	4/08	0824	4/08	1530	(66.0)
D1-15	4/08	1530	4/11	1415	(477.0)
	4/11	1415	4/11	1420	2.0
1-16A	4/11	1420	4/12	0829	(67.2)
Run 12	4/08	1530	4/12	0829	494.0
1-16B	4/11	1420	4/12	1315	(74.3)
1-16C	4/11	1420	4/12	1700	(714.0)
1-16D	4/11	1420	4/13	1514	(1168.0)
1-16	4/11	1420	4/14	1445	881.0
2-14	4/11	1420	4/10	0859	8.21
D1-16B	4/12	0829	4/12	1315	(7.1)
D1-16C	4/12	1315	4/12	1700	(639.7)
D1-16D	4/12	1700	4/13	1514	(454.0)

TABLE VI-4 (Contd.)

Sample I.D.	Time On		Time Off		HTO, μCi
	Date	Hour	Date	Hour	
Run 12 (Contd.)					
D1-16	4/13	1514	4/14	1445	(-287.0)
	4/14	1445	4/14	1444	0.0
1-17A	4/14	1444	4/15	0904	(370.0)
1-17	4/14	1444	4/18	0859	108.0
	4/18	0859	4/18	0903	1.2
Run 13	4/12	0829	4/18	0903	496.0
1-18A	4/18	0903	4/18	1513	(36.9)
1-18B	4/18	0903	4/19	0850	(667.0)
1-18C	4/18	0903	4/19	1602	(678.0)
1-18D	4/18	0903	4/20	0907	(681.0)
1-18	4/18	0903	4/20	1239	670.0
Run 14	4/18	0930	4/20	1239	670.0
2-15	4/18	0903	5/02	0830	84.8
D1-18B	4/19	1513	4/19	0850	(630.1)
D1-18C	4/19	0850	4/19	1602	(11.0)
D1-18D	4/19	1602	4/20	0907	(3.0)
D1-18	4/20	0907	4/20	1239	(-11.0)
	4/20	1239	4/20	1242	0.9
Run 15	4/20	1239	4/20	1242	86.0
1-19A	4/20	1242	4/20	1559	(59.3)
1-19B	4/20	1242	4/21	0914	(36.6)
1-19C	4/20	1242	4/21	1551	(320.0)
1-19D	4/20	1242	4/22	0905	(418.0)
1-19	4/20	1242	4/22	1527	508.0
D1-19B	4/20	1559	4/20	0914	(-22.7)
D1-19C	4/21	0914	4/21	1551	(283.4)
D1-19D	4/21	1551	4/22	0905	(98.0)
D1-19	4/22	0905	4/22	1527	(90.0)
Run 16	4/20	1242	4/22	1527	508.0
	4/22	1527	4/22	1532	2.0
1-20	4/22	1532	4/25	1249	267.3
	4/25	1249	4/25	1253	1.6
Run 17	4/22	1527	4/25	1253	271.0
1-21A	4/25	1233	4/26	0942	(18.5)
1-21B	4/25	1233	4/26	1559	(16.6)
1-21C	4/25	1233	4/27	0906	(15.6)
1-21D	4/25	1233	4/29	0856	(32.0)
1-21	4/25	1233	4/29	1014	32.8

TABLE VI-4 (Contd.)

Sample I.D.	Time On		Time Off		HTO, μCi
	Date	Hour	Date	Hour	
Runs 18,19	4/25	1233	4/29	1014	32.8
	4/29	1014	4/29	1018	0.2
1-22	4/29	1018	5/02	0830	33.4
	5/02	0830	5/02	0846	1.6
1-23	5/02	0846	5/06	0827	69.4
2-16	5/02	0846	5/06	0827	27.6
Runs 20-22	4/29	1014	5/06	0827	132.0
	5/06	0827	5/06	1300	0.00
1-24A	5/06	1300	5/06	1318	(36.6)
1-24B	5/06	1300	5/06	1620	(46.1)
1-24C	5/06	1300	5/07	1152	(172.0)
1-24D	5/06	1300	5/09	0855	(1230.0)
1-24E	5/06	1300	5/09	1156	(1370.0)
Run 23	5/06	0827	5/09	1156	1.37×10^3
1-24F	5/06	1300	5/09	1555	(1540.0)
1-24G	5/06	1300	5/10	0919	(2600.0)
1-24	5/06	1300	5/10	1251	3290.0
2-17A	5/06	1300	5/06	1322	(7.88)
2-17B	5/06	1300	5/06	1618	(7.07)
2-17C	5/06	1300	5/07	1149	(16.7)
2-17D	5/06	1300	5/09	0853	(17.6)
2-17E	5/06	1300	5/09	1153	(25.8)
2-17F	5/06	1300	5/09	1553	(22.8)
2-17G	5/06	1300	5/10	0916	(22.0)
2-17	5/06	1300	5/10	1251	17.2
D1-24B	5/06	1318	5/06	1620	(9.5)
D1-24C	5/06	1620	5/07	1152	(125.9)
D1-24D	5/07	1152	5/09	0855	(1058.0)
D1-24E	5/09	0855	5/09	1156	(140.0)
D1-24F	5/09	1156	5/09	1555	(170.0)
D1-24G	5/09	1555	5/10	0919	(1060.0)
D1-24	5/10	0919	5/10	1251	(690.0)
	5/10	1251	5/10	1257	10.0
Run 24	5/06	1300	5/10	1257	1.947×10^3
1-25A	5/10	1257	5/10	1553	(263.0)
1-25B	5/10	1257	5/11	0830	(2160.0)
1-25C	5/10	1257	5/11	1546	(3890.0)
1-25D	5/10	1257	5/12	0827	(6950.0)

TABLE VI-4 (Contd.)

Sample I.D.	Time On		Time Off		HTO, μCi
	Date	Hour	Date	Hour	
Run 25	5/10	1257	5/12	0827	6.95×10^3
1-25E	5/10	1257	5/12	1555	(8660.0)
1-25	5/10	1257	5/13	0809	13500.0
D1-25B	5/10	1553	5/11	0830	(1897.0)
D1-25D	5/11	1546	5/12	0827	(3060.0)
D1-25E	5/12	0827	5/12	1555	(1710.0)
D1-25	5/12	1555	5/13	0809	(4840.0)
	5/13	0809	5/13	0814	50.0
1-26A	5/13	0814	5/13	1603	(2710.0)
1-26B	5/13	0814	5/16	0934	(70500.0)
1-26	5/13	0814	5/16	0937	41100.0
	5/16	0937	5/16	0942	50.0
Run 26	5/12	0827	5/16	0942	4.775×10^4
1-27A	5/16	0942	5/16	1320	(3310.0)
1-27B	5/16	0942	5/16	1607	(9243.0)
1-27C	5/16	0942	5/17	1051	(52125.0)
1-27	5/16	0942	5/17	1546	4.00×10^4
D1-27B	5/16	1320	5/16	1607	(5933.0)
D1-27C	5/16	1607	5/17	1051	(42882.0)
D1-27	5/17	1051	5/17	1516	(-1.21×10^4)
D'1-27C	5/16	1320	5/17	1051	(48815.0)
D'1-27	5/16	1607	5/17	1546	(30757.0)
D"1-27	5/16	1320	5/17	1546	(36690.0)
	5/17	1546	5/17	1553	210.0
1-28					
1-29A	5/17	1553	5/18	0853	(2.32×10^4)
1-29B	5/17	1553	5/18	1518	(3.25×10^4)
1-29C	5/17	1553	5/19	0830	(6.40×10^4)
1-29D	5/17	1553	5/19	1738	(7.71×10^4)
1-29E	5/17	1553	5/20	0907	(1.09×10^5)
1-29F	5/17	1553	5/20	1315	(1.29×10^5)
1-29	5/17	1553	5/20	1525	1.14×10^5
D1-29B	5/18	0858	5/18	1518	(8.70×10^3)
D1-29C	5/18	1518	5/19	0830	(3.15×10^4)
D1-29D	5/19	0830	5/19	1738	(1.31×10^4)
D1-29E	5/19	1738	5/20	0907	(3.19×10^4)
D1-29F	5/20	0907	5/20	1315	(2.00×10^4)
D1-29	5/20	1315	5/20	1525	(-0.15×10^5)
D'1-29	5/20	0907	5/20	1525	(0.50×10^4)
1-30	5/20	1525	5/23	1002	1.79×10^5
	5/23	1002	5/23	1007	200.0

TABLE VI-4 (Contd.)

Sample I.D.	Time On		Time Off		HTO, μCi
	Date	Hour	Date	Hour	
Run 27	5/16	0942	5/23	1007	3.334×10^5
1-31A	5/23	1007	5/23	1210	(5.80×10^3)
1-31B	5/23	1007	5/23	1455	(1.15×10^4)
1-31C	5/23	1007	5/23	1616	(1.55×10^4)
1-31D	5/23	1007	5/24	0943	(6.98×10^4)
1-31	5/23	1007	5/24	1339	9.49×10^4
D1-31B	5/23	1210	5/23	1455	(5.70×10^3)
D1-31C	5/23	1455	5/23	1616	(4.00×10^3)
D1-31D	5/23	1616	5/24	0943	(5.43×10^4)
D1-31	5/23	0943	5/24	1339	(3.51×10^4)
	5/24	1339	5/24	1344	350.0
1-32A	5/24	1344	5/25	1256	(1.04×10^5)
1-32B	5/24	1344	5/26	0951	(1.85×10^5)
1-32	5/24	1344	5/27	0807	2.64×10^5
D1-32B	5/25	1256	5/26	0951	(0.81×10^5)
D1-32	5/26	0951	5/27	0807	(0.79×10^5)
	5/27	0807	5.27	0811	300.0
1-33A	5/27	0811	5/30	1616	(3.60×10^5)
1-33	5/27	0811	5/31	0826	4.29×10^5
D1-33	5/30	1616	5/31	0826	(0.69×10^5)
2-18	5/10	1257	5/31	0826	64.9
	5/31	0826	5/31	0840	0.00
1-34	5/31	0840	5/31	1639	6.71×10^4
2-19	5/31	0840	5/31	1639	55.9
	5/31	1639	5/31	1645	840.0
Run 28	5/23	1007	5/31	1645	8.57×10^5
1-35A	5/31	1645	6/01	0843	(1.45×10^5)
1-35B	5/31	1645	6/01	1605	(1.78×10^5)
1-35C	5/31	1645	6/02	1006	(2.07×10^5)
1-35D	5/31	1645	6/02	1629	(2.16×10^5)
1-35	5/31	1645	6/03	0751	2.07×10^5
D1-35B	6/01	0843	6/01	1603	(0.33×10^5)
D1-35C	6/01	1603	6/02	1006	(0.29×10^5)
D1-35D	6/02	1006	6/02	1629	(0.09×10^5)
D1-35	6/02	1629	6/03	0751	(-0.09×10^5)
D'1-35	6/02	1006	6/03	0751	(0.0
D"1-35	6/01	1603	6/03	0751	(0.09×10^5)
2-20	5/31	1645	6/03	0751	143.0
	6/03	0751	6/03	0757	60.0
1-36	6/03	0757	6/03	1501	3610.0
	6/03	1501	6/03	1505	4.2

TABLE VI-4 (Contd.)

Sample I.D.	Time On		Time Off		HTO, μCi
	Date	Hour	Date	Hour	
Run 29	5/31	1645	6/03	1505	2.108×10^7
1-37	6/03	1505	6/04	1223	1360.0
	6/04	1223	6/04	1227	4.4
1-38	6/04	1227	6/05	1617	1840.0
	6/05	1617	6/05	1620	3.5
1-39	6/05	1620	6/06	0826	1130.0
	6/06	0826	6/06	0830	8.9
Run 30	6/03	1505	6/06	0830	4.35×10^3
1-40A	6/06	0830	6/06	0849	(42.3)
1-40B	6/06	0830	6/06	0915	(39.9)
1-40C	6/06	0830	6/06	0945	(43.1)
1-40D	6/06	0830	6/06	1015	(88.7)
1-40E	6/06	0830	6/06	1045	(179.0)
1-40F	6/06	0830	6/06	1215	(322.0)
1-40G	6/06	0830	6/06	1600	(561.0)
1-40	6/06	0830	6/07	0830	1610.0
D1-40B	6/06	0849	6/06	0915	(-2.4)
D1-40C	6/06	0915	6/06	0945	(3.2)
D1-40D	6/06	0945	6/06	1015	(45.6)
D1-40E	6/06	1015	6/06	1045	(90.3)
D1-40F	6/06	1045	6/06	1215	(143.0)
D1-40G	6/06	1215	6/06	1600	(239.0)
D1-40	6/06	1600	6/07	0830	(1049.0)
	6/07	0830	6/07	0834	4.0
1-41	6/07	0834	6/08	0840	1480.0
	6/08	0840	6/08	0844	8.3
1-42	6/08	0844	6/08	1055	272.0
	6/08	1055	6/08	1059	6.0
Run 31	6/06	0830	6/08	1059	3.38×10^3
1-43A	6/08	1059	6/08	1242	(154.0)
1-43B	6/08	1059	6/08	1305	(188.0)
1-43C	6/08	1059	6/08	1315	(193.0)
1-43D	6/08	1059	6/08	1325	(207.0)
1-43E	6/08	1059	6/08	1335	(213.0)
1-43F	6/08	1059	6/08	1345	(234.0)
1-43G	6/08	1059	6/08	1355	(247.0)
1-43H	6/08	1059	6/08	1405	(259.0)
1-43I	6/08	1059	6/08	1415	(273.0)
1-43J	6/08	1059	6/08	1430	(285.0)
1-43K	6/08	1059	6/08	1445	(294.0)
1-43L	6/08	1059	6/08	1500	(315.0)
1-43M	6/08	1059	6/08	1530	(337.0)
1-43N	6/08	1059	6/08	1600	(369.0)
1-43O	6/08	1059	6/08	1630	(394.0)
1-43	6/08	1059	6/09	0829	1620.0
	6/09	0829	6/09	0830	1.6

TABLE VI-4 (Contd.)

Sample I.D.	Time On		Time Off		HTO, μCi
	Date	Hour	Date	Hour	
Run 31 (Contd.)					
2-21-1	6/03	0257	6/08	1055	210.0
D1-43B	6/08	1242	6/08	1305	(34.0)
D1-43C	6/08	1305	6/08	1315	(5.0)
D1-43D	6/08	1315	6/08	1325	(14.0)
D1-43E	6/08	1325	6/08	1335	(6.0)
D1-43F	6/08	1335	6/08	1345	(21.0)
D1-43G	6/08	1345	6/08	1355	(13.0)
D1-43H	6/08	1355	6/08	1405	(12.0)
D1-43I	6/08	1405	6/08	1415	(24.0)
D1-43J	6/08	1415	6/08	1430	(12.0)
D1-43K	6/08	1430	6/08	1445	(9.0)
D1-43L	6/08	1445	6/08	1500	(21.0)
D1-43M	6/08	1500	6/08	1530	(22.0)
D1-43N	6/08	1530	6/08	1600	(32.0)
D1-43O	6/08	1600	6/08	1630	(35.0)
D1-43	6/08	1630	6/09	0829	(1226.0)
1-44	6/09	0830	6/10	0804	2270.0
	6/10	0804	6/10	0807	7.5
Run 32	6/08	1059	6/10	0807	4.109×10^3
1-45A	6/10	0807	6/10	0830	(57.7)
1-45B	6/10	0807	6/10	0845	(63.3)
1-45C	6/10	0807	6/10	0900	(73.8)
1-45D	6/10	0807	6/10	0915	(61.0)
1-45E	6/10	0807	6/10	0930	(81.7)
1-45F	6/10	0807	6/10	0945	(121.0)
1-45G	6/10	0807	6/10	1000	(173.0)
1-45H	6/10	0807	6/10	1015	(223.0)
1-45I	6/10	0807	6/10	1030	(263.0)
1-45J	6/10	0807	6/10	1045	(292.0)
1-45K	6/10	0807	6/10	1100	(329.0)
1-45L	6/10	0807	6/10	1115	(354.0)
1-45M	6/10	0807	6/10	1130	(381.0)
1-45N	6/10	0807	6/10	1145	(400.0)
1-45O	6/10	0807	6/10	1200	(424.0)
1-45P	6/10	0807	6/10	1215	(453.0)
1-45Q	6/10	0807	6/10	1245	(544.0)
1-45R	6/10	0807	6/10	1315	(677.0)
1-45S	6/10	0807	6/10	1345	(849.0)
1-45T	6/10	0807	6/10	1415	(1032.0)
1-45U	6/10	0807	6/10	1445	(1238.0)
1-45V	6/10	0807	6/10	1515	(1332.0)
1-45W	6/10	0807	6/10	1545	(1502.0)
1-45X	6/10	0807	6/10	1615	(1628.0)
1-45Y	6/10	0807	6/10	1645	(1788.0)

TABLE VI-4 (Contd.)

Sample I.D.	Time On		Time Off		HTO, μCi
	Date	Hour	Date	Hour	
Run 32 (Contd.)					
1-45	6/10	0807	6/11	0720	4740.0
	6/11	0720	6/11	0723	4.7
D1-45B	6/10	0830	6/10	0845	(5.6)
D1-45C	6/10	0845	6/10	0900	(9.5)
D1-45D	6/10	0900	6/10	0915	(-12.8)
D1-45E	6/10	0915	6/10	0930	(20.7)
D1-45F	6/10	0930	6/10	0945	(39.3)
	6/10	0945	6/10	1000	(52.0)
D1-45H	6/10	1000	6/10	1015	(50.0)
D1-45I	6/10	1015	6/10	1030	(40.0)
D1-45J	6/10	1030	6/10	1045	(29.0)
D1-45K	6/10	1045	6/10	1100	(37.0)
D1-45L	6/10	1100	6/10	1115	(25.0)
D1-45M	6/10	1115	6/10	1130	(17.0)
D1-45N	6/10	1130	6/10	1145	(19.0)
D1-45O	6/10	1145	6/10	1200	(24.0)
D1-45P	6/10	1200	6/10	1215	(29.0)
D1-45Q	6/10	1215	6/10	1245	(91.0)
D1-45R	6/10	1245	6/10	1315	(123.0)
D1-45S	6/10	1315	6/10	1345	(172.0)
D1-45T	6/10	1345	6/10	1415	(183.0)
D1-45U	6/10	1415	6/10	1445	(206.0)
D1-45V	6/10	1445	6/10	1515	(99.0)
D1-45W	6/10	1515	6/10	1545	(165.0)
D1-45X	6/10	1545	6/10	1615	(126.0)
D1-45Y	6/10	1615	6/11	1645	(160.0)
D1-45	6/10	1645	6/10	0720	(2952.0)
1-46	6/11	0723	6/13	0814	4170.0
	6/13	0814	6/13	0818	8.0
1-47	6/13	0818	6/13	0840	72.9
2-22	6/8	1159	6/13	0840	366.0
Run 33	6/10	0807	6/13	0840	9.362×10^3

[a]Molecular sieve bed in front of Trap 3 was left on, thereby removing the HTO. Numbers are estimated.

[b]Numbers in parentheses are for syringe samples taken at various time intervals. These samples are not included in the sum of the total amount collected per run.

[c]Counting time less than 1 min for scintillation sample - accuracy may be reduced about 5%.

The procedure used to apportion the total amount of tritium collected in a sample into the amounts for each run was as follows. The contribution from each run in a sample was assumed to be proportional to three factors: (1) the permeability of the inner cladding at the temperature measured for the run, (2) the square root of the average tritium (HT) pressure, and (3) the time for each run. The tritium permeability for Type 316 stainless steel[46] was used for Type 304 stainless steel cladding in TRIO. [Note: In order to convert the permeability into units of Curies/(m•day•pa), it is necessary to multiply the data in reference 46 by a factor of 677.] The average HT pressure is proportional to the total amount of HT released per unit time. The data for cladding temperature, tritium permeability, calculated amounts of tritium permeation, reciprocal temperature, and the logarithm of the permeation rates are given in Table VI-6.

On observing the permeation data (Table VI-6) some permeation rates appear to be much higher than the rest, particularly those for Samples 2 and 3. These samples include Runs 10-14 which had no hydrogen added to the sweep gas. It appears that the added hydrogen may have reduced the permeation rates for the other runs. It is possible that the addition of hydrogen reduced the permeation rates of tritium by isotopic swamping. This possibility is discussed further in Sec. IX.5.

4. Total Tritium Collected

The data presented in Tables VI-4 and -5 are summarized in Table VI-7. The tritium collected in the three forms, the total (TCOLL), and the cumulative total (CTCOLL) are presented for the 33 runs.

F. Tritium (HT) Release Rates

One of the key features of the TRIO experiment is the on-line measurement of tritium release rate. In the experiment, the level of tritium released in the HT (noncondensable) form was continuously measured with KCl, the line monitor. The HT form accounted for about 94% of the released tritium. Also, for the majority of the experimental runs, the HT form was about 99% of the released tritium. Thus, the dynamic data on HT release rate provide a reasonably good measure of the overall rates of tritium release from the solid.

TABLE VI-5

TRIO Tritium Permeation Data

Run No.	Tritium Produced (T)	Temperature (°C) Nominal	Temperature (°C) Cladding	F, Rel. Perm.	T × F	ϕ[a](Ci)
0	0.002	300	300			5×10^{6}[a]
1	1.081	600	520	0.177	0.191	(0.0038)[a]
2	0.956	700	610	0.260	0.248	(0.0050)[a]
3	0.546	700	620	0.27	0.147	(0.0029)[a]
	Total - Sample 0				0.586	(0.0117)[a]
4	2.365	550	460	0.130	0.307	0.0038
5	0.958	500	410	0.098	0.094	0.0012
6	0.482	550	460	0.130	0.063	0.0008
7	1.470	600	510	0.170	0.250	0.0031
8	0.873	650	560	0.212	0.185	0.0023
9[b]	2.575	650	560	0.212	0.546	0.0068
	Total - Sample 1				1.445	0.018
10[c]	0.406	400	330	0.055	0.022	0.0018
11[c]	0.468	500	420	0.103	0.048	0.0040
12[c]	1.815	550				
13[c]	0.100	600	510	0.170	0.017	0.0014
	Total - Sample 2				0.323	0.027
13[c]	1.937	600	510	0.170	0.329	0.107
14[c,d]	0.983	700	610	0.260	0.256	0.083
15[d]	9.369	700	610	0.260	0.096	0.031[e]
16	0.496	700/(300 SCCM)	610	0.143	0.071	0.023
17	1.316	700/(30 SCCM)	610	0.473	0.622	0.202
18	0.375	700	610	0.260	0.098	0.032
19	0.303	650	560	0.212	0.064	0.021
	Total - Sample 3				1.536	0.499
20[f]	1.570	650	565	0.216	0.339	0.0068
21	0.771	650	570	0.220	0.170	0.0034
22	0.381	600	520	0.177	0.067	0.0013
23	0.290	550	475	0.140	0.041	0.0008
	Total - Sample 4				0.617	0.0123
23	0.956	550	475	0.140	0.123	0.0027
24	0.398	600	520	0.177	0.070	0.0014
25	0.611	560	480	0.143	0.087	0.0018
26	1.441	550	470	0.138	0.199	0.0041
	Total - Sample 5				0.490	0.010

TABLE VI-5 (Contd.)

Run No.	Tritium Produced (T)	Temperature (°C)		F, Rel. Perm.	T × F	ϕ^a (Ci)
		Nominal	Cladding			
27	2.107	525	450	0.124	0.261	0.0103
28	2.488	500	430	0.100	0.269	0.0107
	Total - Sample 6				0.530	0.021
29	0.726	480/(300 SCCM)	410	0.054	0.039	0.0007
30	0.892	480	410	0.098	0.087	0.0016
31	0.718	500	425	0.107	0.077	0.0014
32	0.601	550	470	0.139	0.084	0.0015
33	0.906	650	580	0.230	0.208	0.0038
	Total - Sample 7				0.495	0.009

[a] ϕ = T × F × FF, where FF is assumed to be 0.02 for Sample 0, 0.0125 for Sample 1, 0.0836 for Sample 2, 0.325 for Sample 3, 0.020 for Sample 4, 0.204 for Sample 5, 0.0396 for Sample 6, and 0.018 for Sample 7.

[b] Run 9 had no H_2; tritium produced may be overestimated.

[c] Runs had no H_2.

[d] Some large spikes were noted in Run 14, and especially in Run 15.

[e] Large spike.

[f] Run 20 had no O_2.

TABLE VI-6

Tritium Permeation Data

Run No.	Temp. (°C)	Tritium Permeability (Ci/m·day·Pa)	HT/Day	Permeation (Ci)	1000/T	Log Perm. Rate (Ci/day)
0	170			$(3.3 \times 10^{7})^{a}$		
1	525			$(0.0035)^{a}$		
2	610			$(0.0038)^{a}$		
3	610			$(0.0044)^{a}$		
	Total - Sample 0[a]			(0.012)		
4	460	0.0203	0.74321	0.0021	1.3643	-3.2856
5	410	0.00947	0.55543	3.84×10^{4}	1.4641	-3.7163
6	460	0.0203	0.85147	6.32×10^{4}	1.3643	-3.1996
7	510	0.0395	0.90729	0.0029	1.2771	-2.8829
8	560	0.0709	0.72837	0.0036	1.2005	-2.7243
9	560	0.0709	0.56063	0.0084	1.2005	-2.8379
	Total - Sample 1			0.018		
10	330	0.00215	0.21187	1.96×10^{4}	1.658	-3.6609
11	420	0.0111	0.54772	0.0029	1.443	-2.5355
12	460	0.0203	0.56501	0.0214	1.364	-2.2598
13	510	0.0395	0.67024	0.0024	1.277	-1.8966
	Total - Sample 2			0.027		
13B	510	0.0395	0.67003	0.00759	1.2771	-1.792
14	610	0.119	0.84984	0.1332	1.1325	-1.2098
15	610	0.119	0.91716	0.0566	1.1325	-1.1767
16	610	0.0687	0.67622	0.0312	1.1325	-1.5477
17	610	0.217	10.0531	0.1394	1.1325	-0.8558
18	610	0.119	0.64979	0.0424	1.1325	-1.3264
19	560	0.0709	0.6261	0.0203	1.2005	-1.5674
	Total - Sample 3			0.499		
20	565	0.0749	0.11371	0.00137	1.1933	-3.1957
21	570	0.079	0.77889	0.00829	1.1862	-2.3369
22	520	0.0446	0.59245	0.00198	1.261	-2.704
23A	475	0.025	0.56907	6.65×10^{4}	1.3369	-2.9729
	Total - Sample 4			0.0123		
23B	475	0.025	0.6008	0.0027	1.3369	-30.0063
24	520	0.0446	0.72363	0.0023	1.261	-2.6741
25	480	0.0268	0.55395	0.0017	1.328	-30.0113
26	470	0.0233	0.56131	0.0033	1.3459	-30.0664
	Total - Sample 5			0.010		

TABLE VI-6 (Contd.)

Run No.	Temp. (°C)	Tritium Permeability (Ci/m•day•Pa)	HT/Day	Permeation (Ci)	1000/T	Log Perm. Rate (Ci/day)
27	450	0.0176	0.56065	0.0118	1.3831	-2.7596
28	430	0.013	0.52279	0.0092	1.4225	-2.9215
	Total - Sample 6			0.021		
29	410	0.00947	0.51466	3.48×10^{4}	1.4641	-3.7706
30	410	0.00547	0.51204	2.68×10^{4}	1.4641	-40.0112
31	425	0.012	0.58262	5.30×10^{6}	1.4327	-3.6139
32	470	0.0233	0.83339	0.0012	1.3459	-3.1703
33	580	0.0879	0.76999	0.0066	1.1723	-2.628
	Total - Sample 7			0.090		

[a]Estimated.

TABLE VI-7

Summary of Tritium Collected

Run	Conditions[a]	HT	HTO	ϕ	TCOLL	CTCOLL
0	Tests to 300	0.00186	0.00006	3.3×10^7	0.002	0.002
1	600/STD	0.985	0.026	(0.004)	1.015	1.017
2	700/STD	0.985	0.009	(0.004)	0.998	2.015
3	700/1%H_2	0.513	0.011	(0.004)	0.528	2.543
4	550/STD	2.099	0.006	0.0021	2.107	4.650
5	500/STD	0.617	0.001	0.0004	0.618	5.268
6	550/STD	0.725	0.001	0.0006	0.727	5.995
7	600/STD	1.811	0.002	0.0029	1.816	7.811
8	650/STD	1.008	0.001	0.0036[b]	1.013	8.824
9	650/No H_2	1.823	0.002	0.0084[b]	1.833	10.657
10	400/No H_2	0.040	0.000	0.0004	0.041	10.698
11	500/No H_2	0.300	0.003	0.0029	0.306	11.004
12	550/No H_2	1.245	0.000	0.0214[b]	1.267	12.271
13	600/No H_2	2.197	0.000	0.0783[b]	2.275	14.546
14	700/No H_2	1.560	0.001	0.1332	1.694	16.240
15	700/STD	0.715	0.000	0.0566	0.772	17.012
16	700/(300 SCCM)	0.503	0.001	0.0312	0.535	17.547
17	700/(30 SCCM)	1.109	0.000	0.1394	1.248	18.795
18	700/STD	0.380	0.000	0.0424[b]	0.422	19.217
19	650/STD	0.294	0.000	0.0203[b]	0.314	19.531
20	650/0.2% O_2	0.028	0.000	0.0014	0.029	19.560
21	650/STD	1.092	0.000	0.0083	1.100	20.660
22	600/STD	0.351	0.000	0.0020	0.353	21.013
23	550/STD	1.077	^.001	0.0033[b]	1.082	22.095
24	600/STD	0.576	0.002	0.0023	0.580	22.675
25	560/STD	0.537	0.007	0.0017	0.546	23.221
26	550/STD	1.213	0.048	0.0033[b]	1.264	24.485
27	525/STD	2.128	0.333	0.0118	2.473	26.958
28	500/STD	2.104	0.857	0.0093[b]	2.970	29.928
29	480/(300 SCCM)	0.543	0.211	0.0003	0.754	30.682
30	480/STD	0.721	0.004	0.0003	0.725	31.408
31	500/STD	0.740	0.003	0.0005	0.744	32.152
32	550/STD	1.271	0.004	0.0012	1.276	33.428
33	650/STD	1.666	0.009	0.0066[b]	1.682	35.110
	Total:	32.958	1.543	0.608	35.110	

[a]Numbers on left of slash (/) is temperature (°C); number on right is gas composition; STP means standard conditions, i.e. flow rate of 100 cm^3/min and 0.1% H_3 added.

[b]Permeation samples.

The output of the Kanne chamber records the HT signal in volts, which is equal to the logarithm of the tritium concentration in microcuries per cubic meter. From the outputs of the calibrated transducers which monitor pressure and flow, the HT release rate, in units of microcuries per minute, is then calculated. The absolute accuracy of this release rate was about 30%, owing to the many scale changes (three to four orders of magnitude) which occurred after calibrating the Kanne chamber at low levels. However, the observed data were recalibrated to the data for the HT, which was collected and analyzed by scintillation counting. The latter data had an absolute accuracy of 5%. This calibration procedure involved multiplying the release rates for HT by a factor of 0.65 and subtracting the baseline correction, which increased from zero at the beginning of the experiment to a value of 75 μCi/min at the end. The dynamic data for tritium release, after calibration, agreed with the integral data from the scintillation counting within 10%; thus the absolute accuracy of the HT release rate was about 10%.

For a given run, the experimental parameters (e.g., temperature) are fixed and the tritium (HT) release rate was monitored. At steady state, the release rate is invariant in time and equal to the generation rate. The tritium generation rate was calculated from the recorded neutron flux levels, as later discussed in Sec. VII.D. The absolute accuracy of the tritium generation rate was 10%.

Presented below are the dynamic data for temperature, tritium (HT) release rate, and tritium generation rate for the 33 experimental runs. The time given for all graphical data are in Central Standard Time.

Before the full-power operation of the TRIO irradiation experiment, tests of the ORR were carried out at low power, 3 kW to 12 MW (full power, 30 MW); they were done subsequent to the period of about three months when the reactor was down for repairs to the reactor coolant system. A reactor power of 300 kW, or 1% of full power, is given the name "N_L" because it is considered to be the lowest power that can be quantitavely measured. The data for temperature and tritium release rate data from Run 0 are presented in Figs. VI-6 and -7, respectively.

The recording of temperature began at 2100 on March 10, 1983. One thermocouple element, TR-901, read ~15 deg high owing to an electronic (reference

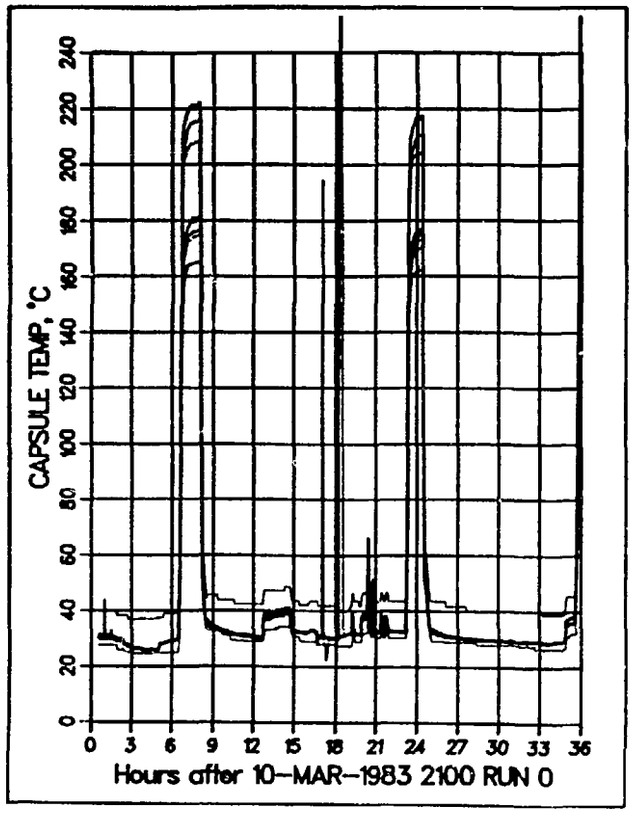

Fig. VI-6. Recorded temperatures for Run 0.

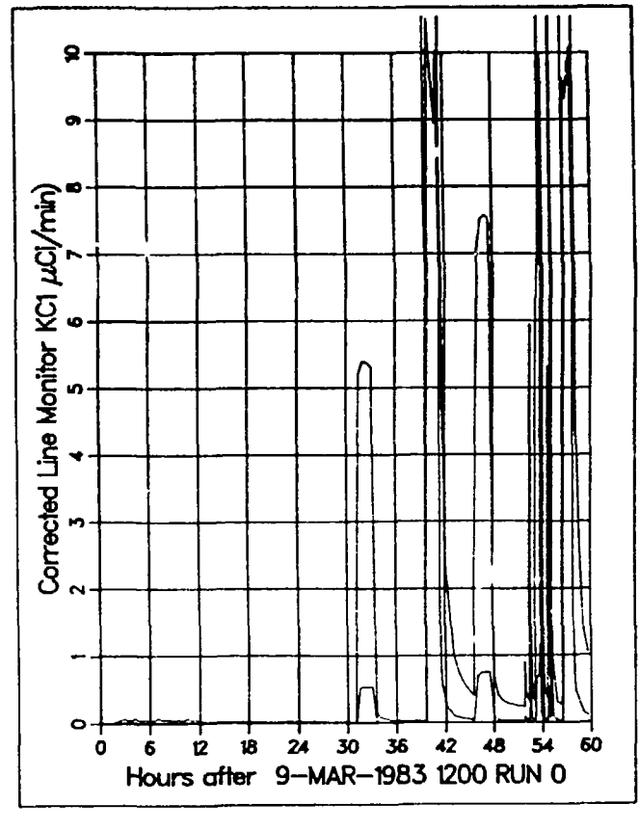

Fig. VI-7. Tritium release rate for Run 0 (shaded). (The unshaded line represents scale expansion by a factor of 100.)

point) problem. As shown, the greatest responses were at 0400 and at 2030 on March 11; these peaks correspond to 1-h tests when the reactor was at 12 MW. With pure helium in the gas gap, the temperature rose to ~200°C when ORR was at 40% full power. Other tests at 1% full power showed a measurable temperature rise of ~4°C. As will be discussed later, the data provide a good deal of information on heat transfer. For example, thermal conductivity of lithium aluminate from 30 to 200°C can be derived from the radial temperature gradient.

The recording of tritium release began on March 9, 1983. Generally, the peak heights are proportional to the tritium generation rate, with approximately 10% of the tritium released. This release is attributed to a recoil mechanism, which is discussed is Sec. IX.A. Another feature is that measurable tritium release occurred on the afternoon of March 9, when the reactor power was at only 3 to 30 kW. These levels are barely detectable by the reactor instruments. It appears that the tritium monitor is the most sensitive detector for neutrons at the ORR facility.

Run 1 had a nominal temperature (the average of T804 and T808) of 600°C with a helium + 0.1% H_2 sweep gas flowing at 100 cm^3/min. The data temperature and tritium release data are given in Figs. VI-8 and VI-9, respectively. The nominal temperature was held at 400°C for 2 h at the start to reduce the chances for thermal shock. At 1200 on March 12, the nominal conditions were established. The thermal data show that the total temperature range is about 180°C, that the radial gradients are about 120°C, and that longitudinal gradients are ~20°C. One thermocouple, TR801 (~630°C) showed a large number of spikes which were caused by the electronic recording system. Also, oscillations in temperature are shown at hours 21 and 31.

The tritium release rate and the generation rate are shown in Fig. VI-8. The ORR reached full power at hour 4, when the generation rate thus reached the level of 350 μCi/min. Because the temperature was low (400°C) from hour 4 until hour 6, tritium accumulated in the solid. When the temperature was increased to nominal conditions, which were chosen such that steady state could be achieved in a few hours, the release curve briefly rose above the generation curve; and some of the excess tritium that had built up over the preceeding two hours was released. Within approximately two hours, the release rate

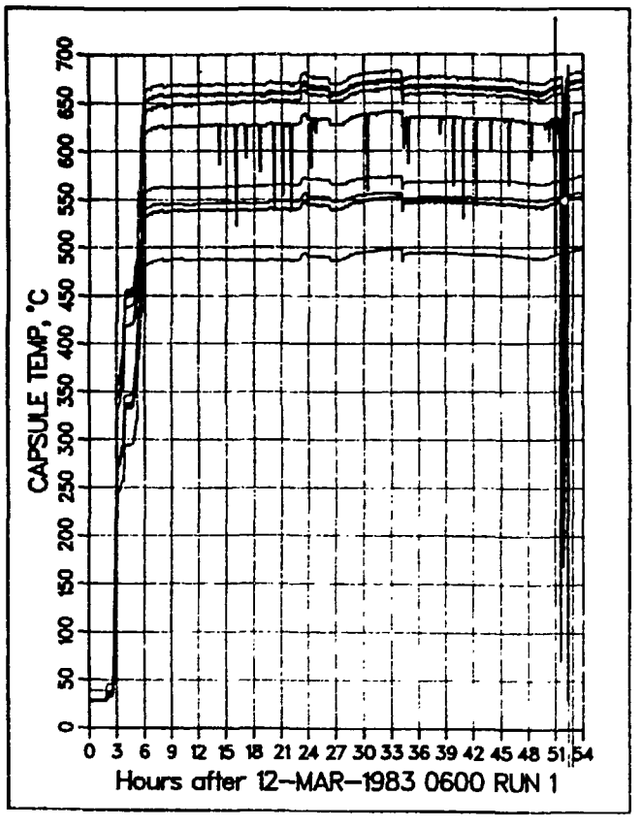

Fig. VI-8. Recorded temperature for Run 1.

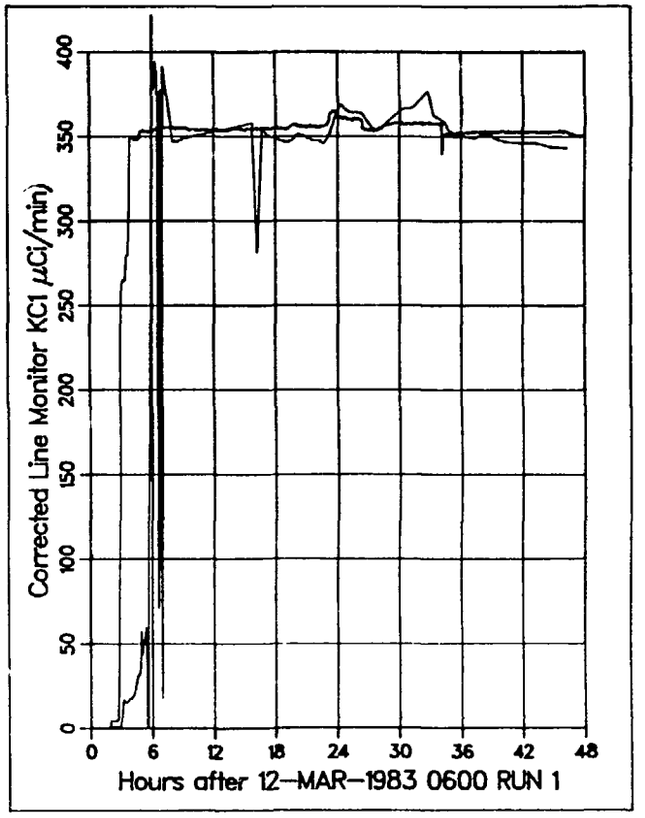

Fig. VI-9. Tritium release rate and generation rate for Run 1.

state was achieved very rapidly in the first run. The negative spike in the release curve at hour 17 is due to changing samples, which briefly altered flow. In addition, the temperature excursions at hours 21 and 31 cause significant perturbations in the tritium release curve.

Run 2 was at a nominal temperature of 700°C with a sweep gas of helium + 0.1% H_2 flowing at a rate of 100 cm^3/min. The temperature and tritium release data are shown in Figs. VI-10 and VI-11, respectively.

The tritium release curve shows a positive spike, followed by a return to steady-state within approximately three hours. The positive spike indicates that the tritium inventory in the solid is less at higher temperatures. There is a temperature spike at 1600 on March 14, which translateds to a small peak in the tritium release curve at 1800 on March 14. There was also a reactor setback at 1000 on March 15, which caused brief temporary fluctuations in temperature and tritium release.

Run 3 was at a nominal temperature of 700°C with a sweep gas flow rate of 100 cm^3/min, as in Run 2. The concentration of hydrogen in the sweep gas was increased from 0.1 to 1.0%. The temperature and tritium release data are shown in Figs. VI-12 and -13, respectively. The temperatures were nearly constant throughout the run except for two small transients which occurred at 1500 on March 16 and at 0800 on March 17. The 150°C decrease at 1400 on March 17 is the start of Run 4. At the beginning of the run, the tritium release curve shows a very sharp spike, which returns to steady state in less than one hour. The positive spike indicates that the increase in hydrogen level in the sweep gas enhances tritium release.

Run 4 was at a nominal temperature of 550°C with a flow rate of 100 cm^3/min for the sweep gas of helium + 0.1% H_2. These sweep gas conditions were used for most of the runs. The temperature and tritium release data are shown in Figs. VI-14 and -15, respectively. The temperature data are generally rather smooth except for a reactor shutdown at 0900 on March 21, a small transient at 1000 on March 19, and a series of oscillations on March 21 and March 22. All these transients are the result of changes in the neutron flux levels, as can be noted by examination of the tritium production curve in Fig. VI-15. The tritium release curve shows a negative peak at the beginning of Run 4, followed by a slow approach to steady state. The transient in tritium release at hour 20 is from changes in flow caused by changing samples. The tritium release curve does not reach steady state during Run 4.

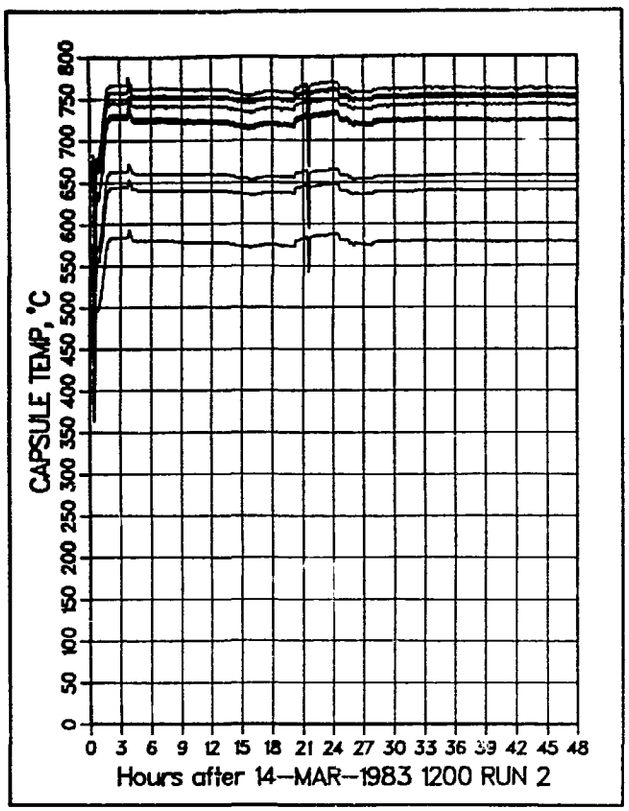

Fig. VI-10. Recorded temperatures for Run 2.

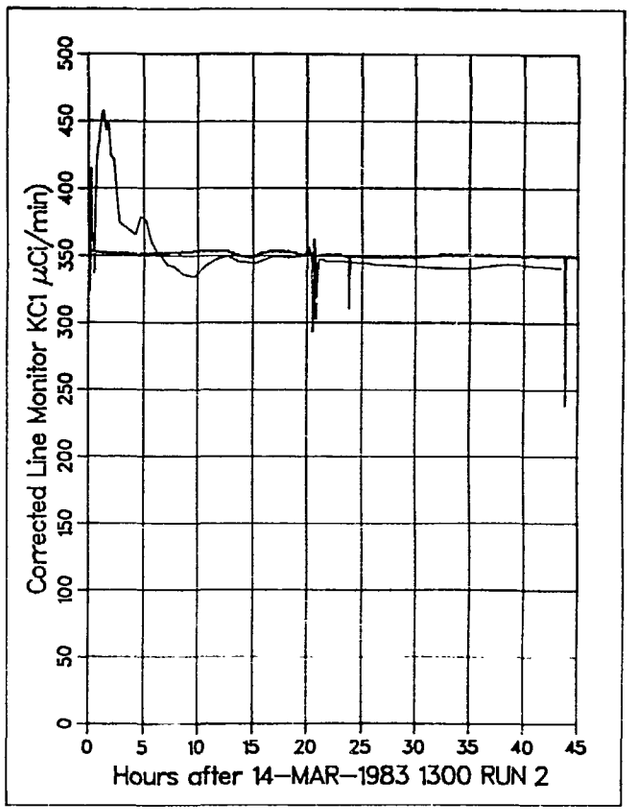

Fig. VI-11. Tritium release rate for Run 2.

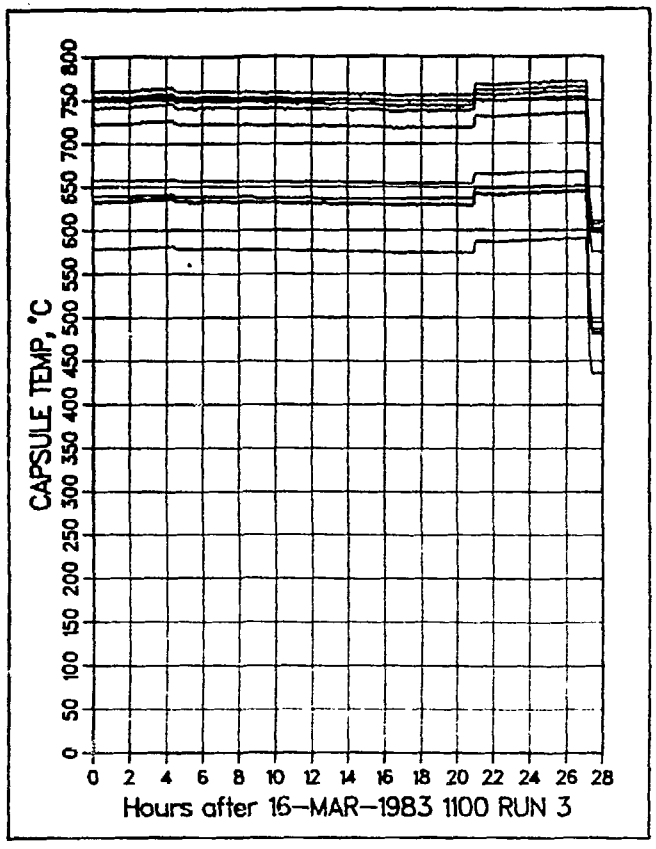

Fig. VI-12. Recorded temperatures for Run 3.

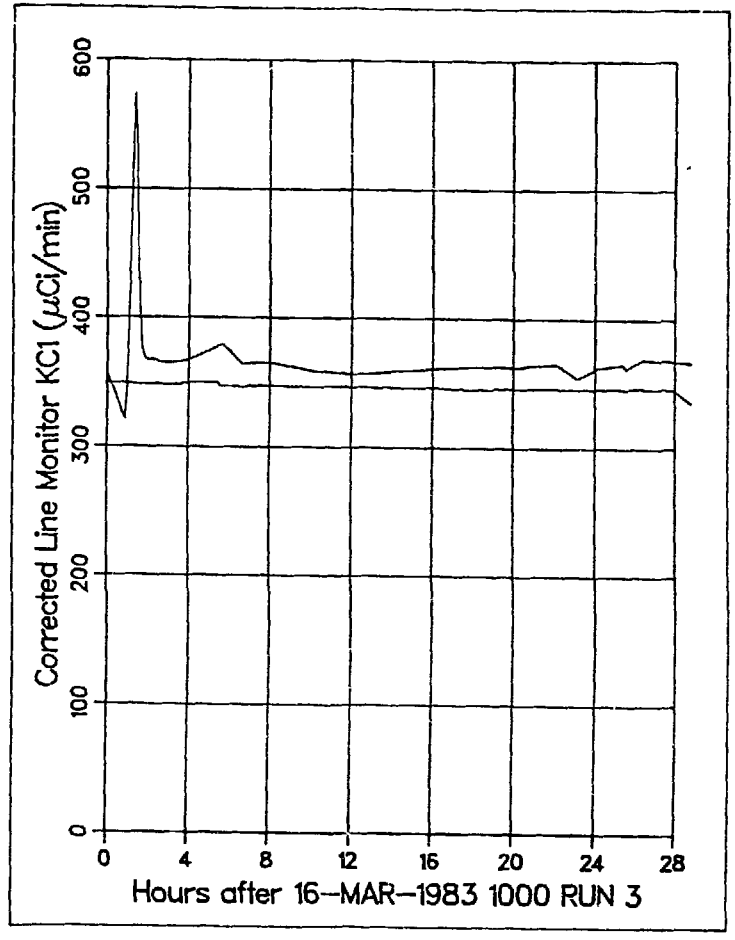

Fig. VI-13. Tritium release rate for Run 3.

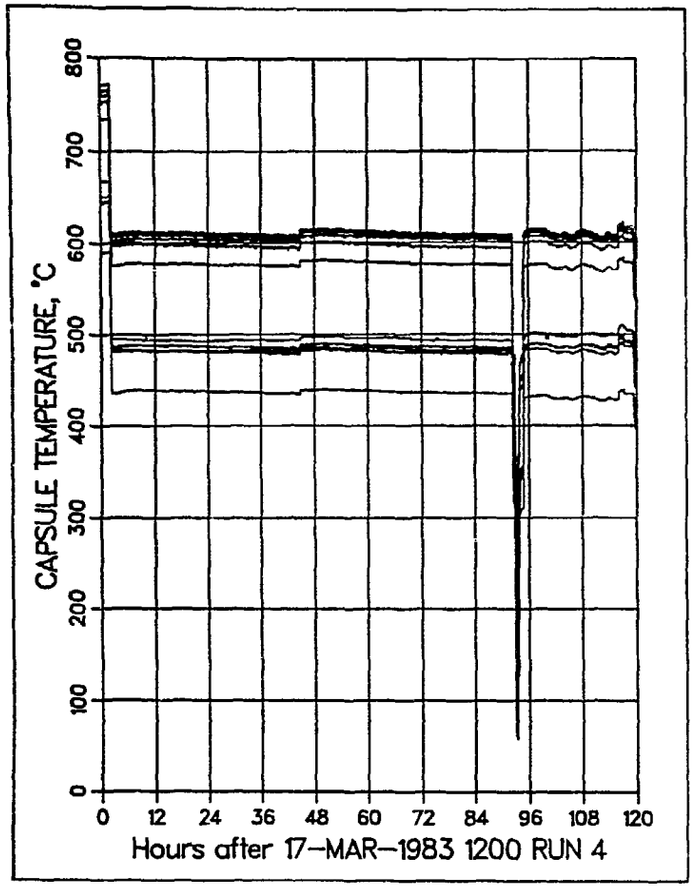

Fig. VI-14. Recorded temperatures for Run 4.

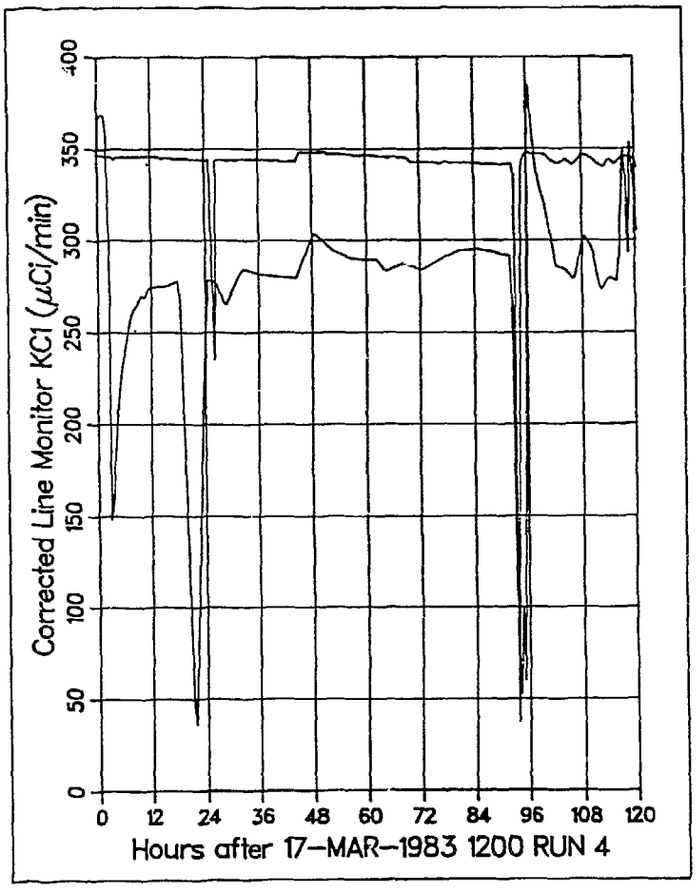

Fig. VI-15. Tritium release rate for Run 4.

Run 5 was at a nominal temperature of 500°C with a flow rate of 100 cc/min and with a sweep gas composition of helium + 0.1% H_2. The temperature and tritium release data are shown in Figs. VI-16 and -17, respectively. The tritium release curve shows a negative peak, followed by a very slow approach to steady state. Steady state is not achieved in Run 5.

Run 6 was at a nominal temperature of 550°C with a flow rate of 100 cm^3/min and for the sweep gas of helium + 0.1% H_2. The temperature and tritium release data are shown in Figs. VI-18 and -19, respectively. Neutron flux and temperature varied by 1% for the entire run. The tritium release curve shows a strong positive peak, followed by a smooth return to steady state at about 20 h.

Run 7 was at a nominal temperature of 600°C with a flow rate of 100 cm^3/min for the sweep gas of helium + 0.1% H_2. The temperature and tritium release data are shown in Figs. VI-20 and -21. The temperatures and the neutron flux are again essentially constant for this run. The apparent temperature excursions for two thermocouples (TR801 and TR901) are due to problems with the electronic recording system. The tritium release curve has a drop in the middle of the peak caused by the scale change. Whenever the signal rises above 1000 μCi/min, the scale changes automatically and this causes an offset problem. The tritium release curve shows a large positive spike followed by a return to steady state within 20 h.

Run 8 was at a nominal temperature of 650°C with a flow rate of 100 cc/min and with a sweep gas composition of helium + 0.1% H_2. The temperature and tritium release data are shown in Figs. VI-22 and -23, respectively. The temperatures and the neutron flux levels were essentially constant throughout Run 8, except for a slight drop in flux and temperature at 0300 on March 29. The tritium release curve shows a positive spike followed by a return to equilibrium in about 12 h.

Run 9 was at a nominal temperature of 650°C with a sweep gas flow rate of 100 cm^3/min. The sweep gas composition was changed, going from 0.1% hydrogen added to pure helium with no hydrogen added. The temperature and tritium release data are shown in Figs. VI-24 and -25, respectively. The temperatures are essentially constant, and all conditions are the same as Run 8 except for the addition of hydrogen to the sweep gas. Removal of the hydrogen additive

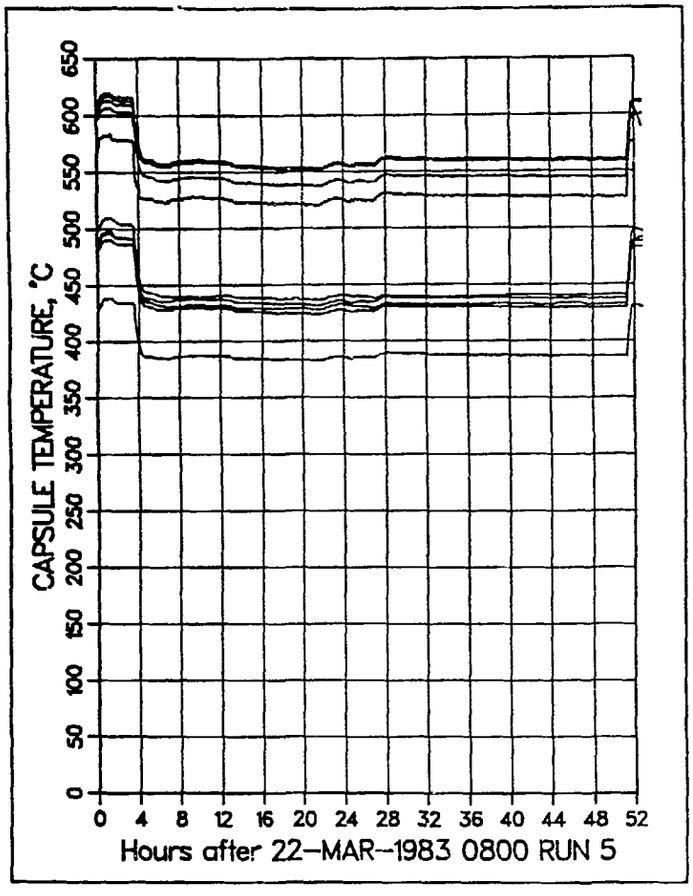

Fig. VI-16. Recorded temperatures for Run 5.

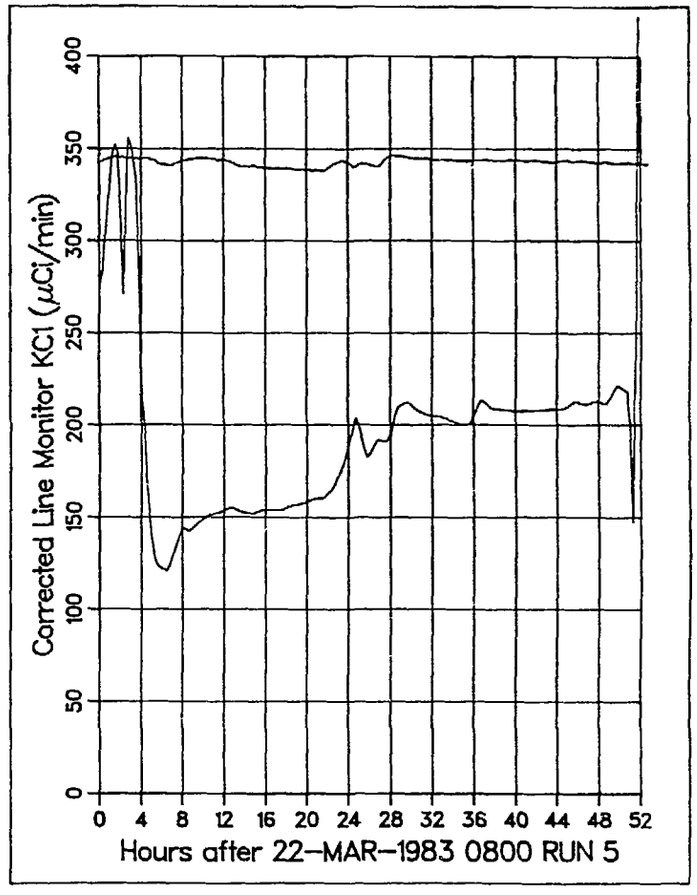

Fig. VI-17. Tritium release rate for Run 5.

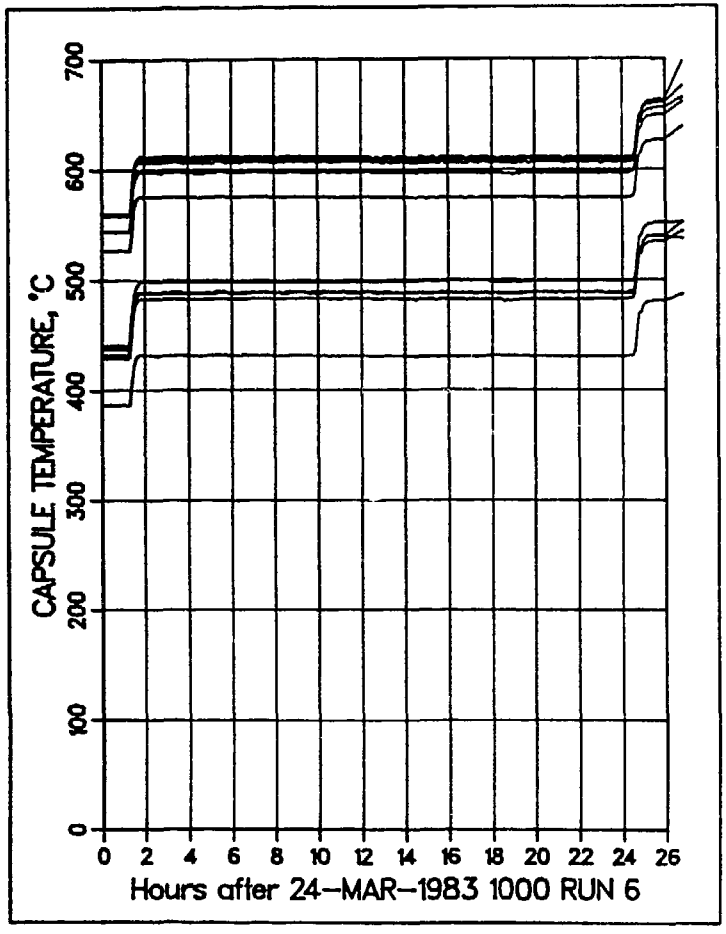

Fig. VI-18. Recorded temperatures for Run 6.

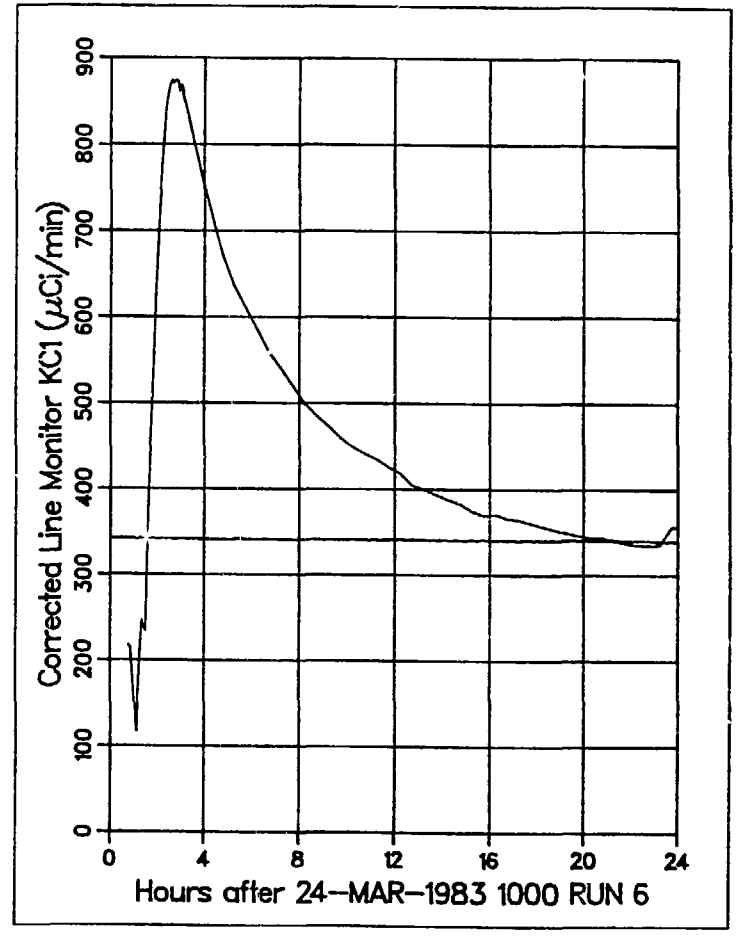

Fig. VI-19. Tritium release rate for Run 6.

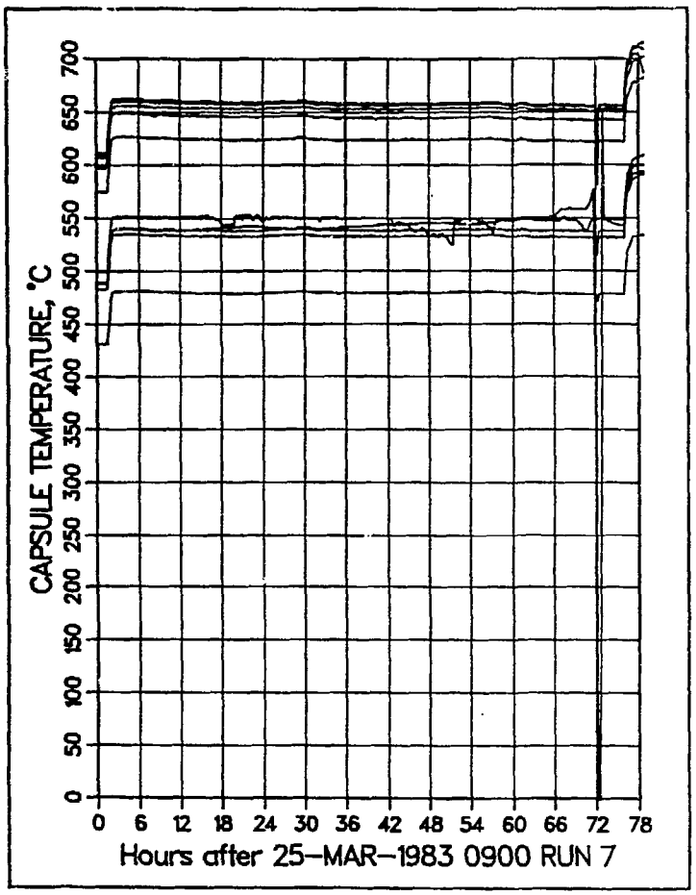

Fig. VI-20. Recorded temperatures for Run 7.

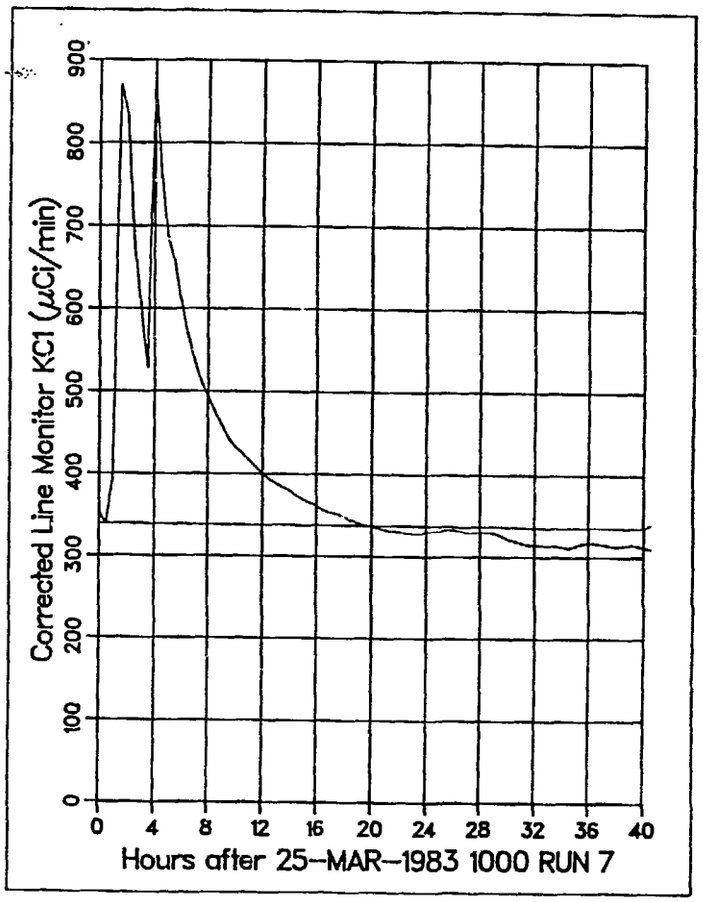

Fig. VI-21. Tritium release rate for Run 7.

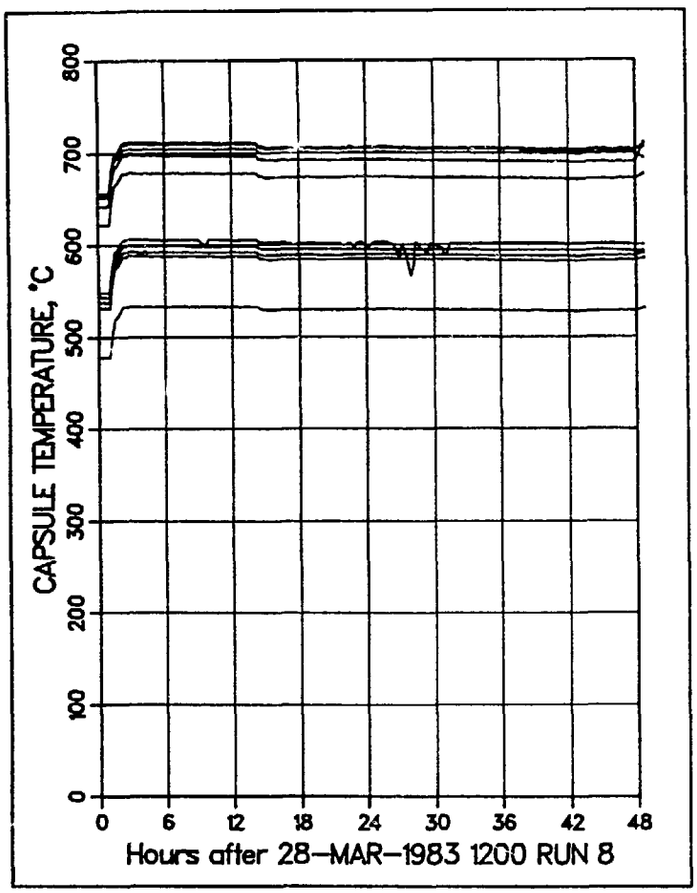

Fig. VI-22. Recorded temperatures for Run 8.

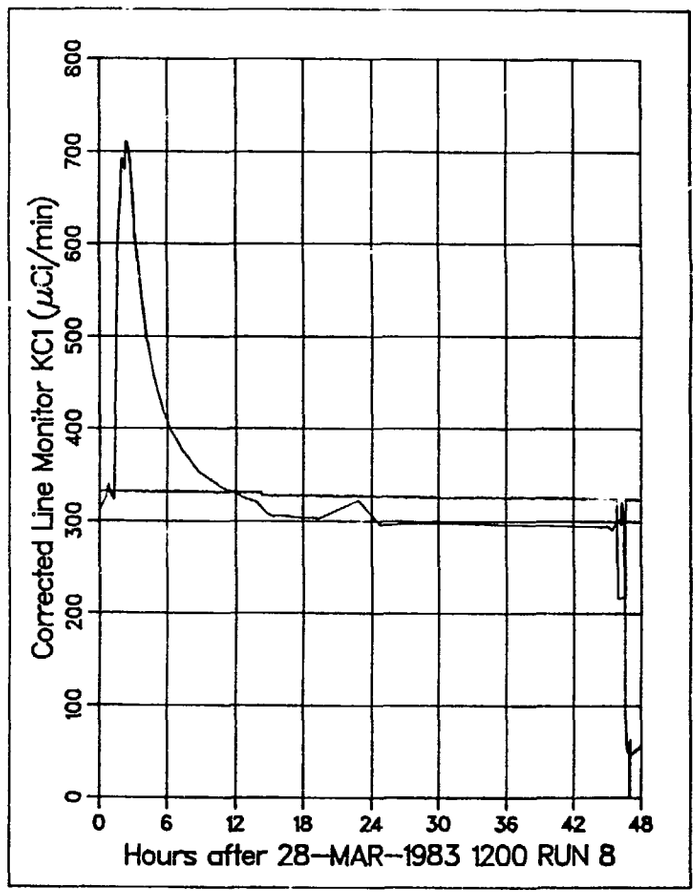

Fig. VI-23. Tritium release rate for Run 8.

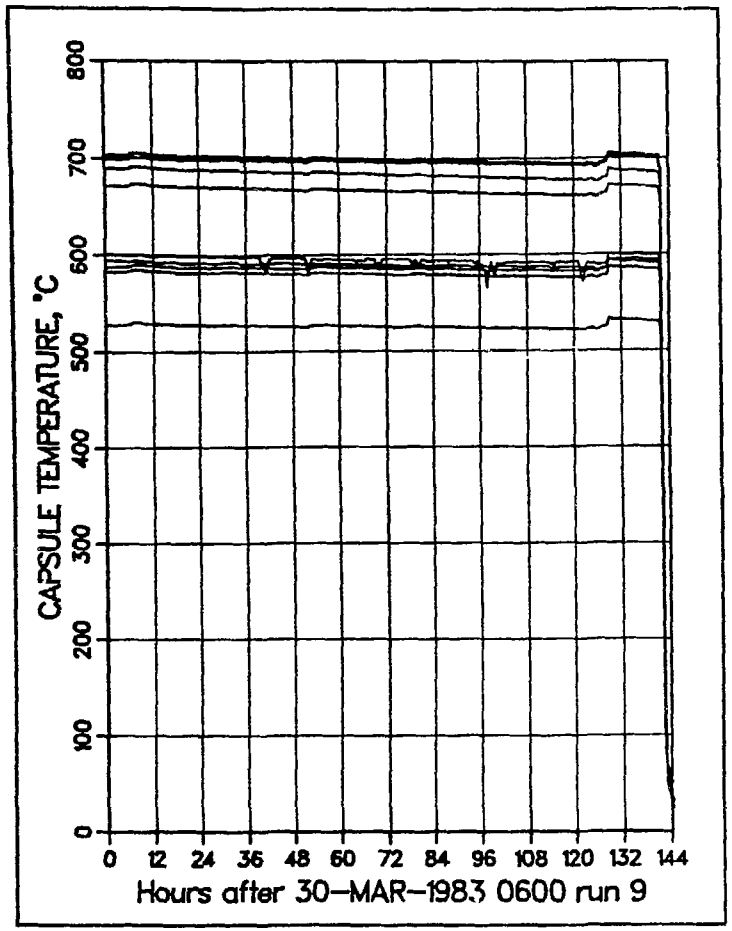

Fig. VI-24. Recorded temperatures for Run 9.

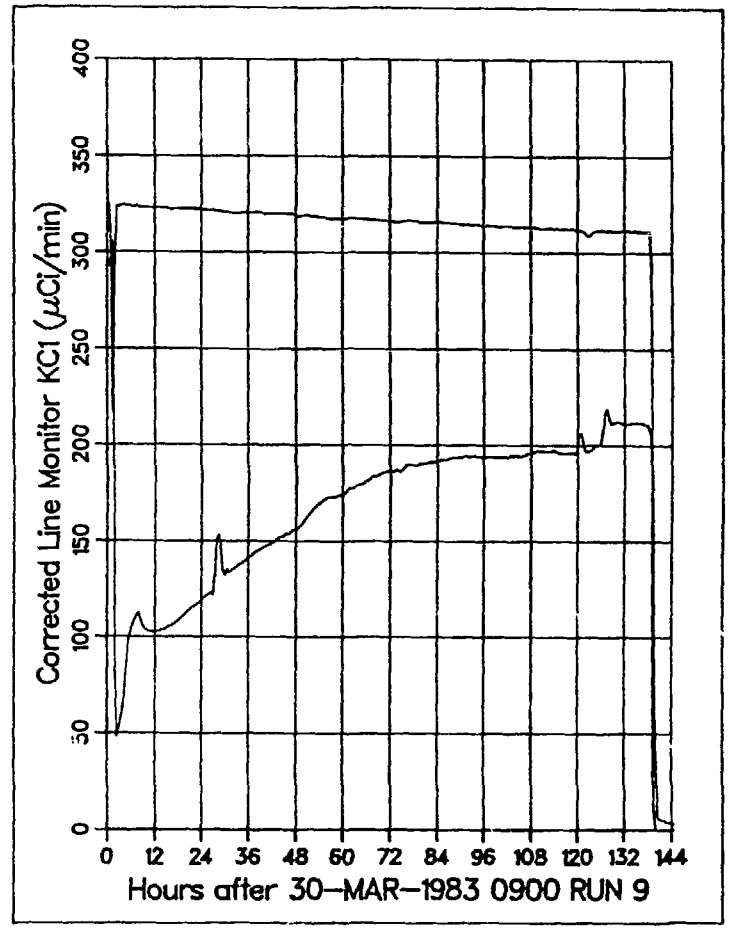

Fig. VI-25. Tritium release rate for Run 9.

has a profoundly negative impact upon tritium release rate, as is evidenced by the large negative peak and the very slow return to equilibrium. Steady state is not achieved in Run 9.

Runs 10 and 11 were performed to investigate the transport rates of radionuclides at lower temperatures. Run 10 was at a nominal temperature of 400°C, and Run 11 was at a nominal temperature of 500°C. The sweep gas was pure helium flowing at 100 cm^3/min. The temperature data for the two runs are shown in Figs. VI-26 and -27. The tritium release data are given in Fig. VI-28. Tritium release was minimal for these runs and steady state was not achieved.

Run 12 was at a nominal temperature of 550°C with a flow rate of 100 cm^3/min for the sweep gas composition of pure helium. The temperature and tritium release data are shown in Figs. VI-29 and -30, respectively. Steady-state tritium was not reached in four days.

Run 13 was at a nominal temperature of 600°C with a flow rate of 100 cm^3/min and for the sweep gas of pure helium. The temperature and tritium release data are shown in Figs. VI-31 and -32, respectively.

There was a reactor shutdown on April 13, as indicated by the low temperatures in Fig. VI-31. The positive spikes in the tritium release curve indicate a net release of tritium after the run had begun, when the reactor was restarted on April 14. The spike is followed by a return to steady state ~100 h after the reactor restart. At 2200 on April 16, a slight decrease in flux caused a drop in temperature of ~5 deg. This temperature drop causes a noticeable dip in the tritium release curve.

Run 14 was at a nominal temperature of 700°C with a flow rate of 100 cm^3/min for the sweep gas of pure helium. The temperature and tritium release data are shown in Figs. VI-33 and -34, respectively. The neutron flux and the temperatures are rather constant throughout the run. The tritium release curve shows a positive spike followed by a return to steady-state conditions.

Run 15 was at a nominal temperature of 700°C with a flow rate of 100 cm^3/min for the sweep gas of helium + 0.1% H_2. The temperature and tritium release data are shown in Figs. VI-35 and -36, respectively. The only change from the previous run is the addition of 0.1% H_2 to the sweep gas. The addition of H_2 has a dramatic effect: the very large positive spike indicates a

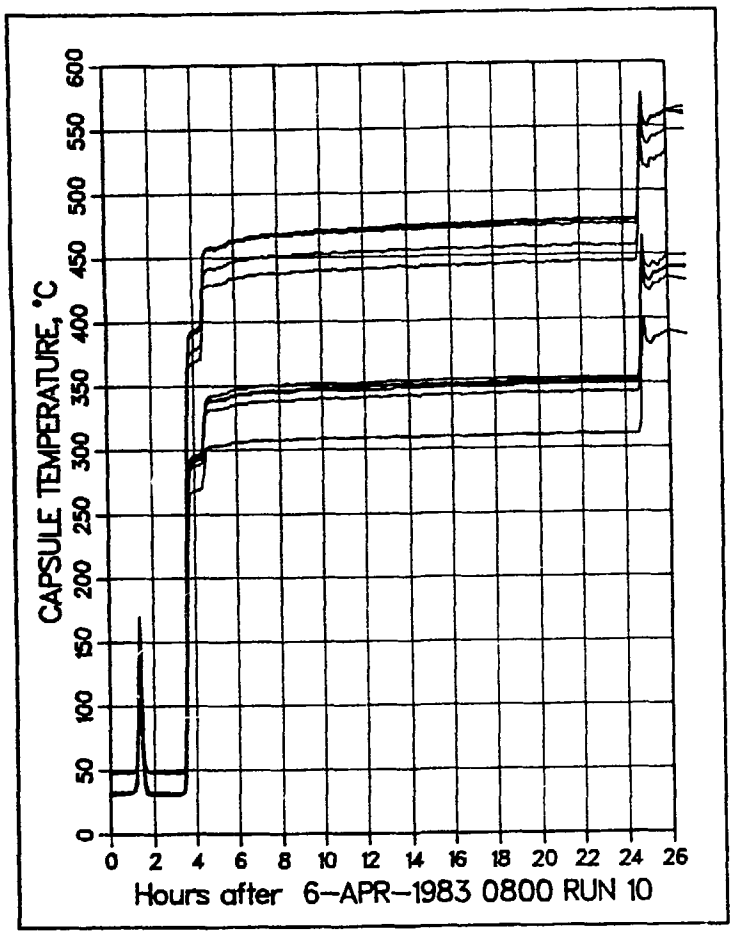

Fig. VI-26. Recorded temperature for Run 10.

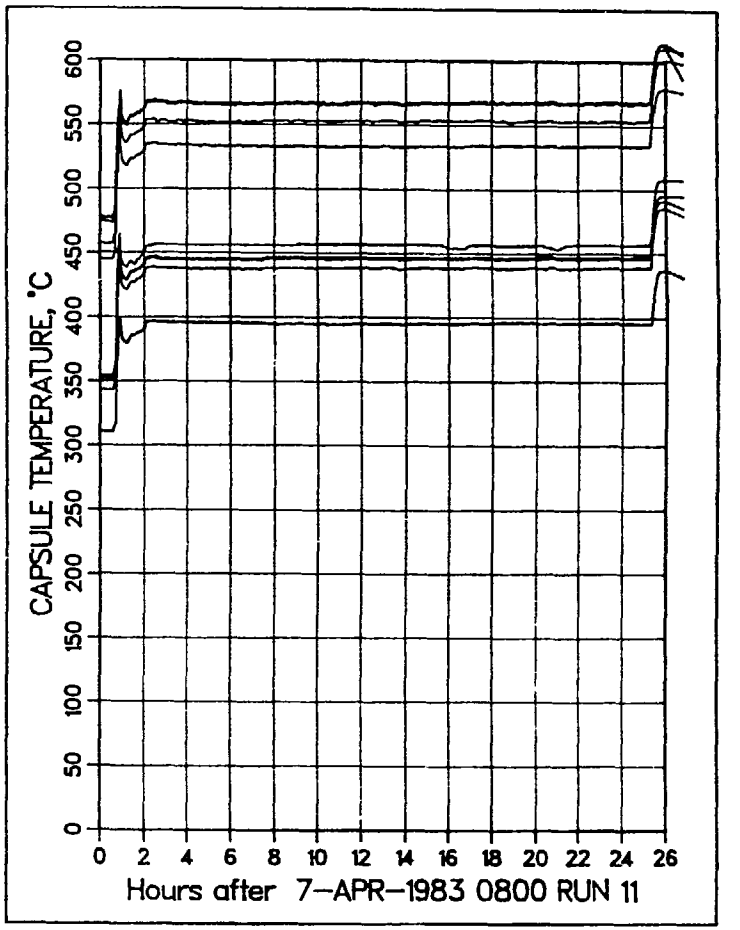

Fig. VI-27. Recorded temperatures for Run 11.

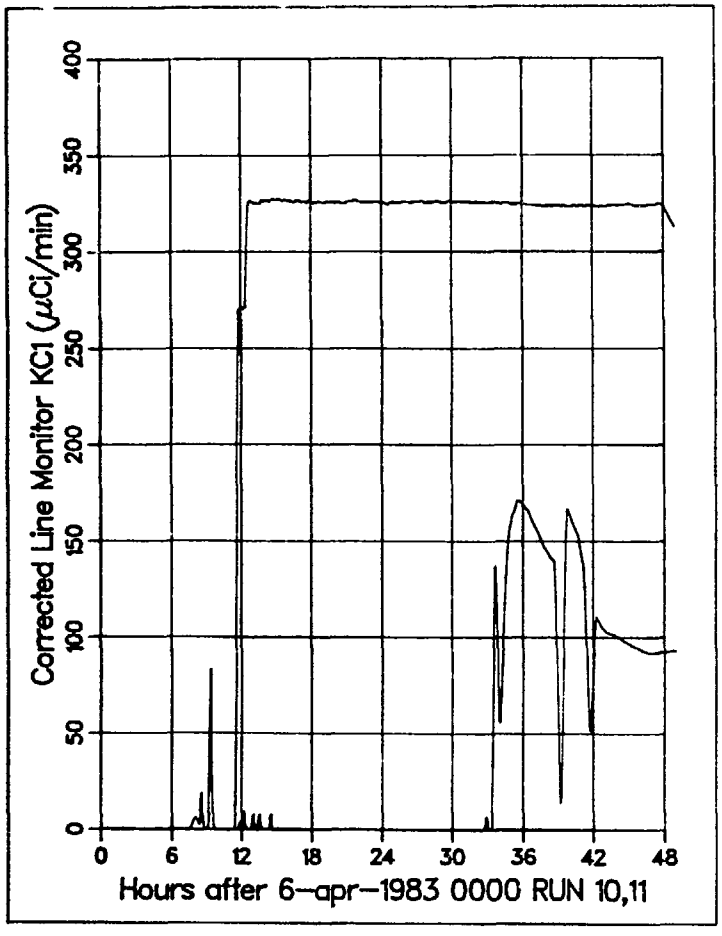

Fig. VI-28. Tritium release rates for Runs 10 and 11.

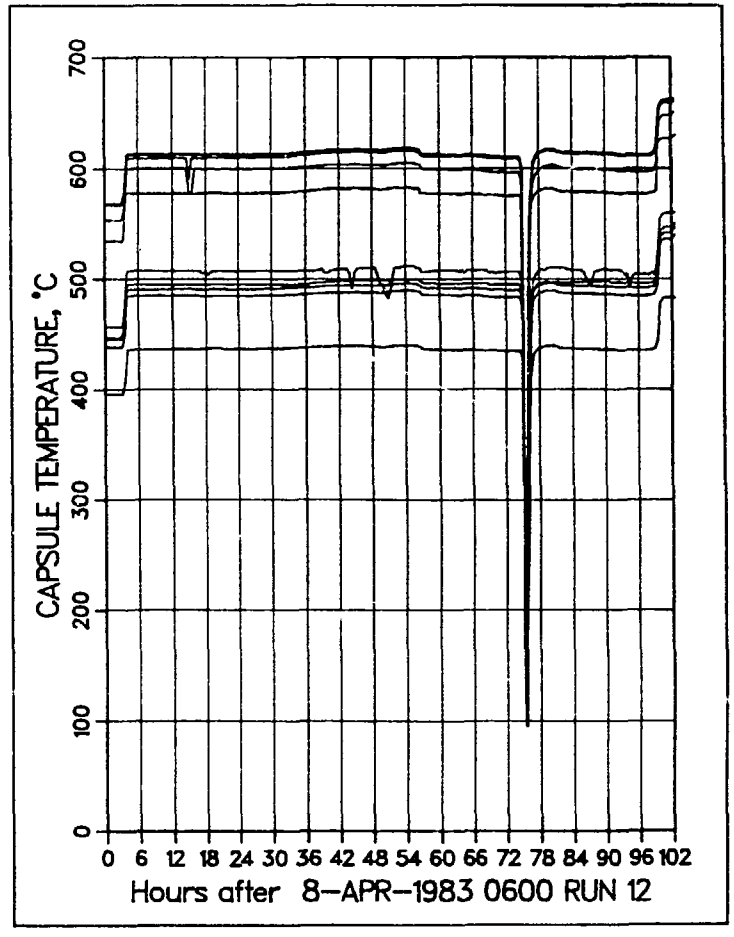

Fig. VI-29. Recorded temperatures for Run 12.

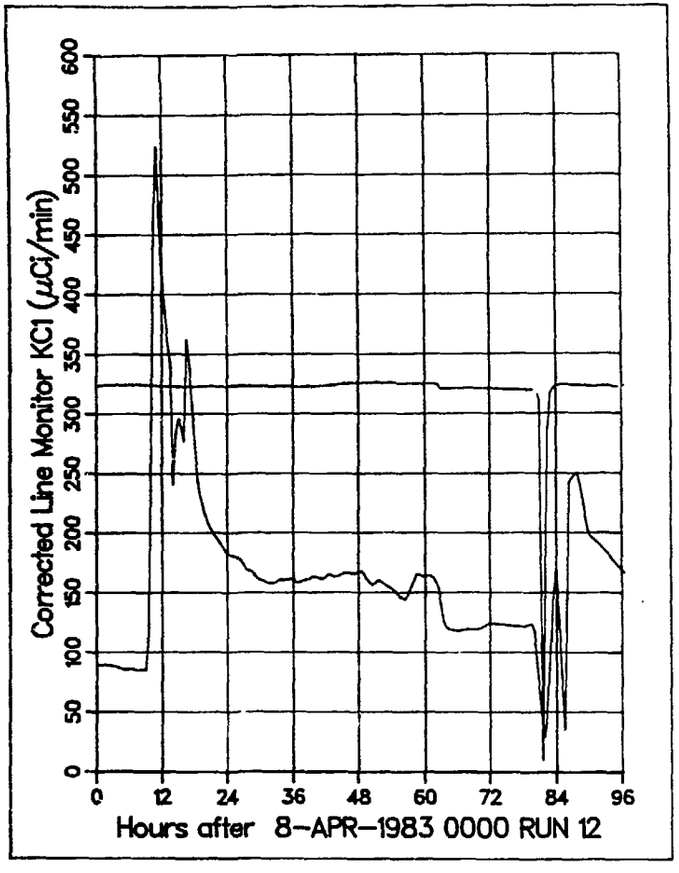

Fig. VI-30. Tritium release rate for Run 12.

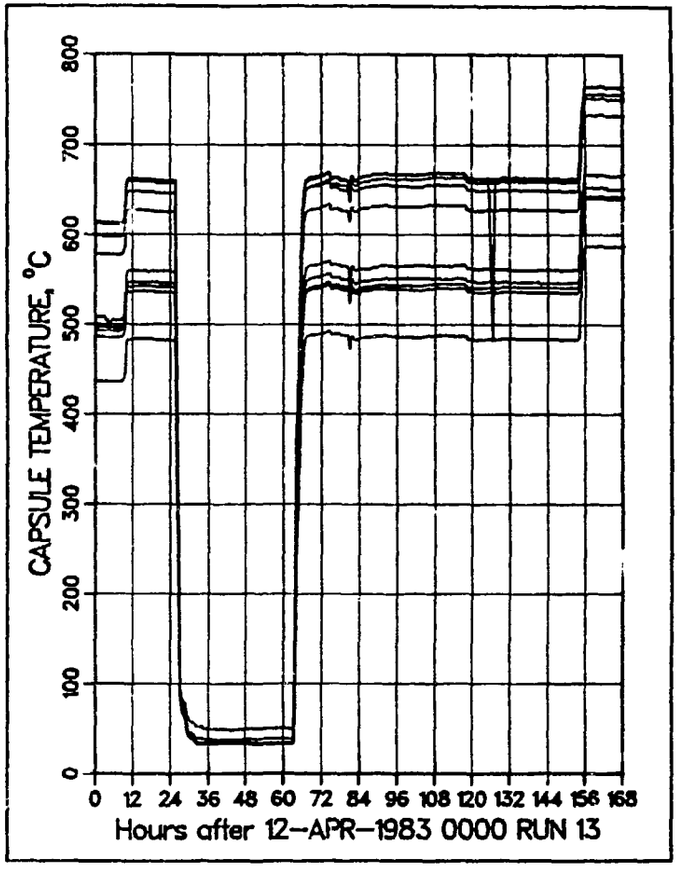

Fig. VI-31. Recorded temperatures for Run 13.

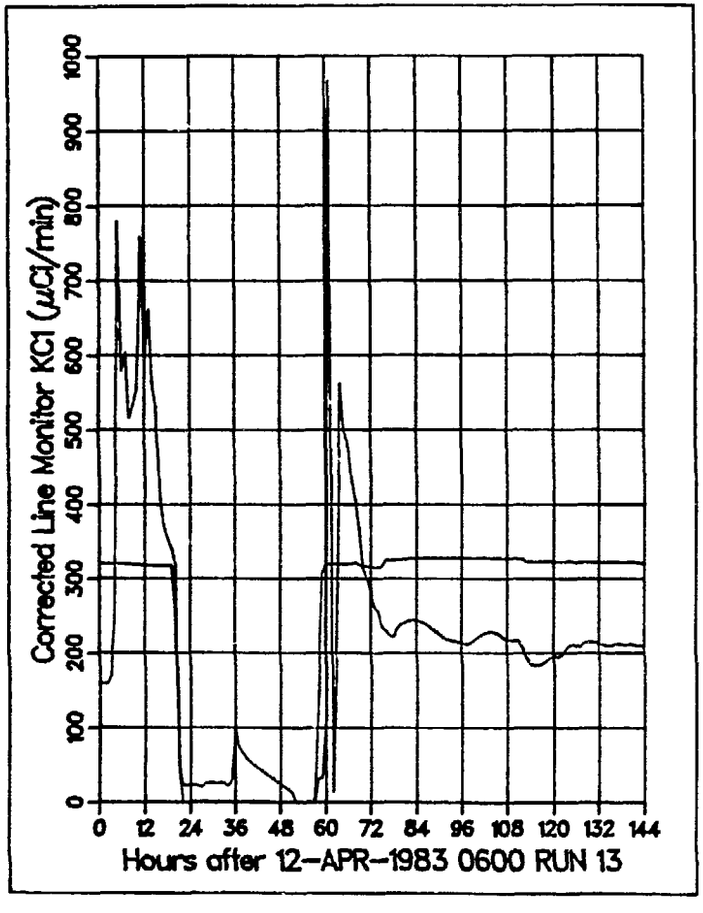

Fig. VI-32. Tritium release rate for Run 13.

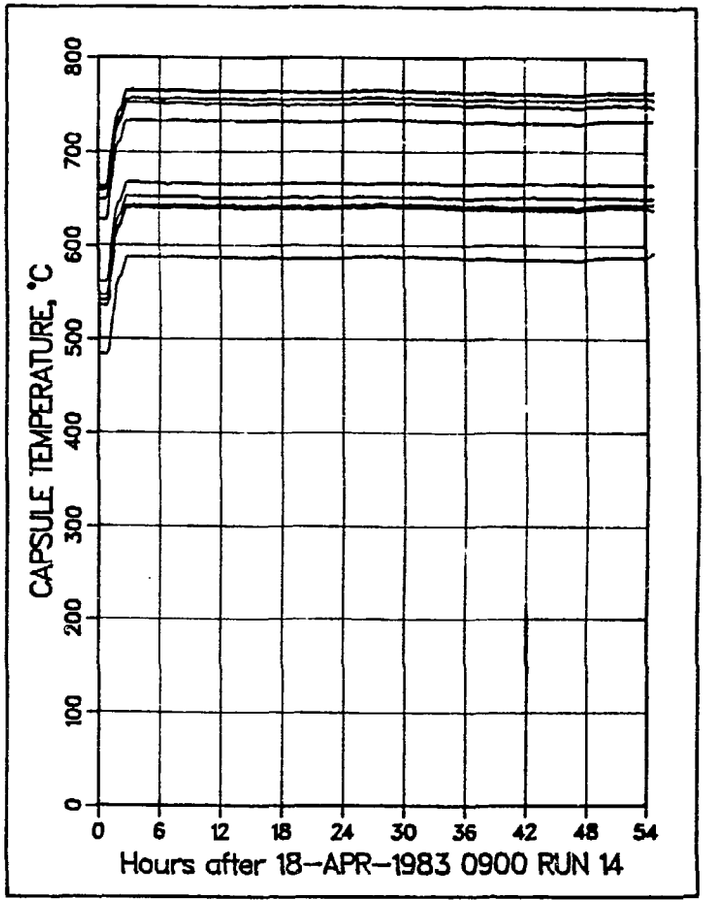

Fig. VI-33. Recorded temperatures for Run 14.

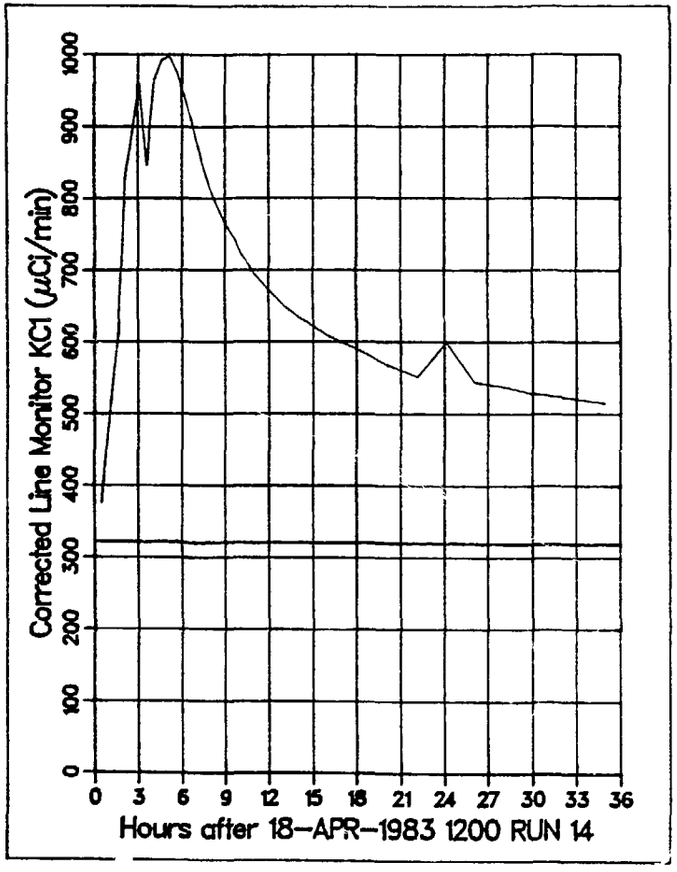

Fig. VI-34. Tritium release rate for Run 14.

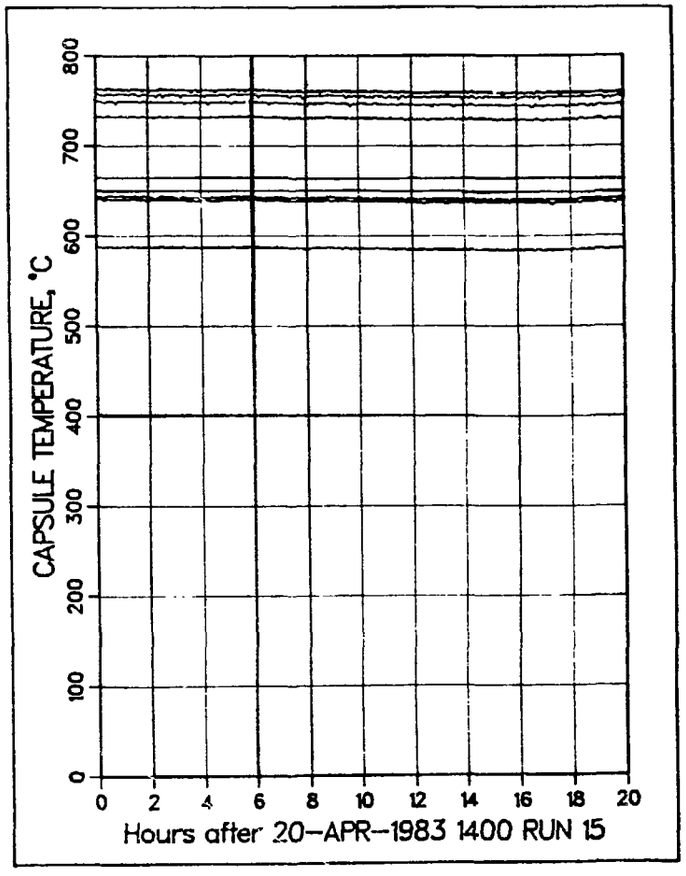

Fig. VI-35. Recorded temperatures for Run 15.

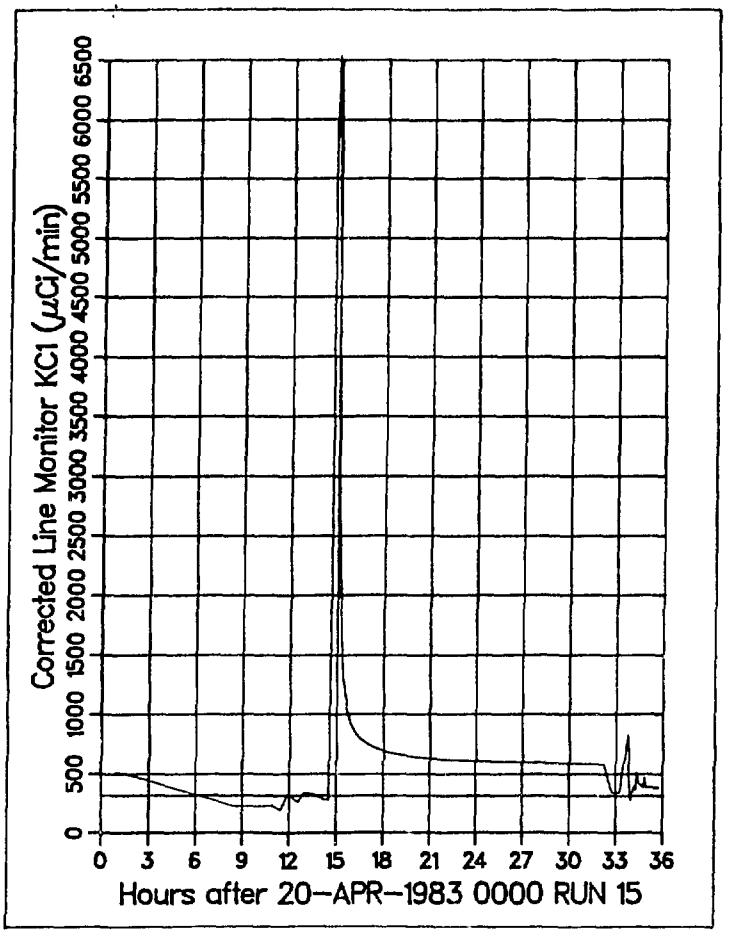

Fig. VI-36. Tritium release rate for Run 15.

large net release of tritium. The addition of hydrogen appears to significantly enhance tritium release. The spike is followed by a return to steady state.

Run 16 was at a nominal temperature of 700°C with a sweep gas flow rate of 300 cc/min and with a sweep gas composition of helium + 0.1% H_2. The temperature and tritium release data are shown in Figs. VI-37 and -38. Pressure and flow conditions in the sweep gas are given in Figs. VI-39 through -42. The only change in conditions from the prior run is an increase in flow rate from 100 to 300 cm^3/min. The increase in flow results in a positive spike at the beginning of the run, followed by a very rapid return to steady state. The second spike seems to be correlated to a temporary drop in pressure (Fig. VI-39) and a brief increase in sweep gas inlet flow. For Run 16 overall, the increase in flow seems to result in an improvement in release.

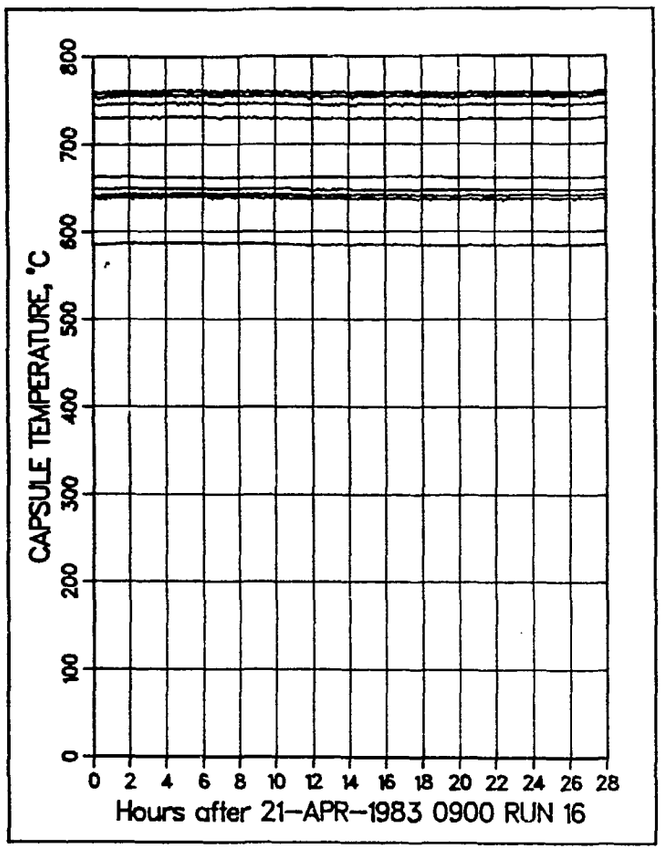

Fig. VI-37. Recorded temperatures for Run 16.

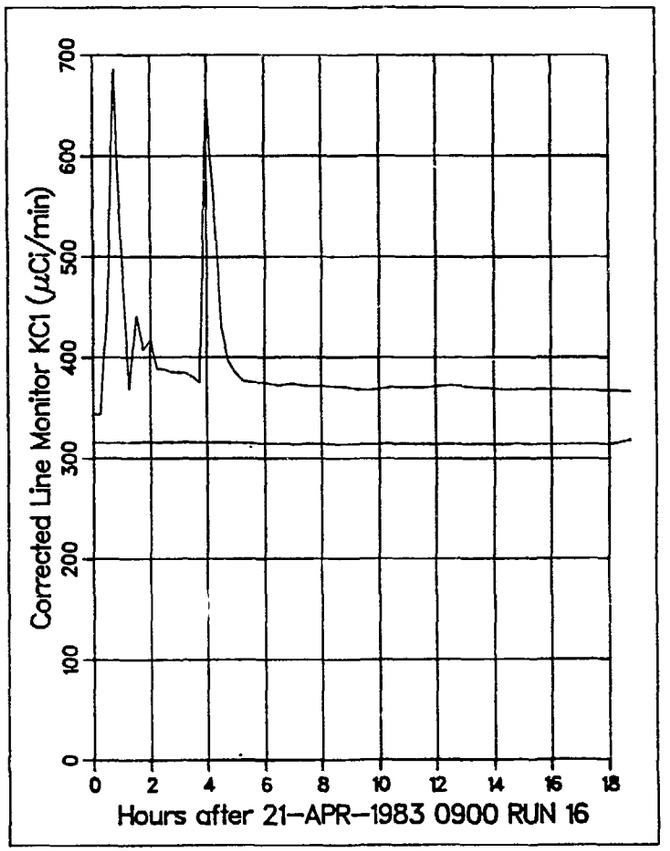

Fig. VI-38. Tritium release rate for Run 16.

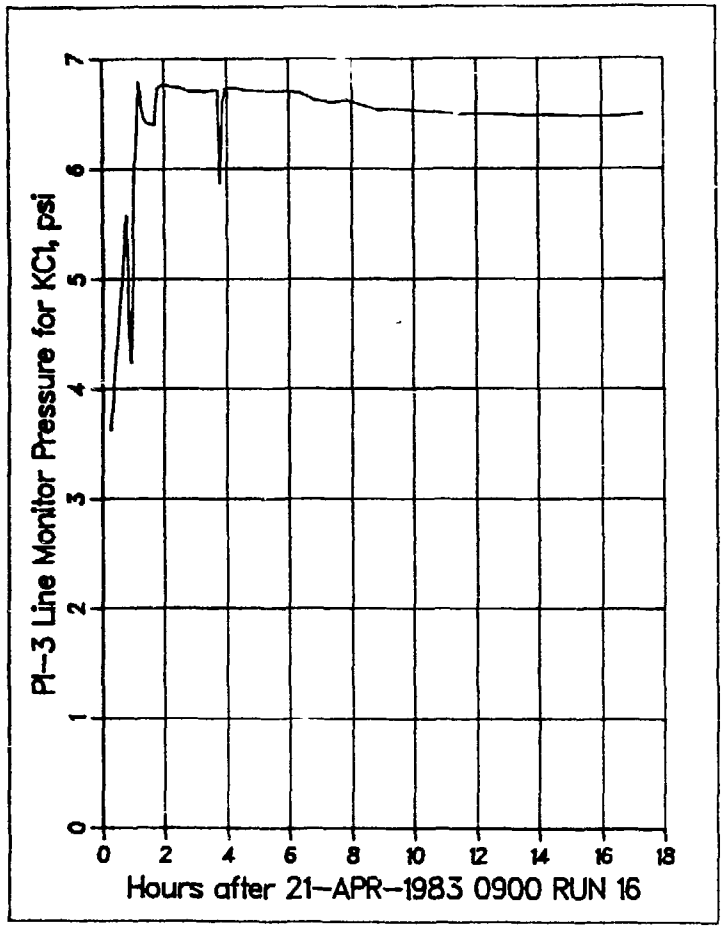

Fig. VI-39. Sweep gas pressure (psig) for Run 16.

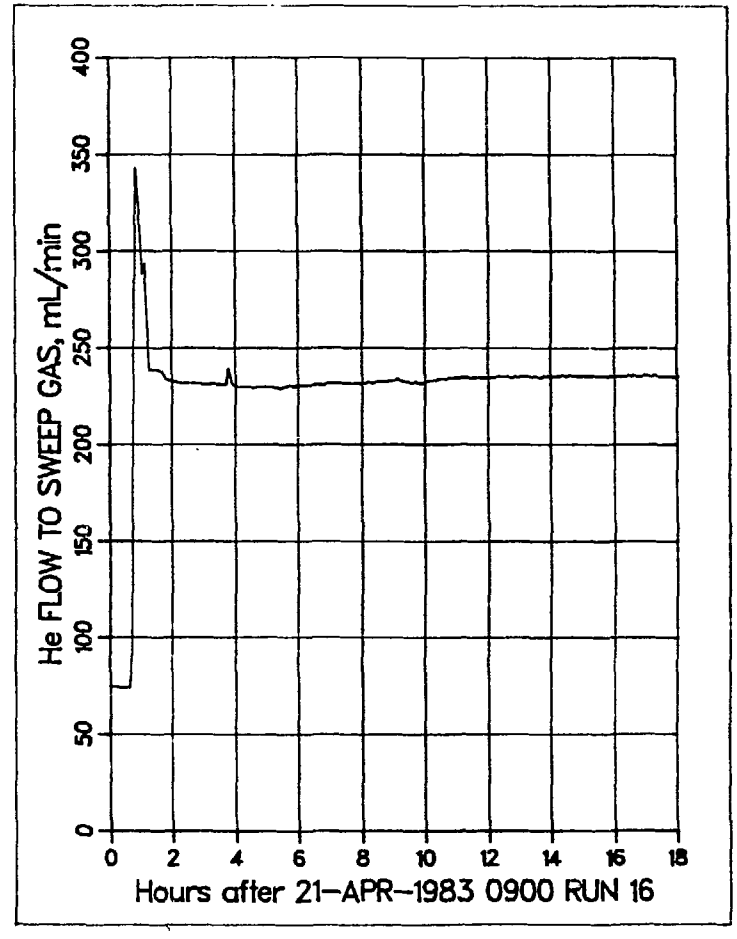

Fig. VI-40. Helium flow to sweep gas for Run 16.

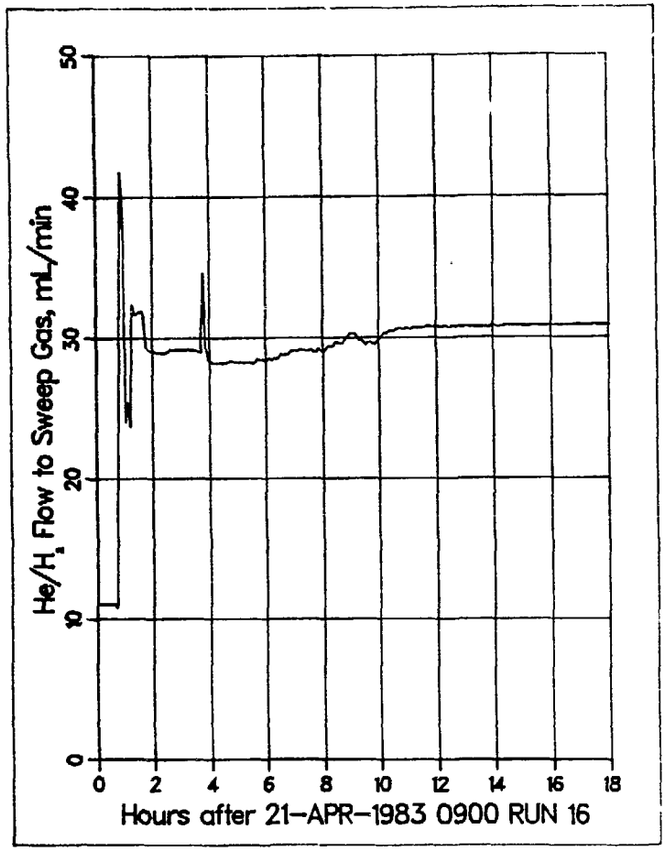

Fig. VI-41. Flow of helium + 4% H_2 to sweep gas for Run 16.

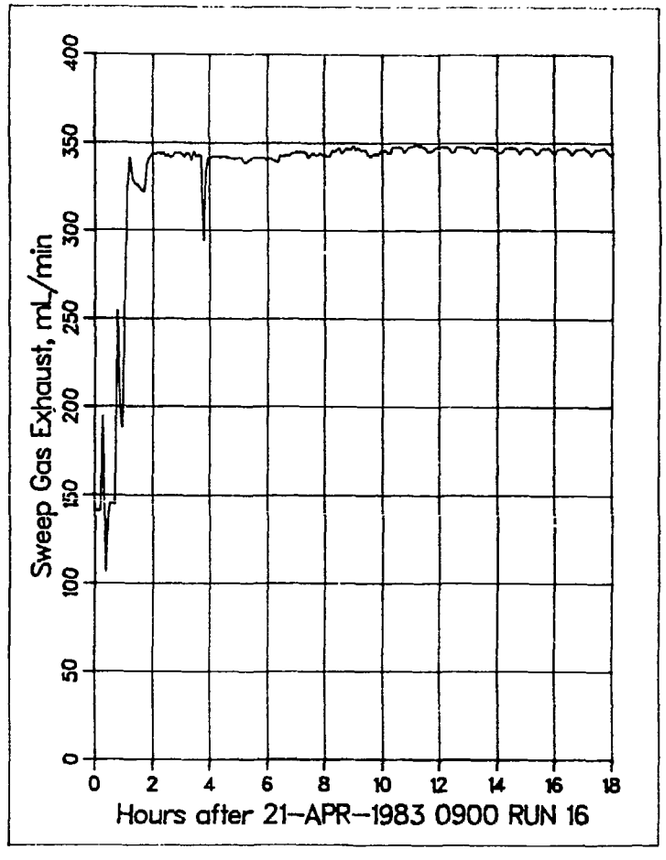

Fig. VI-42. Sweep gas exhaust (cm^2/min) for Run 16.

Run 17 was at a nominal temperature of 700°C with a flow rate of 30 cm^3/min for the sweep gas of helium + 0.1% H_2. The run is the same as the prior run except that the sweep gas flow rate is decreased from 300 cm^3/min to 30 cm^3/min. The temperature and tritium release data are shown in Figs. VI-43 and -44, respectively. A fluctuation in release rate occurs at the beginning of the run, followed by a rapid return to steady state. It is not clear what the effect of decreased flow is. This decreased flow does not seem to have a strong effect upon tritium release.

Run 18 was at a nominal temperature of 700°C with a flow rate of 100 cm^3/min for the sweep gas of helium + 0.1% H_2. The temperature and tritium release data are shown in Figs. VI-45 and -46, respectively. The run has the same conditions as Run 17 except that the flow rate is increased from 30 cm^3/min to 100 cm^3/min. An observable peak in the tritium release curve, followed by a return to steady state within 8 h.

Run 19 was at a nominal temperature of 650°C with a flow rate of 100 cm^3/min for the sweep gas of helium + 0.1% H_2. The temperature and tritium release data are shown in Figs. VI-47 and -48, respectively. The tritium release curve shows oscillations followed by a negative peak and a return to steady state. The oscillations are brought about by temporary pressure and flow changes resulting from changing samples. The rapid fluctuations in the temperature plots were caused by electronic problems with thermocouple TR901.

Run 20 was at a nominal temperature of 650°C with gas flow rate of 100 cm^3/min for the sweep gas of helium + 0.2% oxygen. The temperature and tritium release data are shown in Figs. VI-49 and -50. The temperature profiles show a startup period of about 24 h at low temperature (300-400°C) preceding operation at full temperature. Again, there were problems with thermocouple TR901. The tritium release shows no significant release of tritium in the HT form. As reported previously, no significant release of tritium in the condensable form occurred during the TRIO experiment. The addition of oxygen did not appear to be beneficial to tritium release.

Run 21 was at a nominal temperature of 650°C with a flow rate of 100 cm^3/min for the sweep gas of helium + 0.1% H_2. The temperature and tritium release data are shown in Figs. VI-51 and -52, respectively. The test represents a return to standard conditions following the run with oxygen. The

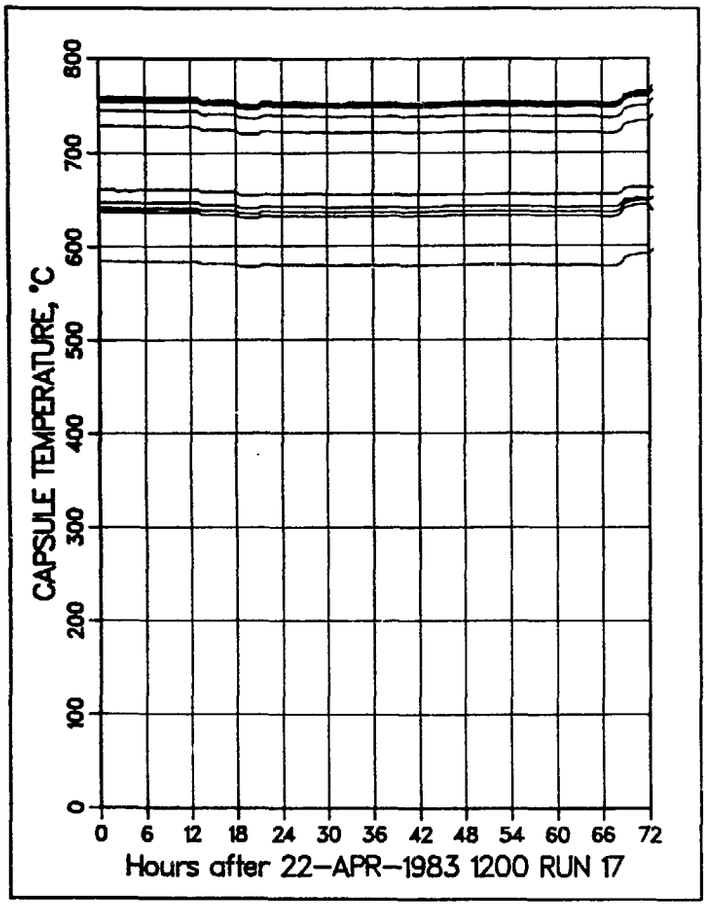

Fig. VI-43. Recorded temperatures for Run 17.

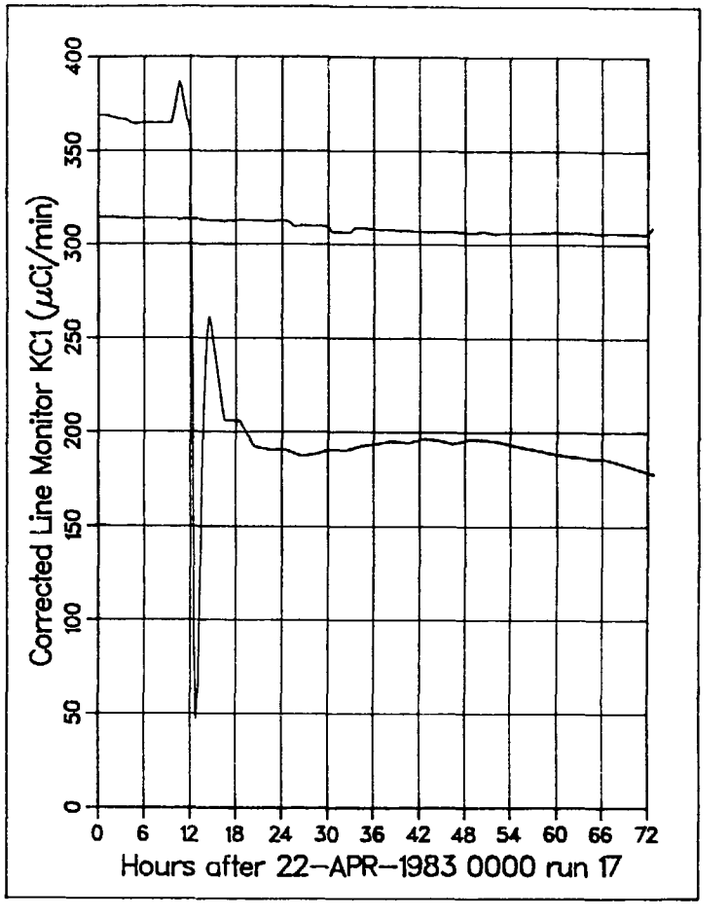

Fig. VI-44. Tritium release rate for Run 17.

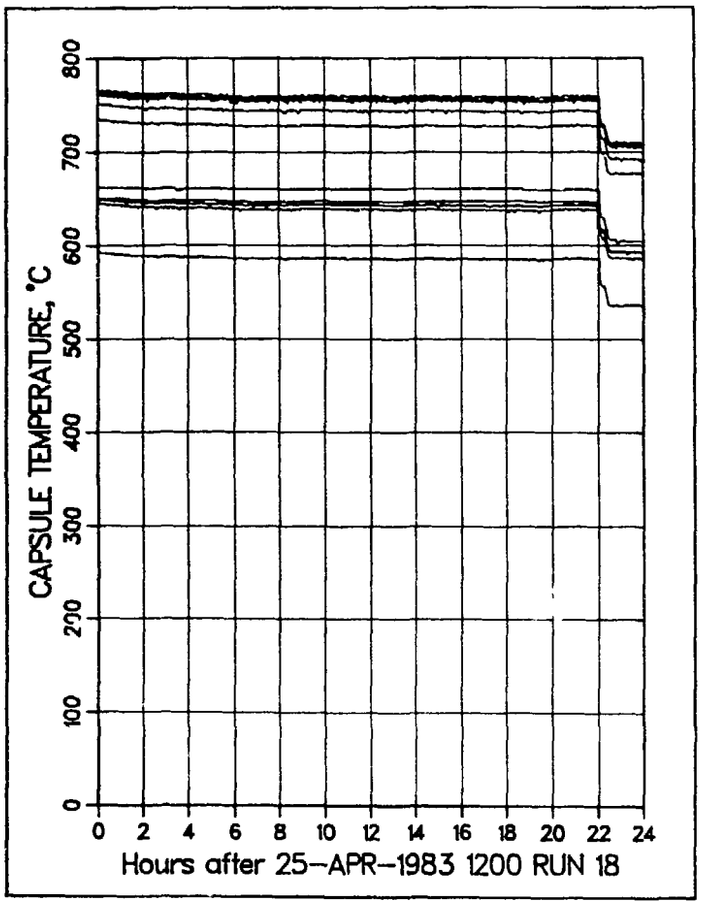

Fig. VI-45. Recorded temperatures for Run 18.

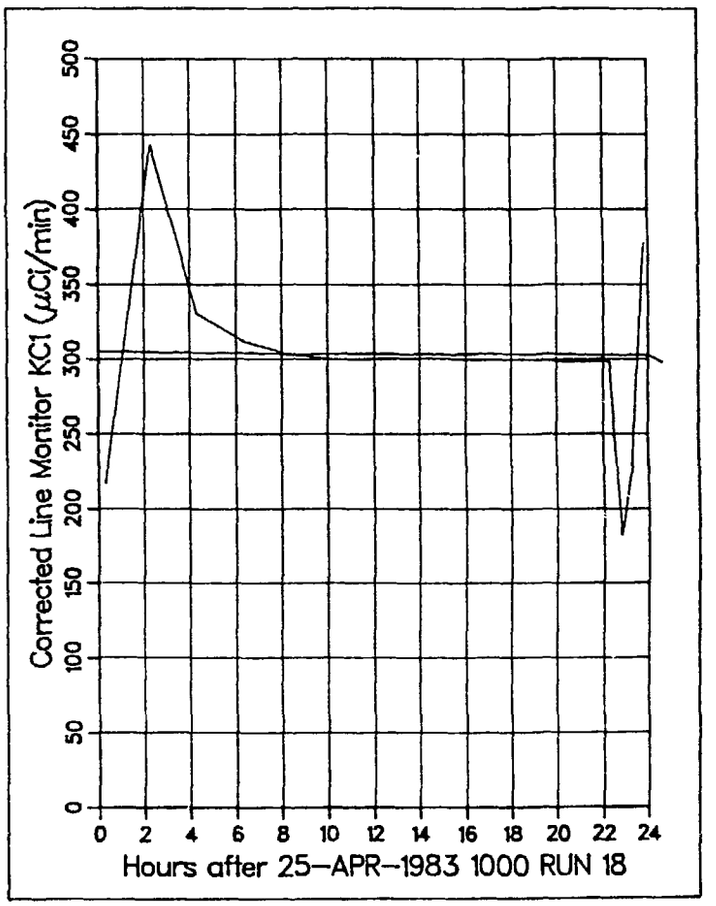

Fig. VI-46. Tritium release rate for Run 18.

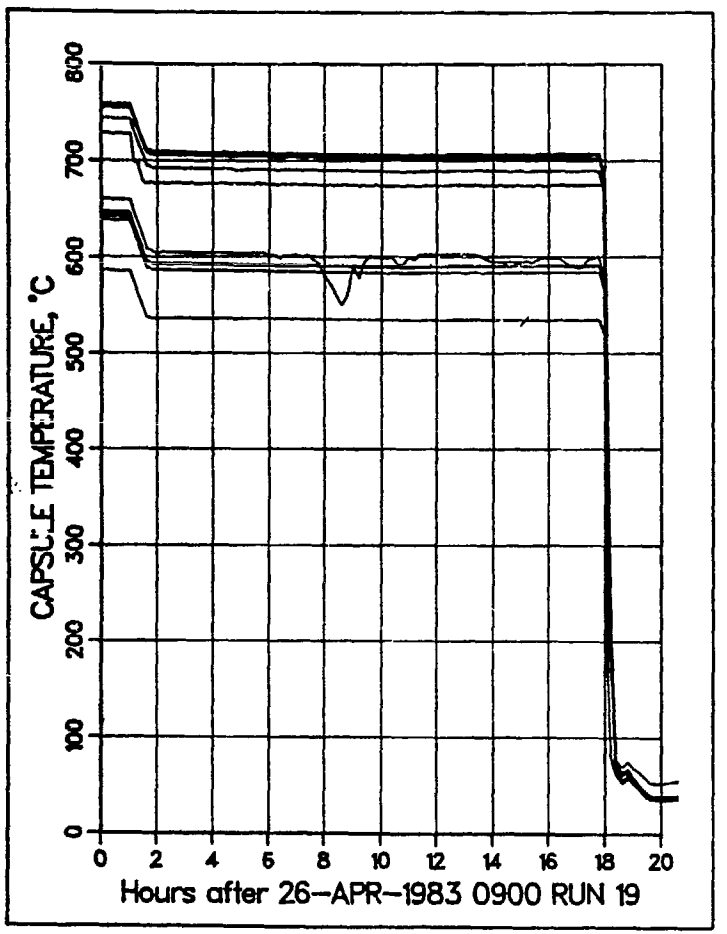

Fig. VI-47. Recorded temperatures for Run 19.

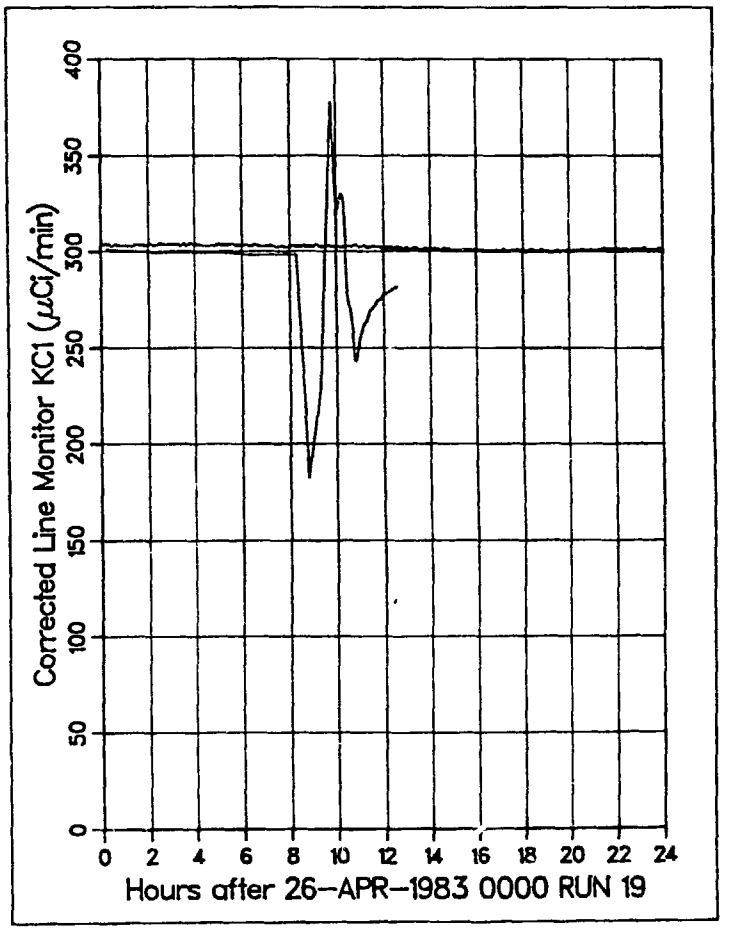

Fig. VI-48. Tritium release rate for Run 19.

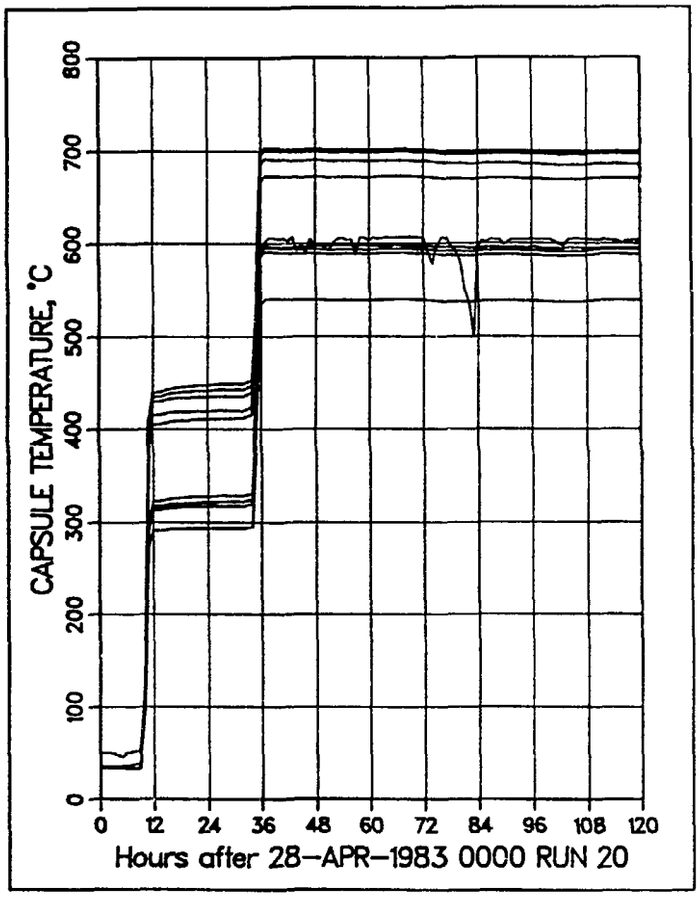

Fig. VI-49. Recorded temperatures for Run 20.

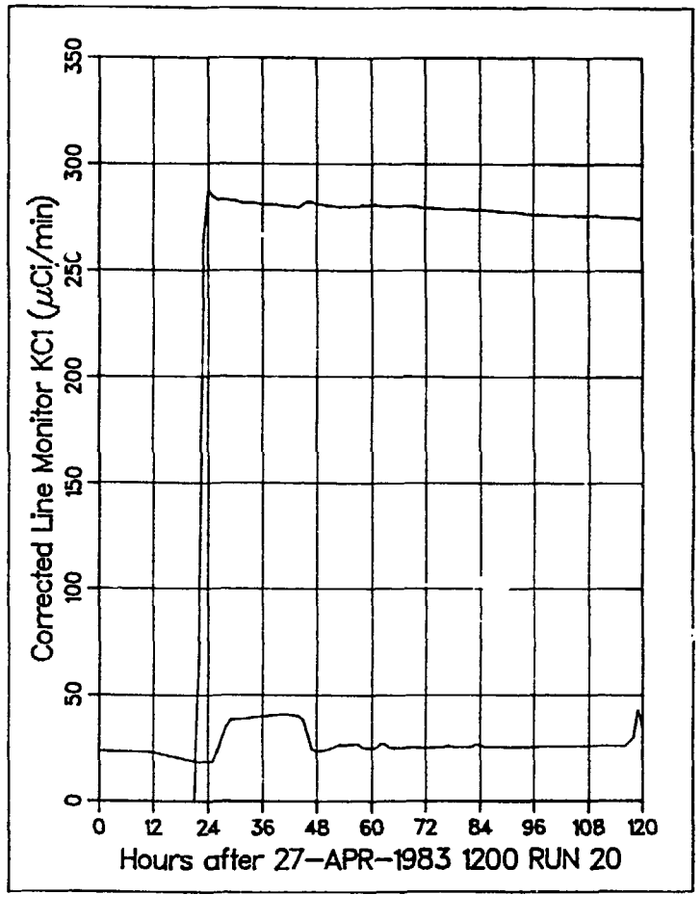

Fig. VI-50. Tritium release rate for Run 20.

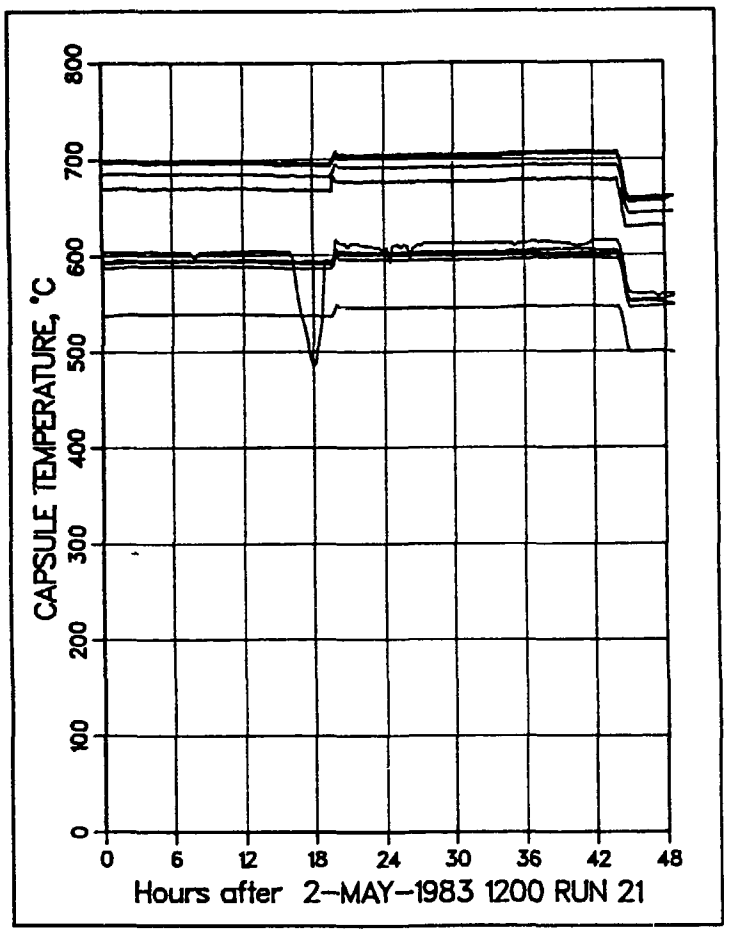

Fig. VI-51. Recorded temperatures for Run 21.

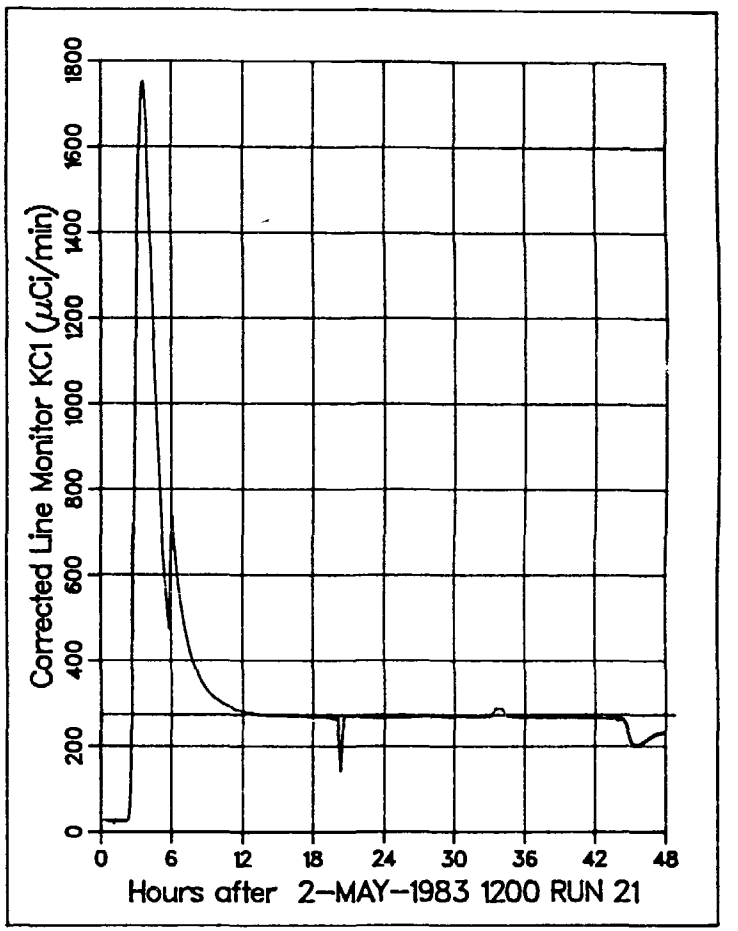

Fig. VI-52. Tritium release rate for Run 21.

tritium release curve shows a very strong positive peak followed by a return to steady state. The temperature perturbation at 0500 on May 3 did not have a noticeable effect upon tritium release.

Run 22 was at a nominal temperature of 600°C with a flow rate of 100 cm^3/min for the sweep gas of helium + 0.1% H_2. The temperature and tritium release data are shown in Figs. VI-53 and -54, respectively. The run represents a decrease of 50°C from Run 21. The temperatures were essentially uniform throughout the course of the run. The tritium release curve has a negative peak, followed by a return to equilibrium conditions. There is a fluctuation at 1500 resulting from temporary pressure and flow changes caused by a sample change.

Run 23 was at a nominal temperature of 550°C with a flow rate of 100 cm^3/min for the sweep gas of helium + 0.1% H_2. The temperature and tritium release data are shown in Figs. VI-55 and -56, respectively. The run represents a decrease in temperature from the prior run. The temperature profiles show the initial temperature drop, followed by an ORR shutdown at 1700 on May 5, an ORR restart at 1900 on May 6, two reactor setbacks, and a number of small step changes in temperature. Owing to the many changes in temperature and neutron flux, the tritium release curve is very complex. It can be said that the temperature decrease at the start of the run caused a negative peak. The release curve at the end of the run appears to approach steady-state conditions.

Run 24 was at a nominal temperature of 600°C with a flow rate of 100 cm^3/min for the sweep gas of helium + 0.1% H_2. The temperature and tritium release data are shown in Figs. VI-57 and -58, respectively. The run was the same as the previous one except that the temperature was higher by 50°C. The temperatures and neutron flux were essentially constant for the duration of the run. The increase in temperature caused a large positive spike in the tritium release curve followed by a return to steady-state conditions within 20 h. The drop in the release curve at the peak maximum is due to a scale change in the tritium monitor.

Run 25 was at a nominal temperature of 560°C with a flow rate of 100 cm^3/min for the sweep gas of helium + 0.1% H_2. The test conditions represent a decrease of 40°C from Run 24. The temperature and tritium release data are shown in Figs. VI-59 and -60, respectively. The temperature data show very

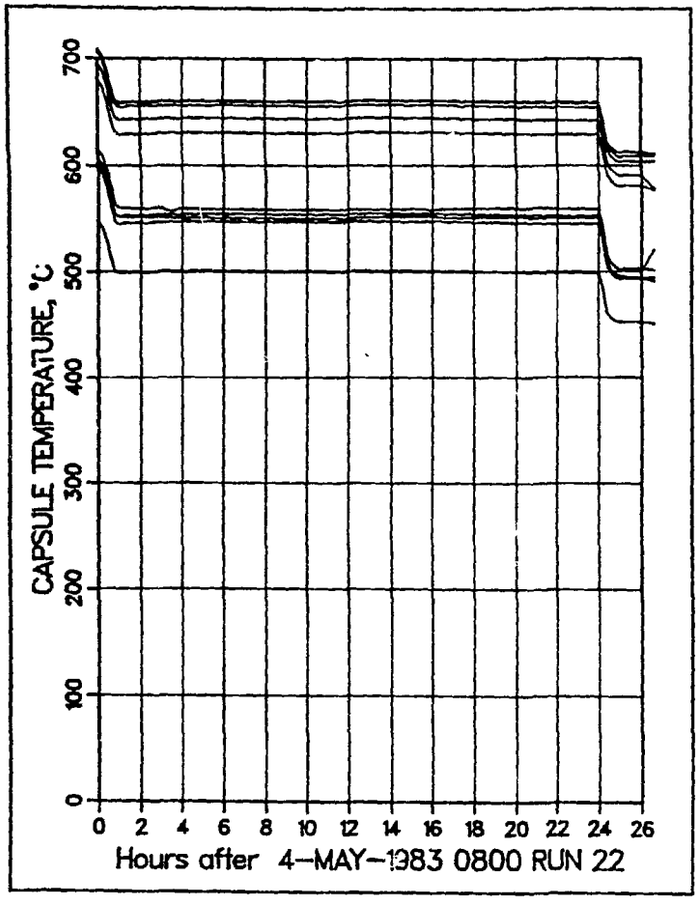

Fig. VI-53. Recorded temperatures for Run 22.

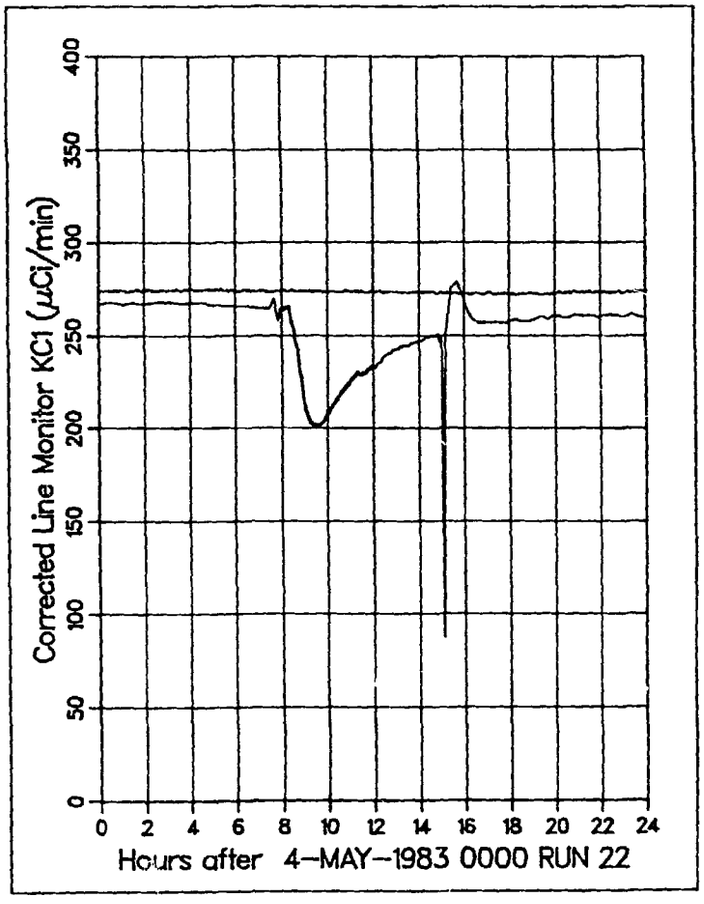

Fig. VI-54. Tritium release rate for Run 22.

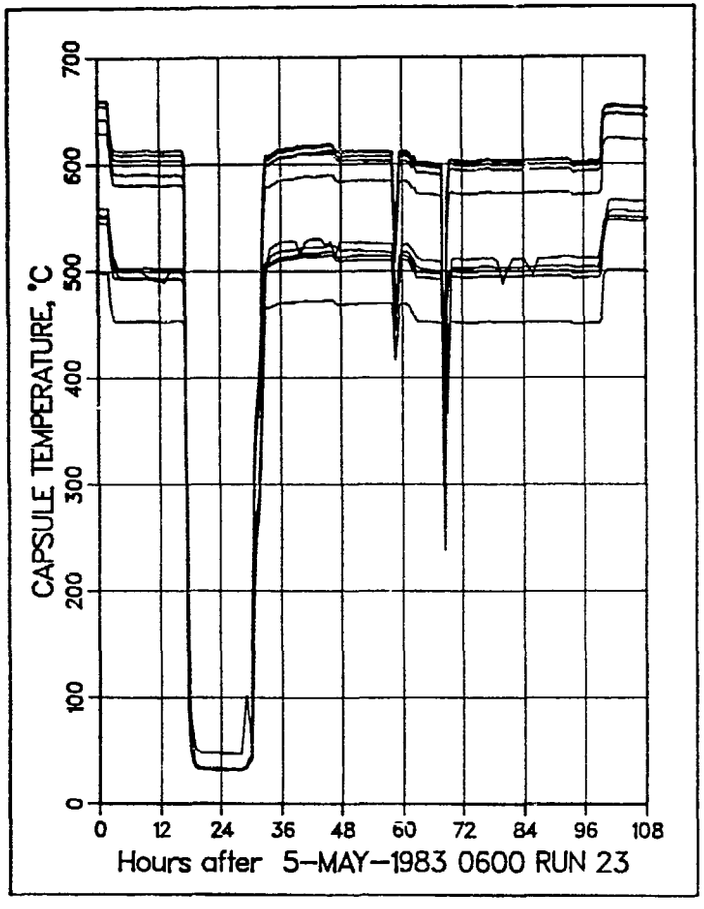

Fig. VI-55. Recorded temperatures for Run 23.

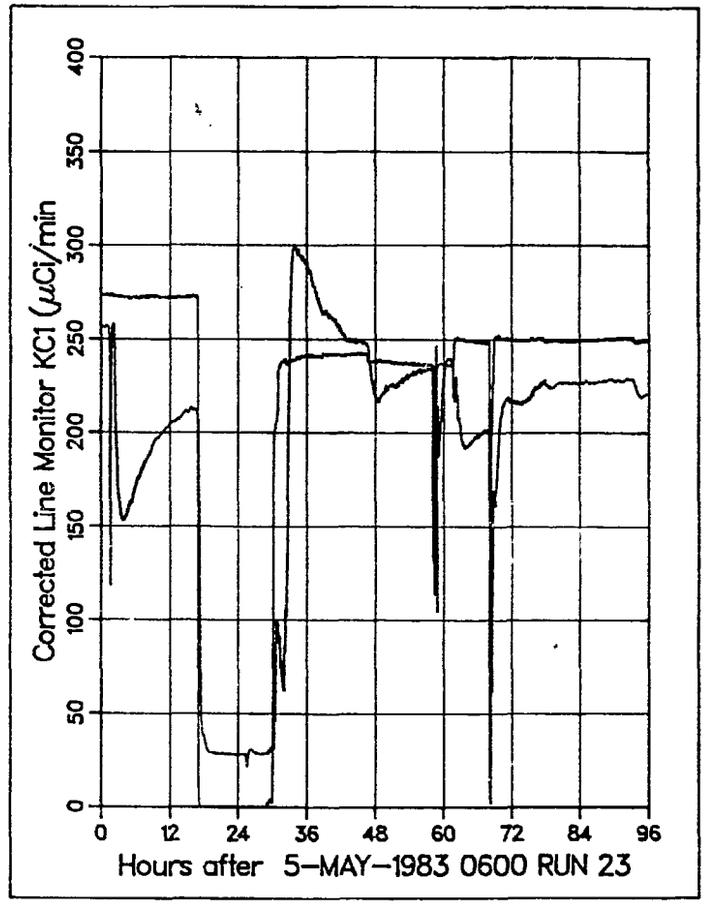

Fig. VI-56. Tritium release rate for Run 23.

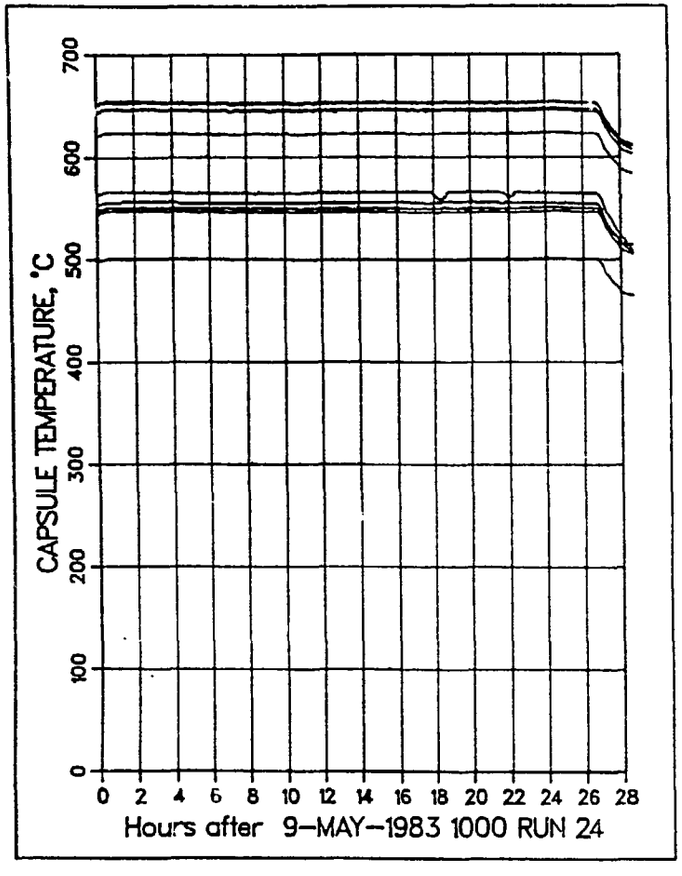

Fig. VI-57. Recorded temperatures for Run 24.

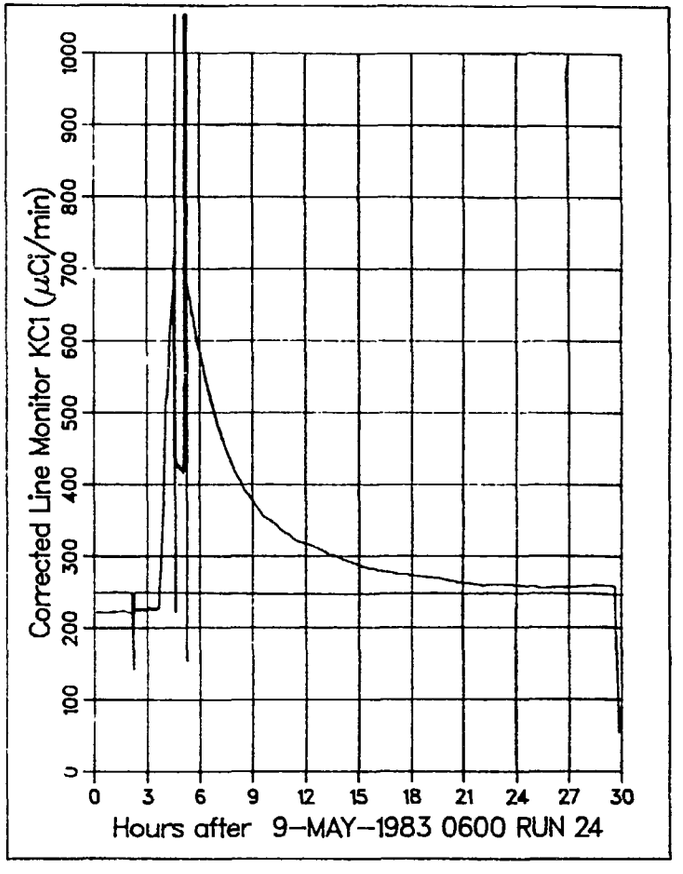

Fig. VI-58. Tritium release rate for Run 24.

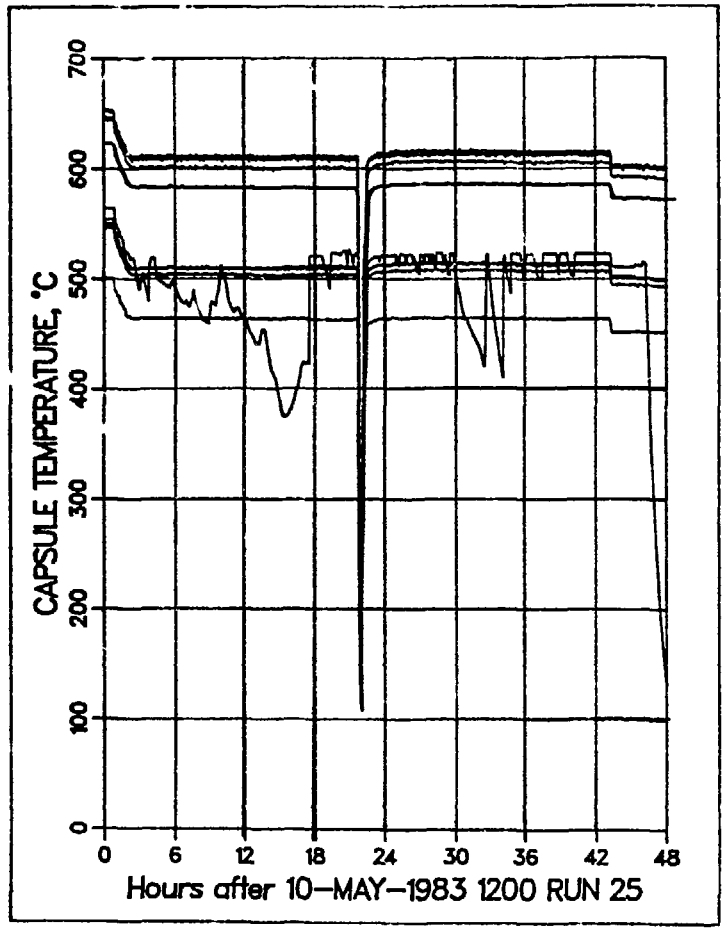

Fig. VI-59. Recorded temperatures for Run 25.

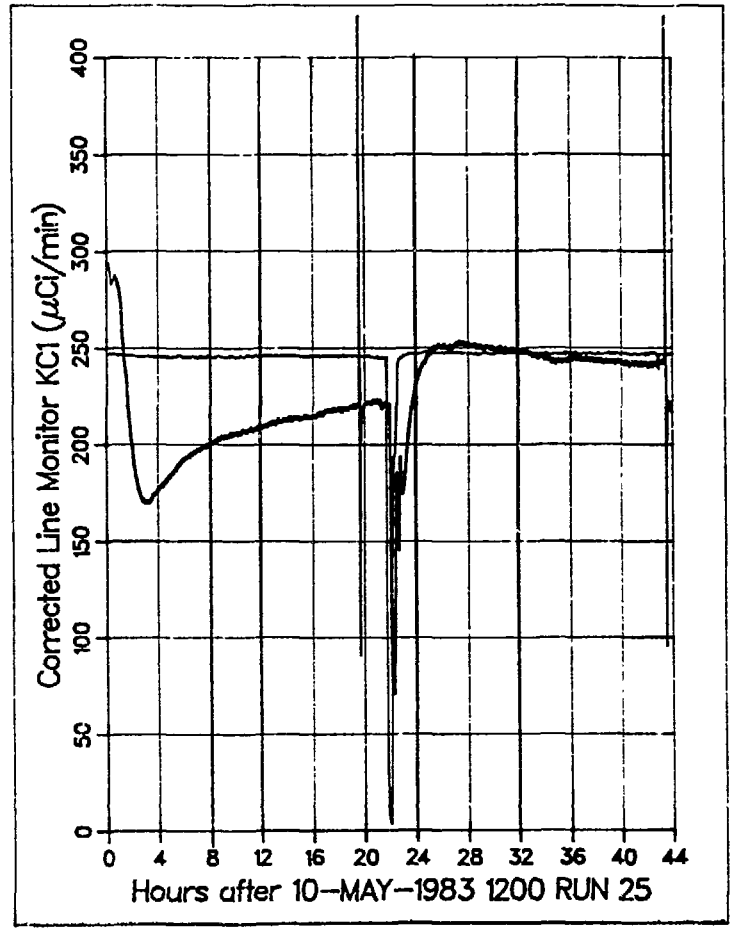

Fig. VI-60. Tritium release rate for Run 25.

constant temperatures except for a reactor setback which occurred at 1045 on May 11. Thermocouple TR901 continued to be erratic. The tritium release curve shows a negative peak followed by a return to equilibrium. The reactor setback resulted in a significant perturbation in the release curve, owing to the drop in temperatures.

Run 26 was at a nominal temperature of 550°C with a flow rate of 100 cm^3/min for the sweep gas of helium + 0.1% H_2. The temperature and tritium release data are shown in Figs. VI-61 and -62, respectively. The test conditions for the run represent a temperature decrease of 10°C from Run 25. In Fig. VI-62 there is a small negative peak followed by a return to steady state in ~70 h. A perturbation resulting from a sample change is observable in this figure at 0700 on May 13.

Run 27 was at a nominal temperature of 525°C with a flow rate of 100 cm^3/min for the sweep gas of helium + 0.1% H_2. The temperature and tritium release data are shown in Figs. VI-63 and -64, respectively. The test conditions of the run represent a temperature decrease of 25°C from Run 26. There was a reactor shutdown followed by a restart at 1400 on May 16. The temperature profiles show that the nominal temperature was dropped from 550 to 525°C at 1200 on May 17. After that time, the reactor power was at 28.5 MW (95% of full power) for the rest of the run. The temperature drop of 25°C results in a negative peak followed by a return to steady state in about 150 h. On the night of May 20, essentially all the sweep gas leaked into a glovebox; the amount lost was calculated to be 0.16 Ci. No measurable tritium was detected in the room. The levels of tritium in the glovebox (Fig. VI-65) rose to about 15,000 $\mu Ci/m^3$.

Run 28 was at a nominal temperature of 500°C with a flow rate of 100 cm^3/min for the sweep gas of helium + 0.1% H_2. The temperature and tritium release data are shown in Figs. VI-66 and -67, respectively. The run represents a decrease in temperature of 25°C from Run 27. The temperature readout from TR901 was still giving problems; thus the negative spikes on May 26 are due to recording problems and not temperature variations. There is a five-degree increase in temperature at 1700 on May 29, owing to a slight increase in neutron flux. The tritium release curve shows a negative peak followed by a slow return to equilibrium after about 170 h (7 days). There are a number of oscillations in the tritium release curve, which were caused by small changes in temperature and in flow conditions.

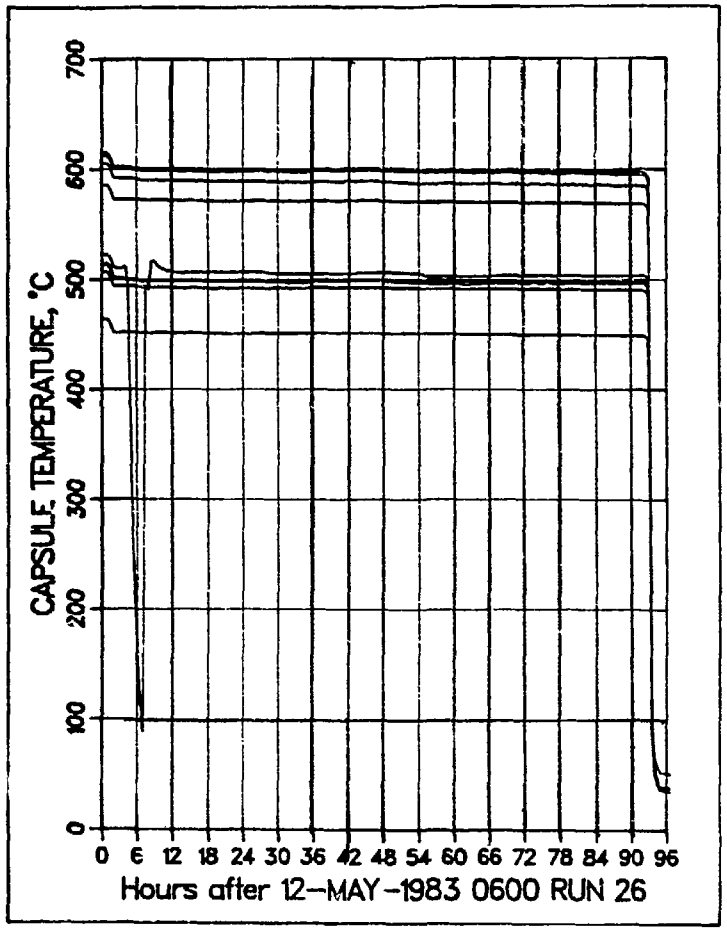

Fig. VI-61. Recorded temperatures for Run 26.

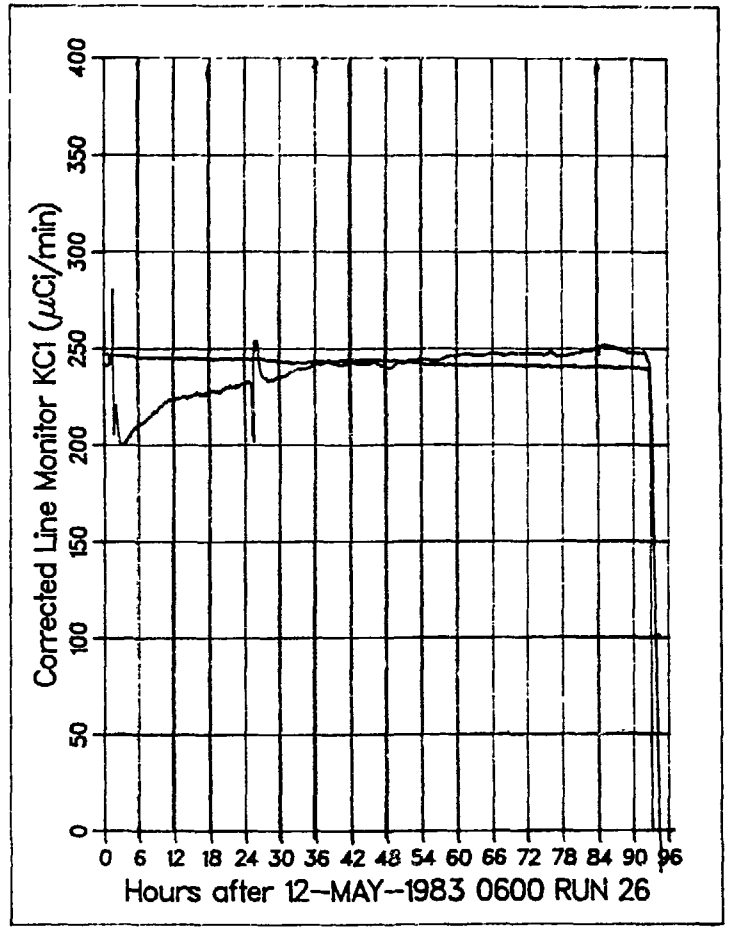

Fig. VI-62. Tritium release rate for Run 26.

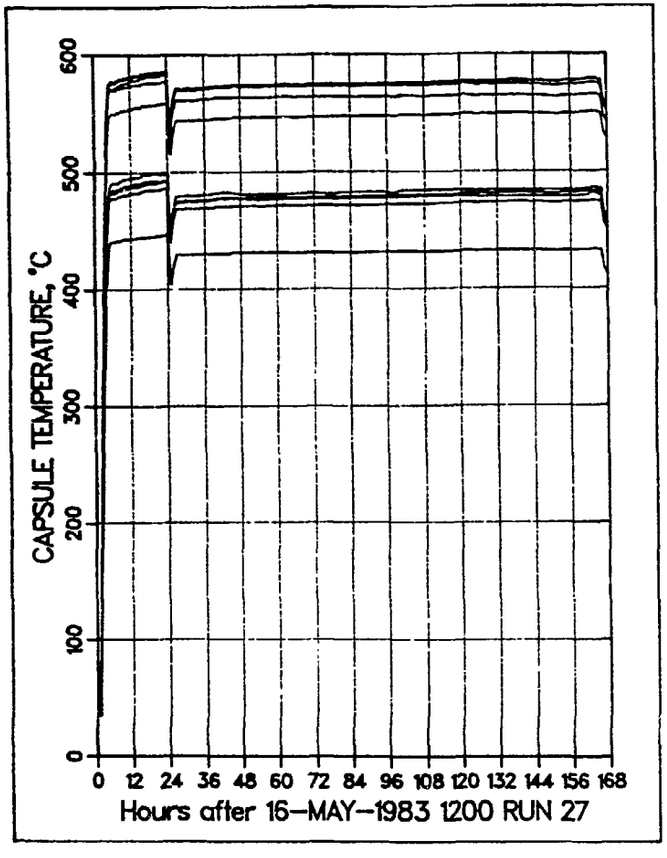

Fig. VI-63. Recorded temperatures for Run 27.

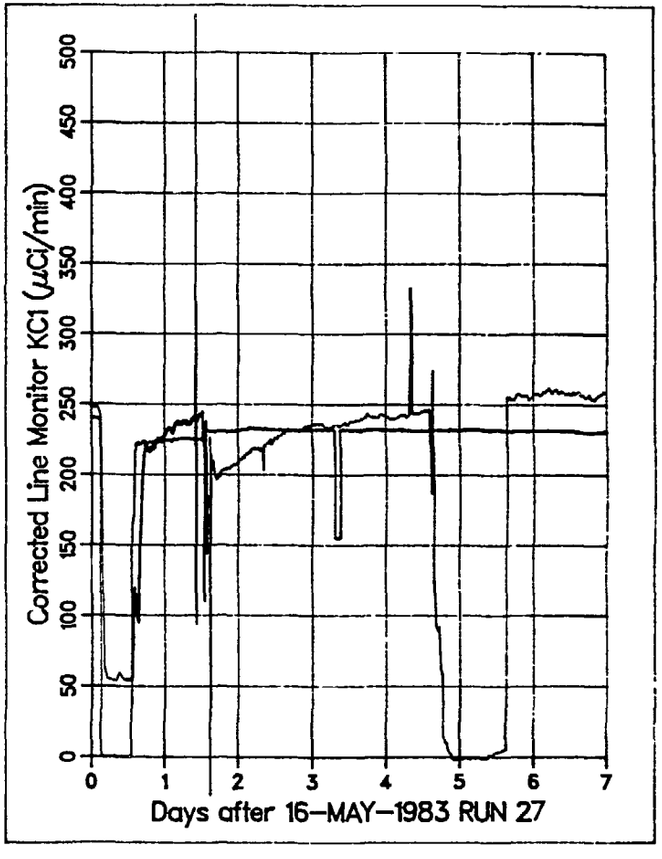

Fig. VI-64. Tritium release rate for Run 27.

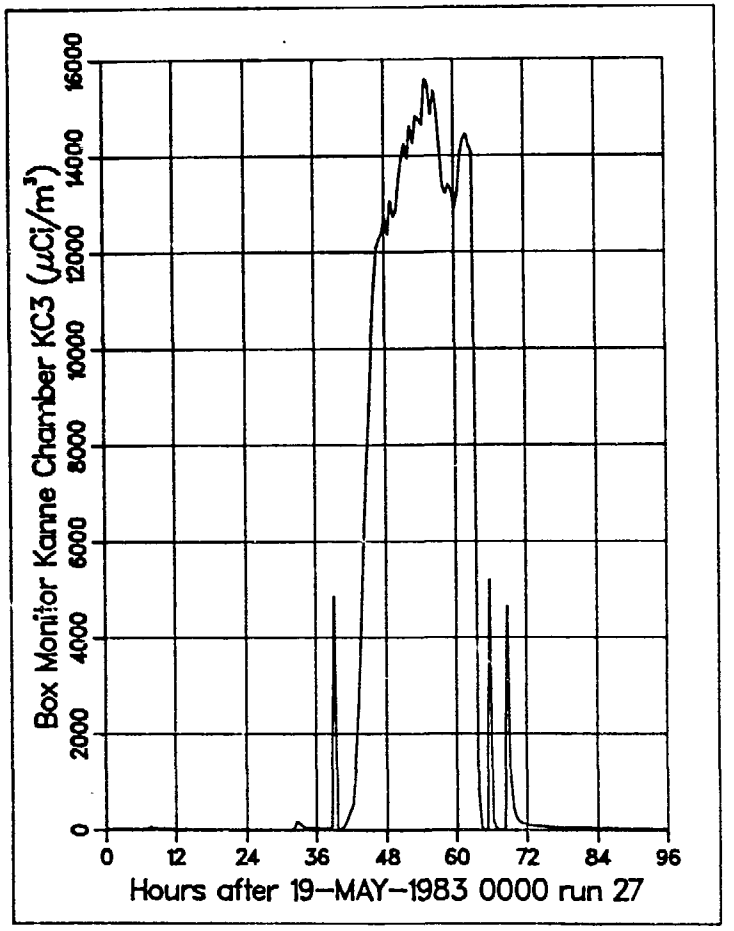

Fig. VI-65. Tritium leaked into glovebox after May 20.

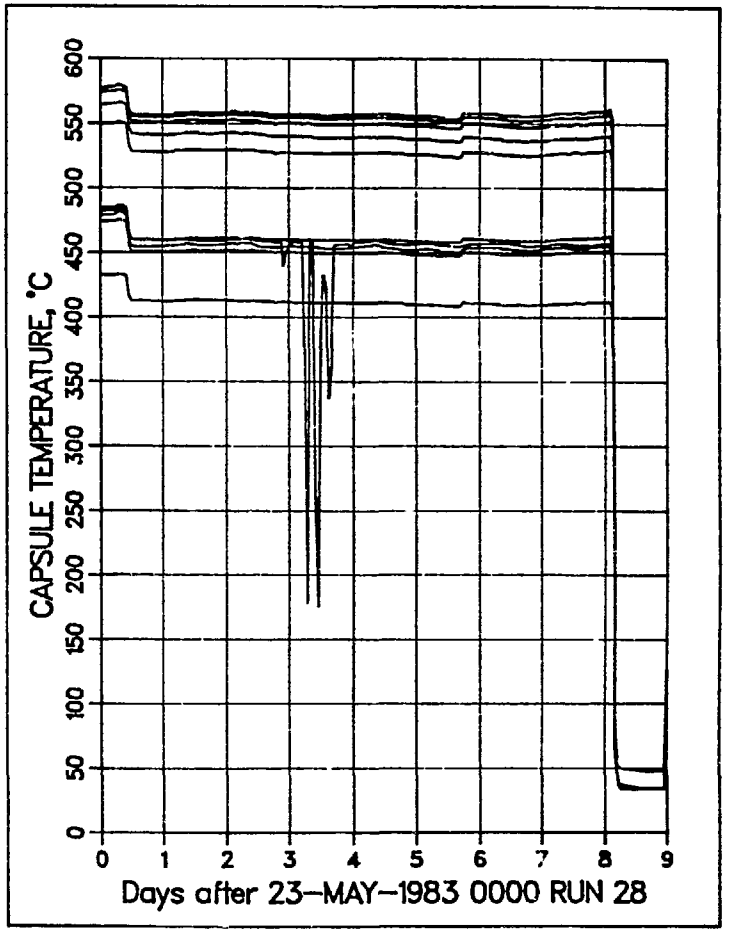

Fig. VI-66. Recorded temperatures for Run 28.

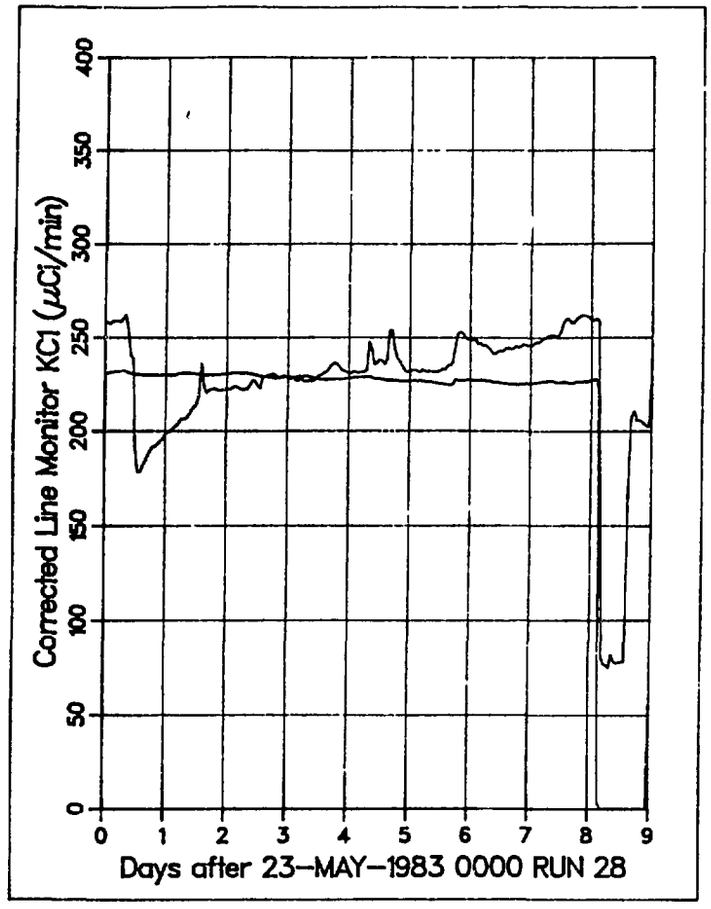

Fig. VI-67. Tritium release rate for Run 28.

Run 29 was at a nominal temperature of 480°C with a flow rate of 300 cm^3/min for the sweep gas of helium + 0.1% H_2. The temperature and tritium release data are shown in Figs. VI-68 and -69, respectively. The test conditions of the run represent a decrease in temperature of 20°C and a threefold increase in flow from Run 28. The temperature profile reflects a reactor shutdown on June 1 and some temperature oscillations on June 2. The tritium release curve shows overall a negative peak followed by a slow approach to equilibrium. The run does not appear to reach steady-state conditions.

Run 30 was at a nominal temperature of 480°C with a flow rate of 100 cm^3/min for the sweep gas of helium + 0.1% H_2. The temperature and tritium release data are shown in Figs. VI-70 and -71, respectively. Figure VI-70 shows that the temperatures were essentially constant for the run. The tritium release curve shows a slow approach to equilibrium; steady-state

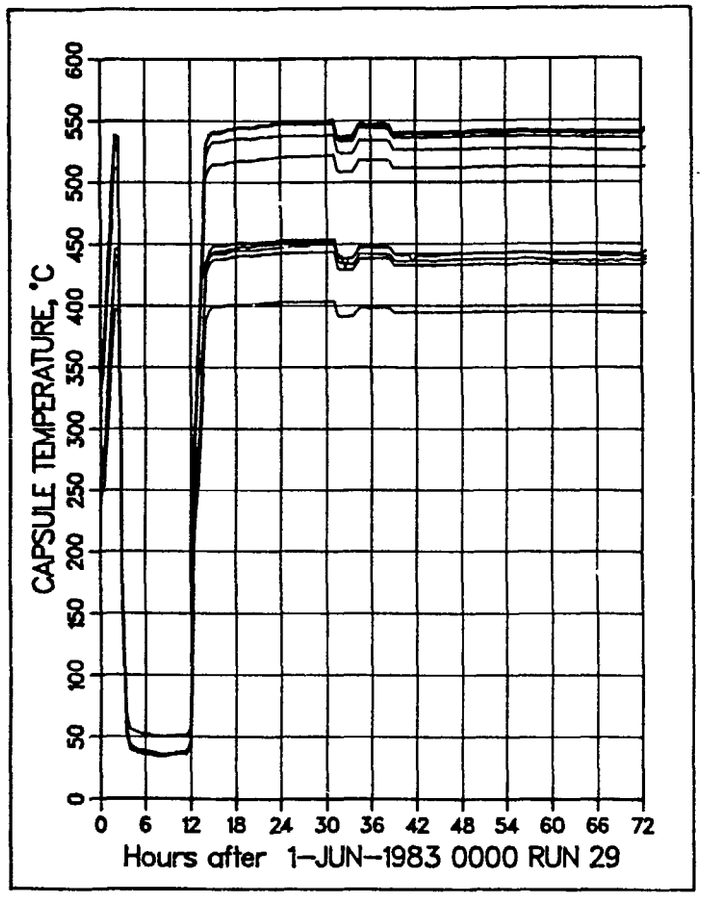

Fig. VI-68. Recorded temperatures for Run 29.

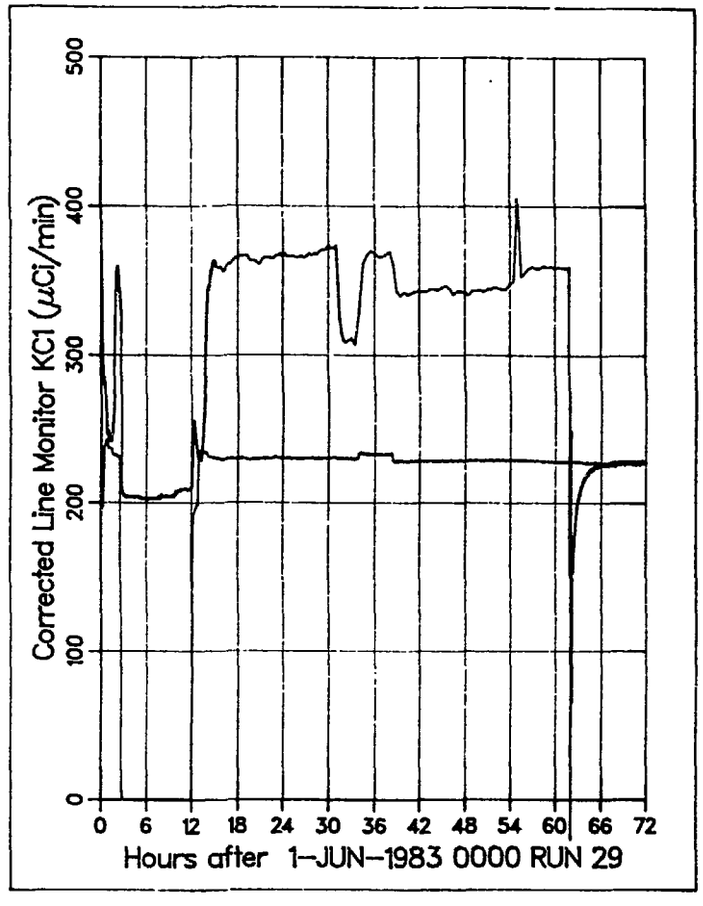

Fig. VI-69. Tritium release rate for Run 29.

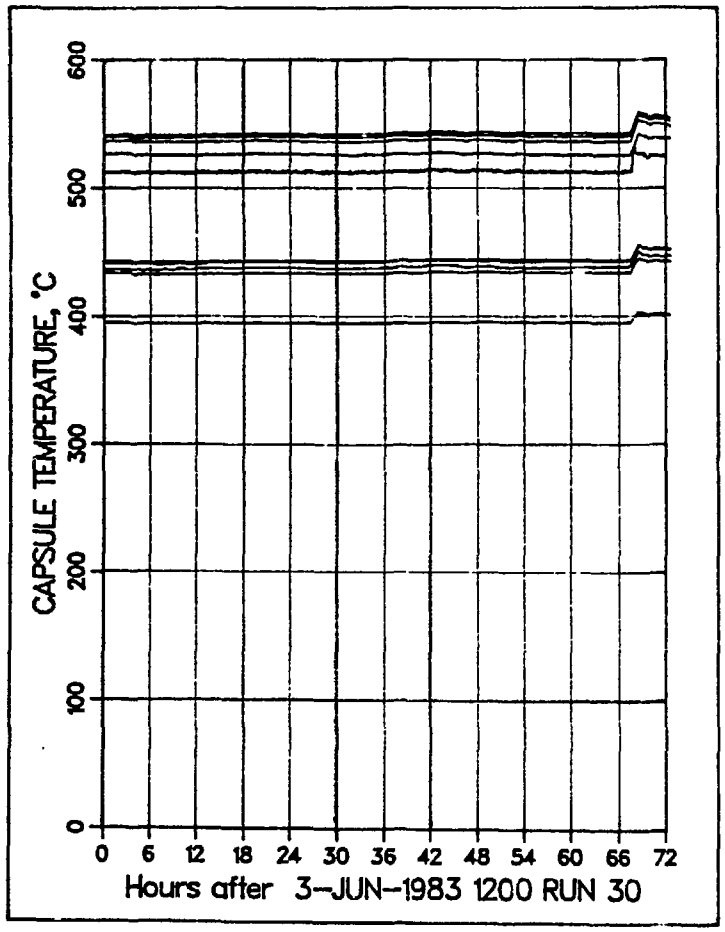

Fig. VI-70. Recorded temperatures for Run 30.

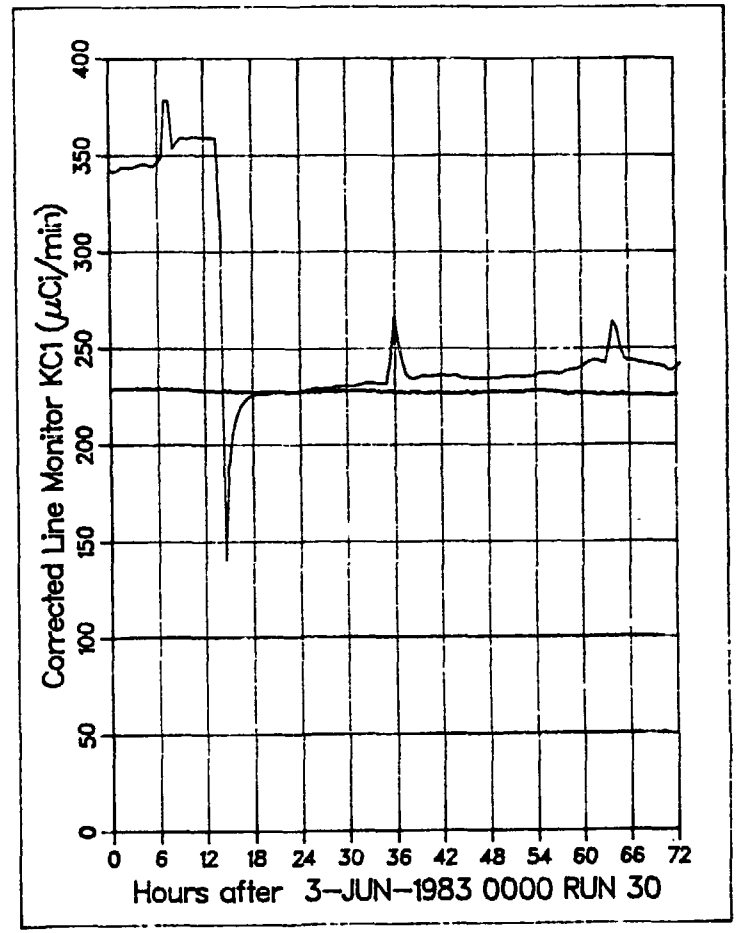

Fig. VI-71. Tritium release rate for Run 30.

conditions are needed after ~6 days at 480°C, including the time at this temperature from Run 29.

Run 31 was at a nominal temperature of 500°C with a flow rate of 100 cm^3/min for the sweep gas of helium + 0.1% H_2. The temperature and tritium release data are shown in Figs. VI-72 and -73, respectively. The run represents a 20°C temperature increase from Run 30. The tritium release curve shows a small positive peak followed by a return to steady state in about 40 h.

Run 32 was at a nominal temperature of 550°C with a flow rate of 100 cm^3/min for the sweep gas of helium + 0.1% H_2. The temperature and tritium release data are shown in Figs. VI-74 and -75, respectively. The run represents a 50°C temperature increase from Run 31. The tritium release curve shows a large positive spike followed by a return to equilibrium conditions. The run was terminated before the system reached steady state. There are again oscillations in the tritium signal owing to changes in scale.

Run 33 was at a nominal temperature of 650°C with a flow rate of 100 cm^3/min for the sweep gas of helium + 0.1% H_2. The temperature and tritium release data are shown in Figs. VI-76 and -77, respectively. The run represents a return to reference conditions. Since Run 33 was the last one, time was allowed to permit equilibration. The tritium release curve shows a very strong peak followed by a return to steady state within 20 h.

G. Release Rates of HTO, Condensable Form

The release rate of the HTO, or the condensable form, was not continually monitored in the way that HT was. Rather, samples were taken over various time intervals. These data were presented in tabular form in Sec. VI.E. It is of some interest to determine the actual release rate of HTO. Therefore, the data presented in Sec. VI.E were used to calculate HTO release rates. These data are not instantaneous but average release rates over the time the sample was collected. Rather than a smooth curve, the release rate appears as a series of bar graphs.

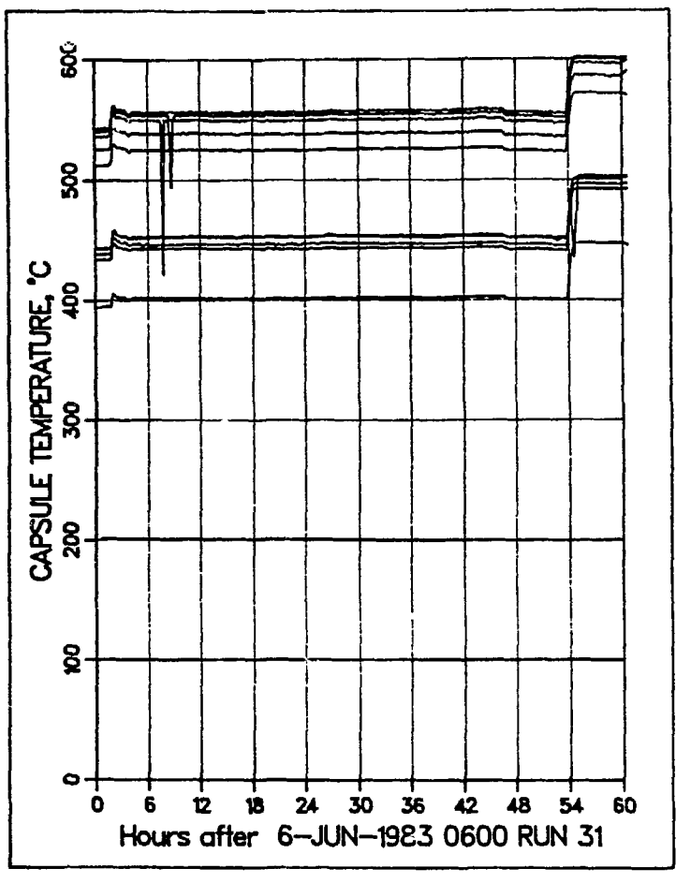

Fig. VI-72. Recorded temperatures for Run 31.

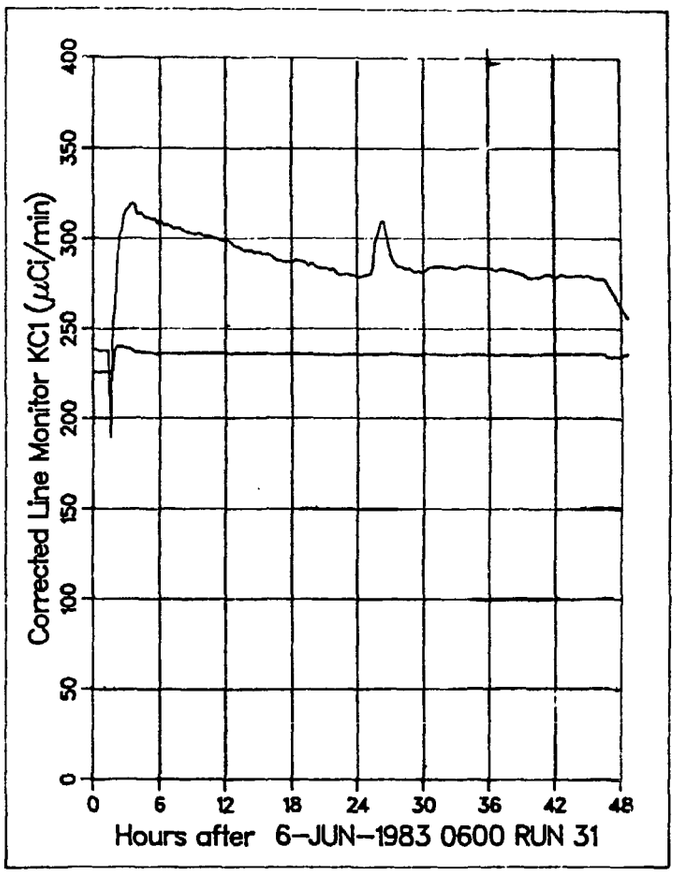

Fig. VI-73. Tritium release rate for Run 31.

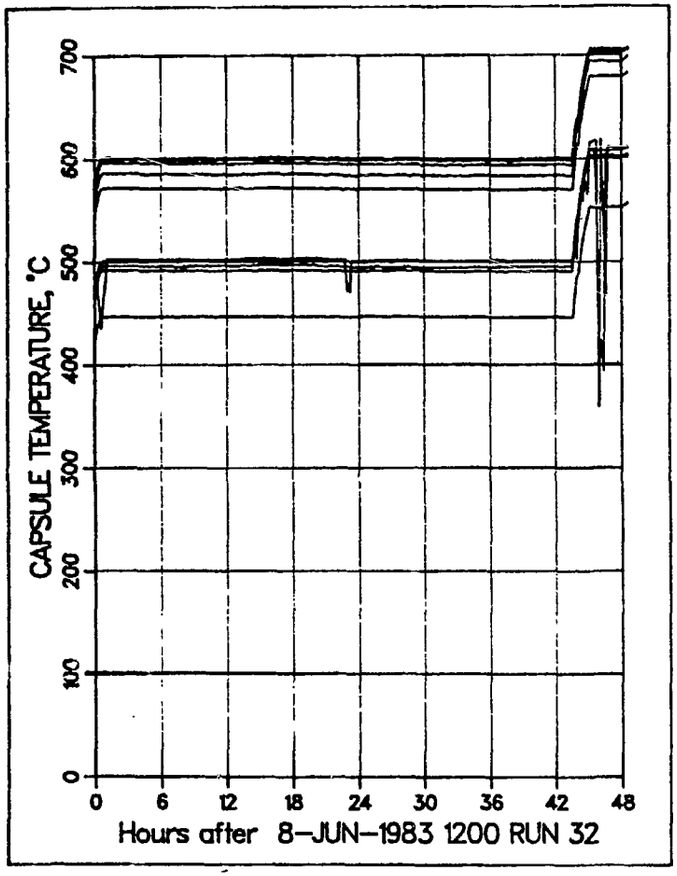

Fig. VI-74. Recorded temperatures for Run 32.

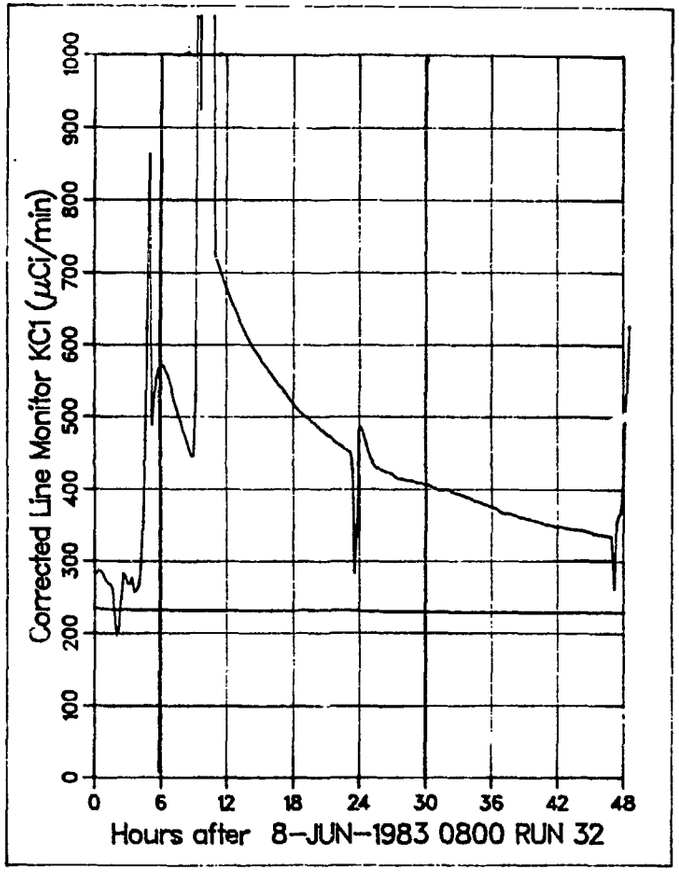

Fig. VI-75. Tritium release rate for Run 32.

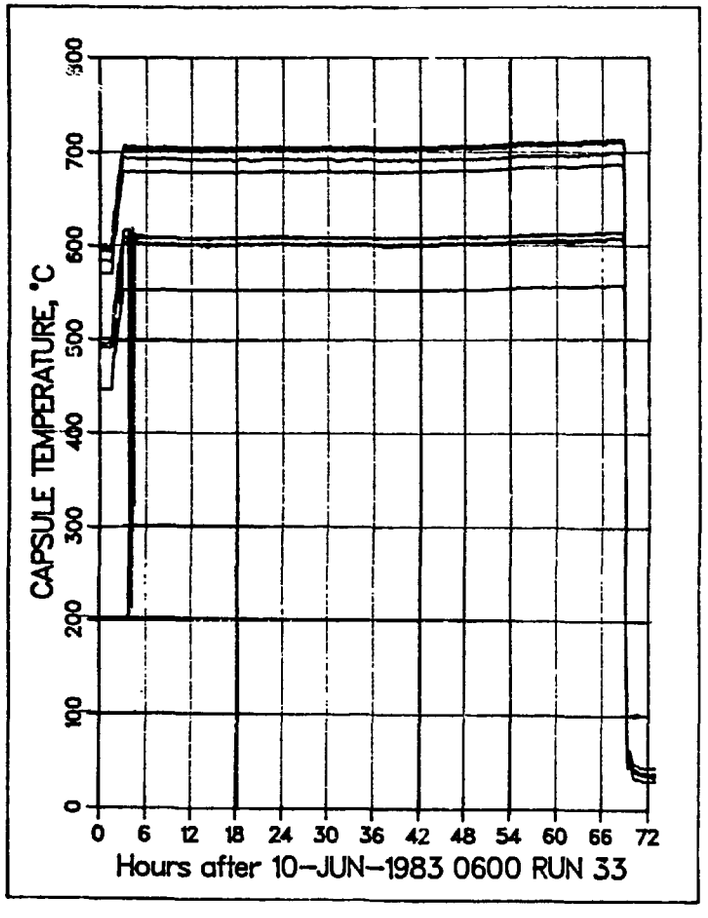

Fig. VI-76. Recorded temperatures for Run 33.

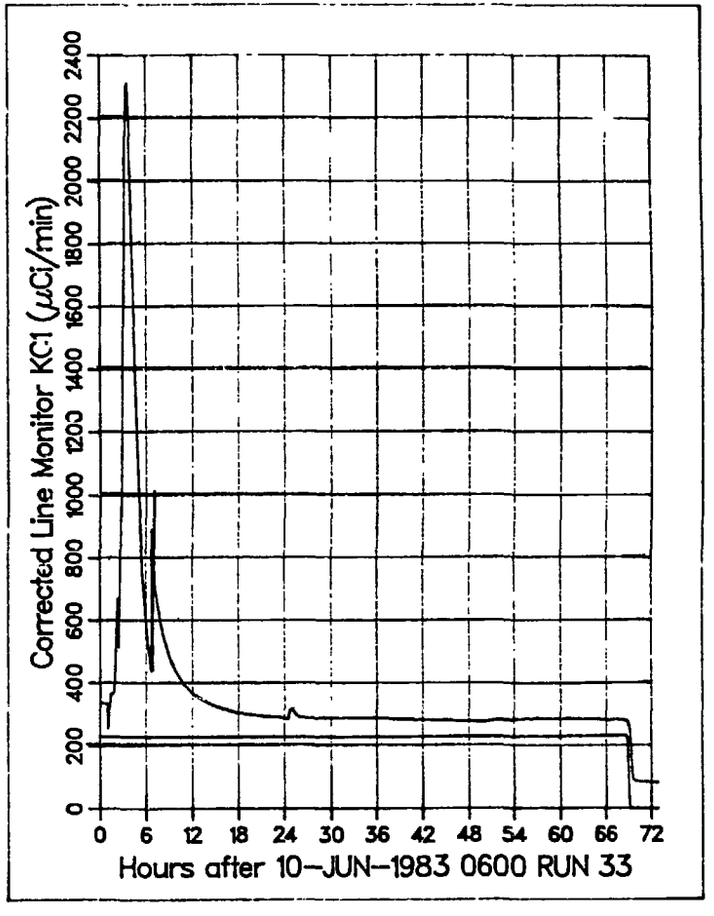

Fig. VI-77. Tritium release rate for Run 33.

1. Runs 0-4

The HTO release rates for the first four runs are given in Fig. VI-78. One can see a small peak for Run 0, which coresponds to a small but finite release of HTO at ~200°C. Run 1 has a rather large peak of ~50 μCi/min followed by rapid decline. This peak is ~15% of the HT release rate (see Fig. VI-9). For an extended period of time, the HTO release rate declines to below 10 μCi/min, then below 1 μCi/min. The initial peak for HTO released appears to be associated with an initial experimental condition, such as outgassing the final traces of moisture from the $LiAlO_2$ ceramic. The HTO release rate for Run 1 is shown in more detail in Fig. VI-79.

A small peak is observed at hour 180 in Fig. VI-78. This peak occurs ~24 h after the sharp spike in the HT release curve, at the beginning of Run 3. Run 3 was at 700°C with 1% H_2 added to the sweep gas.

2. Runs 4-20

The HTO release rates for Runs 4-20 are given in Figs. VI-80 through -83. During this period the HTO release rate was small but finite. The release rate curves may have some structure, but the peaks do not instantaneously correlate to HT peaks. It appears that delays of about a day may occur between the onset of large HT peaks and that of HTO peaks. The HTO release curves for Runs 4-19 are discussed below.

The HT curves in Runs 4 and 5, for which the temperature was decreased to 500-550°C (Figs. VI-15 and -17) show strong negative peaks. These runs are represented by the first 100 h in Fig. VI-80. The HTO release curve shows a continual decrease during this period. Run 6 (temperature increased from 500 to 550°C) begins at hour 108 in Fig. VI-80. There is a strong positive peak in the HT curve (Fig. VI-19); an observable peak occurs in the HTO curve ~12 h later. Run 7 begins at hour 130 in Fig. VI-80, but because only one sample was taken, it is not possible to resolve any HTO peak. Run 8 begins at hour 12 in Fig. VI-81. There may be an HTO peak at the start of the run and one about 36 h after the beginning of the run.

Runs 9 (650°C), 10 (400°C), and 11 (500°C) are represented in Fig. VI-82. All three runs had no hydrogen added to the helium sweep gas. Reactor shutdowns took place at hours 144 and 264; no HTO release is indicated when the

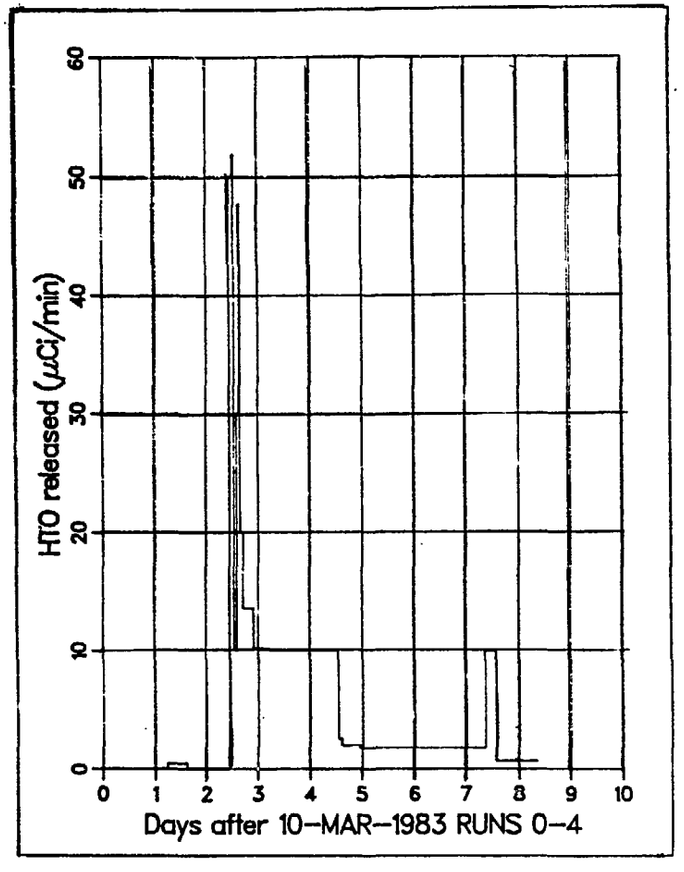

Fig. VI-78. HTO release rates for Runs 1-4.

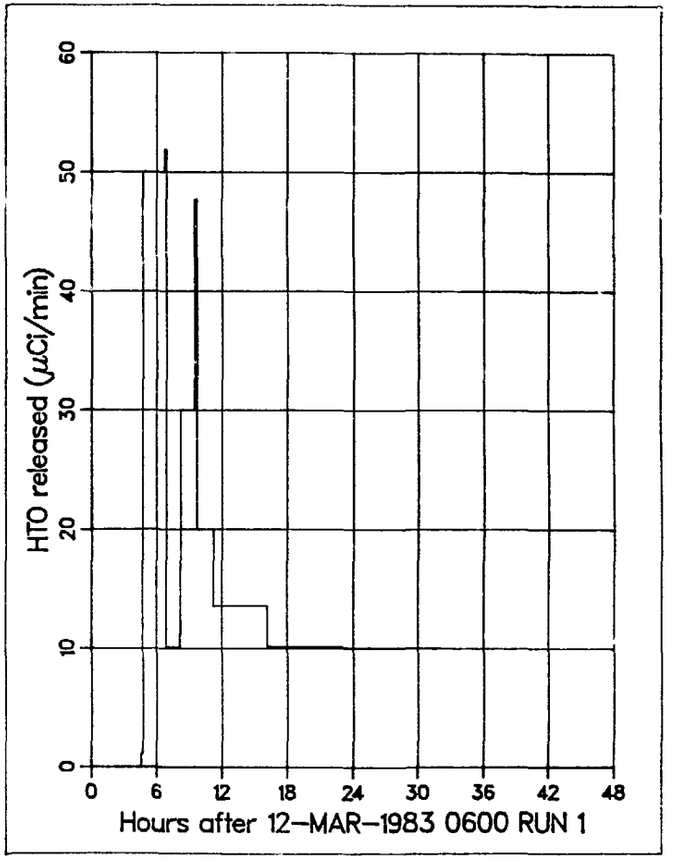

Fig. VI-79. HTO release rate for Run 1.

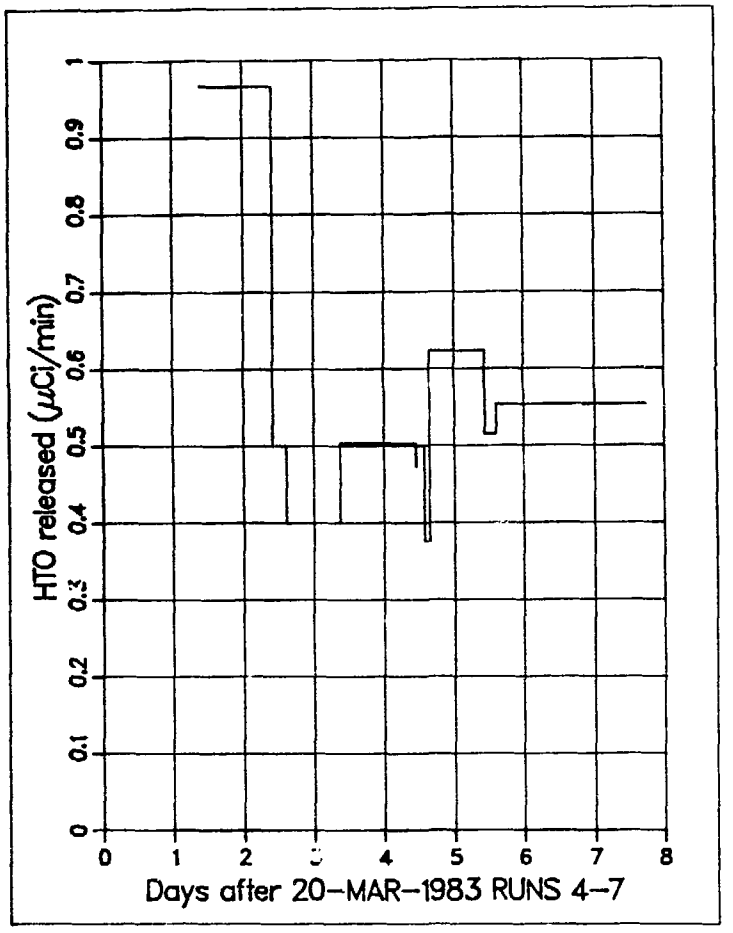

Fig. VI-80. HTO release rate for Runs 4-7.

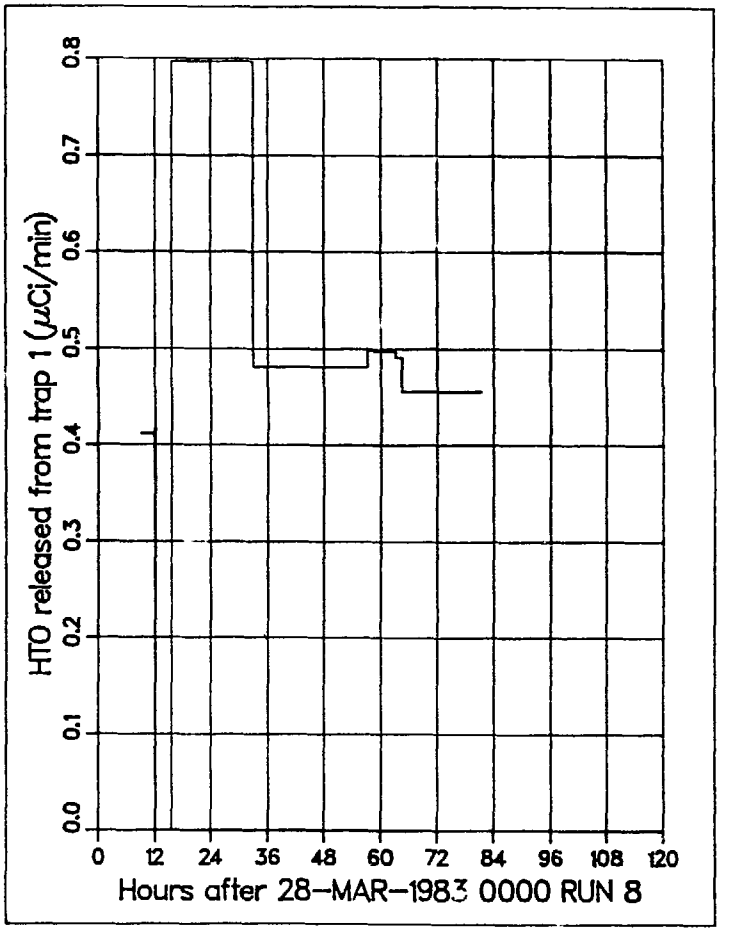

Fig. VI-81. HTO release rate for Run 8.

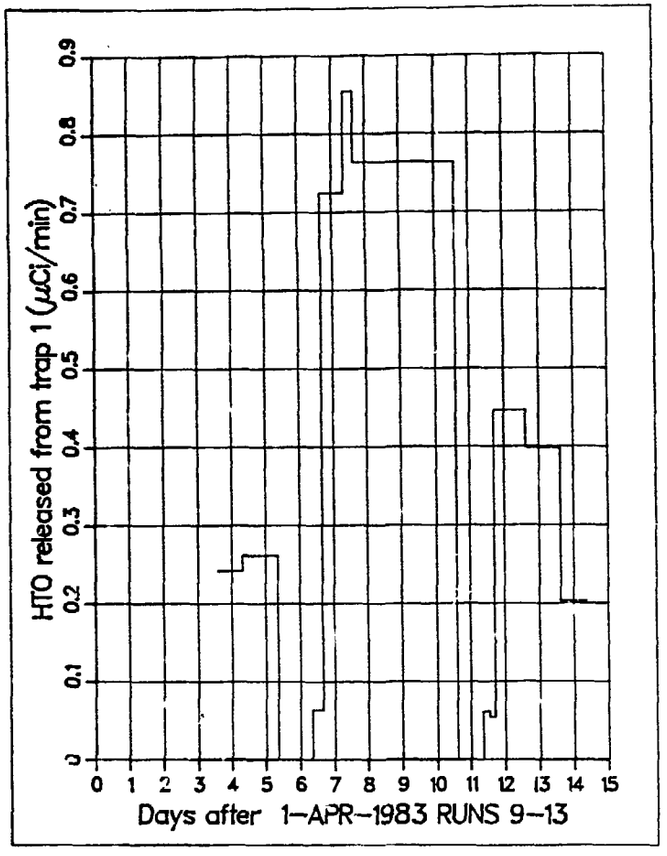

Fig. VI-82. HTO release rate for Runs 9-13.

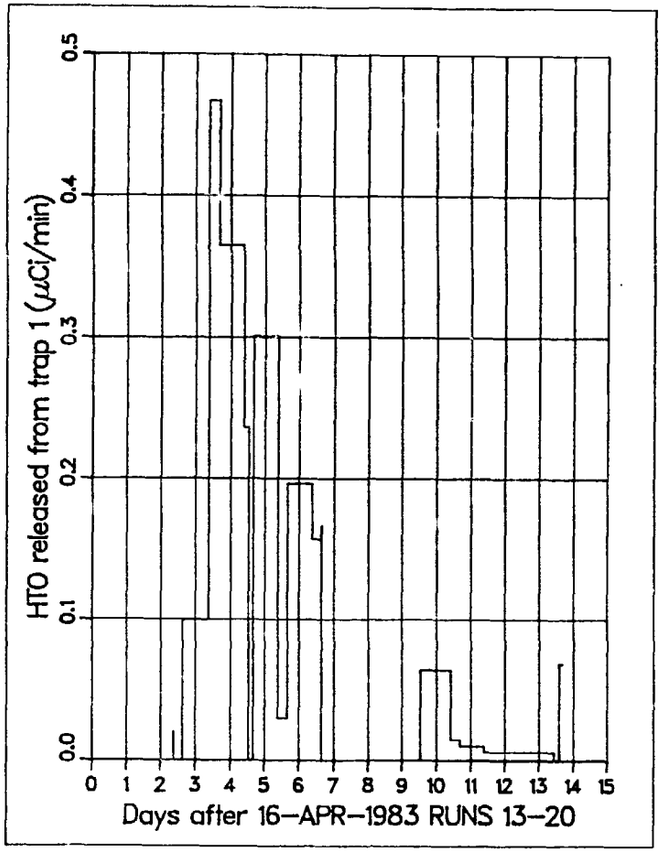

Fig. VI-83. HTO release rate for Runs 13-20.

reactor is down. In each case, a small spike appears in the HTO release curve ~24 h after reactor startup.

Figure VI-83 shows the HTO release rate for Runs 13-20. Run 14 (700°C - no H_2 added) begins at hour 60. The HT release curve (Fig. VI-34) shows a strong positive peak at 1700 on April 18 (hour 65 in Fig. VI-83). The HTO release curve shows a peak ~24 h later. There is not sufficient resolution to tell if there are HTO peaks associated with Runs 15-19.

3. Runs 20-30

Run 20 was at a nominal temperature of 650°C, with 0.1% oxygen added to the sweep gas for April 29 until May 2. The HTO release rate for Runs 20-30 are shown in Figs. VI-84 through -87. During Run 20, essentially no tritium was released, either as HT or HTO. However, for the next several weeks after Run 20, the HTO release curve rose dramatically, to a peak of 150 μCi/min at the beginning of Run 29 (see Figs. VI-86 and -87). This peak occured 30 days after Run 20 had ended. This large peak also does not seem to correlate with the test conditions of Runs 21-30; it is therefore attributed to the effects of Run 20. As noted above, HTO peaks often occur ~24 h after the HT peaks. It is inferred that HTO exits the system ~24 h after it has been released from the breeder in the capsule. The fact that some 30 days elapsed before the HTO created in Run 20 was released suggests that the HTO from Run 20 was trapped on the surface of the breeder material. Over a period of 30 days, the HTO on the breeder surface was gradually released.

In addition to the large HTO peak, there is some evidence of structure in the HTO release curves for Runs 21-30. Run 21 begins at hour 132 in Fig. VI-84. About 12 h later an HTO peak appears to form. A reactor shutdown occurred at hour 216, followed by a restart at hour 224. An observable HTO spike occured ~20 h after startup. Run 24 (600°C) has a large HT spike at 1100 on May 9 (see Fig. VI-58), which corresponds to hour 300 in Fig. VI-84. Some 30 h later the HTO curve showed a peak; which may be associated with the phenomena of Run 20. An HTO peak appears ~24 h after reactor startup (Fig. VI-86), which occurred at hour 108.

Run 31 is depicted in Fig. VI-88. The HT release curve ws given in Fig. VI-73. There appears to be a flow transient at 0800 on June 6, which generated a sharp, narrow spike in both the HT and HTO release curves. The HT peak

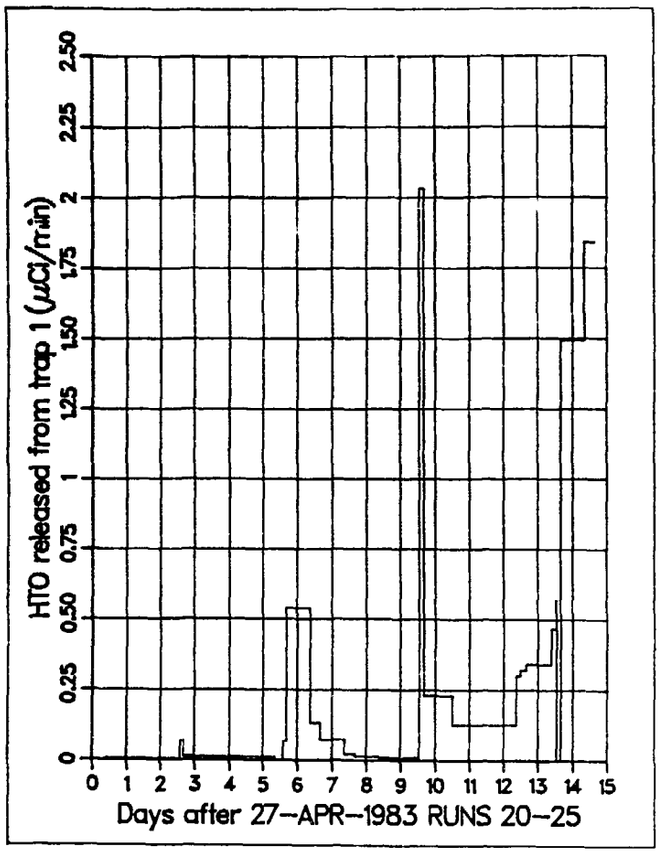

Fig. VI-84. HTO release rate for Runs 20-25.

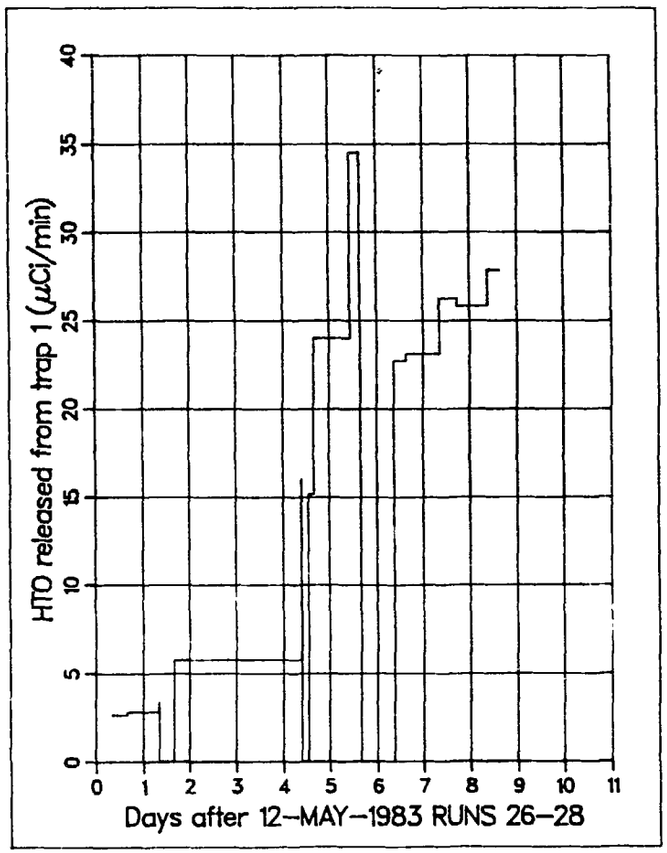

Fig. VI-85. HTO release rate for Runs 26-28.

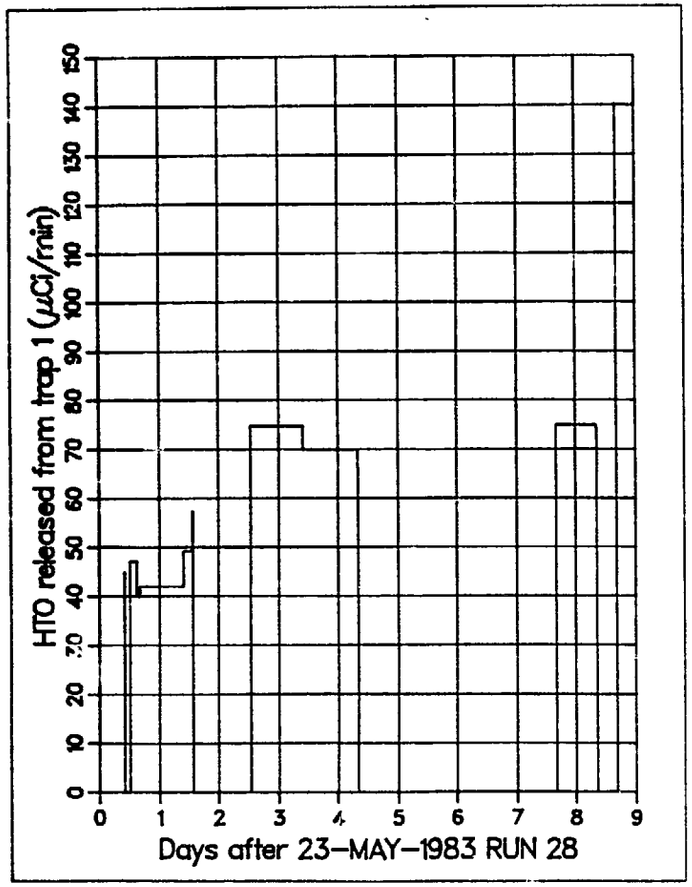

Fig. VI-86. HTO release for Run 28.

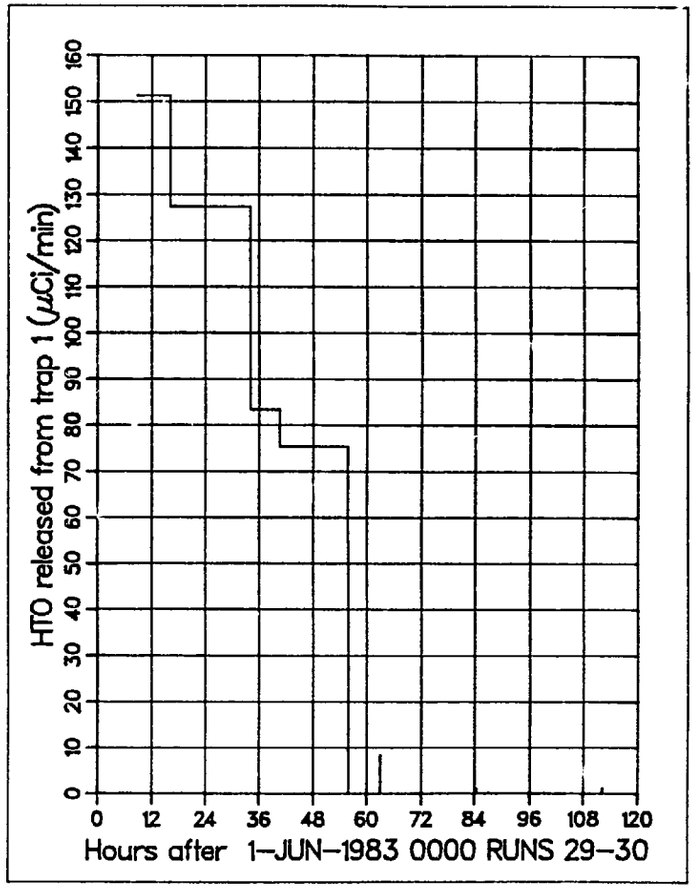

Fig. VI-87. HTO release for Runs 29-30.

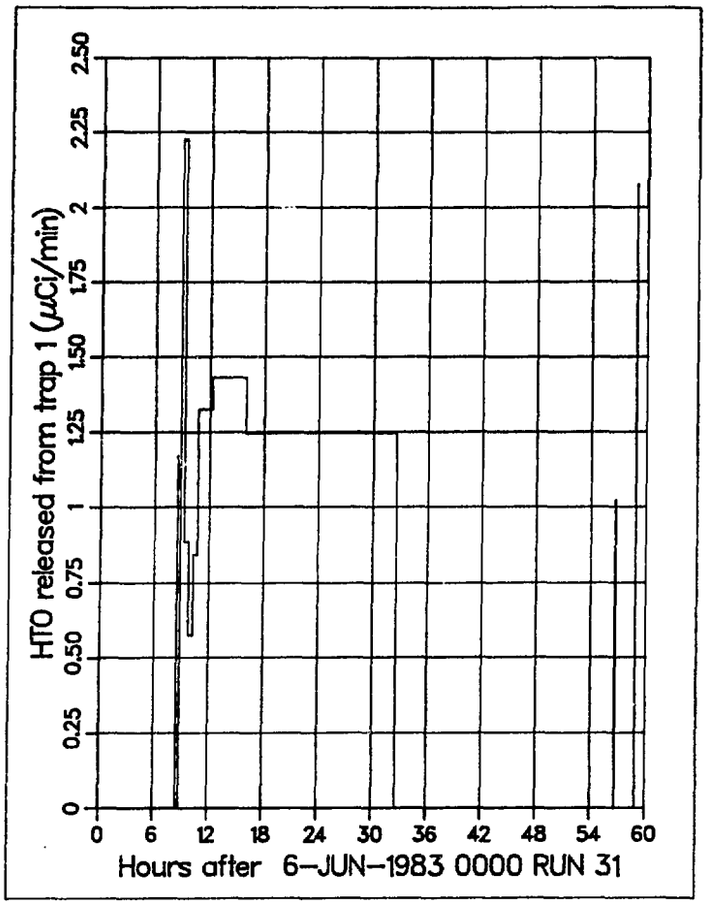

Fig. 88. HTO release for Run 31.

occurred at 1000 on June 6 and is small. The HTO peak, at about 1400 on June 6, is also small.

Run 32 is depicted in Fig. VI-89. The peak in the HT curve (Fig. VI-75) occurred at 1400 on June 8. The peak in the HTO curve at hour 56, at the beginning of the next run, may be associated with Run 32.

Run 33 is shown in Fig. VI-90. The HT curve (Fig. VI-77) showed a very strong peak at 1000 on June 10. There is a very strong peak in the HTO curve 10 to 20 h later.

H. Radionuclides

During operation of the TRIO experiment, a number of radionuclides were observed in the sweep gas stream (Table VI-8). These species were detected by

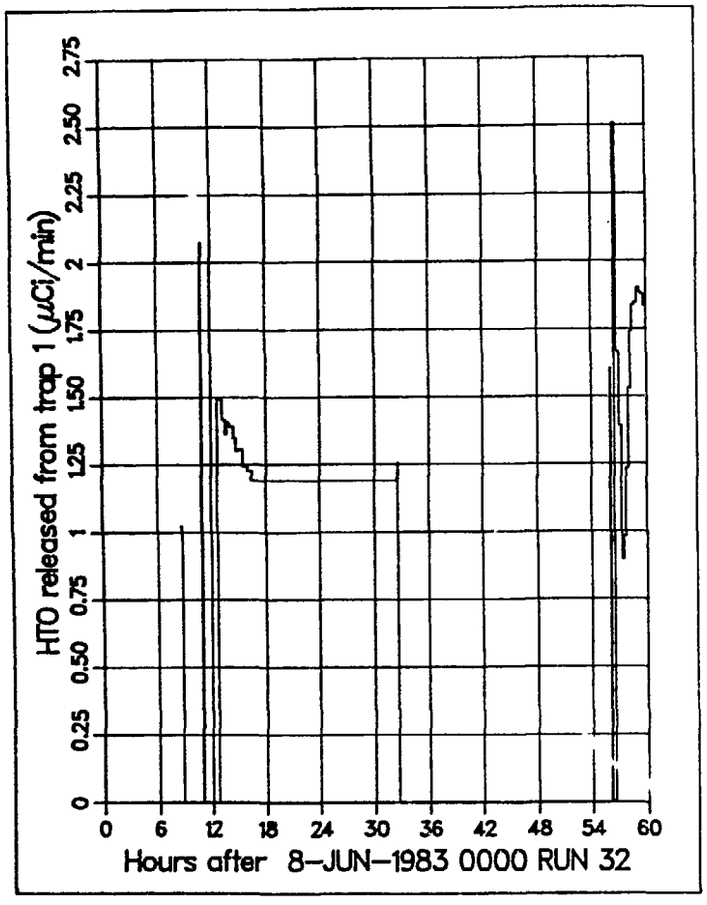

Fig. VI-89, HTO release rate for Run 32.

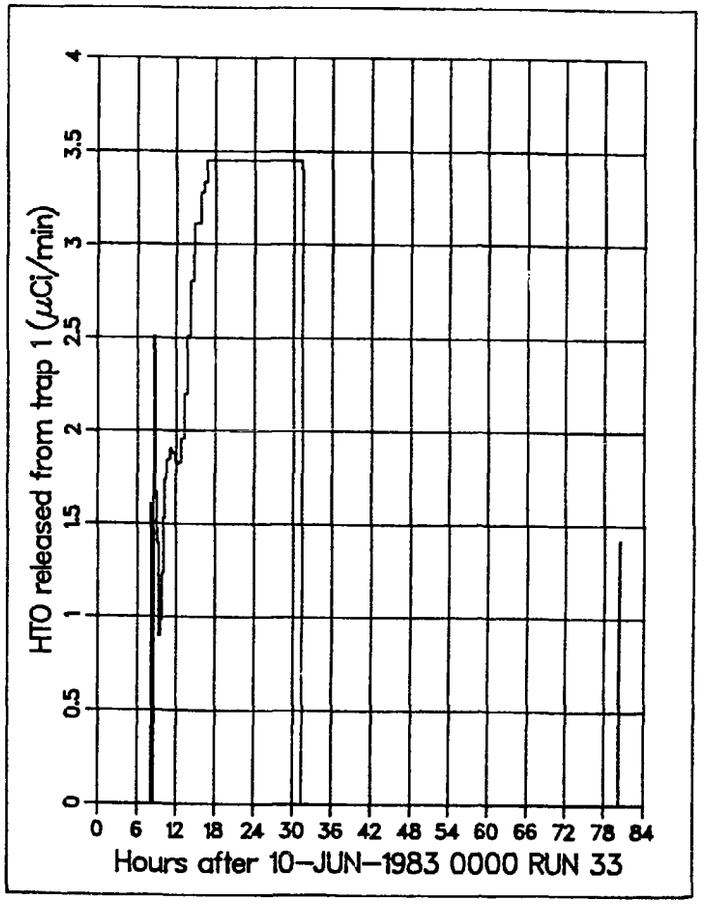

Fig. VI-90. HTO release rate for Run 33.

TABLE VI-8

Radionuclides Observed

Nuclide	Half-Life	Source
^{20}F	11.0 s	Ne
^{23}Ne	37.5 s	Na, Ne
$^{38}Cl8$	37.? mo	Cl
^{41}Ar	1.8 h	Ar, K
^{85m}Kr	4.48	U
^{87}Kr	76.0 mo	U
^{89}Kr	3.15 m	J
^{90}Kr	32.3 s	U
$^{88}Rb8$	17.7 mo	U
$^{89}Rb9$	15.4 mo	U
^{133}Xe	5.25 d	U
^{135m}Xe	15.3 mo	U
^{135}Xe	9.09 h	U
^{137}Xe	3.85 mo	U
^{138}Xe	14.2 mo	U
^{139}Xe	40.0 s	U
^{138}Cs	32.2 mo	U
^{139}Cs	9.4 mo	

gamma spectrometry as previously described (Section IV.C). The levels of these species were not more than 1% of the observed tritium signal, as measured by the Kanne chamber used to monitor the HT level. As shown, these radionuclides arise from the presence of trace levels of certain contaminants present in the breeder material. The presence of these radionuclides is significant because it provides information on radioactivity levels that have to be handled in a fusion reactor. In addition the data on the transport of neon, argon, krypton, and xenon may provide some insight into the transport behavior of a very important species, helium.

SECTION VII

POST-IRRADIATION EXAMINATIONS (PIE)

VII. POST-IRRADIATION EXAMINATIONS (PIE)

The TRIO experiment is comprised of three phases: pre-irradiation, irradiation, and post-irradiation. Data from each phase provide an essential contribution to the overall experiment. The pre-irradiation phase (see Sec. IV) includes: appropriate characterizations of the $LiAlO_2$ breeder material, mockup testing of critical experimental components (e.g., gas analysis system), and characterization of the nuclear environment with core mockup tests. The irradiation phase (see Sec. VI) includes the collection of extensive data on tritium release in its various chemical forms and monitoring of neutron flux and temperature profiles. The post-irradiation examinations (PIE) include the following steps: (1) disassembly of the capsule, (2) measurement of tritium retention in the breeder pellets, (3) determination of lithium burnup by measurement of lithium isotopy, (4) determination of thermal flux with dosimetry wires, (5) microstructural characterization of the pellets by scanning electron microscopy, (6) analysis of radioactivity in the pellets, and (7) characterization of the phase stability of the irradiated γ-$LiAlO_2$ by X-ray diffraction.

A. Capsule Disassembly

The large capsule assembly, nearly 3 m (12 ft) in length (shown as it was fabricated in Fig. IV-8), was removed from the reactor after unbolting the flange at the top and then crimping, disconnecting, and sealing the sweep gas lines with tubing fittings. A 10-m (30-ft) length of the sweep gas exit line was also crimped, then disconnected and sealed at both ends and retained for tritium assay. This line led from the top of the reactor through the pool to the gas analysis system. The large assembly was then brought to the ORR hot cell under water, and the lower portion (45 cm, 16 in.) was sawed off with a motorized hacksaw. This portion of the assembly contained the test capsule and $LiAlO_2$ breeder specimens. The cut part of the lower assembly was then resealed by immersing it into a pot of epoxy, which is expected to be capable of maintaining its integrity to a dose of 10^8 rads. This assembly was loaded into a 2-R container, and a Garden-2 cask, and delivered to ANL.

The capsule disassembly was performed in the ANL Alpha-Gamma Hot Cell facility (AGHC); the log number for the task is AG266A. In this facility, all cuts were made using high-speed grinding wheels with brittle blades. No cutting lubricants were used, and the capsule was rotated during cutting to prevent excessive heating. The temperature of the pieces was not measured, but cutting conditions used were the same as operations that did not melt sodium in similar capsules It is therefore estimated that the temperatures did not exceed 60°C. Photographs were taken after each cut was made and retained in permanent records of the AGHC. Care was taken to retain orientation of all parts with respect to "up" and geographic direction. North was the zero-degree reference angle.

Owing to the large amount of neutron-irradiated steel, the capsule assembly had an activity in excess of 10^6 R. All steel components in the capsule required remote handling. The activity of the lithium aluminate specimens was in the milliroentgens range, and these samples could be handled manually, with appropriate care.

The first cut was through the capsule assembly at a location below the lowest extent of the inner cladding, as shown in Fig. VII-1. The lower portion of the assembly was then discarded. A photograph of the remaining portion of the assembly is shown in Fig. VII-2. The orientation of the photograph is such that the view is looking upward toward the bottom of the inner capsule. The outer cladding and the four fins on the outside of the assembly having been cut through; the cogwheel-shaped centering device at the bottom of the inner capsule is visible. The tube on the outside of the east fin contains dosimetry wires, and the tube on the inside of the east fin is the inlet line for the control gas. Burrs on the inside of the outer cladding resulting from the cut were removed, causing the scratches on the west side of the cog-shaped centering plate. As shown, the centering plate and the inner capsule had been shifted directly to the east side, causing the gap to be smaller and the temperatures to be lower on that side. The nominal gap was 0.051 cm (0.020 in.), and the actual gap dimensions were measured by inserting piano wires of various diameters between the slots in the centering plate into the gap. As can be determined from Table VII-1, the largest gap was on the west side, and the smallest gap was on the east side. The inner capsule (when at ambient temperature) was displaced from center by 0.023 cm (0.009 in.) to

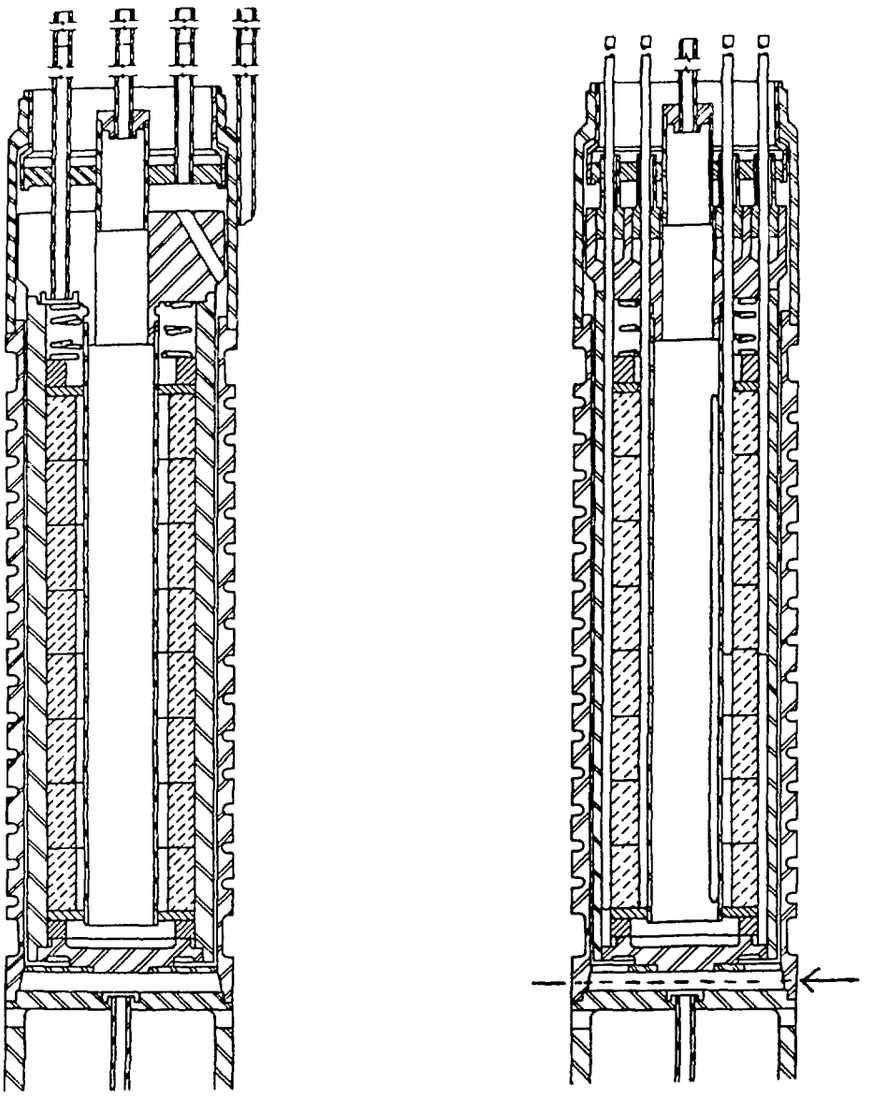

Fig. VII-1. Drawing of TRIO capsule showing location of first cut for the disassembly procedure.

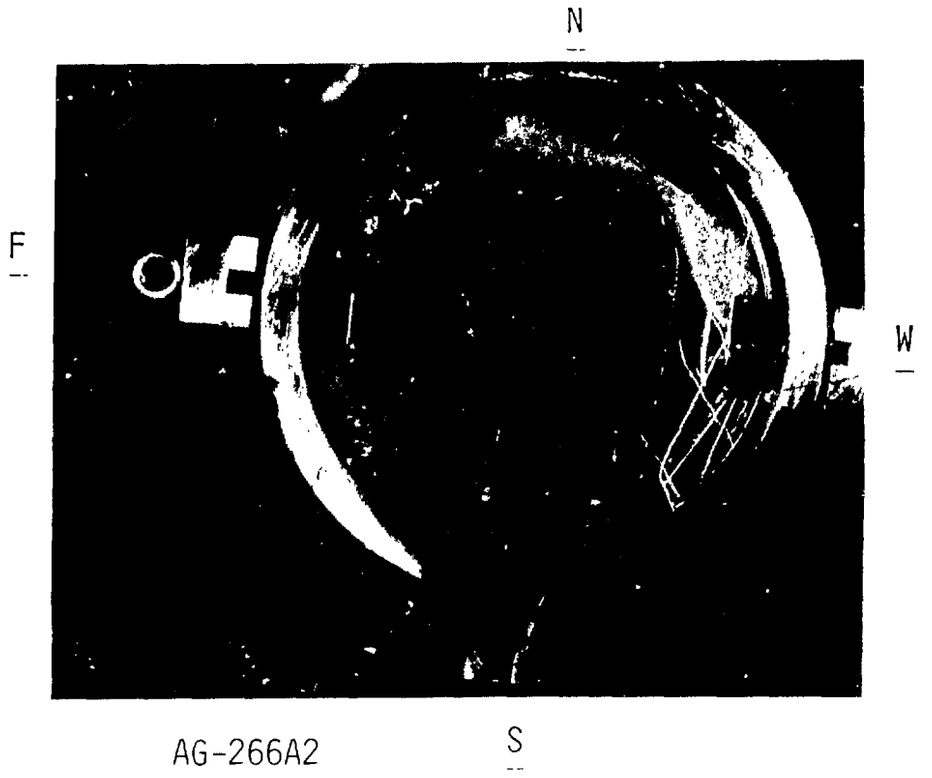

Fig. VII-2. Photograph of TRIO capsule after first cut made. (The view is upward from the bottom.)

TABLE VII-1

Measured Capsule Asymmetry

Angle (deg)	Capsule Asymmetry[a] (in.)				Gap (in.)	
	0.012	0.014	0.020	0.024	Measured	Estimated
30	+	-	-	-	>0.012	0.014
90	-	-	-	-	<0.012	0.011
150	+	-(close)	-	-	0.012	0.014
210	+	+	+	-	>0.020	0.022
270	+	+	+	+	>0.024	0.029[b]
330	+	+	+	+	>0.020	0.022

[a]"+" means wire fit in gap; "-" means that the wire did not fit.

[b]0.029 fits.

the east. The measured temperatures showed that the east side was consistently colder by about 50°C. This effect was due to the gap asymmetry. It is likely that the thermocouples located on the east and west sides directly measured the maximum and the minimum temperatures. It is fortunate that the capsule was not off-center to the north or to the south, because no direct way would have been available to determine the entire temperature range.

The outer cladding was then removed and discarded, and the inner capsule was sectioned to recover the breeder pellets. The breeder pellets appeared to be intact, but broke into four to six pieces when picked up. The lithium-aluminate pellets were numbered 1 to 7 from top to bottom. The orientation of each fragment was marked, and each pellet was placed in a separate container (plastic having a push-fit top) under the ambient cell atmosphere of dry nitrogen. Each plastic container was then placed in a metal "paint-can" type container. The hot cell is generally used to examine fission fuels, and the pellets did become contaminated with fission products. Also, the grinding procedures produced substantial quantities of steel dust, and the pellets probably became contaminated with bits of cladding.

B. Tritium Retention in the Lithium Aluminate Pellets

Pellets 3 and 4 were selected for tritium analysis. Pellet 3 was removed from the AGHC, bagged, placed in a container, and delivered to the Analytical Chemistry Laboratory of ANL. The pellet was in six pieces. The pellet was removed from its containers and reassembled (Fig. VII-3). The activity was quite high, probably owing to contamination as discussed above. The total activity was 1.5 R at a distance of 4 in., with a gamma level of 50 mR. A smear on one of the pellet fragments (the south sector) showed a gamma level of 1.5 million counts per minute (cpm) gamma and 0.15 million cpm alpha, indicating a substantial amount of loose activity. Owing to the amount of loose activity present, an attempt was made to clean the pellet with an ethanol wash. This procedure lowered the total activity to 200 mR, but the gamma level was unchanged. Each pellet fragment was then given an ethanol wash. It was observed that the ethanol rapidly soaked into the sample, because of its porous structure. The tritium content of the ethanol was determined to be 0.22 μCi, less than 0.2% of the amount of tritium in a sample.

-N-

Fig. VII-3. Photograph of irradiated $LiAlO_2$ pellet.

Each pellet fragment (weight about 1 g) was dissolved in 150 mL of 6 N HCl and then neutralized with NaOH. Aliquots of the solution were taken for measurement of lithium isotopy. To measure tritium content, two 15-mL samples were distilled, and two aliquots of each distillate were analyzed for tritium by liquid scintillation counting. Each aliquot was counted twice. The standard deviation of counts for each distillation aliquot was less than 0.7%, and the results for each distillation aliquot agreed within 1.5%.

A sample of distillate was dried and counted to determine if any carryover of nontritium activity had occurred by distillation. The activity counts were 3 cpm alpha and 30 cpm beta, neither of which was above background. The samples all had at least 40,000 accumulated counts so that the error in counting statistics was less than 0.5%. The background counts were less than 3% of the sample counts. Counting efficiencies were typically about 40%, as determined by using NBS standards. The error of a single tritium determination was less than 5%, including errors in the NBS standard (<2%), volumetrics (2%), and distillation (2%).

Fragments, roughly in the shape of 60-deg sectors of the pellet, were taken from the east (coldest side) and the west side of Pellets 3 and 4 for tritium assay. Upon dissolution of the samples of Pellet 3, sniffing for

tritium detected a measurable amount - the order of 10% of the content later found to be in the samples. The amount of tritium in the gas phase evolved during dissolution of the samples from Pellet 4 was then determined quantitatively by circulating the cover gas in a closed loop through a calibrated Kanne chamber (tritium monitor). This procedure has an estimated accuracy of ±10% in the amount of tritium so determined. Once the sealed containers holding the pellet fragments had been opened, a slight amount of tritium was detected, <10 $\mu Ci/m^3$ or less than 0.1 $\mu Ci/m^3$, this amount is less than 0.02 $\mu Ci/g$ of sample.

The data on measured tritium activities are presented in Table VII-2. The amounts of tritium in the solid range from about 100 to about 600 $\mu Ci/g$, or 0.01 to 0.06 wppm. The east side, which was at the lowest temperature, had a much higher tritium content than the west side. The amount of tritium evolved from the samples was about 100 $\mu Ci/g$, representing a content of 0.01 wppm. The average concentration is 303 $\mu Ci/g$ in Pellet 3 and 391.5 $\mu Ci/g$ in Pellet 4, a difference of 23%. This difference is attributed to two factors: the retention is highly temperature dependent, and the temperature distributions within pellet fragments is different. The overall average amount of tritium in the solid is 350 ± 50 $\mu Ci/g$. Since the amount of tritium which evolved upon dissolution is about 100 $\mu Ci/g$, the total content is then estimated as 450 ± 50 $\mu Ci/g$ an average concentration of 0.047 ± 0.005 wppm. The

TABLE VII-2

Measured Tritium Activities Retained in Lithium Aluminate Breeder[a]

Sample I.D.	Tritium in Solid ($\mu Ci/g$ of solid)	Tritium Evolved ($\mu Ci/g$ of solid)
3, east	459 ± 23.0 (0.048)	---
3, west	147 ± 7.0 (0.015)	---
4, east	623 ± 31.0 (0.065)	137 ± 14.0 (0.014)
4, west	160 ± 8.0 (0.016)	77 ± 8.0 (0.008)

[a]The numbers in brackets are tritium concentrations in wppm.

amount of tritium retained in the total amount of breeder (42.9 g) is estimated to be 0.019 ± 0.002 Ci. Of the total amount of tritium recovered (35.1 Ci), more than 99.94% was evolved from the breeder and successfully recovered during operation of the experiment. The value of tritium retention, 0.05 wppm, demonstrates that in-situ tritium recovery can work well for solid breeders, and that tritium inventories in solid breeder blankets can be low.

The length of stainless steel tubing that led from the top of the reactor tank to the glovebox had been crimped and sealed at each end. In an effort to determine if significant quantities of tritium were absorbed on the walls of the tubing, the tubing was opened and connected to tygon tubing, and 50.0 mL of water was recirculated through the tubing for 48 h. The amount of tritium leached into the water was 0.57 mCi. Additional leachings produced a total of 0.11 mCi. The amount of tritium on the tubing is, therefore, estimated as less than 1 mCi.

C. Lithium Isotopy

The ^{6}Li burnup was determined by using isotope dilution mass spectrometry. The initial content had been previously measured as 0.55%. The results for the irradiated pellets are given in Table VII-3. The ^{6}Li content is 0.38%, representing a burnup of 0.17%.

D. Dosimetry

The TRIO assembly contained iron, nickel, and titanium dosimetry wires located in separate tubes on the west and east sides, and in the center of the capsule. The tubes on the west and east sides were on the outside of the capsule assembly and located on the outside surface of the fins (see Fig. IV-10). The 0.25-mm (10-mil) diameter wires were cut into six pieces, each about 1.4 cm long, and counted by gamma spectrometry, using a Ge(Li) detector. The reaction rates were corrected for decay during irradiation using the flux histories measured by the self-powered neutron detectors (see Sec. VI.B). As already noted, the flux histories showed significant variations not observed in the power history, owing to fuel changes. The effect upon interpretation of the dosimetry data is minimal, since the activations used are long lived.

TABLE VII-3

^{6}Li Isotope Content of
Irradiated TRIO Pellets

Sample I.D.	at.% ^{6}Li[a]
3, east (1)	0.379 ± 0.004
3, east (2)	0.379 ± 0.004
3, west (1)	0.378 ± 0.004
3, west (2)	0.378 ± 0.004
4, east	0.383 ± 0.004
4, west	0.385 ± 0.004
Average	0.38%[b]

[a]Values after "±" are precision estimated by the analyst.

[b]Burnup = 0.55% - 0.38% = 0.17%.

The measured activation rates are listed in Table VII-4. The results represent the average of measurements on the six samples. No gradient was measurable over the length of the wires. As can be seen in Table VII-4, the thermal flux is about the same on the two outside (east, west) positions, but drops 32% in the center due to neutron absorption from the stainless steel cladding (total thickness, 1/4 in.) and from the breeder material. The shielding factor (0.68) was calculated to be 0.74 for the stainless steel and 0.95 for the lithium aluminate breeder. The former number corresponds well to the results for the core mockup test (0.77 shielding factor for the steel, see Sec. IV.D). The fast flux gradients are rather steep, decreasing a factor of two from west to east. This decrease is due to the location of the experiment in the A2 position, which is at the edge of the core. This gradient in fast flux has a negligible effect upon tritium production rates and has only a minor effect upon the damage rates. The activation rates are 30 to 40% lower than those in the core mockup test, indicating a correspondingly lower flux in the experiment compared to the core mockup test.

TABLE VII-4

Measured Activation Rates for TRIO

Position	Activation Rate,[a] atom/atom-s		
	$^{58}Fe(n,\gamma)^{59}Fe$	$^{54}Fe(n,p)^{54}Mn$	$^{46}Ti(n,p)^{46}Sc$
West	1.24×10^{-10}	5.34×10^{-12}	7.47×10^{-13}
Center	8.31×10^{-11}	3.42×10^{-12}	5.26×10^{-13}
East	1.22×10^{-10}	2.67×10^{-12}	3.82×10^{-13}

[a]Results are the average of measurements on six samples and normalized to 30 MW.

The activities in Table VII-4 were used to adjust the neutron spectrum measured in the core mockup test (Sec. IV.D). The resultant neutron fluences are listed in Table VII-5.

Table VII-5

Adjusted Neutron Fluences in TRIO

Energy Range	Neutron Fluence (10^{20} nv)		
	Center	West	East
Total	19.1	28.7	19.7
Thermal (<0.5 eV)	6.93	10.3	9.52
Thermal (2200 m/s)	5.32	9.13	8.43
Epithermal (0.5 eV-0.1 MeV)	6.01	8.98	5.13
Fast (>0.1 MeV)	6.15	9.05	5.0

E. Microstructural Characterization of Irradiated Lithium Aluminate Breeder Material

The correlation of microstructural parameters (grain size, surface area, porosity, etc.) of the breeder material to tritium release is essential to understanding the nature of tritium transport. Therefore, the microstructure of the breeder had to be characterized both before and after irradiation. In

the TRIO experiment, scanning electron microscopy (SEM) photographs were taken of the breeder material before irradiation (see Fig. IV-4). In addition, SEM was used to examine the irradiated lithium aluminate breeder material. Moreover, a small section of thermocouple cladding was examined to investigate interactions between the lithium aluminate and stainless steel cladding. The results of these studies are presented below.

A fragment of Pellet 3 (from the northwest sector) was chosen for this investigation. The specimen was fractured and SEM photographs (Figs. VII-4 and -5) were taken. The microstructure appears to be the same as before irradiation. The grain radius is still 0.1 um, and the agglomerates are still about 50 μ in diameter.

A second sample, Pellet 6, was put back together, mounted in epoxy, then ground and polished. The results of the investigation showed that no significant changes in microstructure had occurred as a result of the irradiation in the experiment.

Owing to the radioactivity of the steel components, only a very small metal specimen could be examined with the techniques used, which involved some hands-on operations. A small section of thermocouple from the west inside, ~1 cm in length, was studied to look for breeder-cladding interactions. There was some evidence of corrosion, viz., a light-colored material that was deposited on the surface (probably an oxide) was depleted in iron and enriched in chromium.

F. Radioactivity

A sample of lithium aluminate (the southwest sector of Pellet 3) was analyzed by gamma spectrometry and treated as an activation sample. The measured activities and calculated source concentrations are summarized in Table VII-6. Comparison of these results with pre-irradiation elemental and activation analysis (Table IV-3) that the observed impurities as determined before and after irradiation are generally in agreement. However, the PIE sample has more fission products (Table VII-7), probably owing to contamination from the hot cell. In an effort to remove surface contamination, the sample was washed with ethanol, and both the sample and the wash solution were counted. It was found that only the gamma peaks from long-lived fission products namely ^{134}Cs,

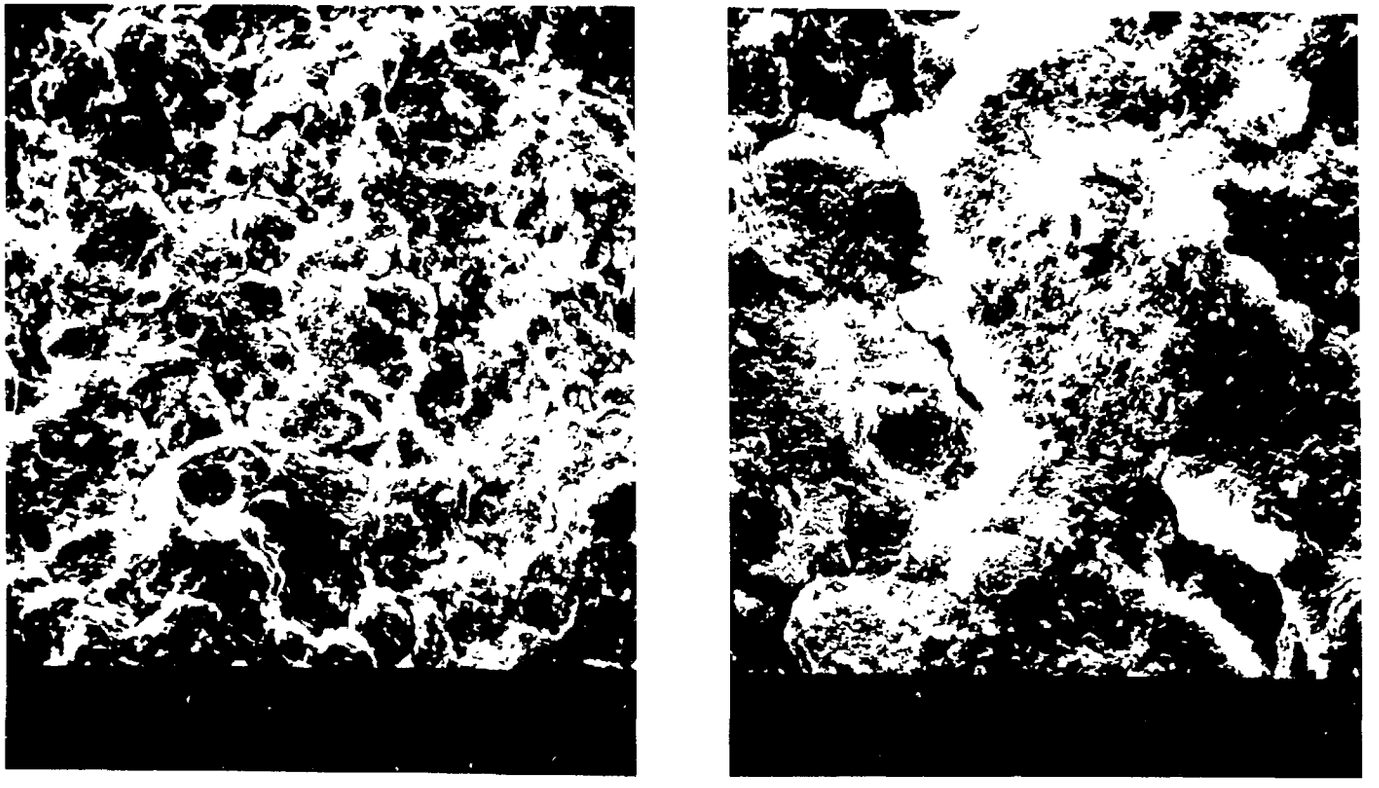

Fig. VII-4. Scanning electron micrographs of irradiated $LiAlO_2$ from TRIO.

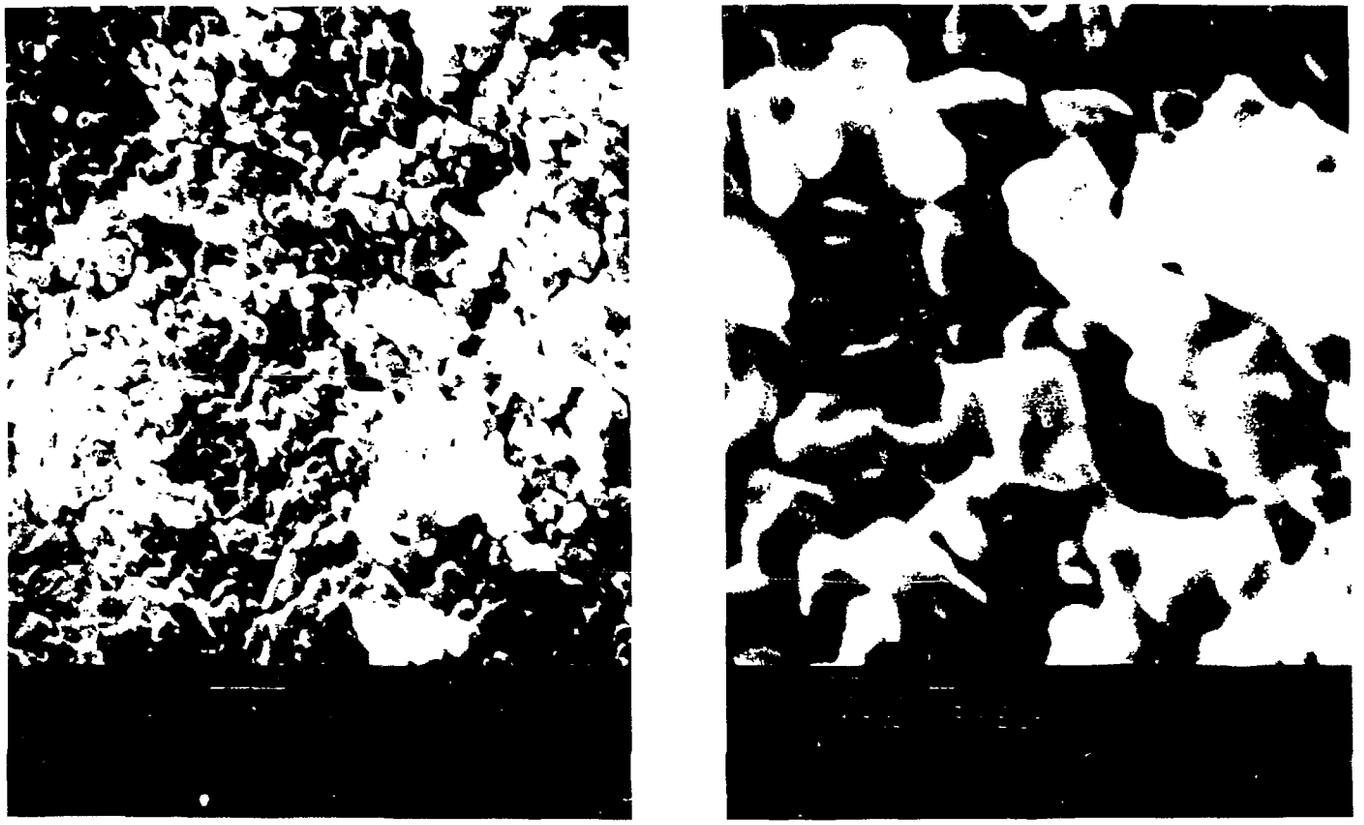

Fig. VII-5. Scanning electron micrographs of irradiated $LiAlO_2$ from TRIO.

TABLE VII-6

Gamma Analysis of Irradiated TRIO Lithium Aluminate Samples

	Before Washing				After Washing with Ethanol			
Isotope	μCi/g	Error (± %)	Element	wppm	μCi/g	Error (± %)	Element	wppm
^{22}Na	0.093	3.5	Na?					
^{46}Sc	28.9		Sc	0.088				
^{51}Cr	489.0		Cr	40.9				
^{54}Mn	1.65		Fe	164.0				
^{59}Fe	6.87		Fe	138.0				
^{57}Co	0.16		Ni?					
^{58}Co	13.1		Ni	40.9				
^{60}Co	8.80		Co	0.38				
^{65}Zn	42.8		Zn	27.0				
^{95}Zr	1.09	4.0	Zr[a]	9.5				
^{103}Ru	0.49	7.4	Ru[a]	0.11				
^{110m}Ag	0.49	1.9	Ag	0.036				
^{124}Sb	2.31	2.9	Sb	0.051				
^{134}Cs	18.0		Cs	0.341	11.0		Cs	0.208
^{137}Cs	0.24		U		0.11		U	
^{141}Ce	0.23	5.0	Ce[a]	0.075				
^{144}Ce	9.28	10.0	U		5.66	10.0	U	
^{181}Hf	8.66	5.1	Hf	0.33				
^{182}Ta	0.846	3.0	Ta	0.011				

[a]Products which can be made either by direct activation or by fission of uranium.

TABLE VII-7

Possible Fission Products
(Uraium/Plutonium) of
Irradiation Aluminate Samples

Isotope	Before Washing (wppm U)	After Washing (wppm U)
^{95}Zr	0.59	0.59
^{103}Ru	0.19	0.19
^{137}Cs	10.9	4.9
^{141}Ce	0.84	0.84
^{144}Ce	17.4	10.6

^{137}Cs, and ^{144}Ce were decreased by washing. Thus, there had been some contamination from fission products.

G. X-Ray Diffraction

Samples of Pellet 3 were taken, powdered, and analyzed by X-ray diffraction. The principal phase in all samples was gamma lithium aluminate. No evidence of alpha or beta phases was observed. The sample from the west inside, which had the highest temperature, showed a minor phase of $LiAl_5O_8$. Both west samples showed a very minor peak of lithium aluminate hydrate, as did the east outside sample. The sample from the east inside had no extra lines. The results show that the material was still lithium aluminate in the same phase. High temperature and lithium burnup may have been starting to produce the lithium-depleted phase. The trace amounts of hydrolysis product could have been caused by handling of the sample after irradiation.

SECTION VIII

DATA ANALYSIS

VIII. DATA ANALYSIS

The raw data accumulated in the course of the experiment, presented in Sec. VII, includes neutron flux, temperatures, and release rates of tritium in the various forms. The translation of the raw data into parameters used for design of fusion reactor blankets is discussed in this section. For example, the raw data on neutron flux and dose are used to determine damage, heating rates, and tritium production rates in the $LiAlO_2$ breeder material. The temperature data, in conjunction with the calculated heating rates, are used to determine heat transfer coefficients and thermal conductivity of the breeder material. The tritium release data, both integral and dynamic, are used to calculate tritium inventory and to quantify the release in terms of specific mechanisms, e.g., intragranular diffusion. A tritium mass transport coefficient, diffusivity, is thus derived.

A. Dosimetry and Damage Analysis

1. Tritium Production Rates

By use of the determined neutron spectrum (Sec. VII.D), the lithium burnup rates were computed. The outer rate was found to be 9.7×10^{-8} atom/atom•s while the inner rate was 6.5×10^{-8} atoms/atom•s. These two values were then used to determine the total burnup; an iterative procedure to calculate the time-dependent burnup and resultant decrease in self-shielding. The stainless steel sleeve was about 0.5-cm thick resulting in a neutron absorption loss factor of about 0.69 (calculated with an analytical approximation for self-shielding). This effect was estimated to be about 0.74 from the previous flux measurements in the mockup experiment (Sec. IV.D). The initial lithium self-shielding was about 0.952, decreasing to about 0.968 by the end of the irradiation. These two factors yield an average lithium burnup rate of 5.87×10^{-8} atom/atom•s. Over the 97 days of the run, this would result in a net burnup of 37.7% of the initial ^6Li atoms and a net tritium activity of 39.2 Ci. Due to the uncertainties in fluence measurements and self-shielding approximations, the tritium values have an estimated accuracy of 10-15%. If the measured lithium-to-iron activity ratios from the mockup experiment are used, the calculated tritium production is 37.5 Ci.

2. Damage Analysis

The SPECTER computer code was used to calculate damage parameters for the TRIO irradiation in ORR. The dose (rads), gas production, and damage rates are listed in Tables VIII-1 through VIII-3. The dose for the lithium aluminate is calculated to be 5.36×10^{12} rads, resulting in 0.81 dpa. Using the measured value of 4.8 W/g for gamma heating (Sec. IV.D), the gamma dose was calculated to be 3.54×10^{12} rads. The displacement damage includes 0.30 dpa from the ^{6}Li reactions, plus the damage (0.51 dpa) from the lithium, aluminum, and oxygen recoils. The total damage is approximately equal to 0.6 MW•yr, or ~2-mo operation in STARFIRE.[1]

3. Nuclear Heating Rates

The data given above on dose rates was translated into nuclear heating rates. The gamma heating rate and the fast neutron heating rate were assumed to be directly proportional to the neutron flux, as continuously measured by the self-powered neutron detectors. The uncertainty of the gamma and fast neutron heating rates so derived was estimated to be <20%. The heating rates in the lithium aluminate from tritium production are in direct proportion to the tritium production rate. The uncertainty in the tritium production rate is less than 10%. The uncertainty in the total heating rate is estimated to be less than 15%. The data for nuclear heating rates are given in Table VIII-4.

B. Analysis of Heat Transfer Data

The TRIO capsule is illustrated schematically in Figure IV-3. As shown, the thermocouples were located on the inside and the outside surfaces of the breeder pellets, both on the east and the west side. The locations of the thermocouple junctions are also illustrated, there are a total of ten, designated thus: T1 (east, inside), T2 (east, outside), T3-T6 (west, inside, top to bottom), and T7-T10 (west, outside, top to bottom). The recorded temperatures for the entire experiment were presented in Secs. VI.C and VI.F. To minimize uncertainties, temperature readings were averaged over those time intervals when the readings were nearly constant. Such data were taken for the 33 runs, and the results are given in Table VIII-5, which lists the run number, the time interval, the number of data points (N), the ten temperatures (T1 through

TABLE VIII-1

Spectral Averaged Kerma (MACKLIB) Factors and Damage per Component Nuclide in the $LiAlO_2$.

	Damage	
	(keV-b)	(rads)
Hydrogen	7.0039×10^{2}	1.2911×10^{13}
Deuterium	4.7055×10^{2}	4.3370×10^{12}
Helium	3.7827×10^{2}	1.7421×10^{12}
Lithium-6	1.3664×10^{6}	3.3340×10^{15}
Lithium-7	2.7662×10^{2}	7.2845×10^{11}
Beryllium	1.8587×10^{2}	3.8018×10^{11}
Boron-10	2.7271×10^{6}	2.1950×10^{15}
Boron-11	1.3459×10^{2}	2.2555×10^{11}
Carbon-12	1.2014×10^{2}	1.8455×10^{11}
Nitrogen	4.9696×10^{2}	6.5403×10^{11}
Oxygen	1.0731×10^{2}	1.2364×10^{11}
Fluorine	1.2503×10^{2}	1.2131×10^{11}
Scdium	1.6840×10^{2}	1.3503×10^{11}
Magnesium	7.2434×10^{1}	5.4920×10^{10}
Aluminum	1.4903×10^{2}	1.0182×10^{11}
Silicon	6.5279×10^{1}	4.2845×10^{10}
Chlorine	3.7211×10^{3}	1.9348×10^{12}
Potassium	1.8804×10^{2}	8.8648×10^{10}
Calcium	1.4646×10^{2}	6.7361×10^{10}
Titanium	1.2790×10^{2}	4.9219×10^{10}
Vanadium	1.6889×10^{2}	6.1113×10^{11}
Chromium	6.2772×10^{1}	2.2254×10^{10}
Manganese	3.1790×10^{3}	1.0667×10^{12}
Iron	3.8452×10^{1}	1.2692×10^{10}
Cobalt	4.0877×10^{1}	1.2786×10^{10}
Nickel	1.0907×10^{2}	3.4247×10^{10}
Copper	6.0413×10^{2}	1.7527×10^{11}
Zirconium	2.7606×10^{1}	5.5787×10^{9}

TABLE VIII-1 (Contd.)

	Damage	
	(keV-b)	(rads)
Niobium	2.9384×10^{1}	5.8301×10^{9}
Molybdenum	3.3340×10^{2}	6.4059×10^{10}
Tin	2.1604×10^{1}	3.3554×10^{9}
Tantalum	2.0110×10^{1}	2.0487×10^{9}
Tungsten-182	1.9420×10^{1}	1.9670×10^{9}
Tungsten-183	1.7868×10^{1}	1.7998×10^{9}
Tungsten-184	1.1409×10^{2}	1.1429×10^{10}
Tungsten-186	1.1629×10^{4}	1.1525×10^{12}
Lead	2.3588×10^{1}	2.0986×10^{9}
Thorium-232	4.7882×10^{3}	3.8045×10^{11}
Protractinium	1.4893×10^{4}	1.1884×10^{12}
Uranium-233	3.0625×10^{7}	2.4229×10^{15}
Uranium-234	4.7042×10^{4}	3.7058×10^{12}
Uranium-235	2.9552×10^{7}	2.3181×10^{15}
Uranium-236	2.0044×10^{4}	1.5656×10^{12}
Uranium-238	1.0036×10^{4}	7.7733×10^{11}
Neptunium	5.6373×10^{4}	4.3846×10^{12}
Plutonium-238	9.7670×10^{5}	7.5648×10^{13}
Plutonium-239	5.8538×10^{7}	4.5149×10^{15}
Plutonium-240	6.7214×10^{4}	5.1625×10^{12}
Plutonium-241	6.4246×10^{7}	4.9141×10^{15}
Plutonium-242	4.9176×10^{4}	3.7459×10^{12}
Americium-241	3.5655×10^{5}	2.7272×10^{13}
Americium-243	3.8848×10^{4}	2.9470×10^{13}

TABLE VIII-2

Spectral Averaged Gas Production File (ENDF 533)

	Gas Production	
	Sigma (mb)	Gas (appm)
^{6}Li (N, Hydrogen)	9.0819×10^{-1}	1.3780
^{6}Li (N, Deuterium)	2.1915×10^{1}	3.3250×10^{1}
^{6}Li (N, Tritium)	2.5198×10^{5}	3.8200×10^{5}
^{6}Li (N, Helium)	2.5200×10^{5}	3.8200×10^{5}
^{7}Li (N, Deuterium)	3.9015×10^{-3}	7.4528×10^{-3}
^{7}Li (N, Tritium)	4.3991	8.4034
^{7}Li (N, Helium)	2.3778×10^{1}	4.5422×10^{1}
^{9}Be (N, Hydrogen)	2.1599×10^{-5}	4.1258×10^{-5}
^{9}Be (N, Deuterium)	3.4889×10^{-5}	6.6647×10^{-5}
^{2}Be (N, Tritium)	1.1636×10^{-3}	2.2228×10^{-3}
^{2}Be (N, Helium)	4.5686×10^{1}	8.7270×10^{1}
^{10}B (N, Hydrogen)	1.6484	1.3750
^{10}B (N, Deuterium)	2.4276×10^{-1}	2.0250×10^{-1}
^{10}B (N, Helium)	1.0321×10^{6}	0.8610×10^{6}
^{11}B (N, Hydrogen)	1.2528×10^{-4}	2.3931×10^{-4}
^{11}B (N, Tritium)	8.3944×10^{-4}	1.6035×10^{-3}
^{11}B (N,X, Helium	6.6045×10^{-3}	1.2616×10^{-2}
^{12}C (N, Hydrogen)	1.9199×10^{-4}	3.6674×10^{-4}
^{12}C (N, Helium)	3.1850×10^{-1}	6.0841×10^{-1}
^{14}N (N, Hydrogen)	4.9821×10^{2}	9.5169×10^{2}
^{14}N (N, Helium)	1.4794×10^{1}	2.8260×10^{1}
^{19}F (N, Hydrogen)	1.9863×10^{-1}	3.7942×10^{-1}
^{19}F (N, Helium)	4.1959	8.0152
^{27}Al (N, Hydrogen)	7.4162×10^{-1}	1.4167
^{27}Al (N, Helium)	1.2538×10^{-1}	2.3950×10^{-1}
^{28}Si (N, Hydrogen)	1.0471	2.0002
^{28}Si (N, Helium)	4.8243×10^{-1}	9.2155×10^{-1}
Ti (N, Hydrogen)	4.8175×10^{-1}	9.2025×10^{-1}
Ti (N, Helium)	1.0830×10^{-1}	2.0688×10^{-1}

TABLE VIII-2 (Contd.)

	Gas Production	
	Sigma (mb)	Gas (appm)
V (N, Hydrogen)	8.6311×10^{-2}	1.6487×10^{-1}
V (N, Helium)	4.6181×10^{-3}	8.8216×10^{-3}
Cr (N, Hydrogen)	7.1945×10^{-1}	1.3743
Cr (N, Deuterium)	2.3418×10^{-5}	4.4734×10^{-5}
Cr (N, Tritium)	1.2795×10^{-4}	2.4441×10^{-4}
Cr (N, Helium-3)	5.6717×10^{-6}	1.0834×10^{-5}
Cr (N, Helium-4)	3.2794×10^{-2}	6.2644×10^{-2}
^{55}Mn (N, Hydrogen)	1.2793×10^{-1}	2.4438×10^{-2}
^{55}MN (N, Helium)	2.6592×1002	5.0797×10^{-2}
Fe (N, Hydrogen)	9.9205×10^{-1}	1.8950
Fe (N, Helium)	5.7466×10^{-2}	1.0977×10^{-1}
^{59}Co (N, Hydrogen)	2.6719×10^{-1}	5.1040×10^{-1}
^{59}Co (N, Helium)	2.6745×10^{-2}	5.1090×10^{-2}
Ni (N, Hydrogen)	1.2307×10^{1}	2.3510×10^{1}
Ni (N, Deuterium)	2.2761×10^{-3}	4.3479×10^{-3}
Ni (N, Helium)	8.5119×10^{-1}	1.6260
Cu (N, Hydrogen)	2.0937	3.9994
Cu (N, Helium)	4.8190×10^{-2}	9.2054×10^{-2}

TABLE VIII-3

Damage from Various Sources of TRIO

Source	dpa	rads
^{6}Li(n,α)t	0.30	1.67×10^{12}
Fast reactions	0.51	0.15×10^{12}
Gamma heating	----	3.54×10^{12}
Total	0.81	5.36×10^{12}

TABLE VIII-4

Nuclear Heating Rates

Days after 3/10/83	Daily Average Flux	Tritium (Ci)	Nuclear Heating (W/g)			
			$^{6}Li(N,\alpha)t$	Fast	Gamma	Total
1	0.0000	0.0000	0.0000	0.0000	0.0000	0.0000
2	0.0000	0.0000	0.0000	0.0000	0.0000	0.0000
3	0.0469	0.0215	0.1183	0.0086	0.2073	0.3342
4	0.6887	0.3155	1.7353	0.1269	3.0448	4.9069
5	1.1146	0.5087	2.7977	0.2053	4.9276	7.9306
6	1.0975	0.4986	2.7421	0.2022	4.8522	7.7965
7	1.1076	0.5008	2.7545	0.2040	4.8970	7.8556
8	1.1080	0.4986	2.7425	0.2041	4.8985	7.8450
9	1.1052	0.4951	2.7228	0.2036	4.8861	7.8125
10	1.0939	0.4878	2.6827	0.2015	4.8364	7.7205
11	1.1157	0.4951	2.7232	0.2055	4.9324	7.8611
12	1.1136	0.4919	2.7055	0.2051	4.9235	7.8341
13	1.0858	0.4774	2.6257	0.2000	4.8005	7.6261
14	1.1225	0.4912	2.7017	0.2068	4.9626	7.8711
15	1.1251	0.4900	2.6952	0.2072	4.9743	7.8768
16	1.1300	0.4898	2.6940	0.2081	4.9959	7.8980
17	1.1276	0.4865	2.6755	0.2077	4.9853	7.8685
18	1.1245	0.4828	2.6553	0.2071	4.9714	7.8338
19	1.1216	0.4793	2.6361	0.2066	4.9589	7.8016
20	1.1173	0.4752	2.6135	0.2058	4.9397	7.7590
21	1.1066	0.4684	2.5763	0.2038	4.8925	7.6727
22	1.0902	0.4593	2.5264	0.2008	4.8200	7.5472
23	1.0976	0.4603	2.5317	0.2022	4.8527	7.5866
24	1.0937	0.4565	2.5110	0.2015	4.8355	7.5479
25	1.0901	0.4529	2.4911	0.2008	4.8195	7.5114
26	1.0870	0.4495	2.4724	0.2002	4.8055	7.4782
27	1.0843	0.4464	2.4550	0.1997	4.7937	7.4484
28	0.1809	0.0743	0.4085	0.0333	0.7997	1.2414
29	0.5851	0.2399	1.3192	0.1078	2.5870	4.0140
30	1.1384	0.4649	2.5569	0.2097	5.0328	7.7994
31	1.1403	0.4634	2.5489	0.2100	5.0414	7.8004
32	1.1457	0.4634	2.5485	0.2110	5.0652	7.8247
33	1.1515	0.4635	2.5490	0.2121	5.0910	7.8521
34	1.1111	0.4451	2.4478	0.2047	4.9125	7.5649
35	1.1502	0.4585	2.5216	0.2119	5.0850	7.8185
36	0.0920	0.0366	0.2011	0.0169	0.4067	0.6248
37	0.4045	0.1606	0.8836	0.0745	1.7883	2.7464
38	1.1710	0.4635	2.5491	0.2157	5.1769	7.9417
39	1.1905	0.4688	2.5787	0.2193	5.2635	8.0615
40	1.1794	0.4621	2.5417	0.2172	5.2143	7.9732
41	1.1800	0.4600	2.5302	0.2174	5.2170	7.9646
42	1.1801	0.4578	2.5177	0.2174	5.2175	7.9526
43	1.1787	0.4549	2.5020	0.2171	5.2111	7.9303
44	1.1762	0.4517	2.4843	0.2167	5.2003	7.9012
45	1.1741	0.4486	2.4673	0.2163	5.1908	7.8743
46	1.1601	0.4410	2.4257	0.2137	5.1289	7.7683
47	1.1596	0.4387	2.4128	0.2136	5.1269	7.7532
48	1.1587	0.4362	2.3990	0.2134	5.1229	7.7354

TABLE VIII-4 (Contd.)

Days after 3/10/83	Daily Average Flux	Tritium (Ci)	Nuclear Heating (W/g)			
			$^{6}Li(N,\alpha)t$	Fast	Gamma	Total
49	1.1549	0.4326	2.3793	0.2127	5.1061	7.6981
50	0.1449	0.0541	0.2977	0.0267	0.6405	0.9649
51	0.6410	0.2390	1.3147	0.1181	2.8340	4.2669
52	1.0811	0.4017	2.2092	0.1991	4.7798	7.1881
53	1.0824	0.4003	2.2014	0.1994	4.7852	7.1860
54	1.0765	0.3962	2.1794	0.1983	4.7593	7.1369
55	1.0736	0.3934	2.1636	0.1978	4.7466	7.1079
56	1.0724	0.3911	2.1512	0.1975	4.7413	7.0900
57	1.0792	0.3918	2.1548	0.1988	4.7712	7.1248
58	1.0367	0.3746	2.0605	0.1910	4.5832	6.8347
59	0.4697	0.1692	0.9305	0.0865	2.0764	3.0935
60	0.9516	0.3418	1.8796	0.1753	4.2072	6.2621
61	0.9845	0.3521	1.9365	0.1813	4.3525	6.4703
62	0.9993	0.3559	1.9572	0.1841	4.4179	6.5592
63	0.9980	0.3539	1.9464	0.1838	4.4124	6.5426
64	0.9824	0.3469	1.9078	0.1810	4.3433	6.4321
65	1.0016	0.3521	1.9367	0.1845	4.4281	6.5492
66	0.9980	0.3493	1.9214	0.1838	4.4121	6.5174
67	0.9969	0.3475	1.9112	0.1836	4.4074	6.5022
68	0.9937	0.3449	1.8969	0.1830	4.3933	6.4732
69	0.5295	0.1832	1.0074	0.0975	2.3408	3.4457
70	0.9465	0.3264	1.7952	0.1744	4.1847	6.1543
71	0.9681	0.3325	1.8286	0.1783	4.2802	6.2871
72	0.9473	0.3240	1.7819	0.1745	4.1883	6.1448
73	0.9747	0.3320	1.8258	0.1795	4.3091	6.3144
74	0.9790	0.3320	1.8261	0.1803	4.3281	6.3345
75	0.9799	0.3309	1.8201	0.1805	4.3322	6.3328
76	0.9826	0.3304	1.8175	0.1810	4.3443	6.3428
77	0.9855	0.3300	1.8151	0.1815	4.3571	6.3537
78	0.9866	0.3290	1.8094	0.1817	4.3620	6.3532
79	0.9844	0.3269	1.7977	0.1813	4.3522	6.3312
80	0.9865	0.3261	1.7938	0.1817	4.3614	6.3369
81	0.9845	0.3241	1.7826	0.1813	4.3526	6.3165
82	0.9871	0.3236	1.7797	0.1818	4.3641	6.3256
83	0.9932	0.3242	1.7830	0.1829	4.3909	6.3568
84	0.1349	0.0439	0.2416	0.0248	0.5964	0.8629
85	0.6087	0.1979	1.0883	0.1121	2.6910	3.8914
86	1.0176	0.3296	1.8130	0.1874	4.4987	6.4991
87	1.0139	0.3270	1.7985	0.1868	4.4825	6.4678
88	1.0150	0.3259	1.7925	0.1870	4.4873	6.4668
89	1.0165	0.3250	1.7873	0.1872	4.4940	6.4686
90	1.0498	0.3341	1.8376	0.1934	4.6411	6.6720
91	1.0663	0.3378	1.8580	0.1964	4.7144	6.7688
92	1.0601	0.3343	1.8387	0.1953	4.6868	6.7207
93	1.0533	0.3307	1.8186	0.1940	4.6569	6.6696
94	1.0514	0.3285	1.8070	0.1937	4.6483	6.6490
95	1.0559	0.3284	1.8064	0.1945	4.6682	6.6691
96	1.0666	0.3302	1.8164	0.1965	4.7156	6.7284
97	0.1344	0.0415	0.2283	0.0248	0.5942	0.8473

TABLE VIII-5

Heat Transfer Data from TRIO: Temperatures

Run	Date	Time On	Time Off	N	Temperature (°C) T1	T2	T3	T4	T5	T6	T7	T8	T9	T10	TE	TW	TAV
0.1	3/11	0346	0500	16	208	165	222	221	223	216	180	177	181	175	186	200	194
0.2	3/11	2020	2120	13	205	162	218	217	218	211	177	173	176	171	184	196	190
1.1	3/12	0856	0920	7	337	248	361	364	365	350	278	274	277	279	292	320	306
1.2	3/12	0936	0950	7	354	257	380	382	384	368	290	286	289	294	306	335	320
1.3	3/12	0950	1040	13	421	296	451	455	458	441	338	334	340	348	358	397	378
1.4	3/12	1040	1050	3	453	322	483	487	492	476	368	365	369	380	388	428	408
1.5	3/12	1054	1124	7	518	384	547	553	560	548	434	432	438	452	451	496	474
1.6	3/12	1200	2400	145	628	489	651	661	670	660	540	540	547	564	558	604	581
1.7	3/13	0000	1800	217	642	499	666	675	684	673	553	552	557	574	570	612	591
1.8	3/13	1800	3900	253	636	496	660	669	668	667	549	548	553	569	566	608	587
2.1	3/14	1600	3100	181	722	580	741	753	763	753	634	635	640	660	651	696	674
2.2	3/15	1700	3500	217	722	579	741	753	761	751	633	634	639	657	650	695	672
3.1	3/16	1100	1500	49	723	579	742	754	761	750	633	634	639	658	651	696	674
3.2	3/16	1600	3200	193	722	579	741	753	760	749	633	633	638	656	650	695	672
3.3	3/17	0900	1300	49	731	587	750	762	768	756	641	642	648	665	659	705	682
4.1	3/17	1800	2400	73	577	438	604	607	612	598	487	482	483	495	508	546	527
4.2	3/18	0000	2400	289	579	439	606	610	613	598	488	483	482	494	509	547	528
4.3	3/19	1200	2400	145	580	439	608	611	614	600	488	482	485	497	510	548	529
4.4	3/20	1200	2400	145	577	436	605	608	610	596	486	480	482	493	507	545	526
5.1	3/23	1200	2400	145	531	390	560	563	564	547	439	431	433	440	475	498	486
5.2	3/24	0000	0800	97	529	388	560	561	561	546	439	431	433	441	474	497	486
6.1	3/24	1200	2400	145	575	431	606	609	611	598	489	483	488	499	518	548	533
6.2	3/25	0000	1000	121	575	431	607	610	612	598	489	483	488	499	519	548	534
7.1	3/25	1500	2400	109	626	481	655	660	662	648	540	535	539	551	554	597	576
7.2	3/26	0900	2100	145	625	479	654	658	660	646	539	534	542	549	552	596	574
8.1	3/28	1500	2400	109	679	533	705	710	712	699	593	588	600	607	606	650	628
8.2	3/30	0000	1200	145	673	529	700	704	705	689	588	583	594	602	601	649	625
9.1	3/30	1200	2400	145	672	529	699	703	704	690	589	583	593	600	600	648	624
9.2	3/31	0000	2400	289	671	529	699	703	703	689	588	583	593	599	600	648	624
9.3	4/01	0000	2400	289	668	526	698	701	700	686	586	581	592	597	597	646	622
9.4	4/02	0000	2400	289	667	526	697	700	699	685	586	580	589	592	596	644	620
9.5	4/03	0000	2400	289	664	524	695	697	696	681	585	578	589	594	594	640	617
9.6	4/04	0000	1200	145	662	522	693	695	693	676	583	576	586	592	592	638	615
9.7	4/04	1800	2400	73	672	532	701	704	702	687	592	586	595	599	602	647	624
10.1	4/06	2000	2400	49	441	309	472	472	470	454	349	341	346	352	375	407	391
10.2	4/07	0000	0800	97	442	309	475	474	472	455	350	342	348	354	376	409	392
11.1	4/07	1000	2400	169	533	394	565	566	565	551	443	436	444	453	464	505	484
11.2	4/08	0000	0900	109	533	395	566	568	567	553	446	438	447	454	464	507	486
12.1	4/08	1100	2400	157	578	436	610	612	613	601	490	485	495	508	507	551	529
12.2	4/09	0000	1800	217	578	437	610	612	612	600	491	485	495	507	508	551	530
12.3	4/10	0000	0600	73	582	439	615	616	617	604	494	488	499	508	510	555	532
12.4	4/10	1400	2400	121	582	439	615	618	617	604	494	489	500	510	510	556	533
12.5	4/11	1600	2400	97	579	438	614	615	614	601	494	488	497	510	508	554	531
12.6	4/12	0000	0800	97	578	436	613	614	612	599	493	486	498	509	507	552	530
13.1	4/12	1200	2400	145	628	484	660	663	662	649	543	537	547	560	556	608	582
13.2	4/15	1800	2400	73	632	87	663	668	668	655	544	540	550	566	560	612	586
13.3	4/16	1200	2000	97	634	488	664	669	668	656	545	541	552	565	561	613	587
13.4	4/17	0000	2400	289	627	483	657	662	662	649	540	536	548	561	557	608	582
13.5	4/18	0000	0800	97	627	483	658	663	662	649	541	536	546	561	557	608	582
14.1	4/18	1200	2400	145	732	587	755	764	765	752	642	640	652	668	660	705	682
14.2	4/19	0000	2400	289	732	586	754	763	763	750	641	638	651	666	659	704	682
14.3	4/20	0000	0800	97	730	585	754	761	760	748	641	638	650	664	658	702	680
15.1	4/20	1400	2400	121	733	588	757	763	763	750	643	641	650	664	660	704	682
15.2	4/21	0000	1000	121	731	586	754	761	760	747	642	639	651	664	658	703	680
16.1	4/21	0900	2400	181	730	586	755	760	759	745	641	638	649	663	658	702	680
16.2	4/22	0000	1300	157	729	585	754	760	758	745	642	638	647	662	657	700	678
17.1	4/22	1200	2400	145	729	585	755	759	758	746	642	638	647	661	657	700	678
17.2	4/23	0900	2400	181	721	579	747	752	750	736	635	631	641	655	650	694	672
17.3	4/24	0000	2400	289	721	579	748	753	751	739	636	632	641	655	650	694	672
17.4	4/25	0000	0800	97	722	580	750	754	751	739	637	632	641	655	651	694	672
18.1	4/25	1800	2400	73	729	586	755	760	757	745	644	639	647	661	658	701	680
18.2	4/26	0000	1000	121	728	586	754	760	757	743	643	639	647	660	658	701	680
19.1	4/26	1100	2400	157	677	536	708	710	706	691	593	587	593	605	606	649	628
19.2	4/27	0000	0300	37	674	534	705	707	702	688	590	583	591	595	604	646	625
20.1	4/28	1100	1200	13	405	291	440	435	430	415	323	313	318	317	348	374	361
20.2	4/28	1200	1300	13	406	291	440	435	430	416	323	314	318	316	348	374	361
20.3	4/28	1300	1400	13	406	292	441	436	431	416	323	314	317	318	349	375	3622
0.4	4/28	1500	1600	13	409	293	444	439	433	418	326	316	320	320	351	377	364
20.5	4/28	1600	1800	25	409	293	444	439	433	419	326	316	319	320	351	377	364

TABLE VIII-5 (Contd.)

Run	Time			N	Temperature (°C)												
	Date	On	Off		T1	T2	T3	T4	T5	T6	T7	T8	T9	T10	TE	TW	TAV
20.6	4/28	1800	2000	25	409	293	446	440	433	419	326	317	320	321	351	378	364
20.7	4/28	2000	2200	25	410	293	446	441	434	419	328	317	321	321	352	379	366
20.8	4/28	2200	2400	25	411	294	448	442	435	420	328	317	321	322	352	380	366
20.9	4/29	0000	0400	49	411	293	447	442	435	420	328	317	322	322	352	380	366
20.10	4/29	0400	0800	49	412	294	449	443	436	420	328	318	322	323	353	380	366
20.11	4/29	0900	1000	13	416	295	453	447	440	423	331	321	324	325	356	383	370
20.12	4/29	1200	2400	145	673	541	701	704	703	691	596	592	599	598	607	650	628
20.13	4/30	0000	2400	289	672	540	699	703	702	690	594	590	598	589	606	648	627
20.14	5/01	0000	2400	289	672	539	699	702	700	689	594	590	598	600	606	648	627
20.15	5/02	0000	1200	145	670	538	696	699	697	685	591	587	596	605	604	645	624
21.1	5/02	1200	2400	145	669	538	696	699	696	684	592	587	595	604	604	644	624
21.2	5/03	0000	0700	85	670	539	697	698	696	685	593	589	596	604	604	644	624
21.3	5/03	0800	2400	193	676	545	703	705	703	692	600	595	604	613	610	651	630
21.4	5/04	0000	0700	85	679	547	705	707	705	694	602	597	605	613	613	653	633
22.1	5/04	0900	2400	181	629	499	659	658	654	643	553	545	552	560	564	604	584
22.2	5/05	0000	0800	97	632	501	662	661	657	645	555	548	552	558	566	606	586
23.1	5/05	0900	2200	157	582	454	614	609	605	592	504	494	497	502	518	554	536
23.2	5/07	0000	0400	49	588	472	610	615	617	608	516	513	522	530	530	570	550
23.3	5/07	0600	1500	109	584	467	607	610	612	603	513	509	519	527	530	566	548
23.4	5/08	0600	2400	217	572	451	597	602	603	594	498	494	503	511	512	550	531
23.5	5/09	0400	0800	49	571	451	598	601	602	593	497	493	502	512	511	550	530
24.1	5/09	1100	2400	157	625	502	648	652	656	647	551	548	556	566	564	603	584
24.2	5/10	0000	1200	145	623	500	647	653	654	646	550	547	556	565	562	602	582
25.1	5/10	1500	2400	109	584	464	608	612	611	601	510	504	509	490	524	559	542
25.2	5/11	0000	0900	109	583	463	609	612	610	601	509	504	510	---	523	559	541
25.3	5/11	1500	2400	109	587	465	613	617	617	607	514	508	515	511	526	564	545
25.4	5/12	0000	0600	73	586	465	613	616	616	606	513	507	514	502	526	563	544
26.1	5/12	0800	2400	193	574	452	601	603	602	593	501	495	502	511	513	550	532
26.2	5/13	0000	2400	289	572	451	599	600	599	590	499	492	499	507	512	548	530
26.3	5/14	0000	2400	289	572	451	600	601	599	590	500	493	499	506	512	548	530
26.4	5/15	0000	2400	289	570	450	598	599	596	587	499	491	496	503	510	546	528
26.5	5/16	0000	0300	37	569	449	597	597	595	585	498	490	496	503	509	544	526
27.1	5/17	1500	2400	109	543	429	569	571	570	561	475	468	474	480	486	520	503
27.2	5/18	0000	2400	289	545	430	571	573	571	563	475	470	475	481	488	522	505
27.3	5/19	0000	2400	289	547	431	574	575	573	564	478	471	477	481	489	524	506
27.4	5/20	0000	2400	289	548	433	575	576	574	565	480	472	479	483	490	526	508
27.5	5/21	0000	2400	289	548	431	576	576	574	564	480	472	479	484	490	526	508
27.6	5/22	0000	2400	289	550	433	577	578	574	565	482	474	479	484	492	526	509
27.7	5/23	0000	0800	97	549	432	577	577	574	564	482	474	479	484	490	526	508
28.1	5/23	1200	2400	145	528	412	557	555	552	542	460	451	454	460	470	503	486
28.2	5/24	0000	2400	289	528	412	557	554	551	541	460	451	455	460	470	503	486
28.3	5/25	0000	2400	289	530	413	559	557	553	543	461	452	457	460	472	505	488
28.4	5/26	0000	2400	289	528	412	558	555	551	541	460	451	455	458	470	503	486
28.5	5/27	0000	2400	289	527	411	556	553	549	539	459	449	454	458	469	501	485
28.6	5/28	0000	1600	195	525	410	556	552	547	537	458	448	452	457	468	500	484
28.7	5/28	1800	2400	73	528	411	557	556	550	540	461	451	453	456	470	502	486
28.8	5/29	0000	1200	145	527	411	558	555	550	539	461	451	454	457	469	502	486
28.9	5/29	1200	2400	145	525	409	556	552	547	537	459	448	452	457	467	500	484
28.10	5/30	1200	2400	145	528	411	559	555	550	539	461	451	453	456	470	502	486
29.1	6/02	0000	0600	73	520	403	548	548	547	538	449	443	447	453	462	496	479
29.2	6/02	0700	0900	25	519	399	548	546	543	535	448	439	445	451	459	494	476
29.3	6/02	1000	1400	49	518	398	547	546	544	534	447	438	443	449	458	493	476
29.4	6/02	1500	2400	109	511	395	540	538	535	525	441	431	435	442	453	485	469
29.5	6/03	0000	2400	289	512	395	541	538	536	527	443	433	438	442	454	486	470
30.1	6/04	0000	2400	289	512	394	542	540	536	526	443	433	438	441	453	486	470
30.2	6/05	0000	2400	289	513	395	543	540	537	526	443	434	438	443	454	487	470
30.3	6/06	0000	0700	85	513	395	543	540	536	526	444	434	438	443	454	487	470
31.1	6/06	1100	2400	157	526	403	557	555	551	540	454	444	447	452	464	498	481
31.2	6/07	0000	2400	289	526	403	558	555	551	540	454	444	447	453	464	498	481
31.3	6/08	0000	0400	49	525	402	557	555	550	539	454	443	447	453	464	498	481
31.4	6/08	0500	1100	73	524	401	556	553	548	536	452	441	446	452	462	496	479
32.1	6/08	1300	2400	133	571	447	601	600	595	586	501	492	497	503	509	546	528
32.2	6/09	0000	2400	289	571	447	601	600	596	583	501	491	497	503	509	546	528
32.3	6/10	0000	0700	85	570	446	600	598	594	584	501	491	495	502	508	544	526
33.1	6/10	1200	2400	145	679	553	702	705	704	693	608	602	602	610	616	653	634
33.2	6/11	0000	2400	289	677	552	701	704	702	691	607	601	600	609	614	651	633
33.3	6/12	0000	0900	109	679	552	703	705	702	691	608	602	600	609	616	652	634
33.4	6/13	0000	0230	31	685	557	708	711	708	697	613	607	604	613	621	658	640

T10), the average temperature in the east and west sides (TE and TW, respectively), and the average overall temperature (TAV). Since thermocouples T3, T7, T9, and T10 were near the ends of the sample, their readings were not used for determining the average temperatures. The measured values have an uncertainty of less than 1% (see Sec. IV.A). Since the error is likely to be a bias, the averaging of many data points will increase the precision but not the accuracy. Examination of the data in Table VIII-5 revealed that the temperatures followed a very consistent pattern throughout the experiment. This demonstrates that the heat transfer pathways were not changed during the experiment and is a good indication that the structural integrity of the breeder and the capsule was maintained.

The data from Table VIII-5 were used to calculate temperature gradients, which are given in Table VIII-6. Also listed are the thermal neutron flux, the reactor power, and the tritium production rate. These quantities are needed to calculate the heating rates in the capsule.

The error in temperature gradient is calculated as follows. Let us assume the error in a single temperature number is 4°C on the west side and 2°C on the east side. Since four temperatures are used to calculate the gradient on the west side, the error in the temperature gradient is calculated to be 2°C. The error for the temperature gradient on the east side (two temperatures) is 1.4°C. The error for the average temperature gradient is less than 2°C.

The data from Table VIII-6 allowed calculation of heating rates in the steel (QSS) and the breeder (QLI). The total heat, QTOT, divided by the average temperature gradient, is approximately proportional to K, the thermal conductivity. The calculated values are given in Table VIII-7. The estimated error in the temperature gradient was less than 2°C, or less than 2%. The uncertainty in heating rates is 15%. The uncertainty in the thermal conductivity values is estimated to be 15%. The values are nearly all about 1.2, except for those at temperatures less than 400°C, which are higher. The results show that the effects of neutron irradiation have not caused large changes in thermal conductivity.

TABLE VIII-6

Heat Transfer Data from TRIO: Temperature Gradients

Run	Time			N	TAV (°C)	Temperature Gradients (°C)							NV[a]	RPWR[b]	TDOC[c]
	Date	On	Off			D2E	D37	D48	D59	D60	DTW	DT			
0.1	3/11	0346	0500	16	194	43	42	40	42	41	41	42	0.432	10.6	137.2
0.2	3/11	2020	2120	13	190	43	41	44	42	40	43	43	0.411	10.5	125.7
1.1	3/12	0856	0920	7	306	89	83	90	88	71	89	89	0.828	20.6	262.8
1.2	3/12	0936	0950	7	320	97	89	96	95	74	96	96	0.874	21.9	279.7
1.3	3/12	0950	1040	13	378	125	113	121	119	94	120	123	1.093	30.1	348.5
1.4	3/12	1040	1050	3	408	131	115	122	123	96	122	126	1.105	30.1	350.1
1.5	3/12	1054	1124	7	474	134	113	121	122	96	122	128	1.105	30.0	351.4
1.6	3/12	1200	2400	145	581	139	111	121	123	96	122	130	1.112	30.1	353.1
1.7	3/13	0000	1800	217	591	143	113	123	127	99	125	134	1.144	30.6	355.3
1.8	3/13	1800	3900	253	587	148	111	121	124	98	122	135	1.113	30.3	351.6
2.1	3/14	1600	3100	181	674	142	107	118	123	93	120	131	1.108	29.8	350.6
2.2	3/15	1700	3500	217	672	143	108	119	122	94	120	131	1.104	30.0	348.6
3.1	3/16	1100	1500	49	674	144	109	120	122	92	121	132	1.110	30.0	349.1
3.2	3/16	1600	3200	193	672	143	108	120	122	93	121	132	1.104	29.9	347.1
3.3	3/17	0900	1300	49	682	144	109	120	120	91	120	132	1.103	30.3	345.5
4.1	3/17	1800	2400	73	527	139	117	125	129	103	127	133	1.105	30.4	345.5
4.2	3/18	0000	2400	289	528	140	118	127	131	104	129	134	1.108	30.3	346.2
4.3	3/19	1200	2400	145	529	141	120	129	129	103	129	135	1.121	30.0	347.7
4.4	3/20	1200	2400	145	526	141	119	128	128	103	128	134	1.111	29.9	343.1
5.1	3/23	1200	2400	145	486	141	121	132	131	107	132	136	1.139	30.6	346.6
5.2	3/24	0000	0800	97	486	141	121	130	128	105	129	135	1.134	30.7	344.3
6.1	3/24	1200	2400	145	533	144	117	126	123	99	124	134	1.128	30.1	341.6
6.2	3/25	0000	1000	121	534	144	118	127	124	99	126	135	1.130	30.2	341.4
7.1	3/25	1500	2400	109	576	145	115	125	123	97	124	134	1.125	30.0	338.9
7.2	3/26	0900	2100	145	574	146	115	124	118	97	121	134	1.127	30.1	338.4
8.1	3/28	1500	2400	109	628	146	112	122	112	92	117	132	1.120	30.2	332.6
8.2	3/30	0000	1200	145	625	144	112	121	111	87	116	130	1.105	29.8	326.2
9.1	3/30	1200	2400	145	624	143	110	120	111	90	116	130	1.098	30.0	323.4
9.2	3/31	0000	2400	289	624	142	111	120	110	90	115	128	1.100	30.2	323.2
9.3	4/01	0000	2400	289	622	142	112	120	108	89	114	128	1.096	30.3	320.3
9.4	4/02	0000	2400	289	620	141	111	120	110	93	115	128	1.092	30.2	317.8
9.5	4/03	0000	2400	289	617	140	110	119	107	87	114	127	1.087	30.1	315.0
9.6	4/04	0000	1200	145	615	140	110	119	107	84	114	127	1.083	30.2	312.3
9.7	4/04	1800	2400	73	624	140	109	118	107	88	114	127	1.084	30.2	311.5
10.1	4/06	2000	2400	49	391	132	123	131	124	102	128	130	1.138	30.0	325.8
10.2	4/07	0000	0800	97	392	133	125	130	124	101	127	130	1.137	30.1	325.4
11.1	4/07	1000	2400	169	484	139	122	130	121	98	126	132	1.140	30.3	325.4
11.2	4/08	0000	0900	109	486	138	120	130	120	99	125	132	1.138	30.2	323.9
12.1	4/08	1100	2400	157	529	142	120	127	118	93	122	132	1.140	30.2	323.7
12.2	4/09	0000	1800	217	530	141	119	127	117	93	122	132	1.140	29.2	322.9
12.3	4/10	0000	0600	73	532	143	121	128	118	96	123	133	1.156	29.9	325.9
12.4	4/10	1400	2400	121	533	143	121	129	117	97	123	133	1.155	30.1	324.6
12.5	4/11	1600	2400	97	531	141	120	127	117	91	122	132	1.157	30.2	323.5
12.6	4/12	0000	0800	97	530	142	120	128	114	90	121	132	1.155	30.1	322.4
13.1	4/12	1200	2400	145	582	144	117	126	115	89	122	133	1.154	30.3	321.4
13.2	4/15	1800	2400	73	586	145	119	128	118	89	124	134	1.190	31.0	328.7
13.3	4/16	1200	2000	97	587	146	119	128	116	89	124	135	1.193	30.1	328.1
13.4	4/17	0000	2400	289	582	144	117	126	114	88	122	133	1.176	30.0	322.8
13.5	4/18	0000	0800	97	582	144	117	127	116	88	122	133	1.179	30.0	322.0
14.1	4/18	1200	2400	145	682	145	113	124	113	84	118	132	1.180	30.0	321.4
14.2	4/19	0000	2400	289	682	146	113	125	112	84	118	132	1.179	30.3	320.2
14.3	4/20	0000	0800	97	680	145	113	123	110	84	116	130	1.179	30.2	318.5
15.1	4/20	1400	2400	121	682	145	114	122	113	86	118	132	1.180	30.1	318.0
15.2	4/21	0000	1000	121	680	145	112	122	109	83	116	130	1.178	30.2	316.7
16.1	4/21	0900	2400	181	680	144	114	122	111	82	116	130	1.176	30.3	315.5
16.2	4/22	0000	1300	157	678	143	112	122	111	83	116	130	1.175	30.3	314.5
17.1	4/22	1200	2400	145	678	143	113	121	111	85	116	130	1.175	30.3	313.7
17.2	4/23	0900	2400	181	672	142	112	121	109	81	115	128	1.154	30.0	306.6
17.3	4/24	0000	2400	289	672	142	112	121	110	84	116	129	1.157	30.1	306.4
17.4	4/25	0000	0800	97	672	142	113	122	110	84	116	129	1.160	30.0	305.8
18.1	4/25	1800	2400	73	680	143	111	121	110	83	116	130	1.155	30.0	303.1
18.2	4/26	0000	1000	121	680	142	111	121	110	83	116	129	1.158	30.1	303.5
19.1	4/26	1100	2400	157	628	141	115	123	113	86	118	130	1.156	30.5	302.5
19.2	4/27	0000	0300	37	625	140	115	124	111	93	118	129	1.153	30.5	300.9
20.1	4/28	1100	1200	13	361	114	117	122	112	98	117	116	1.110	30.7	289.2
20.2	4/28	1200	1300	13	361	115	117	121	112	100	116	116	1.096	30.5	284.6
20.3	4/28	1300	1400	13	362	114	118	122	114	98	118	116	1.088	30.5	283.4
20.4	4/28	1500	1600	13	364	116	118	123	113	98	118	117	1.089	30.0	283.6
20.5	4/28	1600	1800	25	364	116	118	123	114	99	118	117	1.086	30.0	282.7
20.6	4/28	1800	2000	25	364	116	120	123	113	98	118	117	1.083	30.0	282.0

Run	Date	Time		N	TAV (°C)	Temperature Gradients (°C)							NV[a]	RPWR[b]	TDOC[c]
		On	Off			D2E	D37	D48	D59	D60	DTW	DT			
20.7	4/28	2000	2200	25	366	117	118	124	113	98	118	118	1.081	30.1	281.3
20.8	4/28	2200	2400	25	366	117	120	125	114	98	120	118	1.081	30.1	281.3
20.9	4/29	0000	0400	49	366	118	119	125	113	98	119	118	1.078	30.1	280.5
20.10	4/29	0400	0800	49	366	118	121	125	114	97	120	119	1.078	30.1	280.1
20.12	4/29	1200	2400	145	628	132	105	112	104	93	108	120	1.082	30.5	280.7
20.13	4/30	0000	2400	289	627	132	105	113	104	101	108	120	1.086	30.5	281.0
20.14	5/01	0000	2400	289	627	133	105	112	102	89	107	120	1.081	29.8	278.5
20.15	5/02	0000	1200	145	624	132	105	112	101	80	106	119	1.074	30.3	275.5
21.1	5/02	1200	2400	145	624	131	104	112	101	80	106	118	1.072	30.3	274.3
21.2	5/03	0000	0700	85	624	131	104	109	100	81	104	118	1.075	30.0	274.4
21.3	5/03	0800	2400	193	630	131	103	110	99	79	104	118	1.068	30.0	272.3
21.4	5/04	0000	0700	85	633	132	103	110	100	81	105	118	1.078	30.3	274.0
22.1	5/04	0900	2400	181	584	130	106	113	102	83	108	119	1.079	30.2	273.8
22.2	5/05	0000	0800	97	586	131	107	113	105	87	109	120	1.083	30.6	273.9
23.1	5/05	0900	2200	157	536	128	110	115	108	90	112	115	1.079	30.2	272.5
23.2	5/07	0000	0400	49	550	116	94	102	95	78	98	107	0.960	28.5	241.3
23.3	5/07	0600	1500	109	548	117	96	101	93	76	97	107	0.948	28.1	238.0
23.4	5/08	0600	2400	217	531	121	99	108	100	83	104	112	0.999	30.6	249.6
23.5	5/09	0400	0800	49	530	120	101	108	100	81	104	112	0.998	30.1	248.6
24.1	5/09	1100	2400	157	584	123	98	104	100	81	102	112	1.003	29.8	249.5
24.2	5/10	0000	1200	145	582	123	97	106	98	81	102	112	1.002	29.7	248.6
25.1	5/10	1500	2400	109	542	120	98	108	102	101	105	112	0.993	29.7	245.6
25.2	5/11	0000	0900	109	541	120	100	108	100	---	104	112	0.997	29.7	246.2
25.3	5/11	1500	2400	109	545	122	99	109	102	96	106	114	1.006	30.1	247.8
25.4	5/12	0000	0600	73	544	121	100	109	102	96	106	114	1.005	30.1	247.3
26.1	5/12	0800	2400	193	532	122	100	108	100	82	104	113	1.006	30.2	247.0
26.2	5/13	0000	2400	289	530	121	100	108	100	83	104	112	1.000	30.0	245.0
26.3	5/14	0000	2400	289	530	121	100	108	100	84	104	112	1.002	30.2	244.4
26.4	5/15	0000	2400	289	528	120	99	108	100	84	104	112	0.994	30.0	241.3
26.5	5/16	0000	0300	37	526	120	99	107	99	82	103	112	0.993	30.2	240.0
27.1	5/17	1500	2400	109	503	114	94	103	96	81	100	107	0.959	28.6	230.6
27.2	5/18	0000	2400	289	505	115	96	103	96	82	100	108	0.964	28.6	231.5
27.3	5/19	0000	2400	289	506	116	96	104	96	83	100	108	0.969	28.6	231.8
27.4	5/20	0000	2400	289	508	116	95	104	95	82	100	108	0.976	28.7	232.6
27.5	5/21	0000	2400	289	508	117	96	104	95	80	100	108	0.977	28.6	231.8
27.6	5/22	0000	2400	289	509	117	95	104	95	81	100	108	0.980	28.9	231.6
27.7	5/23	0000	0800	97	508	117	95	103	95	80	99	108	0.981	28.8	230.8
28.1	5/23	1200	2400	145	486	116	97	104	98	82	101	108	0.980	28.7	230.0
28.2	5/24	0000	2400	289	486	116	97	103	96	81	100	108	0.982	28.6	229.9
28.3	5/25	0000	2400	289	488	117	98	105	96	83	100	108	0.990	28.8	230.9
28.4	5/26	0000	2400	289	486	116	98	104	96	83	100	108	0.987	28.8	229.3
28.5	5/27	0000	2400	289	485	116	97	104	95	81	100	108	0.987	28.7	227.9
28.6	5/28	0000	1600	95	484	115	98	104	95	80	100	108	0.984	28.7	226.5
28.7	5/28	1800	2400	73	486	117	96	105	97	84	101	109	0.991	29.2	227.4
28.8	5/29	0000	1200	145	486	116	97	104	96	82	100	108	0.991	29.2	227.2
28.9	5/29	1200	2400	145	484	116	97	104	95	80	100	108	0.986	29.1	225.5
28.10	5/30	1200	2400	145	486	117	98	104	97	83	100	108	0.992	29.1	225.9
29.1	6/02	0000	0600	73	479	117	99	105	100	85	100	85	1.016	28.7	230.1
29.2	6/02	0700	0900	25	476	120	100	107	98	84	102	111	1.018	28.7	230.3
29.3	6/02	1000	1400	49	476	120	100	108	101	85	104	112	1.033	28.8	233.6
29.4	6/02	1500	2400	109	469	116	99	107	100	83	104	110	1.009	28.7	227.9
29.5	6/03	0000	2400	289	470	117	98	105	98	85	102	110	1.013	28.8	228.5
30.1	6/04	0000	2400	289	470	118	94	107	98	85	102	110	1.012	29.0	227.3
30.2	6/05	0000	2400	289	470	118	100	106	99	83	102	110	1.017	28.9	227.3
30.3	6/06	0000	0700	85	470	118	99	106	98	83	102	110	1.015	29.2	226.0
31.1	6/06	1100	2400	157	481	123	103	111	104	88	108	116	1.068	30.2	237.2
31.2	6/07	0000	2400	289	481	123	104	111	104	87	108	116	1.068	30.0	236.6
31.3	6/08	0000	0400	49	481	123	103	112	103	86	108	116	1.067	30.1	235.3
31.4	6/08	0500	1100	73	479	123	104	112	102	86	107	115	1.061	29.8	233.8
32.1	6/08	1300	2400	133	528	124	100	108	98	83	103	114	1.055	30.1	232.1
32.2	6/09	0000	2400	289	528	124	100	109	99	80	104	114	1.054	30.1	231.3
32.3	6/10	0000	0700	85	526	124	99	109	99	82	104	114	1.049	30.0	229.1
33.1	6/10	1200	2400	145	634	126	94	103	102	83	102	114	1.051	30.1	229.2
33.2	6/11	0000	2400	289	633	125	94	103	102	82	102	114	1.051	30.0	228.7
33.3	6/12	0000	0900	109	634	127	95	103	102	82	102	114	1.057	30.1	228.8
33.4	6/13	0000	0230	31	640	128	95	104	104	84	104	116	1.075	30.2	231.6

[a]NV is the thermal neutron flux, 10^{14} n/cm^2·s.

[b]RPWR is the reactor power, MW.

[c]TDOT is the tritium production rate, μCi/min.

TABLE VIII-7

Heat Transfer Data from TRIO: Thermal Conductivity

Run	Date	TAV	DT	NV	THTG	GAMM	QSS	QLI	QTOT	Q/DT	K, est.
0.1	3/11	194	42	0.432	1.076	1.986	3.09	5.12	8.21	0.195	1.43
0.2	3/11	190	43	0.411	0.986	1.890	2.94	4.80	7.74	0.180	1.32
1.1	3/12	306	89	0.828	2.062	3.808	5.93	9.81	15.74	0.177	1.29
1.2	3/12	320	96	0.874	2.194	4.019	6.26	10.38	16.64	0.173	1.27
1.3	3/12	378	123	1.093	2.734	5.026	7.79	12.96	20.76	0.169	1.24
1.4	3/12	408	126	1.105	2.747	5.081	7.91	13.07	20.99	0.167	1.22
1.5	3/12	474	128	1.105	2.757	5.081	7.90	13.09	20.99	0.164	1.20
1.6	3/12	581	130	1.112	2.770	5.114	7.96	13.17	21.13	0.157	1.15
1.7	3/13	591	134	1.144	2.787	5.261	8.19	13.44	21.63	0.161	1.18
1.8	3/13	587	135	1.113	2.759	5.118	7.97	13.16	21.13	0.157	1.15
2.1	3/14	674	131	1.108	2.751	5.095	7.93	13.10	21.03	0.161	1.18
2.2	3/15	672	131	1.104	2.735	5.076	7.90	13.05	20.95	0.160	1.17
3.1	3/16	674	132	1.110	2.739	5.104	7.94	13.10	21.04	0.159	1.17
3.2	3/16	672	132	1.104	2.723	5.076	7.90	13.03	20.93	0.159	1.16
3.3	3/17	682	132	1.103	2.711	5.072	7.90	13.00	20.90	0.158	1.16
4.1	3/17	527	133	1.105	2.711	5.081	7.91	13.02	20.93	0.157	1.15
4.2	3/18	528	134	1.108	2.716	5.095	7.93	13.05	20.98	0.157	1.15
4.3	3/19	529	135	1.121	2.728	5.155	8.02	13.17	21.19	0.157	1.15
4.4	3/20	526	134	1.111	2.692	5.109	7.95	13.03	20.98	0.157	1.15
5.1	3/23	486	136	1.139	2.719	5.238	8.15	13.29	21.44	0.158	1.15
5.2	3/24	486	135	1.134	2.701	5.215	8.12	13.22	21.34	0.158	1.16
6.1	3/24	533	134	1.128	2.680	5.187	8.07	13.14	21.21	0.158	1.16
6.2	3/25	534	135	1.130	2.678	5.196	8.09	13.15	21.24	0.157	1.15
7.1	3/25	576	134	1.125	2.659	5.173	8.05	13.08	21.13	0.158	1.15
7.2	3/26	574	134	1.127	2.655	5.183	8.07	13.09	21.16	0.158	1.16
8.1	3/28	628	132	1.120	2.609	5.150	8.02	12.96	20.98	0.159	1.16
8.2	3/30	625	130	1.105	2.559	5.081	7.91	12.76	20.67	0.159	1.16
9.1	3/30	624	130	1.098	2.537	5.049	7.86	12.67	20.53	0.158	1.16
9.2	3/31	624	128	1.100	2.535	5.058	7.87	12.68	20.55	0.161	1.18
9.3	4/01	622	128	1.096	2.513	5.040	7.84	12.62	20.46	0.160	1.17
9.4	4/02	620	128	1.092	2.493	5.022	7.82	12.55	20.37	0.159	1.16
9.5	4/03	617	127	1.087	2.471	4.999	7.78	12.48	20.26	0.160	1.17
9.6	4/04	615	127	1.083	2.450	4.980	7.75	12.41	20.16	0.159	1.16
9.7	4/04	624	127	1.084	2.444	4.985	7.76	12.41	20.17	0.159	1.16
10.1	4/06	391	130	1.138	2.556	5.233	8.15	13.01	21.16	0.163	1.19
10.2	4/07	392	130	1.137	2.553	5.228	8.14	13.00	21.14	0.163	1.19
11.1	4/07	484	132	1.140	2.553	5.242	8.16	13.02	21.18	0.160	1.17
11.2	4/08	486	132	1.138	2.541	5.233	8.15	12.99	21.14	0.160	1.17
12.1	4/08	529	132	1.140	2.540	5.242	8.16	13.00	21.16	0.160	1.17
12.2	4/09	530	132	1.140	2.533	5.242	8.16	12.99	21.15	0.160	1.17
12.3	4/10	532	133	1.156	2.557	5.316	8.27	13.15	21.42	0.161	1.18
12.4	4/10	533	133	1.155	2.547	5.311	8.27	13.13	21.40	0.161	1.18
12.5	4/11	531	132	1.157	2.538	5.320	8.28	13.13	21.41	0.162	1.19
12.6	4/12	530	132	1.155	2.529	5.311	8.27	13.10	21.37	0.162	1.19
13.1	4/12	582	133	1.154	2.522	5.307	8.26	13.08	21.34	0.160	1.17
13.2	4/15	586	134	1.190	2.579	5.472	8.52	13.45	21.97	0.164	1.20
13.3	4/16	587	135	1.193	2.574	5.486	8.54	13.47	22.01	0.163	1.19
13.4	4/17	582	133	1.176	2.533	5.408	8.42	13.27	21.69	0.163	1.19
13.5	4/18	582	133	1.179	2.526	5.422	8.44	13.28	21.72	0.163	1.19
14.1	4/18	682	132	1.180	2.522	5.426	8.45	13.28	21.73	0.165	1.21
14.2	4/19	682	132	1.179	2.512	5.422	8.44	13.25	21.69	0.164	1.20
14.3	4/20	680	130	1.179	2.499	5.422	8.44	13.23	21.67	0.167	1.22
15.1	4/20	682	132	1.180	2.495	5.426	8.45	13.23	21.68	0.164	1.20
15.2	4/21	680	130	1.178	2.485	5.417	8.43	13.20	21.63	0.166	1.22
16.1	4/21	680	130	1.176	2.475	5.408	8.42	13.17	21.59	0.166	1.22
16.2	4/22	678	130	1.175	2.467	5.403	8.41	13.15	21.56	0.166	1.21
17.1	4/22	678	130	1.175	2.461	5.403	8.41	13.14	21.55	0.166	1.21
17.2	4/23	672	128	1.154	2.405	5.307	8.26	12.88	21.14	0.165	1.21
17.3	4/24	672	129	1.157	2.404	5.320	8.28	12.90	21.18	0.164	1.20
17.4	4/25	672	129	1.160	2.399	5.334	8.30	12.92	21.22	0.164	1.20
18.1	4/25	680	130	1.155	2.378	5.311	8.27	12.85	21.12	0.162	1.19
18.2	4/26	680	129	1.158	2.381	5.325	8.29	12.87	21.16	0.164	1.20
19.1	4/26	628	130	1.156	2.373	5.316	8.27	12.85	21.12	0.162	1.19
19.2	4/27	625	129	1.153	2.361	5.302	8.25	12.80	21.05	0.163	1.19
20.1	4/28	361	116	1.110	2.269	5.104	7.94	12.32	20.26	0.175	1.28
20.2	4/28	361	116	1.096	2.233	5.040	7.85	12.15	20.00	0.172	1.26
20.3	4/28	362	116	1.088	2.223	5.003	7.79	12.07	19.86	0.171	1.25

TABLE VIII-7 (Contd.)

Run	Date	TAV	DT	NV	THTG	GAMM	QSS	QLI	QTOT	Q/DT	K, est.
20.4	4/28	364	117	1.089	2.225	5.008	7.80	12.08	19.88	0.170	1.24
20.5	4/28	364	117	1.086	2.218	4.994	7.77	12.05	19.82	0.169	1.24
20.6	4/28	364	117	1.083	2.212	4.980	7.75	12.01	19.76	0.169	1.24
20.7	4/28	366	118	1.081	2.207	4.971	7.74	11.99	19.73	0.167	1.22
20.8	4/28	366	118	1.081	2.207	4.971	7.74	11.99	19.73	0.167	1.22
20.9	4/29	366	118	1.078	2.201	4.957	7.72	11.96	19.66	0.167	1.22
20.10	4/29	366	119	1.078	2.198	4.957	7.72	11.95	19.65	0.165	1.21
20.11	4/29	370	121	1.088	2.217	5.003	7.79	12.06	19.85	0.164	1.20
20.12	4/29	628	120	1.082	2.202	4.976	7.75	11.99	19.74	0.164	1.20
20.13	4/30	627	120	1.086	2.205	4.994	7.77	12.03	19.80	0.165	1.21
20.14	5/01	627	120	1.081	2.185	4.971	7.74	11.95	19.69	0.164	1.20
20.15	5/02	624	119	1.074	2.161	4.939	7.69	11.86	19.55	0.164	1.20
21.1	5/02	624	118	1.072	2.152	4.930	7.67	11.83	19.50	0.165	1.21
21.2	5/03	624	118	1.075	2.153	4.943	7.69	11.85	19.54	0.166	1.21
21.3	5/03	630	118	1.068	2.136	4.911	7.64	11.77	19.42	0.165	1.20
21.4	5/04	633	118	1.078	2.150	4.957	7.72	11.87	19.59	0.166	1.22
22.1	5/04	584	119	1.079	2.148	4.962	7.72	11.88	19.60	0.165	1.21
22.2	5/05	586	120	1.083	2.149	4.980	7.75	11.91	19.66	0.164	1.20
23.1	5/05	536	115	1.079	2.138	4.962	7.72	11.86	19.58	0.170	1.25?
23.2	5/07	550	107	0.960	1.893	4.415	6.87	10.54	17.41	0.163	1.19
23.3	5/07	548	107	0.948	1.867	4.359	6.78	10.40	17.18	0.161	1.18
23.4	5/08	531	112	0.999	1.958	4.594	7.15	10.95	18.10	0.162	1.18
23.5	5/09	530	112	0.998	1.950	4.589	7.14	10.92	18.06	0.161	1.18
24.1	5/09	584	112	1.003	1.957	4.612	7.18	10.97	18.15	0.162	1.19
24.2	5/10	582	112	1.002	1.950	4.608	7.18	10.95	18.13	0.162	1.18
25.1	5/10	542	112	0.993	1.927	4.566	7.11	10.85	17.96	0.160	1.17
25.2	5/11	541	112	0.997	1.932	4.585	7.14	10.89	18.03	0.161	1.18
25.3	5/11	545	114	1.006	1.944	4.626	7.20	10.98	18.18	0.159	1.17
25.4	5/12	544	114	1.005	1.940	4.621	7.19	10.97	18.16	0.159	1.17
26.1	5/12	532	113	1.006	1.938	4.626	7.20	10.98	18.18	0.161	1.18
26.2	5/13	530	112	1.000	1.922	4.598	7.16	10.89	18.05	0.161	1.18
26.3	5/14	530	112	1.002	1.917	4.608	7.18	10.90	18.08	0.161	1.18
26.4	5/15	528	112	0.994	1.893	4.571	7.12	10.80	17.92	0.160	1.17
26.5	5/[illegible]6	526	112	0.993	1.883	4.566	7.11	10.77	17.88	0.160	1.17
27.1	5/[illegible]7	503	107	0.959	1.809	4.410	6.86	10.39	17.25	0.161	1.18
27.2	5/18	505	108	0.964	1.816	4.433	6.90	10.44	17.34	0.161	1.18
27.3	5/19	506	108	0.969	1.819	4.456	6.94	10.48	17.42	0.161	1.18
27.4	5/20	508	108	0.976	1.825	4.488	6.99	10.55	17.54	0.162	1.19
27.5	5/21	508	108	0.977	1.819	4.493	6.99	10.55	17.54	0.162	1.19
27.6	5/22	509	108	0.980	1.817	4.507	7.02	10.56	17.58	0.163	1.19
27.7	5/23	508	108	0.981	1.811	4.511	7.02	10.56	17.58	0.163	1.19
28.1	5/23	486	108	0.980	1.804	4.507	7.02	10.55	17.57	0.163	1.19
28.2	5/24	486	108	0.982	1.804	4.516	7.03	10.56	17.59	0.163	1.19
28.3	5/25	488	108	0.990	1.812	4.553	7.09	10.63	17.72	0.164	1.20
28.4	5/26	486	108	0.987	1.799	4.539	7.07	10.59	17.66	0.164	1.20
28.5	5/27	485	108	0.987	1.788	4.539	7.07	10.58	17.65	0.163	1.20
28.6	5/28	484	108	0.984	1.777	4.525	7.05	10.55	17.60	0.163	1.19
28.7	5/28	486	109	0.991	1.784	4.557	7.09	10.60	17.69	0.162	1.19
28.8	5/29	486	108	0.991	1.783	4.557	7.09	10.60	17.69	0.164	1.20
28.9	5/29	484	108	0.986	1.769	4.534	7.06	10.53	17.59	0.163	1.19
28.10	5/30	486	108	0.992	1.772	4.562	7.10	10.58	17.68	0.164	1.20
29.1	6/02	479	85?	1.016	1.805	4.672	7.27	10.82	18.09	0.212	1.56?
29.2	6/02	476	111	1.018	1.807	4.681	7.29	10.84	18.13	0.163	1.20
29.3	6/02	476	112	1.033	1.833	4.750	7.39	11.00	18.39	0.164	1.20
29.4	6/02	469	110	1.009	1.788	4.640	7.22	10.74	17.96	0.163	1.20
29.5	6/03	470	110	1.013	1.793	4.658	7.25	10.78	18.03	0.164	1.20
30.1	6/04	470	110	1.012	1.783	4.654	7.24	10.75	17.99	0.164	1.20
30.2	6/05	470	110	1.017	1.783	4.677	7.28	10.79	18.07	0.164	1.20
30.3	6/06	470	110	1.015	1.773	4.667	7.26	10.75	18.01	0.164	1.20
31.1	6/06	481	116	1.068	1.861	4.911	7.64	11.31	18.95	0.163	1.20
31.2	6/07	481	116	1.068	1.856	4.911	7.64	11.30	18.94	0.163	1.20
31.3	6/08	481	116	1.067	1.846	4.907	7.64	11.28	18.92	0.163	1.19
31.4	6/08	479	115	1.061	1.834	4.879	7.59	11.21	18.80	0.163	1.20
32.1	6/08	528	114	1.055	1.821	4.851	7.55	11.15	18.70	0.164	1.20
32.2	6/09	528	114	1.054	1.815	4.847	7.54	11.13	18.67	0.164	1.20
32.3	6/10	526	114	1.049	1.798	4.824	7.51	11.06	18.57	0.163	1.19
33.1	6/10	634	114	1.051	1.798	4.833	7.52	11.07	18.59	0.163	1.19
33.2	6/11	633	114	1.051	1.794	4.833	7.52	11.07	18.59	0.163	1.19
33.3	6/12	634	114	1.057	1.795	4.861	7.57	11.12	18.69	0.164	1.20
33.4	6/13	640	116	1.075	1.817	4.943	7.69	11.29	18.98	0.164	1.20

C. Integral Tritium Release and Tritium Inventory

The amounts of tritium accounted for and ^6Li and lithium quantities for lithium burnup are given in Table VIII-8. The different methods for determining the various integral quantities are in excellent agreement; all the measurements agree within the estimated error. There is thus confidence that all the tritium is accounted for: 35 Ci was produced and 35 Ci collected. The uncertainty in the total amount produced, the average of the four determinations, is estimated as 3%, or about 1 Ci. In addition, as previously discussed (Sec. VII.B), the stainless steel tubing leading from the reactor to the sweep gas analysis system was leached with recirculating water for 18 h, and an insignificant quantity of tritium was recovered.

TABLE VIII-8

Integral Tritium Data

Method Used	Tritium (Ci)	^6Li Burnup (%)	Lithium Burnup (%)	Estimated Error (%)
Tritium collected	35	33	0.18	5
^6Li assay	32	31	0.17	10
Thermal gradient	35	33	0.18	10
Dosimetry	39	38	0.21	10
Average	35	33	0.18	8.7

The amounts of tritium generated during each run were then calculated, normalized to a total production of 35.1 Ci. The tritium residue for each run was calculated, and the tritium inventory at the end of each run from the difference between the total amount generated (CTGEN) and the total amount recovered (CTCOL), as given in Table VIII-9. The tritium retention is known to be zero before irradiation and was measured as 0.019 ± 0.002 Ci at the end of the irradiation. The uncertainty is thus small at the beginning and at the end of the experiment. The uncertainty for the first 15 runs is estimated as 3% of the amount produced at the end of each run. For the last 18 runs, the uncertainty is estimated as 3% of the difference between the total amount of

TABLE VIII-9

Total Tritium

Run	Amount of Tritium (Ci)						
	TCOLL	CTCOL	TGEN	CTGEN	DEL T	TINV	±
0	0.002	0.002	0.022	0.022	0.020	0.020	0.001
1	1.015	1.017	1.094	1.116	0.079	0.099	0.03
2	0.999	2.016	0.966	2.082	-0.033	0.066	0.06
3	0.527	2.543	0.552	2.634	0.025	0.091	0.08
4	2.109	4.652	2.391	5.025	0.282	0.373	0.15
5	0.619	5.273	1.050	6.076	0.431	0.804	0.18
6	0.727	5.998	0.406	6.482	-0.321	0.484	0.19
7	1.816	7.814	1.486	7.968	-0.330	0.154	0.24
8	1.011	8.825	0.882	8.850	-0.129	0.025	0.27
9	1.832	10.657	2.603	11.453	0.771	0.796	0.34
10	0.042	10.699	0.421	11.875	0.379	1.175	0.36
11	0.307	11.006	0.462	12.337	0.155	1.331	0.37
12	1.265	12.271	1.835	14.172	0.570	1.901	0.42
13	2.305	14.576	2.061	16.232	-0.244	1.657	0.50
14	1.644	16.220	0.994	17.227	-0.650	1.007	0.52
15	0.746	16.966	0.373	17.600	-0.373	0.634	0.53
16	0.527	17.493	0.502	18.102	-0.025	0.609	0.51
17	1.311	18.804	1.331	19.433	0.020	0.629	0.47
18	0.412	19.216	0.380	19.813	-0.032	0.597	0.46
19	0.315	19.531	0.306	20.119	-0.009	0.588	0.45
20	0.035	19.566	1.585	21.705	1.550	2.139	0.40
21	1.095	20.661	0.783	22.488	-0.312	1.827	0.38
22	0.352	21.013	0.385	22.873	0.033	1.860	0.37
23	1.082	22.095	1.260	24.134	0.178	2.038	0.33
24	0.579	22.674	0.397	24.530	-0.182	1.856	0.32
25	0.546	23.220	0.618	25.148	0.072	1.928	0.30
26	1.265	24.485	1.414	26.562	0.149	2.077	0.26
27	2.471	26.956	2.169	28.731	-0.302	1.775	0.19
28	2.972	29.928	2.509	31.240	-0.463	1.312	0.12
29	0.755	30.683	0.732	31.972	-0.023	1.289	0.09
30	0.727	31.410	0.899	32.871	0.172	1.461	0.067
31	0.744	32.154	0.723	33.594	-0.021	1.440	0.045
32	1.277	33.431	0.605	34.199	-0.672	0.768	0.027
33	1.679	35.110	0.912	35.111	-0.767	0.019	0.002[a]
Total	35.110		35.111				

[a]Measured.

tritium produced (35.1 Ci) and the cumulative total produced at the end of each run.

The experimental conditions, the amounts of the different forms of tritium collected, and the calculated tritium inventories for the 33 runs are summarized in Table VIII-10. Those runs which did not reach equilibrium are indicated by "<" or ">" as appropriate. There were no experimental tritium permeation data for the first three runs, and the estimated tritium inventory values (in pararenthesis) could be in error by the order of 0.01 Ci. This possible error is small in comparison to the estimated uncertainty, however.

D. Analysis of Integral Tritium Inventory Using Steady-State Diffusion

A calculational method was devised to explore the degree to which intragranular diffusion is the rate limiting step in determining the tritium retention and release characteristics. For the ideal case of a spherical grain under isothermal conditions with a constant tritium generation rate and the assumption that intragranular diffusion is the dominant mechanism, the tritium inventory (tritium retention) in the grain is given by the relationship:

$$I_g = (r_g^2/15\ D)\dot{g} \ , \qquad (1)$$

where I_g = the tritium inventory, g; r_g = the grain radius, cm; D = the diffusivity, cm^2/s; and $\dot{g}$ = the generation rate, g/s. The diffusivity has a temperature dependance as:

$$D = D_0 \exp(-Q/RT) \ , \qquad (2)$$

where D_0 is a pre-exponential factor, Q is the activation energy, R is the gas constant, and T is the absolute temperature. In the ideal case (for isothermal conditions), if the logarithm of the tritium retention is plotted versus 1/T, a linear relationship is expected.

However, the TRIO experiment had a significant temperature variation; therefore, Eq. (1) has to be integrated over the volumetric temperature distribution in the sample. In this case, if a uniform tritium generation rate $(\dot{G})$ is assumed, the expression for tritium diffusive inventory, I_d, is:

$$I_d = (r_g^2/15)f\dot{G}/[D(\bar{T})] \ , \qquad (3)$$

TABLE VIII-10

Calculated Tritium Inventory for each TRIO Run.

Run No.	Conditions (°C)	HT	HTO	PERM	TCOLL	TGEN	TINV	±
0	Tests to 300°C	0.00186	0.00006	5×10^{-7}	0.002	0.022	0.020	0.001
1	600/STD	0.985	0.026	(0.004)	1.015	1.094	0.099	0.03
2	700/STD	0.985	0.009	(0.005)	0.999	0.966	0.066	0.06
3	700/1% H_2	0.513	0.011	(0.003)	0.527	0.552	0.091	0.08
4	550/STD	2.099	0.006	0.0038	2.109	2.391	>0.373	0.15
5	500/STD	0.617	0.004	0.0012	0.619	1.050	>0.804	0.18
6	550/STD	0.725	0.001	0.0008	0.727	0.406	0.484	0.19
7	600/STD	1.811	0.002	0.0031	1.816	1.486	0.154	0.24
8	650/STD	1.008	0.001	0.0023	1.011	0.882	0.025	0.27
9	650/No H_2	1.823	0.002	0.0068[a]	1.832	2.603	>0.796	0.34
10	400/No H_2	0.040	0.000	0.0018	0.042	0.421	>1.175	0.36
11	500/No H_2	0.300	0.003	0.0040	0.307	0.462	>1.331	0.37
12	550/No H_2	1.245	0.000	0.0197	1.265	1.835	>1.901	0.42
13	600/No H_2	2.197	0.000	0.108[a]	2.305	2.061	1.657	0.50
14	700/N H_2	1.560	0.001	0.083	1.644	0.994	1.007	0.52
15	700/STD	0.715	0.000	0.031	0.746	0.373	0.634	0.53
16	700/300 SCCM	0.503	0.001	0.023	0.527	0.502	0.609	0.51
17	700/30 SCCM	1.109	0.000	0.202	1.311	1.331	0.629	0.47
18	700/STD	0.380	0.000	0.032	0.412	0.380	0.597	0.46
19	650/STD	0.294	0.000	0.021[a]	0.315	0.306	0.588	0.45
20	650/0.2% O_2	0.028	0.000	0.0068	0.035	1.585	>2.139	0.40
21	650/STD	1.092	0.000	0.0034	1.095	0.783	1.827	0.38
22	600/STD	0.351	0.000	0.0013	0.352	0.385	1.860	0.37
23	550/STD	1.077	0.001	0.0035[a]	1.082	1.260	2.038	0.33
24	600/STD	0.576	0.002	0.0014	0.579	0.397	1.856	0.32
25	560/STD	0.537	0.007	0.0018	0.546	0.618	1.928	0.30
26	550/STD	1.213	0.048	0.0041[a]	1.265	1.414	2.077	0.26
27	525/STD	2.128	0.333	0.0103	2.471	2.169	1.775	0.19
28	500/STD	2.104	0.857	0.0107	2.972	2.509	1.312	0.12
29	480/300 SCCM	0.543	0.211	0.0007	0.755	0.732	>1.289	0.09
30	480/STD	0.721	0.004	0.0016	0.727	0.899	1.461	0.067
31	500/STD	0.740	0.003	0.0014	0.744	0.723	1.440	0.045
32	550/STD	1.271	0.004	0.0015	1.277	0.605	<0.768	0.027
33	650/STD	1.666	0.009	0.0038	1.679	0.912	0.019	0.002
	Total	32.958	1.543	0.608	35.110	35.111		

[a]"STD" = 100 SCCM, 0.1% H_2.

[b]Permeation sample taken.

where $\bar{T}$ is the volume-averaged temperature, and f is a factor to account for the temperature distribution. The factor f is the ratio between the tritium inventory for the actual distribution and the idealized isothermal inventory at a temperature of $\bar{T}$. For the TRIO experiment, the generation rate is reasonably uniform, having a range of less than 10% throughout the sample. In addition, although the generation rate does vary considerably throughout the course of the experiment (see Sec. VI), it is reasonably constant during a single run. The grain size did not measurably change over the course of the experiment, as noted in Sec. VII.

For purposes of calculational simplicity, a radial temperature profile is assumed. This temperature profile is characterized by two integrated parameters: $\bar{T}$ and $\Delta\bar{T}$ (average radial temperature drop across the pellet thickness). For the capsule geometry (hollow cylinder of outer radius r_0 and inner radius r_i) and an unknown activation energy Q, the f factor is given by

$$f = f(\bar{T},\Delta\bar{T},Q) = (\beta - 1)^{-1} \int_1^{\beta} \exp\left[(Q/R\bar{T})(\bar{T}/T - 1)\right] d\eta \ , \qquad (4)$$

where $\beta = r_0^2/r_i^2 = 2.56$; $\eta = r^2/r_i^2$; and T = local temperature.

Equation (3) can be inverted to solve for the diffusivity as a function of measured and calculated data:

$$D(\bar{T}) = (r_g^2/15) f(\dot{G}/I_d) \ . \qquad (5)$$

The generation rate $(\dot{G})$, the inventory values (I_d), the volume-averaged temperatures $(\bar{T})$, and temperature gradients $(\Delta\bar{T})$ are obtained from data previously presented. The grain radius r_g is taken to be 0.1 μm. If intragranular diffusion is the dominant mechanism, then the calculated diffusivity values should vary linearly with 1/T on a semilog plot. Because f and D depend on the unknown activation energy, Q, iteration is required.

The TRIO runs at conditions optimal for tritium release (i.e., hydrogen added to the sweep gas) were postulated to be diffusion controlled. Since the uncertainties in the calculated tritium inventories were smallest at the beginning and at the end of the experiment, the first eight runs and the last six runs were used for the analysis. The data are summarized in Table VIII-11.

TABLE VIII-11

Calculated Diffusivities from TRIO Data

Run No.	Volume-Averaged Temp. (°C)	Temp. Gradient (°C)	$I_d/\dot{G}$ (10^4 s)	f	Diffusivity (10^{-16} cm^2/s)
1	592	126	1.70	2.62	10.3
2	677	122	1.13	2.38	14.1[a]
3	685	122	1.56	2.36	10.1[a]
4	627	125	>6.49	2.99	<3.08
5	481	125	>14.0	3.30	<1.58
6	530	20	8.54	2.97	2.32
7	578	130	2.73	2.73	6.65
8	627	130	0.462	2.50	36.1
28	489	107	34.5	2.74	0.532
29	474	107	>34.5	2.84	<0.551
30	474	107	37.3	2.84	0.507
31	484	112	37.4	2.88	0.513
32	531	111	<20.0	2.64	0.883
33	642	113	0.498	2.33	31.2

[a]Uncertainty in inventory is large relative to its magnitude.

The data were then plotted in Figure VIII-1. The solid circles in the figure represent runs that achieved equilibrium and the open circles represent those that did not. The calculated diffusivity (diffusion coefficient) shows excellent agreement with the equation

$$D = 1.1 \times 10^{-6} \exp(-35.8/RT) , \quad (6)$$

where R = the gas constant in Kcal/mol. The activation energy is 35.8 Kcal/mol (150 kJ/mol). The excellent agreement with the linear relationship provides strong evidence that the tritium release for these selected runs is diffusion-controlled.

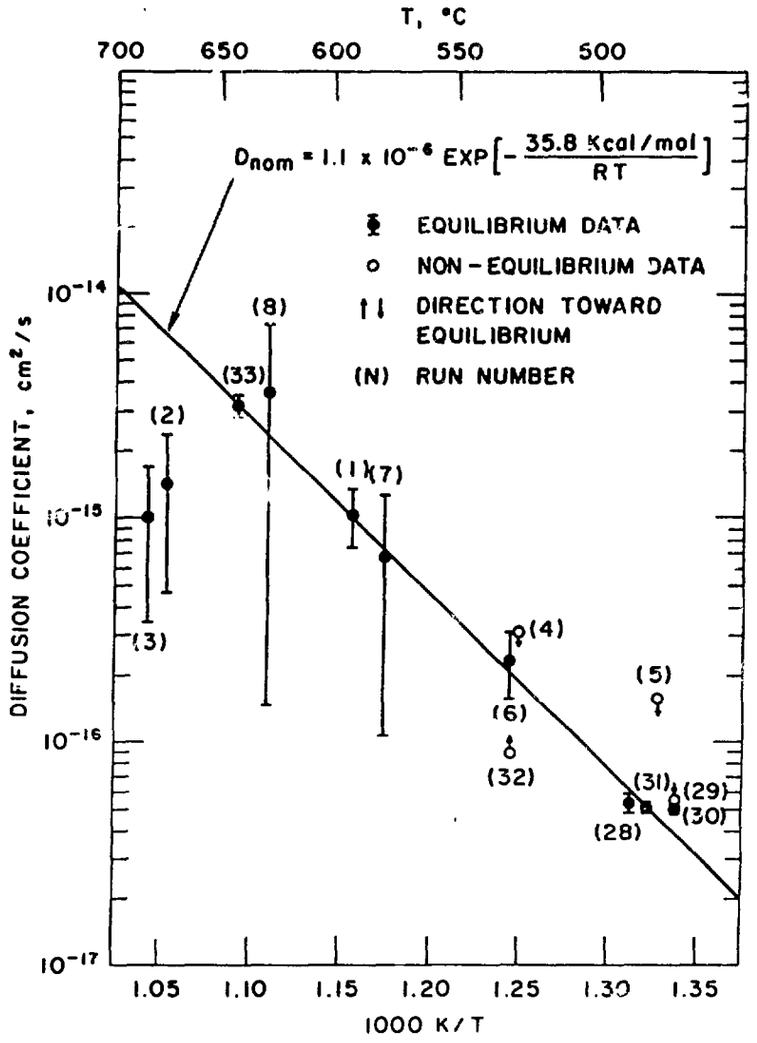

Fig. VIII-1. Diffusion coefficient for tritium in $LiAlO_2$ determined from selected TRIO runs in which intragranular diffusion appeared to be the rate-limiting phenomenon in tritium transport. The one-sigma bands are based on uncertainties in the experimental generation rate ($\dot{G}$) and inventory (I).

Based on an error generation analysis which includes the uncertainties in generation rate and derived inventory, the diffusion coefficient for $LiAlO_2$ deduced from the TRIO data can be written as:

$$\ell n\left(D/cm^2 \cdot s^{-1}\right) = \left(-13.7 \pm 2.3\right) - \left(35.8 \pm 3.9\right)\ Kcal/mol/RT\ . \qquad (7)$$

If the variability in grain size (±30%) is also included in the uncertainty analysis, then the following equation should be used when comparing to single crystal data:

$$\ell n\left(D/cm^2 \cdot s^{-1}\right) = \left(-13.7 \pm 1.8\right) - \left(35.8 \pm 3.9\right)\ Kcal/mol/RT\ . \qquad (8)$$

No attempts were made to include uncertainties in temperature distribution in the error analysis. While the accuracy of the thermocouples was quite good, the asymmetry of the temperature profile introduces uncertainty into the calculation which could not be easily estimated because of the limited number of data points.

The above relationship was then used to calculate inventories for Runs 9-26. These calculated inventories, given in Table VIII-12, are called the "diffusive inventories". For these runs in general, the diffusion model does not account for all the tritium retained.

E. Analysis of Dynamic Tritium Release Data

The dynamic tritium release curves (see Sec. VI.F) provide additional information on the transport behavior of tritium. Steady-state diffusion analysis was utilized above to investigate runs that appear to be diffusion controlled. An independent way to study these runs is to use transient diffusion kinetics. Described herein is analysis of the dynamic tritium release data using a transient diffusion method.

The dominant mechanism for tritium release is postulated to be intragranular diffusion for selected runs. The grains are assumed to be uniform spheres, 0.1 μm in radius. The generation rate is assumed to be uniform and constant for a given run. The steady-state release rate is equal to the generation rate. The time to reach any fraction of the steady-state release rate is sensitive to the diffusivity, and the diffusivity is in turn sensitive to temperature.

First, let us consider an idealized case for a step change in temperature at a constant generation rate. For an isothermal grain with an initial temperature T_1 and a final temperature T_2, the time-dependent solutions for the release rate, $\dot{R}_g$, and the inventory, I_g, are:

$$\dot{R}_g/\dot{g} = 1 + (D_2/D_1 - 1)(6/\pi^2) \sum_{n=1}^{\infty} (1/n^2) \exp(-n^2\pi^2 t/\tau_2) \qquad (9)$$

$$I_g/(I_g)_{SS} = 1 + (D_2/D_1 - 1)(90/\pi^4) \sum_{n=1}^{\infty} (1/n^4) \exp(-n^2\pi^2 t/\tau_2) \ , \qquad (10)$$

TABLE VIII-12

Diffusive Inventories for Runs 9-27

Run No.	Volume Averaged Temp. (°C)	Temp. Gradient (°C)	f	Diffusive Tritium Inventory (Ci)
9[a]	630	128	2.51	0.02
10[a]	396	127	4.10	<67.8
11[a]	488	128	3.18	>2.02
12[a]	605	128	2.60	0.07
13	582	128	2.08	0.12
14	684	126	2.35	0.01
15	684	126	2.35	0.01
16	682	126	2.36	0.01
17	677	125	2.36	0.01
18	683	125	2.34	0.01
19	628	126	2.50	0.04
20[a]	639	116	2.36	0.03
21	639	116	2.36	0.03
22	588	117	2.52	0.09
23	533	109	2.60	0.34
24	585	109	2.43	0.08
25	546	113	2.61	0.23
26	530	109	2.62	0.76
27	513	106	2.64	0.56

[a]These runs did not achieve steady state.

where

$$(I_g)_{SS} = (\tau_2/15)\,\dot{G}$$

t = time from change in temperature

$$\tau_2 = r_g^2/D_2$$

$$D_1 = D(T_1)$$

$$D_2 = D(T_2)\ .$$

Figure VIII-2 is a plot of Eq. (9) for the case of $D_2/D_1 = 19.4$, which corresponds to a step change of 100°C from 500 to 600°C. An observation can be made with regard to Eq. (9). Since the size of the spike in the release rate is given by $(\dot{R}_g)_2/(\dot{R}_g)_1 = D_2/D_1$, an increase in temperature results in a positive spike and a decrease results in a negative spike with reference to

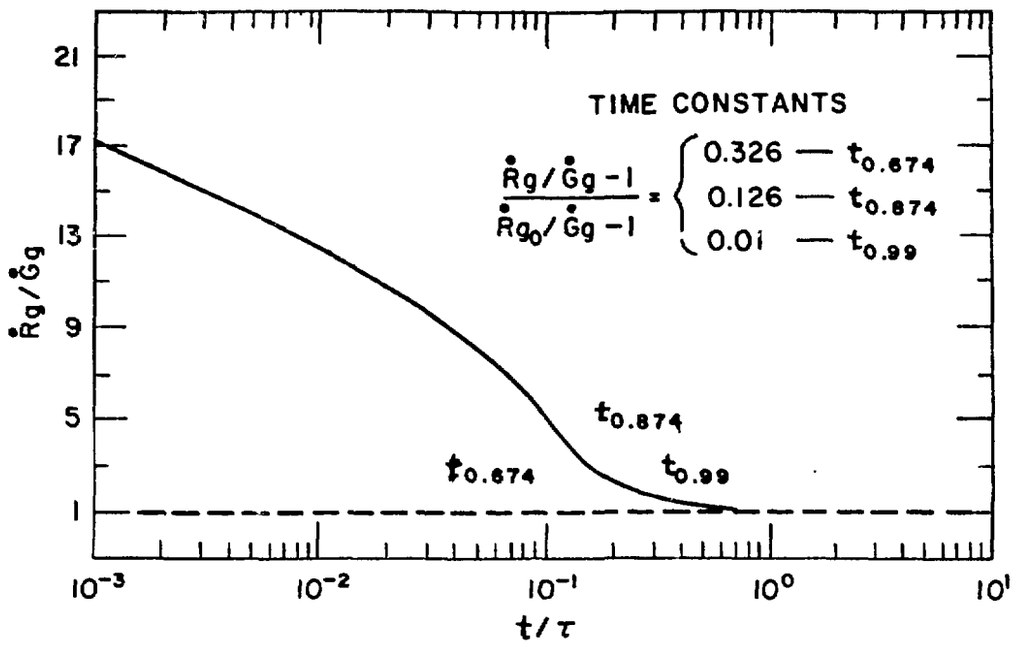

Fig. VIII-2. Fractional release rate for step increase in temperature $(\tau_1/\tau_2 = 19.4)$.

the generation rate line. As previously discussed (Sec. VI.F), this pattern was consistently observed throughout the course of the experiment for nearly all 33 runs.

The effect of spatial temperature distribution is more complicated than it was for the steady-state case. Let $T_1 = T_1(\eta)$ be the temperature before the temperature jump and $T_2 = T_2(\eta)$ be the temperature distribution after the jump. Integration of Eqs. (9) and (10) yields

$$\dot{R}/\dot{G} = 1 + (6/\pi^2) \sum_{n=1}^{\infty} (1/n^2)(\beta - 1)^{-1} \int_1^{\beta} (D_2/D_1 - 1) \times \exp(-n^2\pi^2 t/\tau_2)\, d\eta \,, \tag{11}$$

$$I/I_{SS} = 1 + (90/\pi^4) \sum_{n=1}^{\infty} (1/n^4) \times \frac{\int_1^{\beta} (\tau_1 - \tau_2) \exp(n^2\pi^2 t/\tau_2)}{\int_1^{\beta} \tau_2\, d\eta} \,. \tag{12}$$

Figures VIII-3 through -5 show the experimentally determined tritium release rate $(\dot{R}_e)$ versus the analytically determined [(Eq. (11)] release rate $(\dot{R}_{min}, \dot{R}_{nom}, \dot{R}_{max})$ for Runs 8, 28, and 31. In all three cases, the size of the calculated spike is greater than the experimentally determined value. This finding is to be expected because the model assumes an instantaneous temperature change and the monitoring instrumentation lag time is not included in the analysis. The general shapes of the analytical and experimental curves have some similarity, but the quantitative results are somewhat different. Owing to the sensitivity of response to temperature, the differences may be due to the modeling of the temperature profiles.

Equation (9) can be manipulated to show that the time response of the system depends only on T_2 for step changes in isothermal temperatures. Let

$$F_e \equiv 1 - (\dot{R}_g/\dot{g} - 1)(\dot{R}_{g_0}/\dot{g} - 1)^{-1} , \tag{13}$$

where F_e is related to the approach to equilibrium and $\dot{R}_{g_0}/\dot{g} = D_2/D_1$. Substituting Eq. (9) into Eq. (13) gives

$$F_e = 1 - (6/\pi^2) \sum_{n=1}^{\infty} (1/n^2) \exp(-n^2 t/\tau_2) . \tag{14}$$

The variable F_e is a measure of the extent of approach to equilibrium, being equal to zero at the beginning of the transient and reaching unity at steady state; F_e is a function only of τ_2, which is equal to r_g^2/D_2. Equation (13) can then be used to compare calculated and experimental values of F_e for the non-isothermal TRIO runs. This procedure was employed to calculate the time required to reach 67% of the way to equilibrium. The calculations are compared to the experimental data in Table VIII-13. Once again, the results are encouraging but not conclusive.

While the transient analysis strongly suggests that bulk diffusion is the dominant release mechanism during temperature changes, a more accurate analysis, which models the actual temperature history, is required before this is demonstrated quantitatively. Such efforts, however, would be hampered by the uncertainties in the generation and release rates.

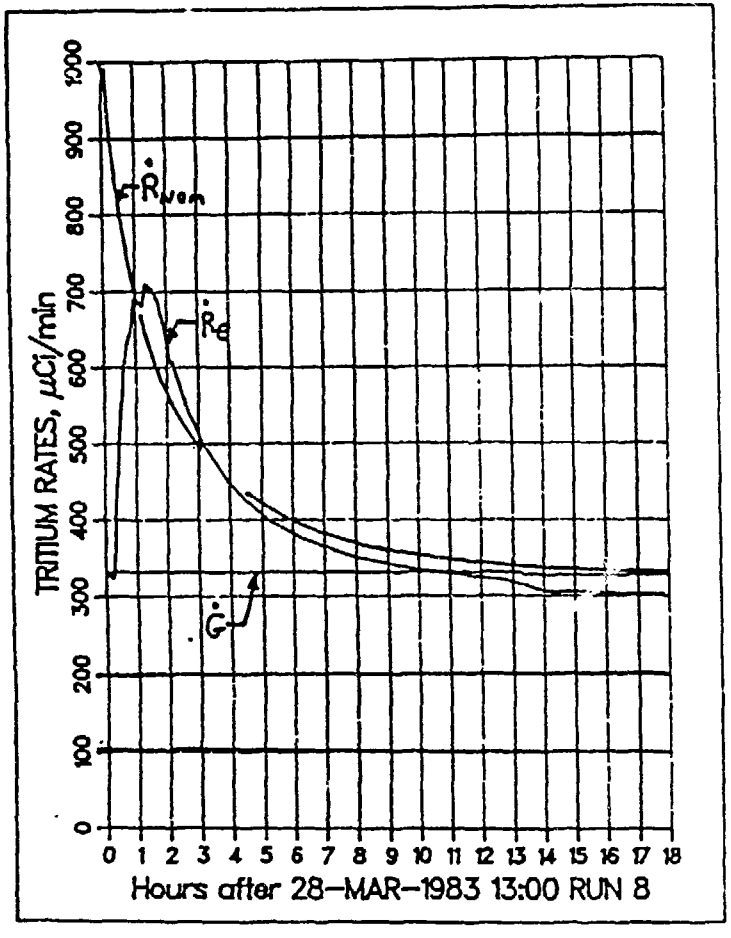

Fig. VIII-3. Comparison between analytical predictions ($\dot{R}_{nom}$) for Run 8 and TRIO tritium rate ($\dot{R}_e$) for a mean temperature increase from 578°C to 627°C. The generation rate ($\dot{G}$) is also shown.

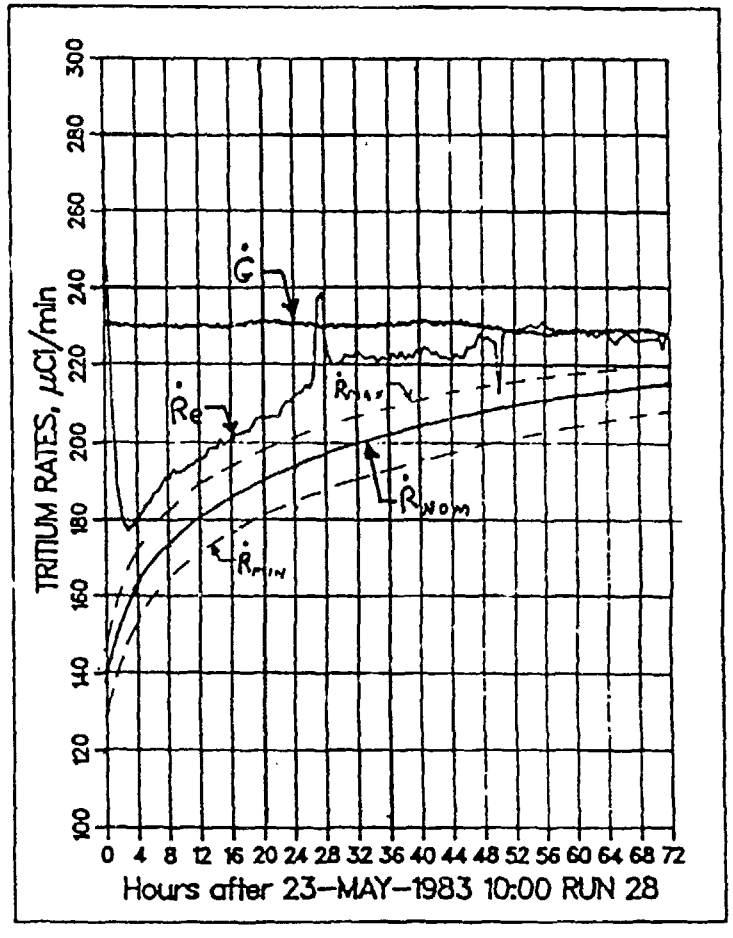

Fig. VIII-4. Comparison between analytical predictions ($\dot{R}_{min}$, $\dot{R}_{nom}$, $\dot{R}_{max}$) for Run 28 and TRIO tritium release rate ($\dot{R}_e$) for a mean temperature decrease from 513°C to 489°C. The generation rate ($\dot{G}$) is also shown.

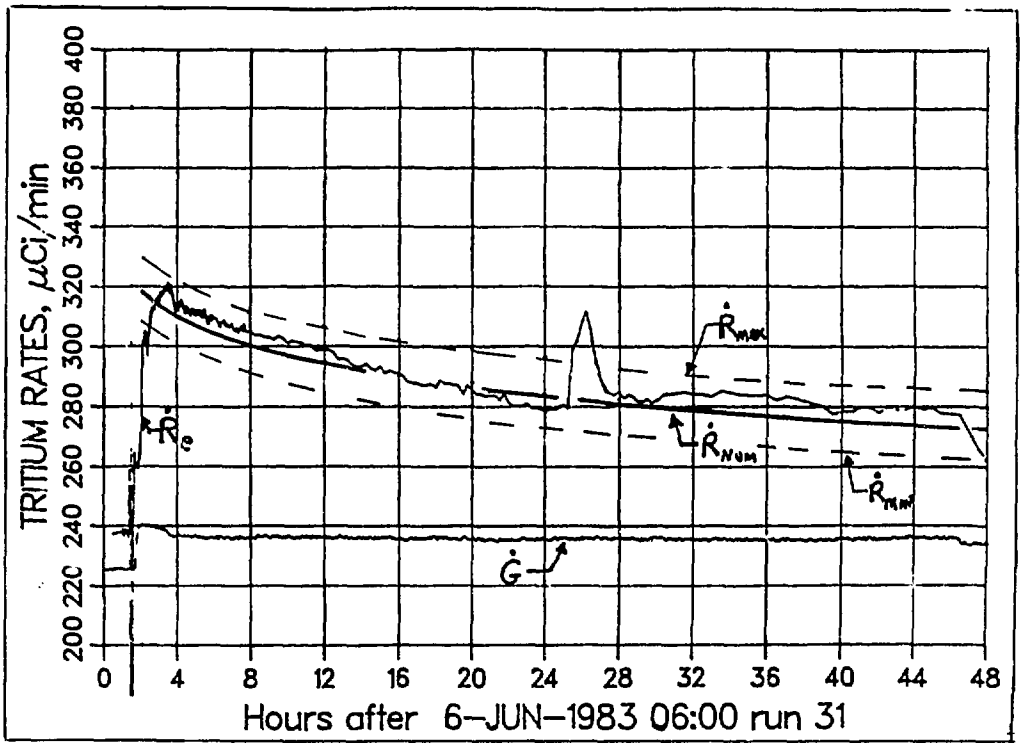

Fig. VIII-5. Comparison between analytical prediction $(\dot{R}_{nom})$ for Run 31 and TRIO tritium release rate $(\dot{R}_e)$ for a mean temperature increase from 474°C to 484°C. The generation rate $(\dot{G})$ is also shown.

TABLE VIII-13

Comparison Between Predictions and TRIO Results (in Parentheses) for Time to Reach 67% of Steady-State Release Rate After a Temperature Change

Run No.	T_i (°C)	T_{i+1} (°C)	ΔT_i (°C)	ΔT_{i+1} (°C)	$t_{0.67}$[a] (h)
8	530	578	130	126	1.8 (2.5)
28	513	489	106	107	33.0 (21.0)
31	474	484	107	112	81.0 (38.0)

[a] $[\dot{R}(t_{0.67})/\dot{G} - 1]/[\dot{R}_0/\dot{G} - 1] = 0.33 \rightarrow t_{0.67}$.

SECTION IX

DISCUSSION

IX. DISCUSSION

The most important results from the TRIO experiment are those which contribute to the fundamental understanding of transport of tritium and the transport of heat in a fusion reactor blanket. Since a limited parameter space is tested in an experiment of this kind, models have to be developed so that the results can be extrapolated to anticipated conditions in a fusion reactor blanket. Experimental results were obtained on the amount of tritium retained, or the tritium inventory, as a function of test conditions for the 33 runs. The results also provided quantitative data for intragranular diffusion and information on surface effects and on the chemical species of tritium evolved from the capsule. In addition, the permeation rate of tritium through the inner capsule wall was measured, and an analysis of temperature profiles and heating rates provided data on heat transfer. It was concluded that the irradiation produced measurable amounts of volatile radionuclides and activation products in the lithium aluminate breeder material. These results and their implication for blanket design are discussed.

A. Tritium Inventory in the Solid Breeder

1. Tritium Inventory Model

A tritium transport model was developed in support of the STARFIRE study.[1] This model is used to predict the steady-state tritium inventory in a solid breeder blanket. Five transport mechanisms were identified: (1) bulk diffusion, (2) surface desorption, (3) gas-phase transport through interconnected pores in the solid, (4) dissolution -- sometimes called "solubility", and (5) trapping. Each mechanism can contribute to the tritium inventory in the blanket. The total inventory is estimated as the sum of the individual contributions.

For bulk diffusion, probably the best understood of the five transport mechanisms, there is at least some semi-quantitative data for a number of candidate solid breeders. Bulk diffusion is considered to contribute significantly to the tritium inventory in the blanket. Based on diffusion, the tritium inventory is a strong function of grain size and temperature. Activation

energies for diffusion are typically a few tens of kilocalaries per mole. Thus, the tritium inventory rapidly increases as temperature decreases. It is primarily this temperature dependence which establishes the lower temperature limits for solid breeders.[1] Under steady-state conditions, where the tritium generation rate equals the tritium release rate which equals a constant, the following expression has been developed for spherical particles (single-crystal grains):[38]

$$I_d = \dot{g} r_g^2 / 15\ D\ , \qquad (1)$$

where I_d = the diffusive inventory, i.e., the inventory one would calculate with the assumption that bulk diffusion is the only process contributing significantly to tritium inventory. The other terms are: $\dot{g}$ = the generation rate of tritium; r_g = the radius of the spheres; and D = diffusivity. For STARFIRE, at 500°C, if r_g = 0.1 μm, D = 10^{16} cm^2/s, and τ = 6 × 10^3 g/s, the diffusive inventory would be 400 g, assuming uniform temperature throughout the blanket. For the TRIO experiment, assuming the same conditions except that $\dot{g}$ = 5 μCi/s, the steady-state inventory is estimated to be 0.33 Ci. In practice, the temperatures have a significant range in both the TRIO experiment and in a fusion reactor blanket. Under this circumstance, the volumetric temperature distribution must be integrated to calculate the diffusive inventory.

Surface desorption processes could affect tritium transport, particularly for microstructures having high porosity and small grain size, as is the case for the $LiAlO_2$ material used in TRIO. The tritium inventory associated with surface effects is directly dependent on surface area. Presence of hydrogen gas or water may help tritium release by isotopically swamping available surface sites. The activation energies for adsorption/desorption are rather low, on the order of a few kilocalories per mole, and the temperature dependance is thus rather weak.

Because of the small grain size of the TRIO pellets, the surface area is large, estimated to be the order of 10 m^2/g. If one assumes a surface site has an area of 10 $Å^2$, for the 42 g of $LiAlO_2$, there are 4.2 × 10^{21} sites, which if completely filled would hold 200 Ci of tritium atoms. In the experiment, only a small fraction of the sites is likely to be occupied by a hydrogen or a tritium atom. In addition, protium is present at a concentration

three orders of magnitude higher than tritium for most of the experiment. Under these circumstances, the surface inventory is expected to be orders of magnitude less than 200 Ci.

Gas phase transport through the interconnected porosity establishes the tritium partial pressure in contact with the solid breeder. The tritium inventory is estimated by considering the solid to be in equilibrium with the gas phase; the tritium dissolution is then estimated. During the STARFIRE study, considerations of gas phase transport indicated that a reasonable amount of interconnected porosity (20-30%) was desirable for minimizing tritium inventories.[1,18] In addition, larger pore sizes, >1 μm, are beneficial. In order to have large pore sizes and, at the same time, small grain sizes, a microstructure having a bimodal pore size distribution was proposed for the breeder material in STARFIRE.[1] This type of microstructure was selected and fabricated for the TRIO experiment (see Sec. IV.B.)

Tritium dissolution was considered to be a potentially significant problem, particularly for Li_2O, on the basis of some idealized thermodynamic calculations.[1] The primary assumption in these calculations is that activity coeffients are unity. More recent measurements of H_2O-Li_2O phase equilibria have shown that activity coefficients are very large, approaching 1000 at some temperatures. As a result, tritium dissolution in Li_2O is very small, the order of 1 wppm. The tritium solubility in ternary ceramics is expected to be even less. Therefore, tritium dissolution is not expected to make a significant contribution to the tritium inventory.

Trapping could conceivably result in very high tritium inventories in solid breeders. In the STARFIRE study, it was considered a possibility that radiation-induced trapping could lead to unacceptably high tritium inventories. However, the literature contains no applicable data for solid breeders which could have allowed even qualitative limits on this effect to be established.

2. Tritium Inventory Results from the TRIO Experiment

For the TRIO experiment, the tritium inventory for the 33 runs was given in Table VIII-10. As previously discussed, the data from the first eight runs and the last six runs provided an excellent fit to a steady-state diffusion model. These runs represent optimal conditions for tritium release, namely,

0.1% hydrogen added to the sweep gas stream. It is inferred that, when hydrogen is added, surface release is enhanced but intragranular diffusion is not appreciably changed. Under these conditions intragranular diffusion is the rate-limiting step for tritium release; the tritium release is diffusion controlled.

For Runs 9-27, the inventory was assumed to be a sum of two components, the diffusive inventory (I_d) and the surface (including solubility) inventory (I_S). The derived diffusion relationship from Runs 1-8 and 28-33 [Eq. (6), Sec. VIII] was used to calculate diffusive inventories for Runs 9-27. Each surface inventory (I_S) was taken to be the total inventory minus the diffusive inventory (I_d). The results are given in Table IX-1. Certain trends appear upon examination of the data in Tables VIII-10 and IX-1. For Runs 1-8, the surface inventory term is negligible because the inventories are ascribed to intragranular diffusion. This set of runs had hydrogen added to the sweep gas, generally 0.1% or a thousand-fold excess with respect to tritium.

Runs 9-14 had no hydrogen added to the sweep gas stream (the actual hydrogen concentration was about 3 ppm, or about three times the tritium level). For this set of runs the surface inventory increased from a negligible quantity to about 1 Ci. As discussed above, the surface site population of tritium could well account for a tritium inventory of 1 Ci for the conditions of Runs 9-14. Addition of 0.1% hydrogen should decrease the surface inventory by more than an order of magnitude; as a result, the surface inventory for the first eight runs is expected to be less than 0.1 Ci. The tritium inventories for the first eight runs appear to be diffusion controlled, and the actual surface inventories for these runs do indeed appear to be less than 0.1 Ci.

Runs 15-19 represent a return to "standard" conditions; i.e., hydrogen was again added to the sweep gas. The calculated diffusive inventories for these runs do not account for all the tritium, which is 0.6 Ci. However, the uncertainty in tritium inventory for these runs is estimated as 0.5 Ci. Therefore, it cannot be concluded that the surface inventory is significantly large for these runs.

TABLE IX-1

Tritium Inventories for Runs Which Were Not Diffusion Controlled

Run No.	Conditions[a]	HT	HTO	PERM	TCOLL	TGEN	I_d	I_s
9[b]	650/No H_2	1.823	0.002	0.0068	1.832	2.603	0.02	>0.78
10	400/No H_2	0.040	0.000	0.0018	0.042	0.421	(67.8)	---
11	500/NO H_2	0.300	0.003	0.0040	0.307	0.462	(2.02)	---
12	550/No H_2	1.245	0.000	0.0197	1.265	1.835	0.07	>1.83
13	600/No H_2	2.197	0.000	0.108	2.305	2.061	0.12	1.54
14	700/No H_2	1.560	0.001	0.083	1.644	0.994	0.01	1.00
15[c]	700/STD	0.715	0.000	0.031	0.746	0.373	0.01	0.62
16	700/300 SCCM	0.503	0.001	0.023	0.527	0.502	0.01	0.60
17	700/30 SCCM	1.109	0.000	0.202	1.311	1.331	0.01	0.62
18	700/STD	0.380	0.000	0.032	0.412	0.380	0.01	0.59
19	650/STD	0.294	0.000	0.021	0.315	0.306	0.04	0.55
20[d]	650/0.2% O_2	0.028	0.000	0.0068	0.035	1.585	0.03	>2.11
21	650/STD	1.092	0.000	0.0034	1.095	0.783	0.03	1.80
22	600/STD	0.351	0.000	0.0013	0.352	0.385	0.09	1.77
23	550/STD	1.077	0.001	0.0035	1.082	1.260	0.34	1.70
24	600/STD	0.576	0.002	0.0014	0.579	0.397	0.08	1.78
25	560/STD	0.537	0.007	0.0018	0.546	0.618	0.23	1.70
26	550/STD	1.213	0.048	0.0041	1.265	1.414	0.36	1.72
27	525/STDF	2.128	0.333	0.0103	2.471	2.169	0.56	1.22

NOTE: "STD" = 100 SCCM, 0.1% H_2.

[a]Value on the right of slash (/) is temperature (°C); value on left is gas composition.

[b]Hydrogen was removed from the sweep gas after Run 8 and up to Run 14.

[c]0.1% H_2 was added to the sweep gas after Run 14 and up to Run 19.

[d]Oxygen was added to the sweep gas in Run 20.

Run 20 had 0.2% oxygen added to the sweep gas. Very little tritium was evolved during this run, and the retention was more than 2 Ci when the run was ended. Given the temperature (700°C), the diffusive inventory was calculated to be negligible in comparison to the total inventory. Furthermore, this excess inventory of about 2 Ci persisted for Runs 21-26 even though hydrogen was added for these runs. In addition, a large amount (about 1.5 Ci) of HTO (tritium in the condensable form) was released in Runs 25-29, about a month after Run 20 had ended. About 2 Ci of tritium was retained either in the breeder material or somewhere else in the system for an extended period of time as a result of the oxygen addition. As previously discussed (Sec. VI.G)

small HTO spikes consistently occurred about one day after large HT spikes. The response time of the system to a release of HTO from the breeder was concluded to be ~1 day. Therefore, the 2 Ci of excess tritium is associated with either the surface or the bulk of the breeder material.

The last six runs (28-33) appear to be diffusion controlled. The agreement between the calculated diffusivities for Runs 1-8, 28-33, and the derived diffusivity relationship [Eq. (6) in Sec. VIII-D] is quite good, shown in Fig. VIII-2.

There is another point regarding Table VIII-10 that is useful to place the data in context. Both the tritium generation rate and the mass of breeder material in a 4000-MW fusion reactor[1,9] are just about 10 million times those in the TRIO experiment. Since 1 kg of tritium is 10 million Ci, the inventories listed in Curies for TRIO would translate to inventories in such fusion reactor blankets in units of kilograms.

B. Intragranular Diffusion

Diffusivity values have been reported for polycrystalline alumina,[47-48] single-crystal alumina,[49] and lithium aluminate itself.[29,50-52] Selected literature data on diffusivity are compared to the TRIO results in Fig. IX-1. Since Wiswall et al.[29] obtained lithium aluminate from the same source used for TRIO, the grain size was assumed to be the same for the two studies. In addition, the diffusivity values were recalculated from their tritium release curves to correct for a small error. Yunker[50] did not report grain size or diffusivity, but his activation energy agrees with the TRIO results. The grain size for Yunker's experiment was assumed to be 0.3 μm. The activation energy of 35.8 Kcal/mol is rather large in comparison to that of other solid breeders, but the value is in agreement with Wiswall et al.[29] and Yunker.[50] In addition, the activation energy for tritium and hydrogen diffusion in alumina[47-49] is similar. Both Guggi et al.[51] and Vasiliev et al.[52] report much lower activation energies and higher diffusivities for tritium in lithium aluminate than derived from TRIO. In both these cases, the particle sizes are reported as two to three orders of magnitude larger than those of TRIO. It is also possible that the true grain size in these experiments is much smaller than the grain size which would explain the large difference in magnitude but not activation energy. Another point is that activation energies as high as

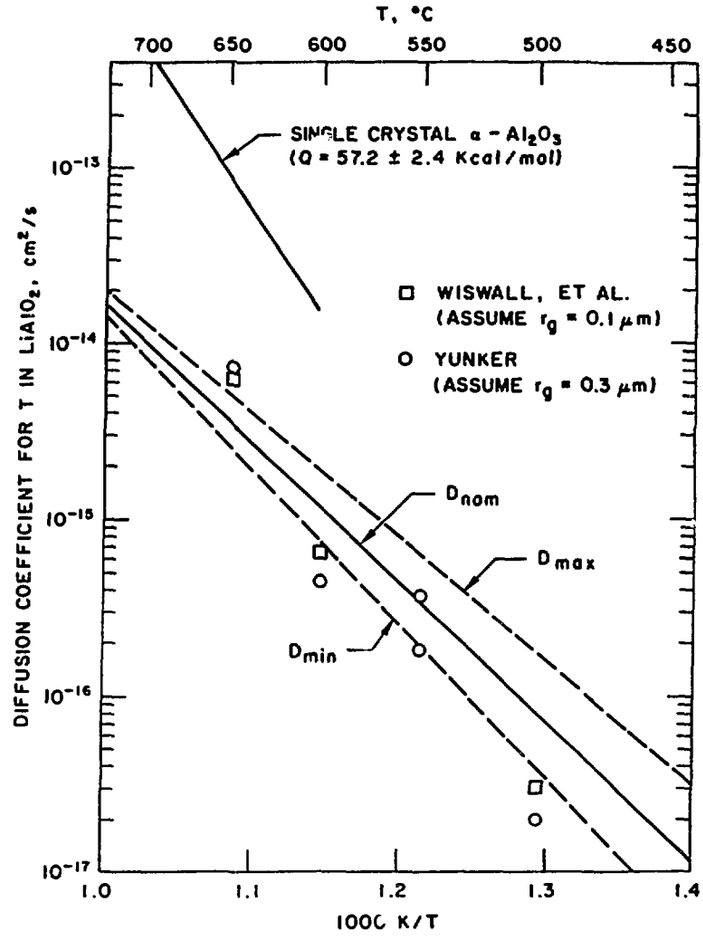

Fig. IX-1. Comparison of selected data for tritium diffusion in γ-$LiAlO_2$ with the TRIO correlation (includes uncertainties in grain size, inventory, and generation rate).

35.8 Kcal/mol are most probably due to intragranular diffusion. Other processes such as surface sorption and grain edge diffusion are expected to have much lower activation energies. Based on the high value of the activation energy, the good fit of the experimental data to the diffusivity relationship, and the agreement of the experimental data with results of two other independent studies, it is considered likely that the diffusivity values derived from the TRIO experiment represent intragranular diffusion.

The data for runs at the beginning and end of the experiment indicate that the controlling mechanism for tritium transport, when hydrogen is added to facilitate surface desorption, is intragranular diffusion. Over the limited temperature range, the data fit a single equation. Based on this observation, no evidence exists for trapping, which was earlier considered[1] to

possibly be a dominant effect. Thus, for the limited conditions and burnup of the TRIO experiment, trapping is not considered a significant contributor to tritium inventory.

A material such as lithium aluminate could show a wide range of diffusivities owing to impurities and solid-state effects.[53] The diffusivity could be affected by oxide vacancy concentration. Since low oxygen potentials tend to form more vacancies, diffusivity could be enhanced. Conversely, when oxygen potential is high (e.g., Run 20), defect content is reduced and diffusion is correspondingly reduced. This possibility cannot be resolved with the TRIO results.

It is of interest to assess the impact of the derived diffusivity in terms of tritium inventory in a fusion reactor blanket. With the calculational method previously described (Sec. VIII.D), the temperature distributions given in the Blanket Comparison and Selection Study (BCSS)[9] were used to estimate tritium inventories. In that study, the tritium generation rate is 0.006 g/s for the entire blanket of the 4000-MW reactor. The maximum temperature is fixed at 950°C, and the minimum temperature is varied from 300 to 550°C. As was the case for TRIO, capsule geometry for this study was a hollow cylinder, but the coldest temperatures was on the inside of the cylinder rather than on the outside.

The results of this analysis are presented in Table IX-2. In this table, the temperature distribution is characterized by a volume-averaged temperature (TVAV), over the range from the maximum temperature (TMAX) to the minimum temperature (TMIN). The f factor has the same meaning as before, viz., the ratio between tritium inventory for the actual case and that for the isothermal (T = TVAV) case. The results show that the diffusive tritium inventory rises very rapidly as the minimum temperature is decreased. If the diffusive inventory is not to exceed 1 kg, then the minimum temperature for the blanket must be no lower than 350°C.

C. Surface Effects

As noted above, the presence of hydrogen appears to enhance the release of tritium. For example, hydrogen addition of 0.1% (a thousand-fold excess) enhanced tritium release rates and reduced tritium inventories associated with the surface. A simple argument presented above showed that isotope swamping

TABLE IX-2

Calculated Diffusive Inventories for a
4000-MW Fusion Reactor Blanket

TMAX (°C)	TMIN (°C)	TVAV (°C)	f	Tritium Inventory (kg)
950	550	846	1.180×10^{1}	7.10×10^{-3}
950	500	534	3.009×10^{1}	2.16×10^{-3}
950	450	823	9.384×10^{1}	7.92×10^{-2}
950	400	811	3.831×10^{2}	0.388
950	350	800	2.080×10^{3}	2.50
950	300	789	3.664×10^{4}	23.5

of surface sites with hydrogen could account for the reduction in tritium inventory when hydrogen was added.

There is further evidence of surface effects. Namely, in Run 3, the hydrogen content was increased from 0.1 to 1%. The HT release curve (see Fig. VI-13) shows a positive spike followed by a very rapid return to equilibrium. The time constant is the order of ten minutes. This rapid response is not characteristic of processes in the bulk of the breeder solid, such as intragranular diffusion, but is characteristic of a surface process, which is much more rapid.

For Run 20, oxygen was added, and very little tritium came out. The tritium inventory increased by about 2 Ci as a result. Run 21 (0.1% H_2) shows a large positive peak, followed by a return to steady state as shown in the HT release curve (Fig. VI-52). The release curve for Run 21 does not appear to show a different response than other similar runs (e.g., Run 33). Thus, although the tritium retention is higher for Run 21, the release kinetics do not appear to be affected. The excess tritium, which appears to be in the oxide form, does not seem to inhibit release of the rest of the tritium. If this excess tritium is on the surface, it is probably not affecting surface release rates.

One other issue should be mentioned: The surface could affect the ratio of HT to HTO. This possibility is discussed in the next section.

D. Species of Tritium Evolved

The predominant form of tritium evolved during the experiment was the HT, or noncondensable form. Prior to the experiment, the expectation was that the oxide breeder would give rise to the oxide form of tritium. This result has serious implications for blanket design because the permeation rates for HT are much greater than those for HTO, and thus tritium loss rates by permeation could become high. A number of rationales for this observation exist, including kinetic and thermodynamic arguments discussed below.

Perhaps the simplest way to look at the system is first to assume that lithium aluminate produces T_2O and the T_2O reacts with H_2 to form HT and H_2O. For the runs when 0.1% H_2 was added, which is 1000 times the tritium level in the sweep gas, one would expect HT to be the dominant tritium form. However, this rationale does not account for the fact that the noncondensable HT form was dominant even when H_2 was not added.

Another possibility is that the structural material, Type 304 stainless steel, is playing a role in the equilibrium process by affecting the oxygen potential of the system. In vapor effusion studies, Guggi et al.[51] noted that the presence of a stainless steel container caused a very significant increase in the vapor pressure of elemental lithium over lithium aluminate. In other words, the oxygen potential was very low in Guggi's test. A series of thermodynamic calculations were performed to assess the effect of the steel cladding on the system. To perform the rather complex set of equilibrium calculations, the SOLGASMIX code was used.

The calculations are for a system that was initially 1 mole of lithium aluminate at 1000 K. It is assumed that 100 mole ppm of the lithium was burned up to form 100×10^{-6} g atoms tritium, 99% tritium was released and recovered from the system, and 50 g atoms oxygen were produced by burnup and remained in the system. The effect of the steel is approximated by assuming the system contains 0.01 g atom iron. The condensed phases are simulated by $LiAlO_2$, $LiAl_5O_8$, iron, and iron oxide.

In the first calculation, the results of which are shown in Table IX-3, the oxygen activity was fixed at a value derived from the results of Guggi et al[51], 2×10^{-35} atm. Based upon these results, the ratio of T_2O to T_2 is very small, 5×10^{-6}. This result is consistent with the TRIO observations. The tritium content of the condensed phase is 5.6% of the total amount of tritium.

If the H_2-H_2O couple sets the oxygen potential (assuming 1 ppm water and 0.1% H_2 in the gas phase), the oxygen potential is about 10^{-26} atm at 1000 K. Under this condition, the HTO:HT ratio is still very small, less than 0.001.

If the iron-iron oxide couple is dominant, then the oxygen potential is still higher, as shown in Table IX-4. The reduced T_2 form is only a factor of two higher than the T_2O form. In this case, over 99% of the tritium in the system is in solid solution as the tritoxide in the lithium aluminate condensed phase. This represents a considerable increase over the first case (Table IX-3) and indicates that the oxygen potential may affect the tritium retention.

A final calculation, summarized in Table IX-5, corresponds to the oxygen level set at 0.1% in the gas phase (approximately Run 20). The oxide form does become dominant in the gas phase, but 99.85% of all the tritium in the system is retained in the solid as the tritoxide.

The above calculations have considerable uncertainty in a number of areas; in particular, the activity coefficient of the tritoxide in solution is unknown. Nonetheless, the trends are meaningful. For example, it was found that the stainless steel cladding may control the oxygen potential sufficiently to yield the observed results In the TRIO tests, the cladding temperature was rather high; the tube on the inside was hotter than the breeder material, and the cladding was near the temperature at the colder surface of the breeder. In a fusion reactor with pressurized water coolant, the temperature of the steel structural material will be considerably lower. In this case, the effect of the cladding as a reducing agent will be much less. In addition, if the cladding is oxidized before use with an oxide layer on the steel, the steel may not participate in the equilibrium. Under this circumstance the fraction of the condensable form will be considerably larger.

A second point of interest is that the amount retained in the solid by dissolution rose dramatically as the oxygen potential was increased. The release enhancement observed when hydrogen was added to the sweep gas may be explained by this effect. Conversely, the effect is consistent with the observation that addition of oxygen was detrimental to tritium release.

TABLE IX-3

Lithium Aluminate Equilibria: Fixed Oxygen Content

Species	Moles at Equilibrium	Partial Pressure (atm)
Inert gas	0.35000×10^{-3}	0.99999
T_2 (G)	0.23414×10^{-8}	0.66895×10^{-5}
O_2 (G)	0.82058×10^{-25}	0.23445×10^{-21}
T_2O (G)	0.71875×10^{-9}	0.20536×10^{-5}
LiOT (G)	0.31388×10^{-14}	0.89680×10^{-11}
$(LiOT)_2$ (G)	0.73446×10^{-21}	0.20984×10^{-17}
LiO (G)	0.72859×10^{-25}	0.20817×10^{-21}
Li_2O (G)	0.64548×10^{-23}	0.18442×10^{-19}
LiT (G)	0.86381×10^{-20}	0.24680×10^{-16}
Li (G)	0.20134×10^{-16}	0.57524×10^{-13}
AlO_2T (G)	0.38082×10^{-25}	0.10880×10^{-21}
AlOT (G)	0.95695×10^{-26}	0.27341×10^{-22}
Al (G)	0.21823×10^{-32}	0.62351×10^{-29}
$LiAlO_2$ (S)	0.99987	Mole Fraction 0.10000×10^{1}
LiOT (L)	0.99385×10^{-6}	0.99398×10^{-6}
$LiAl_5O_8$ (S)	0.25248×10^{-4}	Mole Fraction 0.10000×10^{1}
LiOT (L)	0.25096×10^{-10}	0.99398×10^{-6}

Note: Thermodynamic equilibrium conditions in a 1-mole $LiAlO_2$ system that contains no protium. The oxygen activity is taken as that for the Fe/FeO system. Total system pressure is 1 atm at 1000 K. Assumes that 100-mole ppm burnup of lithium has occurred, that 1% of the produced tritium is still present, and that no oxygen has been lost. The system contains, therefore, 0.9999 g•atom oxygen, 1.0 g•atom aluminum, and 1×10^{-6} g•atom tritium.

TABLE IX-4

Lithium Aluminate Equilibria: Low Oxygen Activity

Species	Moles at Equilibrium	Partial Pressure (atm)
Inert gas	0.35000×10^{-3}	0.99865
T_2 (G)	0.47181×10^{-6}	0.13462×10^{-2}
O_2 (G)	0.20994×10^{-34}	0.59902×10^{-31}
T_2O (G)	0.23151×10^{-11}	0.66057×10^{-8}
LiOT (G)	0.17826×10^{-15}	0.50863×10^{-12}
$(LiOT)_2$ (G)	0.23657×10^{-23}	0.67501×10^{-20}
LiO (G)	0.29168×10^{-27}	0.83226×10^{-24}
Li_2O (G)	0.64635×10^{-23}	0.18442×10^{-19}
LiT (G)	0.30691×10^{-16}	0.87570×10^{-13}
Li (G)	0.50426×10^{-14}	0.14388×10^{-10}
AlO_2T (G)	0.21628×10^{-26}	0.61710×10^{-23}
AlOT (G)	0.34000×10^{-22}	0.97013×10^{-19}
Al (G)	0.34194×10^{-25}	0.97566×10^{-22}
$LiAlO_2$ (S)	0.10000×10^{1}	Mole Fraction 0.10000×10^{1}
LiOT (L)	0.56375×10^{-7}	0.56375×10^{-7}
$LiAl_5O_8$ (S)	0.28189×10^{-7}	Mole Fraction 0.10000×10^{1}
LiOT (L)	0.15891×10^{-14}	0.56375×10^{-7}

Note: Analogous to Table IX-3 except that the lithium activity is fixed (and the oxygen activity is also thereby fixed) at the value taken from Guggi's study of $LiAlO_2$ in a stainless steel cell.

TABLE IX-5

Lithium Aluminate Equilibria: High Oxygen Activity

Species	Moles at Equilibrium	Partial Pressure (atm)
Inert gas	0.35000×10^{-3}	0.99900
T_2 (G)	0.11455×10^{-17}	0.32696×10^{-14}
O_2 (G)	0.35035×10^{-6}	0.10000×10^{-2}
T_2O (G)	0.72624×10^{-9}	0.20729×10^{-5}
LiOT (G)	0.31567×10^{-14}	0.90101×10^{-11}
$(LiOT)_2$ (G)	0.74211×10^{-21}	0.21182×10^{-17}
LiO (G)	0.33144×10^{-20}	0.94602×10^{-17}
Li_2O (G)	0.64613×10^{-23}	0.18442×10^{-19}
LiT (G)	0.42064×10^{-29}	0.12006×10^{-25}
Li (G)	0.44347×10^{-21}	0.12658×10^{-17}
AlO_2T (G)	0.38299×10^{-25}	0.10932×10^{-21}
AlOT (G)	0.46599×10^{-35}	0.13301×10^{-31}
Al (G)	0.0	0.0
$LiAlO_2$ (S)	0.99987	Mole Fraction 0.10000×10^{1}
LiOT (L)	0.99852×10^{-6}	0.99865×10^{-6}
$LiAl_5O_8$ (S)	0.25250×10^{-4}	Mole Fraction 0.10000×10^{1}
LiOT (L)	0.25216×10^{-10}	0.99865×10^{-6}

Note: Analogous to Tables IX-3 and -4 except that the oxygen activity is set at 0.001 to correspond to a doped sweep gas with 0.1% oxygen.

The species evolved could be affected by a number of other factors, such as surface effects and internal kinetic factors. For example, if the diffusion rate of tritium atoms is much faster than that of oxygen atoms, more of the HT form could be released, at least for a short period of time. This process could be affected by surface effects. The experimental results are not sufficient to prove or disprove such effects. It is not considered likely that radiolysis of HTO can account for the experimental results.

E. Tritium Permeation

The data on tritium permeation through the primary cladding (see Sec. VI.E) were translated into permeation rates in units of curies per day. The resultant permeation rates are illustrated in Fig. IX-2. The data appear to follow a definite pattern.

During Runs 9-15, no hydrogen was added to the sweep gas, as illustrated by the solid squares. For those runs (solid squares in Fig. IX-2), the permeation rate is close to the calculated rate for the tritium pressure and geometry of the capsule, as is shown by the reference lines which used data for austenitic stainless steel.[46] When hydrogen gas was added to the sweep gas, permeation rates decreased by an order of magnitude. This effect is attributed to isotope swamping. For the idealized case, a 1000-fold excess of hydrogen would be expected to reduce the permeation by a factor of $\sqrt{1000}$, or about 30. The observed decrease is close to that value.

F. Heat Transfer Results

The heat transfer results were presented in Sec. VIII.B. The most significant results were the in-pile measurement of thermal conductivity for the lithium aluminate. These data are plotted in Fig. IX-3. The large open circles represent the data for the first few experimental runs; the dots represent the later runs. The estimated precision is <10%. The data show no significant changes in thermal conductivity as a result of increased irradiation. It is inferred that, for the temperature range of interest, limited radiation damage (equivalent to about two months in a fusion reactor) does not significantly affect thermal conductivity.

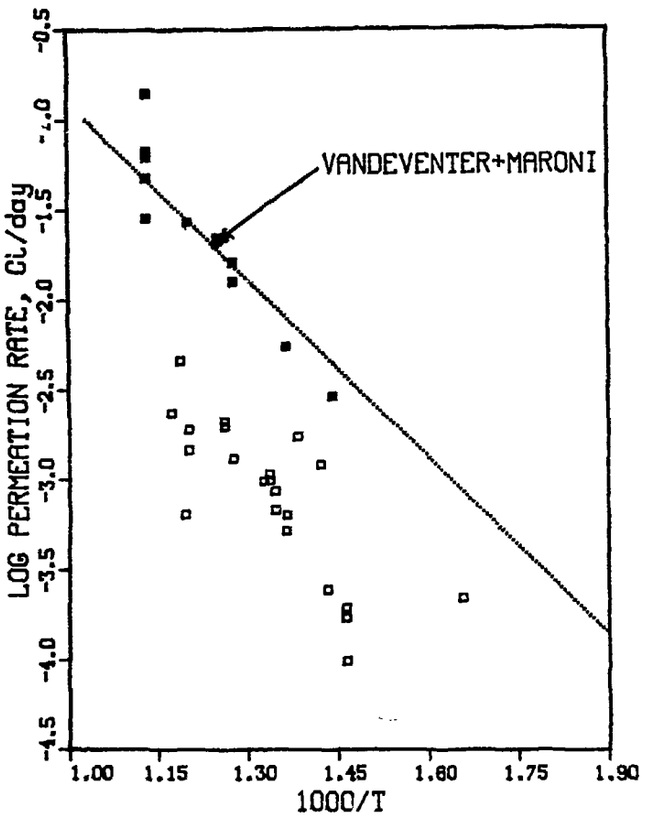

Fig. IX-2. Tritium permeation results for TRIO.

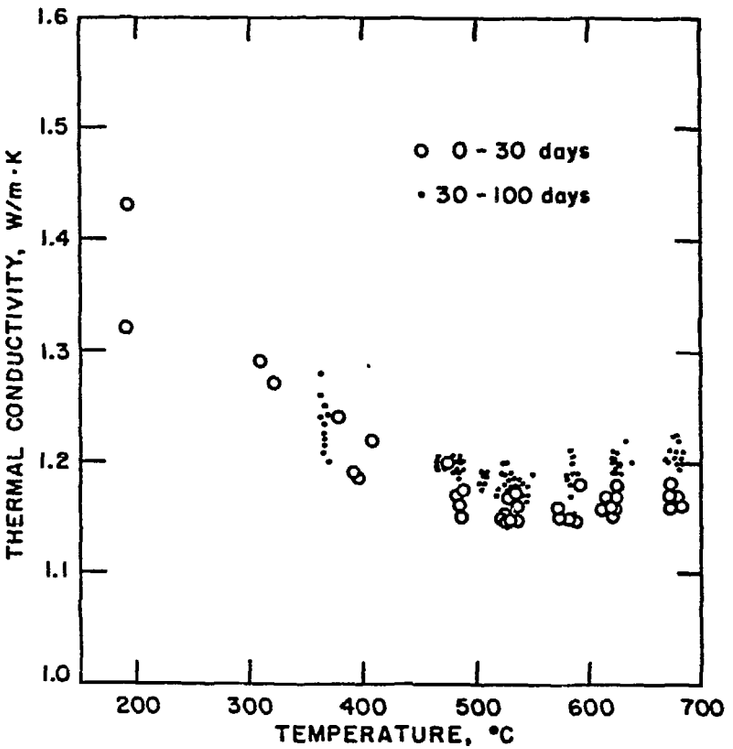

Fig. IX-3. Thermal conductivity of γ-$LiAlO_2$ measured in-pile.

G. Radioactivity

As previously discussed, impurities in the breeder material resulted in generation of measurable quantities of a number of volatile radionuclides during radiation. The levels measured showed significant temperature dependence, but the data were not adequate to calculate release rates.

Chemical analysis including neutron activation was performed prior to irradiation. In addition, the irradiated material was analysed by gamma spectrometry. The data should be useful in providing guidance to calculations of fusion blanket radioactivity and afterheat.

SECTION X

CONCLUSIONS

X. CONCLUSIONS

The purpose of the TRIO experiment was to test in-situ tritium recovery and heat transfer performance of a candidate breeder material, lithium aluminate. Seven objectives were proposed for the experiment (see Sec. II), and all of them were met. A large amount of data was collected and analyzed. From the results of the experiment, the conclusions are:

1. In-situ tritium recovery can work very well. The inventory levels at the end of the experiment were less than 0.1 wppm. More than 99.9% of the tritium generated in the lithium aluminate was recovered.

2. Intragranular diffusion was found to be an important tritium transport mechanism. For runs at the beginning and end of the experiment when hydrogen was added to the sweep gas, the experimental data showed excellent agreement with the derived diffusivity given by the relationship:

$$D = 1.1 \times 10^{-6} \exp(-35.8 \text{ Kcal/RT})$$

The derived diffusivity appears to be consistent with other data in the literature.

3. The tritium inventories and tritium release rates are accounted for by consideration of intragranular diffusion, surface effects, and tritium dissolution ("solubility"). There is no evidence of detrimental or anomalous effects of radiation on tritium transport, such as trapping.

4. Addition of hydrogen to the sweep gas enhanced the release of tritium. This release enhancement is ascribed to improvement in surface release kinetics.

5. The addition of oxygen to the sweep gas was detrimental to release of tritium. This effect is consistent with thermodynamic calculations showing increased retention of tritium as the oxygen potential is increased. In addition, the oxygen might have had a detrimental effect upon the surface of the lithium aluminate.

6. The predominant form of tritium observed in the experiment was the noncondensable, or HT, form. Thermodynamic calculations correctly predict this form for the experimental conditions. The amount of HT is expected to be less in a fusion reactor blanket, but permeation rates could still be a problem

7. Permeation rates measured in the experiment were extrapolated to rates of about 1000 Ci/day for a fusion reactor blanket, owing to the predominance of the HT form. Permeation rates of 1000 Ci/day are lower than the rates of tritium currently estimated to transport from the plasma edge through the first wall. Thus, the HT form results in high permeation rates, but such rates may be manageable.

8. The total damage was 0.18% lithium burnup, with 0.81 dpa and a dose of 5.36×10^{12} rads. This burnup is equivalent to ~0.6 MW•yr/m^2 or about two months in a fusion reactor like STARFIRE. Under these damage conditions and temperatures ranging nearly up to 800°C, no evidence was found of significant change in the microstructure of the breeder material.

9. Temperatures were effectively controlled with the gap gas technique.

10. Heat transfer coefficients and thermal conductivity did not significantly change as a result of irradiation.

11. Trace impurities produced a number of volatile radionuclides, which were observed in the sweep gas.

SECTION XI

RECOMMENDATIONS FOR FURTHER RESEARCH

XI. RECOMMENDATIONS FOR FURTHER RESEARCH

The TRIO experiment produced a considerable amount of useful data on tritium transport and heat transfer in the breeder material of lithium aluminate. More information in these areas is needed, as well as more data on the effects of radiation damage on solid breeder materials in general. The requirements of in-situ tritium recovery establish the operating limits (such as temperature and porosity) for solid breeder blankets.[1] Tritium recovery from solid breeders is potentially affected by a number of factors, including temperature, temperature gradient, tritium production rate, grain size, porosity, surface area, surface condition (sites), oxygen potential, hydrogen potential, tritium partial pressure, defects/vacancies in the lattice, impurities in the solid and/or sweep gas, and transport of other species (e.g., helium). The role of these factors needs to be quantified in order to establish meaningful limits for blanket design.

Radiation damage needs to be studied because it can alter some of these factors. For example, radiation damage can change grain size, change porosity, and create defects in the solid.

Temperature is a key factor because it directly affects tritium transport rates and can, particularly in concert with radiation, change the microstructural properties of the ceramic. Owing to the importance of temperature, the control of temperature profiles in a solid breeder blanket is a key issue. Temperature profiles must be controlled both in an experiment of this kind and in a fusion reactor. Therefore, data on heat transfer coefficients and thermal conductivity and the effects of irradiation on these properties is needed.

It is unlikely that a single experiment can effectively solve all the programmatic needs. Nonetheless, TRIO demonstrated that experiments of this type can effectively address many different research needs on breeder blankets. Therefore, it is recommended that more experiments of this type be undertaken. Considered herein is a single experiment which logically follows the successful completion of the TRIO experiment.

The follow-on experiment should first of all retain the many useful features incorporated in the TRIO experiment. These features include a number of on-line capsule monitors, thermocouples, and flux monitors placed in appropriate locations in the test capsule. In addition, the gas analysis system for TRIO included provision for real-time and integral monitoring of tritium in its various chemical forms, as well as tritium permeation and measurement of impurities. This basic experimental setup should be upgraded to include the following modifications and/or improvements:

1. The temperature gradient should be minimized to simplify the interpretation of temperature-dependent behavior such as diffusion. It is recommended that the temperature gradient not exceed 50°C. In addition, it would be beneficial to use a material with a lower activation energy for diffusion. Li_2O appears to have an activation energy about one-fourth that of $LiAlO_2$.

2. The temperature range should, if possible, span the recommended temperature limits, viz. 300-1000°C. Investigation of low temperature allows direct determination of the lower temperature limit. Investigation of high temperature allows direct determination of the effects of swelling, sintering, etc., on tritium transport.

3. The experimental system should have improved monitoring capability for oxygen potential becasue of its importance to tritium release. The following items are needed: an oxygen meter, a moisture meter, and a mass analyzer.

4. More quantitative measurements of real-time tritium response are needed. This can be achieved with minor modification of the apparatus and with appropriate provision for extensive manual operations.

5. Experimental runs should go to equilibrium, i.e., each run should last one to two weeks. Longer runs would permit more quantitative measurement of release for volatile radionuclides.

6. In order to reduce uncertainties in measured heat transfer coefficients and thermal conductivity, a more accurate determination of gamma heating rates is needed. This could be done by making a number of measurements of gamma heating throughout the course of the experiment.

7. Because of its high thermal conductivity, Li_2O is the best choice of breeder material to study decreases in thermal conductvity owing to radiation damage. In addition, the radial temperature gradient should be at least 50°C so that thermal conductivity can be accurately measured.

In addition to consideration of the experimental setup, there are a number of operational choices which should be considered, such as the test matrix, the number of capsules, etc.

The first choice is whether the temperature should be a variable. In the TRIO experiment, the temperature was systematically changed every few days. With this approach, data for many temperatures were obtained from a single test capsule; however, frequent temperature changes complicated the interpretation of the results. A single set temperature has two disadvantages: the amount of data that can be obtained is very limited, and no information can be derived on temperature-dependent behavior, unless one goes to a large number of capsules. Because irradiation experiments of this kind are expensive to conduct, care should be taken to obtain the maximum amount of data possible. Therefore, each capsule should have the capability of changing the temperature in a controlled way. For purposes of planning, each temperature run should last one to two weeks. For similar reasons, each capsule should have capabilities for operating with a sweep gas of variable flow and oxygen potential.

The next choice is the number of capsules. The recommended approach is not to do anything that will adversely affect the monitoring capability for each capsule. Thus, each capsule should have appropriate instrumentation. The cost per capsule will be somewhat less for experiments with multiple capsules, but the difference will not be large. The number of capsules will most likely be set by cost constraints. An option that should be evaluated is running a number of single-capsule tests in series. For the purpose of setting a reference point, it is recommended that the next TRIO-type test include two capsules.

Another choice to be made is the material to be tested. In TRIO, lithium aluminate was tested. Lithium aluminate should be similar to a number of the ternary lithium oxides because of its high melting point, low thermal conductivity, and chemical inertness. Lithium oxide, which is rather different in

the above aspects and is a generally attractive candidate breeder material, should be tested in a TRIO-type test. Lithium oxide has been tested in-pile in experiments at JAERI,[27,30] but those experiments were somewhat limited in scope. Lithium oxide remains the most logical choice for the next experiment. The high thermal conductivity and the low activation energy for diffusion are favorable for this material. Therefore, it is recommended that one capsule contain lithium oxide. The selection of material for the second capsule is now an open question. It could be lithium oxide of different morphology, an appropriate ternary oxide, or some advanced material.

REFERENCES

REFERENCES

1. C. C. Baker et al., "STARFIRE - A Commercial Tokamak Fusion Power Plant Study," Argonne National Laboratory, ANL/FPP-80-1 (1980).

2. B. Badger et al., "UWMAK-II," University of Wisconsin, UWFDM-112 (1975).

3. M. A. Abdou, L. J. Wittenberg, and C. W. Maynard, "A Fusion Design Study of Nonmobile Blankets with Low Lithium and Tritium Inventories," Nucl. Technol. 26, 400 (1975).

4. J. R. Powell et al., "Preliminary Reference Design of a Fusion Reactor Blanket Exhibiting Very Low Residual Radioactivity," Brookhaven National Laboratory, BNL-19565 (1974).

5. K. R. Schultz et al., "Blanket, Shield, and Power Conversion System for a Small Field Reversed Mirror Fusion Center," General Atomic Company, GA-A15533 (1979).

6. R. L. Hagenson et al., "The Reversed-Field Pinch Reactor (RFPR) Concept," Los Alamos National Laboratory, LA-7973-MS (1979).

7. D. W. Kearney et al., "Doublet Demonstration Fusion Power Reactor Study," General Atomic Company, GA-A14742 (1978).

8. D. L. Smith et al., "Fusion Reactor Blanket/Shield Design Study," Argonne National Laboratory and McDonnell Douglas Astronautics Company, ANL/FPP-79-1 (1979).

9. M. Abdou et al., "Blanket Comparison and Selection Study - Interim Report," Argonne National Laboratory, ANL/FPP/TM-177 (1983).

10. M. Abdou et al., "A Demonstration Power Plant Study," Argonne National Laboratory, ANL/FPP/82-1 (1982).

11. D. Steiner et al., "ORNL Fusion Power Demonstration Study," Oak Ridge National Laboratory, ORNL/TM-5813 (1977).

12. K. Sako et al., "Design Study of a Tokamak Reactor," Japan Atomic Energy Research Institute, IAEA-CN-33/G1-2 (1982).

13. U.S. FED-INTOR Activity and U.S. Contribution to the International Tokamak Reactor Phase-2A Workshop, USA FED-INTOR/82-1 (1982).

14. Standard Mirror Fusion Reactor Design Study, Lawrence Livermore National Laboratory, UCID-17644 (1978).

15. ELMO Bumpy Torus Reactor and Power Plant, Los Alamos National Laboratory, LA-8882-MS (1981).

16. E. M. Larsen, R. G. Clemmer, and D. K. Sze, Trans. Am. Nucl. Soc. 23, 56 (1976), and references therein.

17. R. G. Clemmer, "The Development of Tritium Breeding Blankets for DT-Burning Fusion Reactors," Proc. 4th Top. Mtg. on The Technology of Controlled Nuclear Fusion, USDOE, CONF-801011, p. 526 (1980), and references therein.

18. D. L. Smith et al., "Analysis of In-Situ Tritium Recovery from Solid Breeder Blankets," ibid, p. 560, and references therein.

19. D. Okula and D. K. Sze, "Tritium Recovery from Solid Breeders: Implications of the Existing Data," University of Wisconsin, UWFDM-351 (1980), and references therein.

20. J. W. Davis et al., Proc. Workshop on Tritium Breeding Solids - Research and Development, USDOE, DOE/ET-52039/1 (1981) and references therein.

21. S. Nasu, "Data Base for Breeder Choice," Japan Atomic Energy Research Institute, JAERI-M-8510 (1979) and references therein; also published as Appendix C, Ref. 19.

22. D. L. Smith et al., "Assessment of Solid Breeding Blanket Options for Commercial Tokamak Reactors," Proc 8th Symp. on Engineering Problems of Fusion Research, San Francisco, IEEE Pub. No. 79CH1441-5, p. 433 (1979).

23. C. E. Johnson, R. G. Clemmer, and G. W. Hollenberg, "Solid Breeder Materials," J. Nucl. Mater. 103, 547 (1981), and references therein.

24. C. E. Johnson and G. W. Hollenberg, "Recent Advances in the Development of Solid Breeder Blankets," Proc. 3rd Top. Mtg. on Fusion Reactor Materials, Albuquerque, New Mexico, September 19-22, 1983.

25. R. G. Clemmer et al., "The TRIO-01 Experiment: In-Situ Tritium Recovery Results," ibid.

26. G. W. Hollenberg, "Fast Neutron Irradiation Results on Li_2O, Li_4SiO_4, Li_2ZrO_3, and $LiAlO_2$," ibid.

27. T. Kurasawa et al., "In-Situ Tritium Recovery Experiment from Lithium Oxide Under High Neutron Fluence," ibid.

28. R. G. Clemmer, R. F. Malecha, and I. T. Dudley, "The TRIO-01 Experiment," Nucl. Technol./Fusion 4, 83 (1983).

29. R. Wiswall, E. Wirsing, and K. C. Hong, "The Removal of Tritium from Fusion Reactor Blankets," Brookhaven National Laboratory, BNL-50748 (1977); see also, R. H. Wiswall and E. Wirsing, "Tritium Recovery from Fusion Blankets Using Solid Lithium Compounds-II: Experiments on Tritium Removal and Absorption," Proc. Intern. Conf. on Radiation Effects and Tritium Technology for Fusion Reactors, Gatlinburg, TN, USA, October 1-3, 1975; and R. Wiswall, E. Wirsing, and K. C. Hong, " The Removal of Bred Tritium from Solid Lithium Compounds in Fusion Reactor Systems," Proc. 14th IECEC (1976).

30. S. Nasu, "A Preliminary In-Pile Test of Tritium Release from Li_2O Pellets," Japan Atomic Energy Research Institute, JAERI-Memo 9276 (1980).

31. L. Yang et al., "Irradiation Study of Lithium Compound Samples for Tritium Breeding Applications," GA Technologies, GA-A17407 (1981).

32. D. L. Porter et al., "Irradiation and Compatibility Testing of Li_2O Materials at EBR-II," Argonne National Laboratory, ANL/FPP/TM-167 (1982).

33. M. S. Ortman and E. M. Larsen, "The Preparation, Characterization, and Melting Point of Lithium Oxide," J. Am. Ceramic Soc., 66(9), 645 (1983).

34. G. W. Hollenberg, in "Fifth Annual Progress Report On Special Purpose Materials for Magnetically Confined Fusion Reactors," USDOE, DOE/ER-0113/2 (1983).

35. T. Takahashi and T. Kikuchi, J. Nucl. Mater. 91, 93 (1980).

36. R. W. McCulloch, Oak Ridge National Laboratory, personal communication (1983).

37. M. S. Ortman and E. M. Larsen, "Preparation and Melting Point of Octalithium Zirconate," Comm. Am. Ceramic Soc. C-142 (August 1983).

38. W. Jost, Diffusion in Solids, Liquids, and Gases, Academic Press, New York, p. 60 (1960).

39. R. Treybal, Mass-Transfer Operations, McGraw-Hill, New York, pp. 79-81 (1968).

40. W. G. Sheehan, M. L. Curtis, and D. C. Carter, "Development of a Low Cost Versatile Method for Measurement of HTO and HT in Air," Mound Laboratory, MLM-2205 (1975).

41. Union Carbide Data Sheet on Linde Molecular Seive Type 4A Pellets (1982).

42. K. R. Thoms, Oak Ridge National Laboratory, personal communication.

43. L. R. Greenwood, "Dosimetry Results for the TRIO test in ORR" in Damage Analysis and Fundamental Studies, Quarterly Progress Report, April-June 1982, U.S. Department of Energy, DOEE/ER-0046, p. 9 (1982).

44. D. W. Knef, B. M. Oliver, M. M. Nakata, and H. Farrar IV, "Helium Production in Li-6 and B-10 from ORR-TRIO," in Damage Analysis and Fundamental Studies, Quarterly Progress Report, July-September 1982, U.S. Department of Energy, DOE/ER-0046/10, p. 36 (1982).

45. P. A. Finn et al., "The Design, Fabrication, and Testing of the Gas Analysis System for the Tritium Recovery Experiment, TRIO-01," 10th Symp. on Fusion Engineering, Philadelphia, PA, December 5-9, 1983.

46. E. H. Van Deventer and V. A. Maroni, "Hydrogen Permeation Characteristics of Some Austenitic and Ferritic Alloys," J. Nucl. Mater. 92, 103 (1980); see also V. A. Maroni, "Materials Considerations in Tritium Handling Systems," Proc. 1st Top. Mtg. on Fusion Reactor Materials, January 29-31, 1979, Miami, Florida, and references therein.

47. E. W. Roberts and J. P. Roberts, Bull. Soc. Franc. Ceram., 77, 3 (1967).

48. V. K. Hauffe and O. Hoeffgren, Berichte Bunsen-Gesell., Phsyikal. Chem. 74, 537 (1970).

49. T. S. Elleman et al., Proc. 3rd Top. Mtg. on the Technology of Controlled Nuclear Fusion, Santa Fe, NM, Vol. 2, p. 763 (1978).

50. W. Yunker, "Continuous Extraction of Tritium From Irradiated Lithium Aluminate," Hanford Engineering Development Laboratory, TC-1745 (1980).

51. D. Guggi, H. Ihle, A. Neubert, and R. Wolfe, "Tritium Release from $LiAlO_2$," Intern. Conf. on Radiation Effects and Tritium Technology for Fusion Reactors, Gatlinburg, TN, October 1-3, 1975; see also D. Guggi, H. Ihle, and U. Kurz, "Tritium Release from Neutron-Irradiated Lithium-Aluminum Oxides," Proc. 9th Symp. on Fusion Technology, EUR-5602, p. 337 (1975).

52. V. G. Vasiliev et al., "Investigation of the Physical-Chemical Properties of Irradiated Inorganic Compounds of Lithium Oxides, Aluminates, and Silicates," US/USSR Workshop on Engineering and Economic Problems of ETF, Moscow and Lenningrad (USSR), September 10-21, 1979.

53. S. W. Tam, Argonne National Laboratory, private communication (1978).

54. F. G. Perry, "Least-Square Spectral Adjustment: The Computer Code STAYSL," Oak Ridge National Laboratory, ORNL/TM-6062 (1979); modified by L. R. Greenwood.

ACKNOWLEDGMENTS

The authors wish to acknowledge the many people and organizations who contributed to the success of this project. The work was supported by the Office of Fusion Energy, U.S. Department of Energy. Of the many people at Argonne, a few deserve special mention: V. A. Maroni who conceived the idea for the experiment and provided much useful guidance; C. C. Baker who provided guidance, advice, and leadership; C. Hytry who prepared and assembled this document; and the many people from the Chemical Technology Division and the Materials Science Division who made numerous valuable contributions. The authors are indebted to J. R. Conlin, C. D. West, and other people from Oak Ridge National Laboratory.

DISTRIBUTION FOR ANL-84-55

Internal:

C. Baker
M. Billone
D. Bowers
Y. Cha
R. Clemmer (50)
D. Diercks
A. Fischer
F. Fradin
L. Greenwood
D. Gruen
P. Finn
A. Fischer
C. Johnson
Y. Liu
R. Malecha
V. Maroni
R. Mattas
B. Misra
L. Neimark
R. Poeppel
D. Porter
W. Praeg
J. Roberts
G. T. Reedy
D. L. Smith
M. Steindler
D. K. Sze
S. W. Tam
H. Thresh
M. Tetenbaum
FPP Files (10)
ANL Contract File
ANL Libraries
ANL Patent Dept.
TIS Files (6)

External:

DOE-TIC, for distribution per UC-20, 20c, 20d, 20e (196)
Manager, Chicago Operations Office, DOE
University of Chicago Special Committee for the Fusion Program:
- S. Baron, Brookhaven National Laboratory
- H. Forsen, Bechtel Group, Inc.
- J. Maniscalco, TRW, Inc.
- G. Miley, University of Illinois-Urbana
- P. Reardon, Brookhaven National Laboratory
- P. Rutherford, Princeton University
- D. Steiner, Rensselaer Polytechnic Institute
- K. Symon, University of Wisconsin-Madison
- K. Thomassen, Lawrence Livermore National Laboratory

University of Chicago Review Committee for the Chemical Technology Division:
- K. H. Keller, U. Minnesota
- T. A. Milne, Solar Energy Research Inst.
- H. Perry, Resources for the Future, Washington
- R. Winston, U. Chicago
- W. L. Worrell, U. Pennsylvania
- R. Wymer, Oak Ridge National Lab.
- E. B. Yeager, Case Western Reserve U.

M. A. Abdou, University of California-Los Angeles
R. Alire, Lawrence Livermore National Laboratory
J. Anderson, Los Alamos National Laboratory
R. Arons, Celenase Resarch Company
A. Bancroft, Chalk River Nuclear Laboratories, Canada
J. Bartlit, Los Alamos National Laboratory
S. Berk, U. S. Department of Energy, Office of Fusion Energy
S. Buchsbaum, Bell Telephone Laboratories, Inc.
G. Casini, Joint Research Centre, Ispra Establishment, Italy
G. Caskey, E. I. DuPont de Nemours, Savannah River Laboratory
G. Catchen, Pennsylvania State University
R. Childs, Oak Ridge National Laboratory
E. Clemmer, Oak Ridge National Laboratory
F. Clinard, Jr., Los Alamos National Laboratory
M. Cohen, U. S. Department of Energy, Office of Fusion Energy
J. Conlin, Oak Ridge National Laboratory

R. Conn, University of California-Los Angeles
J. Darvas, Commission of the European Communities, Belgium
R. Conrad, JRC Petten, The Netherlands
J. Davis, McDonnell Douglas Astronautics Company
S. Dean, Fusion Power Associates, Gaithersburg, MD
D. DeFreece, McDonnell Douglas Astronautics Company
D. Doran, Hanford Engineering Development Laboratory
I. Dudley, Oak Ridge National Laboratory
F. Dyer, Oak Ridge National Laboratory
K. Ehrlich, Kernforschungszentrum Karlsruhe, Federal Republic of Germany
R. Eichelberger, Rockwell International, Canoga Park, CA
B. Engholm, GA Technologies Inc.
J. Fillo, Brookhaven National Laboratory
P. Fisher, Oak Ridge National Laboratory
C. Flanagan, Westinghouse Electric Corporation, Oak Ridge, TN
T. Galloway, Lawrence Livermore National Laboratory
P. Gildea, Sandia National Laboratories, Livermore, CA
J. Gilligan, North Carolina State University
R. Gold, Westinghouse Electric Corporation, Madison, PA
D. Graumann, GA Technologies Inc.
E. Hager, GA Technologies Inc.
C. Henning, Lawrence Livermore National Laboratory
R. Hickman, Lawrence Livermore National Laboratory
N. Hoffman, Energy Technology Engineering Center, Canoga Park, CA
G. Hollenberg, Westinghouse Hanford Company
G. Hopkins, GA Technologies Inc.
P. Hsu, EG&G Idaho, Inc.
P. Hubberstey, University of Nottingham, United Kingdom
G. Hurley, Los Alamos National Laboratory
J. Hurley, Rockwell International, Golden, CO
D. Jassby, Princeton Plasma Physics Laboratory
K. Keller, University of Minnesota
C. Kershner, Monsanto Research Corporation
D. Kneff, Rockwell International, Canoga Park, CA
M. Kinoshita, Japan Atomic Energy Research Institute
R. Krakowski, Los Alamos National Laboratory
S. Kulcinski, University of Wisconsin-Madison
M. Kwast, Netherlands Energy Research Foundation, ECN, The Netherlands
E. Larsen, University of Wisconsin-Madison
G. Longhurst, EG&G Idaho, Inc.
P. Lykoudis, Purdue University
L. McGrath, Sandia National Laboratories, Albuquerque, NM
S. Merrill, EG&G Idaho, Inc.
M. Migge, Hahn-Meitner Institut für Kernforschung Berlin, FRG
M. Mintz, Sandia National Laboratories, Livermore, CA
L. Moir, Lawrence Livermore National Laboratory
M. Morgan, McDonnell Douglas Astronautics Company
C. O'Kula, E. I. DuPont de Nemours, Savannah River Laboratory
A. Opdenecker, U. S. Department of Energy, Office of Fusion Energy
M. Overhoff, Overhoff and Associates
M. Pierini, ISPRA, Varese, Italy
T. Ruether, U. S. Department of Energy, Office of Fusion Energy
M. Rogers, Monsanto Research Corporation
M. Roth, CEA, Centre d'Etudes Nucleaires de Saclay, France

A. Scandora, Science Applications, Inc.
K. Schultz, GA Technologies Inc.
F. Scott, Electric Power Research Institute, Palo Alto
J. Scott, Oak Ridge National Laboratory
T. Shannon, FEDC, Oak Ridge National Laboratory
H. Takeshita, Japan Atomic Energy Research Institute, Japan
A. Tobin, Grumman Aerospace Corporation, Bethpage, NY
P. Tortorelli, Oak Ridge National Laboratory
C. Trachsel, McDonnell Douglas Astronautics Company
V. Vassiliev, International Atomic Energy Agency, Vienna, Austria
R. Verbeek, Commission of the European Communities, Belgium
L. Waganer, McDonnell Douglas Astronautics Company
H. Watanabe, Japan Atomic Energy Research Institute, Japan
C. D. West, Oak Ridge National Laboratory
P. Wienhold, Institute für Plasmaphysick, Kernforschungsanlage Jülich, FRG
H. Willenberg, Mathematical Science N.W.
L. Wittenberg, Univesity of Wisconsin-Madison
W. Wolfer, University of Wisconsin-Madison
C. Wong, GA Technologies Inc.
C. Wu, Institute für Chemie, Kernsforschungsanlage Jülich, FRG